Molekularbiologische und physiologische Analyse des Oligomerisierungsverhaltens von humanen Connexinen

Von der Naturwissenschaftlichen Fakultät der

Gottfried Wilhelm Leibniz Universität Hannover

zur Erlangung des Grades

Doktor der Naturwissenschaften (Dr. rer. nat.)

genehmigte Dissertation

von

Patrik Klaus Schadzek, M. Sc.

[2019]

Referent: Prof. Dr. Anaclet Ngezahayo

Korreferent: Prof. Dr. Peter Claus

Korreferent: Prof. Dr. Ralf Jacob

Tag der Promotion: 20.03.2019

Inhaltsverzeichnis

Abkürzungsverzeichnis

ACh	Acetylcholin
AFM	Rasterkraftmikroskop (*atomic force microscope*)
AleI	Restriktionsendonuklease (*blunt cutter* 5' CACNN ↓ NNGTG 3')
ANOVA	Varianzanalyse *(analysis of variance)*
ATP	Adenosintriphosphat
C-Terminus	Carboxy-Terminus
cAMP	zyklisches Adenosinmonophosphat
cDNA	*complementary desoxyribonucleic acid*
cGMP	zyklisches Guanosinmonophosphat
CL	Zytoplasmatische (intrazelluläre) Schleife *(cytoplasmatic loop)*
CLSM	Konfokales Laser Scanning Mikroskop
cRNA	coding *ribonucleic acid*
Cx	Connexin
DNA	*desoxyribonucleic acid*
DSP	3,3-Dithio-*bis*-(succinimidyl)propionat
DTSSP	3,3-Dithio-*bis*-(sulfosuccinimidyl)propionat
E1	Erste extrazelluläre Schleife
E2	Zweite extrazelluläre Schleife
eGFP	*enhanced green fluorescent protein*
ER	Endoplasmatisches Retikulum
ERGIC	*ER-Golgi intermediate compartment*
ERp29	*ER-localized protein 29 kDa, thioredoxin-family protein*
FRET	*Fluorescence Resonance Energy Transfer*
G	Leitfähigkeit
GABA	γ-Aminobuttersäure

GFP	*green fluorescent protein*
HCVp	Hepatitis C Virus Protease
hCx	Humanes Connexin
HeLa	Henrietta Lacks: Spenderin der Cervixkarzinom-Epithelzelllinie
IP$_3$	Inositoltriphosphat
kDa	Einheit für die Proteingröße (1 kDa $\stackrel{\wedge}{=}$ 1000 u)
LY	*Lucifer Yellow*, Gap Junction permeabler Farbstoff
N-Terminus	Amino-Terminus
N2A	Neuro-2A: Maus-Neuroblastoma Zelllinie
NAMD	*nanoscale molecular dynamics*
ODDD	Okulodentodigitale Dysplasie
p-Wert	Wahrscheinlichkeits-Wert
Panx	Pannexin
PhoCl	*photocleavable protein*
R	Widerstand
RIN	Ratten-Bauchspeicheldrüsen Zelllinie
RNA	*ribonucleic acid*
SEM	Standardfehler *(standard error of the mean)*
SKHep1	Leber-Zelllinie aus dem Menschen
SRP	*signal recognition particle*
TEV	*Tobacco Etch Virus*
TGN	trans-Golgi Netzwerk
TM	Transmembrandomäne
WGA	*wheat germ agglutinin*
wt	Wildtyp

Abbildungsverzeichnis

Zusammenfassung

Für multizelluläre Organismen ist die Zell-Zellkommunikation lebensnotwendig, die durch Gap Junctions zwischen benachbarten Zellen innerhalb eines Gewebes vermittelt wird. Connexine, die die Untereinheit von Gap Junction-Kanälen bei Vertebraten bilden, sind somit maßgeblich für die Organfunktionalität verantwortlich, indem sie die einzelnen Zellen zu einer physiologischen Einheit vereinen. Die Funktionalität der Gap Junction-Kanäle ist von der Oligomerisierung der Connexin-Untereinheiten, wovon beim Menschen bisher 21 verschiedene Isoformen bekannt sind, abhängig.

In dieser Arbeit wurde das Oligomerisierungsverhalten von Connexinen, sowohl in Hinblick auf das Hexamerisieren von sechs Connexinen zu einem Connexon (Halbkanal), als auch in Hinblick auf das Docking von zwei Connexonen zu einem Gap Junction-Kanal, analysiert. Ausgehend von der Mutation N188T des humanen Connexin46 (hCx46), welche mit einer Kataraktbildung assoziiert ist, wurden die strukturellen und funktionellen Konsequenzen dieses Aminosäureaustauschs untersucht. Es konnte erstmals gezeigt werden, dass die Mutation N188T das Docking der Connexone stört, da durch die Mutation die benötigte Stabilisierung des Gap Junction-Kanals über ausreichend viele Wasserstoffbrückenbindungen nicht mehr möglich ist. Die Aminosäure N188 stellt die Schlüssel-position beim Docking von hCx46 dar. Um auf molekularer Ebene zu untersuchen, wie die Patienten pathophysiologisch betroffen sind, die die Mutation zusammen mit dem Wildtyp hCx46 exprimieren (heterozygot), wäre es wünschenswert, die Anzahl und die stöchiometrische Zusammensetzung mutierter Connexine innerhalb eines Connexons determinieren zu können. Hierfür wurden Connexine konkatemerisiert. Es konnte erstmals gezeigt werden, dass konkatemerisierte Connexine transportiert und in die Plasmamembran insertiert werden, wo sie funktionale Halbkanäle und Gap Junction-Kanäle bilden können. Durch das Bilden von Konkatemeren, bestehend aus hCx46N188T und dem Wildtyp, in Kombination mit Molekül-Dynamik-Simulationen konnte die postulierte dominant-negative Eigenschaft der Mutation auf das Docking strukturbiologisch bestätigt werden. hCx46N188T reduziert die Anzahl der zwischen den Zellen gebildeten hCx46-Gap Junction-Kanäle und erschwert dadurch die metabolische Homöostase der Linse, was die Katarakt-Bildung begünstigt. Durch diese innovative Herangehensweise der Connexin-Konkatemerisierung eröffnen sich neue Möglichkeiten für die Analyse heteromerer Connexone und heterotypischer Gap Junction-Kanäle mit einer definierten Stöchiometrie. Homodimere und heterodimere Konkatemere, bestehend aus hCx46 und hCx26, wurden im Vergleich zu den beiden Monomeren in Zellen exprimiert und auf ihre physiologischen Eigenschaften untersucht. Die heterodimeren Kanäle wiesen einzigartige Kanaleigenschaften auf, die von denen der homodimeren Kanäle abwichen, was weitere Hinweise auf die postulierte Spezifizierung von Connexonen durch Heterooligomerisierung gibt. Eine weitere Analyse stöchiometrisch spezifischer heteromerer Kanäle mit dieser Methode ist somit sehr vielversprechend.

Schlagworte: Gap Junctions, Halbkanal-Docking, Connexin-Konkatemer, heteromere Connexone, Oligomerisierung, Kanalstöchiometrie

Abstract

For multicellular organisms the cell-to-cell communication is essential, mediated by gap junctions between neighboring cells within a tissue. Connexins are the subunits of vertebrate gap junction channels and are responsible for multiple organ functions by uniting individual cells to a physiological system. The functionality of the gap junctions channels depends on the oligomerization of the connexin subunits. In human 21 different connexin isoforms are known.

In this dissertation, the oligomerization behavior of connexins was analyzed with regard to the hexamerization of six connexins to a connexon and to the docking of two connexons to form a gap junction channel. Based on the N188T mutation of human connexin46 (hCx46), which is associated with a congenital nuclear pulverulent cataract, the structural and functional consequences of this amino acid exchange were investigated. It could be shown for the first time that the N188T mutation disrupts the docking of the connexons by not allowing the required stabilization of the channel via a sufficient number of hydrogen bonds. The N188 residue is the key position for the docking of the hemichannels. In order to molecularly analyze how patients are pathophysiologically affected who express the mutation hCx46N188T together with the hCx46 wild type (heterozygous for the mutation hCx46N188T), it would be desirable to be able to determine the number of the mutant connexins and the stoichiometric composition within a connexon. Therefore, connexins were concatemerized. It was shown for the first time that concatenation of connexins is compatible with trafficking of the hemichannels to the membrane and the formation of functional hemichannels and gap junction channels. By constructing concatemers consisting of hCx46N188T and the wild type, in combination with molecular dynamics simulations, the postulated negative dominate property of the mutation for the hemichannel docking was structural biologically verified. hCx46N188T reduces the amount of gap junction channels between cells, making it more difficult to catabolize the metabolic homeostasis of the lens and thereby promoting the formation of cataract. This innovative approach of concatemerizing connexins opens up new possibilities to analyze heteromeric connexons and heterotypic gap junction channels with a defined stoichiometry. Homodimeric and heterodimeric concatemers, consisting of hCx46 and hCx26, were expressed in cells. Their physiological properties were analyzed in comparison to cells expressing the monomers. The heterodimeric channels showed unique channel properties that deviated from those of the homodimeric channels, giving further evidence regarding the postulated specification of the connexons by hetero-oligomerization. Future analysis of the stoichiometrically specified heteromeric channels by concatenating connexins is very promising.

Keywords: gap junctions, hemichannel docking, concatenated connexins, heteromeric connexons, oligomerization, channel stoichiometry

1. Einleitung

Die Gap Junction-vermittelte Zell-Zellkommunikation stellt die Grundvoraussetzung für die Existenz und das Überleben von multizellulären Vertebraten dar. Krankheiten, die mit den Gap Junction-bildenden Connexinen in Verbindung stehen, gehen mit einer Störung der Zell-Zellkommunikation einher und äußern sich oft bei der Geburt bzw. in den ersten Lebensjahren, wo sie zu abnormaler Organentwicklung sowie Organversagen von lebenswichtigen Organen führen (Kelly *et al.*, 2015). Die bisher bekannten mit Connexinen in Verbindung stehenden Krankheiten lassen sich in sechs Bereiche klassifizieren: Hörverlust, Störung der Myelinisierung, Okulodentodigitale Dysplasie (ODDD), Hauterkrankungen, Katarakt-Bildung und Herz-Kreislauferkrankungen (Kelly *et al.*, 2006; Mathias *et al.*, 2010; Kleopa *et al.*, 2012; Van Norstrand *et al.*, 2012; Chan & Chang, 2014; Martin *et al.*, 2014).

Des Weiteren sind Connexine beispielsweise für die metabolische Homöostase und die Physiologie der avaskulären Linse verantwortlich (Mathias *et al.*, 2007). Für die gezielte Versorgung und den Abtransport von Stoffwechselprodukten aus der Linse wird angenommen, dass die Zellen durch die Oligomerisierung verschiedener Connexine zu spezialisierten Gap Junction-Kanälen und Halbkanälen eine metabolische Selektivität schaffen und so die Flussrichtung von Metaboliten steuern können.

1.1 Connexine und Gap Junctions

Gap Junction-Kanäle verbinden das Zytoplasma von benachbarten Zellen. Sie erlauben den direkten Austausch von Ionen und Metaboliten und ermöglichen somit die Zell-Zell-Kommunikation (Nielsen *et al.*, 2012; Leybaert *et al.*, 2017). Gap Junctions sind permeabel für Moleküle bis zu einer Größe von etwa 1,5 kDa und daher können wichtige Metaboliten, beispielsweise ATP, Glucose und sekundäre Botenstoffe wie cAMP, cGMP oder IP_3 (Alexander & Goldberg, 2003; Sáez *et al.*, 2003; Li *et al.*, 2012) und sogar kleine RNAs, zwischen den Zellen ausgetauscht werden (Brink *et al.*, 2012). Gap Junctions sind in nahezu allen tierischen Geweben exprimiert und verbinden eine Vielzahl von Geweben zu physiologischen Einheiten und gewährleisten so beispielsweise die elektrische Reizweiterleitung im Herzen (Dhein, 2004; Leybaert *et al.*, 2017), den Reifungsprozess von Eizellen (Nicholson & Bruzzone, 1997) und die Nährstoffversorgung und metabolische Homöostase der Linse (Donaldson *et al.*, 2001; Berthoud & Ngezahayo, 2017).

Ein Gap Junction-Kanal wird bei Vertebraten aus Connexin-Untereinheiten (Nicholson & Bruzzone, 1997; Harris, 2001; Nielsen *et al.*, 2012) und bei Invertebraten aus Innexinen (Phelan, 2005; Yen & Saier, 2007) gebildet. Connexine sind Membranproteine und besitzen vier Transmembrandomänen, zwei extrazelluläre Schleifen, eine intrazelluläre Schleife, sowie einen zytoplasmatisch lokalisierten

N- und C-Terminus (Zimmer *et al.*, 1987; Falk *et al.*, 1994). Sechs Connexine bilden in der Plasmamembran ein Connexon (Falk *et al.*, 1994; Unger *et al.*, 1999), einen Halbkanal (siehe Abbildung 1), der einen Stoffaustausch mit dem extrazellulären Milieu ermöglicht (Nielsen *et al.*, 2012; Retamal & Sáez, 2014; Leybaert *et al.*, 2017; Harris, 2018). Zwei Connexone benachbarter Zellen können miteinander interagieren und so einen Gap Junction-Kanal bilden (Kumar & Gilula, 1996; Foote *et al.*, 1998). Ihren Namen erhielten die Kanäle, da zwischen adhärent wachsenden Zellen in Bereichen von Gap Junction-Kanal-Ansammlungen eine Verengung des Zellzwischenraums auf einen definierten Abstand von 2 – 4 nm beobachtet wurde, welcher „*gap*" (wörtlich übersetzt: „Lücke") genannt wird (Revel & Karnovsky, 1967).
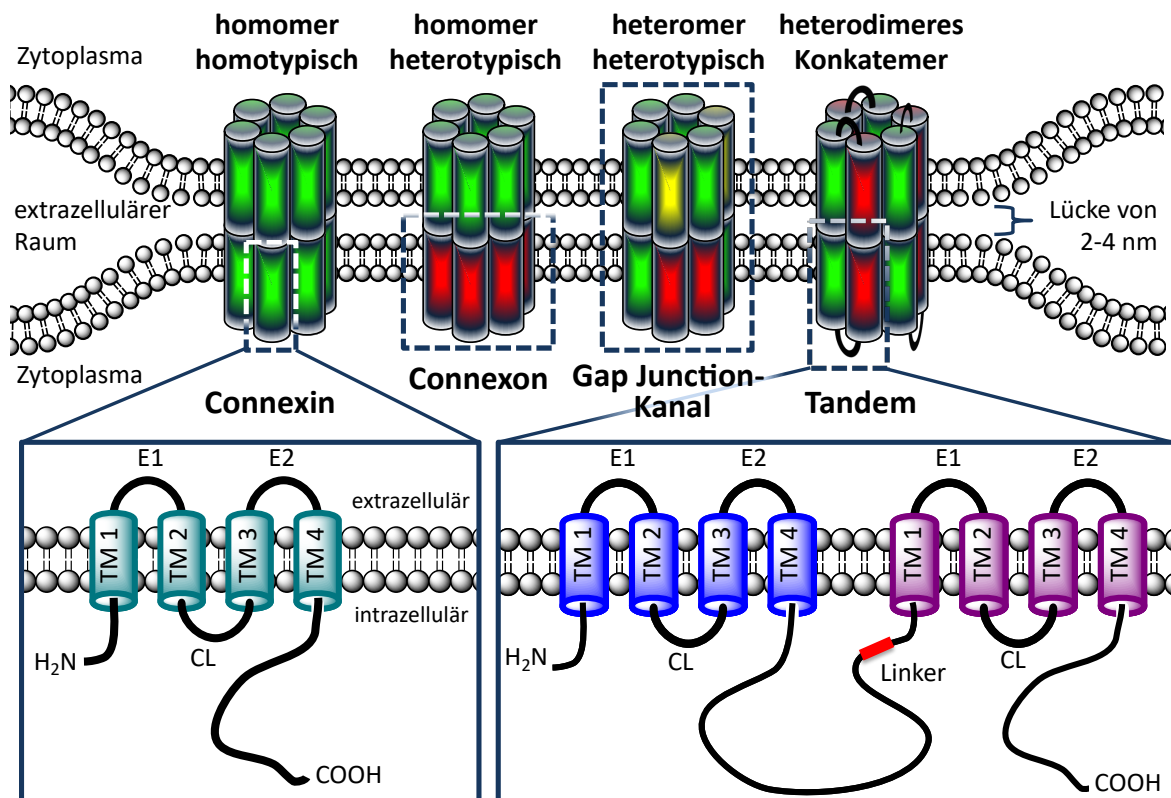

Abbildung 1: Struktureller Aufbau von Connexinen und Gap Junction-Kanälen. Ein Gap Junction-Kanal wird aus zwei Connexonen bzw. Halbkanälen gebildet, die wiederum aus jeweils sechs Connexinen aufgebaut sind. Connexine sind Membranproteine mit vier Transmembrandomänen (TM1-TM4), zwei extrazellulären Schleifen (E1 & E2), einer zytoplasmatischen Schleife (CL), sowie einem zytoplasmatisch lokalisierten N- und C-Terminus. Homomere Connexone und homotypische Gap Junction-Kanäle werden aus einer Connexin-Isoform gebildet. Im Gegensatz dazu werden die postulierten heteromeren Connexone und heterotypischen Kanäle aus verschiedenen Connexin-Isoformen zusammengefügt. Um das Oligomerisierungsverhalten zu analysieren, wurden während dieser Arbeit Connexin-Konkatemere generiert, was unten rechts gezeigt ist (modifiziert nach Schadzek *et al.*, 2018).

Bei der Benennung der Connexine werden zwei parallel existierende verschiedene Nomenklaturen verwendet. Die eine basiert auf der Aminosäurehomologie (Kumar & Gilula, 1996), während der anderen das ungefähre Molekulargewicht zugrunde liegt (Beyer *et al.*, 1987). Die auf die

Aminosäurehomologie zurückzuführende Nomenklatur unterteilt die Connexine anhand der Sequenzhomologie in drei Cluster. Die beiden größeren Cluster, die α- und β-Connexine, unterscheiden sich deutlich voneinander. Neben der Aminosäurehomologie variieren die Connexine deutlich in ihrer Länge der zytoplasmatischen Schleife. Diese ist bei den zur α-Gruppe gehörenden Connexinen fast doppelt so lang wie bei den β-Connexinen (Harris, 2001; Maeda *et al.*, 2009). Das dritte Cluster wird von Connexinen gebildet, die eine gemischte Homologie tragen, und wird daher noch weiter in γ-, δ- und ε-Connexin-Gruppen aufgespalten (Berthoud & Beyer, 2009; Abascal & Zardoya, 2013).

Die zweite geläufige Nomenklatur bezieht sich, wie einleitend bereits erwähnt, auf das ungefähre Molekulargewicht in kDa der Connexine. Das Molekulargewicht wird der Abkürzung Cx für Connexin angehängt. Die Unterscheidung zwischen verschiedenen Spezies erfolgt über das Voranstellen eines Präfixes. Fehlt dieses Präfix, so ist definitionsgemäß das humane Connexin gemeint. Jedoch wird von den meisten Autoren, um Verwechselungen auszuschließen, hCx als Abkürzung für humanes Connexin verwendet (Söhl & Willecke, 2003; Nielsen *et al.*, 2012). In dieser Arbeit wird die zuletzt vorgestellte Nomenklatur verwendet. So bezeichnet hCx46 beispielsweise das humane Connexin46.

Bisher sind beim Menschen 21 Isoformen der Connexin-Familie bekannt (Söhl & Willecke, 2004; Beyer & Berthoud, 2008). Bei Nagetieren und Zebrafischen sind 20 bzw. 38 verschiedene Connexin-Typen beschrieben worden (Willecke *et al.*, 2002; Eastman *et al.*, 2006). Die verschiedenen Isoformen, die ein Molekulargewicht von 25 bis 62 kDa haben (Willecke *et al.*, 2002; Cruciani & Mikalsen, 2006; Scemes *et al.*, 2009), unterscheiden sich hauptsächlich in der Länge des C-Terminus. Auch die Länge der intrazellulären Schleife ist variabel. Die Aminosäuresequenz des relativ kurzen N-Terminus ist bei allen Connexinen stark konserviert (Segretain & Falk, 2004).

Die meisten Zellen exprimieren zeitgleich mehr als eine Connexin-Isoform (Bevans *et al.*, 1998; White *et al.*, 2007; Leybaert *et al.*, 2017), weshalb postuliert wurde, dass ein Connexon mehrere verschiedene Connexine enthalten kann, was dann heteromeres Connexon genannt wird (siehe Abbildung 1). Ist nur eine Connexin-Isoform an der Bildung eines Halbkanal beteiligt, so wird dieses Connexon homomer genannt. Parallel wird bei der Bildung eines Gap Junction-Kanals zwischen homotypischen (bestehend aus zwei gleichen Connexonen) und heterotypischen (gebildet aus zwei unterschiedlichen Connexonen) Kanälen unterschieden (Kumar & Gilula, 1996; Nicholson, 2003). Aus diesen Kombinationsmöglichkeiten resultiert eine Kanalvielfalt, die die Bildung von Kanälen mit definierten Eigenschaften ermöglicht, wie etwa eine spezifische Permeabilität für bestimmte Metaboliten (Zhong *et al.*, 2017) oder eine Variabilität in der Spannungssensitivität, was eine zusätzliche Möglichkeit zur Regulation der intrazellulären Kommunikation darstellt (Koval *et al.*,

2014). Es können allerdings nicht alle Connexin-Isoformen heteromere Connexone, bzw. heterotypische Gap Junction-Kanäle miteinander bilden. Erklärt werden kann dieses unterschiedliche Heteromerisierungsverhalten durch eine nähere Betrachtung der Synthese von Connexinen.

1.2 Synthese und Degradation von Connexinen und Gap Junctions

Wie andere Membranproteine oder sekretorische Proteine werden Connexine auch in die Membran des Endoplasmatischen Retikulums (ER) translatiert (Pfeffer & Rothman, 1987; Jordan *et al.*, 1999). Dafür bindet während der Translation das SRP (*signal recognition particle*) an die Signalsequenz des entstehenden Connexins und dirigiert dieses durch die Interaktion mit dem SRP-Rezeptor an das Translokon in der ER-Membran (Görlich & Rapoport, 1993). Das Connexin wird daraufhin kotranslational in die ER-Membran insertiert, sodass N- und C-Terminus zytoplasmatisch lokalisiert sind (Falk & Gilula, 1998). Während des vesikulären Transports zur Plasmamembran hexamerisieren die Connexine zu Connexonen, wobei nicht alle Connexin-Isoformen in demselben Kompartiment oligomerisieren.

Basierend auf der Sequenzhomologie können Connexine bezüglich ihres Oligomerisierungsverhaltens in zwei Gruppen eingeordnet werden (siehe Abbildung 2). Die beiden Gruppen lassen sich anhand der Sequenz am Übergang von der zytoplasmatischen Schleife zur dritten Transmembrandomäne unterscheiden (CL-TM3-Motiv). Die meisten der zur β-Gruppe gehörenden Connexine haben an dieser charakteristischen Stelle zwei aufeinanderfolgende Tryptophan (W)-Aminosäuren und gehören daher zum W-Typ (Koval *et al.*, 2014). Sie folgen eher dem traditionellen Stoffwechselweg, was bedeutet, dass die vollständige Oligomerisierung zu Hexameren Voraussetzung für den Transport vom ER zum *cis*-Golgi-Kompartiment ist (Maza *et al.*, 2005; Das *et al.*, 2009; Jara *et al.*, 2012). Die Oligomerisierung findet für die W-Typ-Connexine also entweder im ER selbst oder im ERGIC (*ER-Golgi intermediate compartiment*) statt (Maza *et al.*, 2005; Koval, 2006).

Im Gegensatz dazu oligomerisieren die zur zweiten Gruppe gehörenden Connexine erst im TGN (*trans*-Golgi Netzwerk). Sie werden R-Typ-Connexine genannt, da sie am Übergang von der zytoplasmatischen Schleife zur dritten Transmembrandomäne eine geladene Arginin (R)-Aminosäure in der Sequenz aufweisen (Lagree *et al.*, 2003; Smith *et al.*, 2012). Chaperone interagieren im ER mit den monomeren Connexinen, um sie zu stabilisieren. Für Cx43, das am besten erforschte R-Typ-Connexin, wurde gezeigt, dass die Interaktion mit dem Chaperon ERp29 (ER-*localized protein* 29 kDa, *thioredoxin-family protein*) die Monomere stabilisiert. Hierfür interagiert ERp29 mit dem R-Typ-Connexin über ein Motiv mit der Aminosäuresequenz QYFLYGF, welche

zwischen dem Ende der dritten Transmembrandomäne und dem Anfang der zweiten extrazellulären Schleife liegt. W-Typ-Connexine tragen dort das Motiv FYxLYxG (x steht für eine beliebige Aminosäure), an das ERp29 nicht binden kann. Auch für andere R-Typ-Connexine (Cx40 und Cx46) ist experimentell nachgewiesen worden, dass sie erst später in ihrem Syntheseweg, also im TGN, nach dem Dissoziieren der Chaperone hexamerisieren (Musil & Goodenough, 1993; Koval *et al.*, 1997; Smith *et al.*, 2012). Da R-Typ-Connexine zum Zeitpunkt der Oligomerisierung von W-Typ-Connexinen durch Chaperone stabilisiert sind und somit noch nicht oligomerisieren können (Lagree *et al.*, 2003; Koval *et al.*, 2014), ist eine Bildung von heteromeren Connexonen aus R- und W-Typ-Connexinen *in vivo* nicht möglich.

Nach dem Oligomerisieren werden die Connexone über einen vesikulären mikrotubuliabhängigen Transport zur Plasmamembran transportiert (Martin *et al.*, 2001; Thomas *et al.*, 2001). Die Vesikel fusionieren mit der Membran, sodass die Connexone in die Zellmembran gelangen. Um einen Gap Junction-Kanal zu formen, diffundieren die Connexone lateral in der Plasmamembran zum Rand von sogenannten Gap Junction-Plaques. Dabei handelt es sich um eine Ansammlung von wenigen bis über tausend Gap Junction-Kanälen (Friend & Gilula, 1972; Nicholson, 2003).

Dort interagieren die stark konservierten extrazellulären Schleifen der Connexone zweier benachbarter Zellen miteinander (Cole *et al.*, 1996; Thomas *et al.*, 2005). Einige Studien zeigten die kritische Rolle der zweiten extrazellulären Schleife (E2) für das Kopf-an-Kopf-Docking, um einen funktionalen Gap Junction-Kanal zu formen (Zhou *et al.*, 1997; Foote *et al.*, 1998; Harris, 2001; Kronengold *et al.*, 2003). Der Gap Junction-Kanal wird durch spezifische Wasserstoffbrückenbindungen sowie ionische Wechselwirkungen zwischen den E2-Domänen der an der Kanalbildung beteiligten Connexone stabilisiert. Das konnte insbesondere anhand der Röntgenkristallstruktur von hCx26 belegt werden. In der E2-Domäne von hCx26 nimmt die Asparagin-Aminosäure N176 eine Schlüsselposition ein und bildet jeweils eine Wasserstoffbrückenbindung zu Lysin an Position 168 (K168), zu Threonin an der Position 177 (T177), sowie zur Asparaginsäure an der Position 179 (D179) des gegenüberliegenden Connexins aus (Maeda *et al.*, 2009; Maeda & Tsukihara, 2011). Neben den Wasserstoffbrückenbindungen zwischen den E2-Domänen wird der Gap Junction-Kanal auch durch Wasserstoffbrückenbindungen zwischen den E1-Domänen stabilisiert. Bei hCx26 sind jeweils eine Wasserstoffbrückenbindung zwischen N54-L56 und zwei Bindungen zwischen den beiden Q57-Aminosäuren der Kopf-an-Kopf-orientierten Connexine zu finden. Insgesamt wird ein hCx26-Kanal somit von 60 Wasserstoffbrückenbindungen stabilisiert.
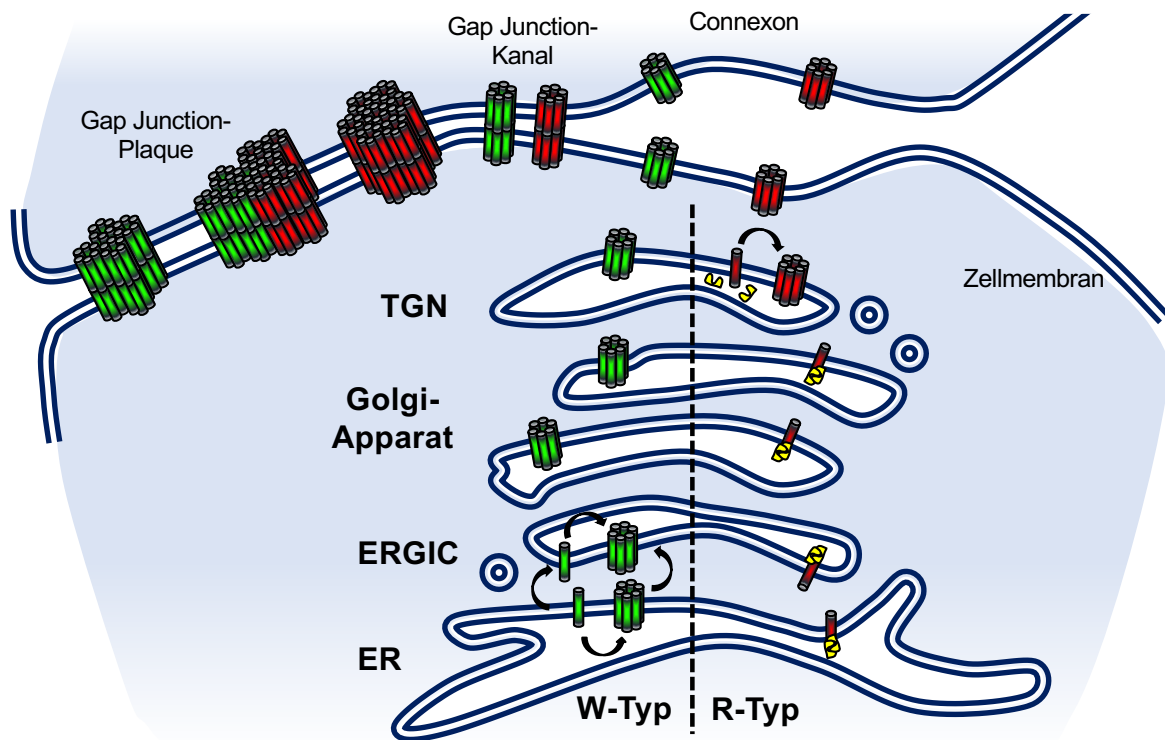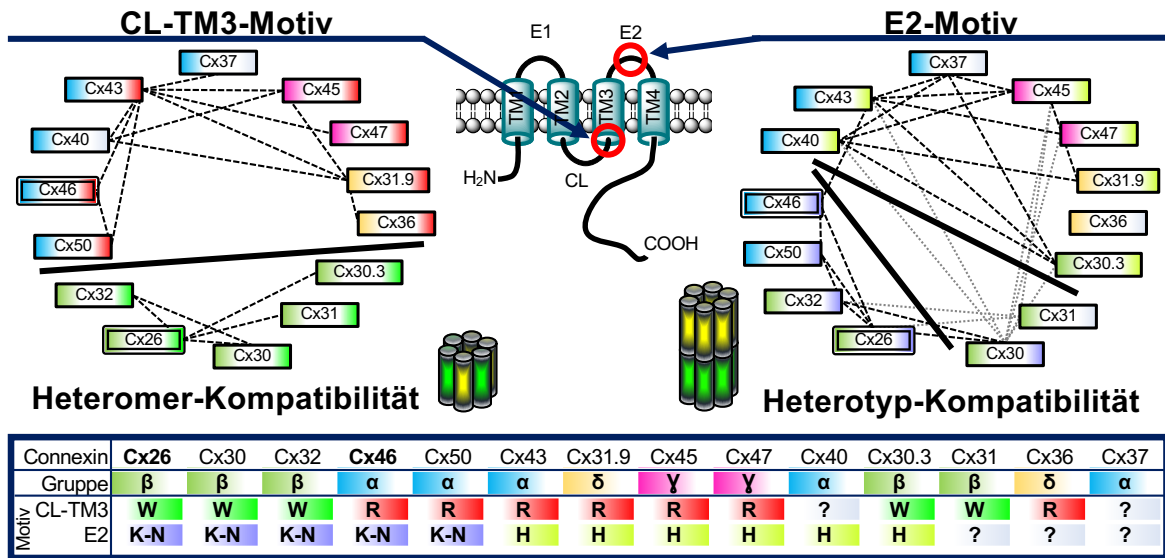
CL-TM3-Motiv

E2-Motiv

Heteromer-Kompatibilität

Heterotyp-Kompatibilität

Connexin	**Cx26**	Cx30	Cx32	**Cx46**	Cx50	Cx43	Cx31.9	Cx45	Cx47	Cx40	Cx30.3	Cx31	Cx36	Cx37
Gruppe	β	β	β	α	α	α	δ	γ	γ	α	β	β	δ	α
Motiv CL-TM3	W	W	W	R	R	R	R	R	R	?	W	W	R	?
Motiv E2	K-N	K-N	K-N	K-N	K-N	H	H	H	H	H	H	?	?	?

Gap Junction-Kanal

Connexon

Gap Junction-Plaque

Zellmembran

TGN

Golgi-Apparat

ERGIC

ER

W-Typ R-Typ

Abbildung 2: Heteromere und heterotypische Kompatibilität. Oben: Die Fähigkeit einiger gut erforschter Connexine, heteromere Connexone oder homomer heterotypische Gap Junction-Kanäle miteinander auszubilden, ist dargestellt. Für die Bildung von heteromeren Connexonen wurde gezeigt, dass das CL-TM3-Motiv entscheidend für die Kompatibilität ist. Die Connexine lassen sich in zwei Gruppen unterteilen: W- und R-Typ. Bezüglich des Dockings von zwei Connexonen zu einem Gap Junction Kanal ist das E2-Motiv ausschlaggebend für die Kompatibilität. Die schwarzen gestrichelten Linien verbinden kompatible Connexine. Die hellgrauen gestrichelten Linien weisen auf widersprüchliche Daten bezüglich der Heterotyp-Kompatibilität von Cx30 und Cx31 hin. In dem Diagramm sind die Connexine links bezüglich ihrer Sequenzhomologie in α-, β-, γ- und δ-Connexine farbig kodiert dargestellt. Die farbige Markierung am rechten Rand der Box weist auf die Gruppierung in W-/R-Typ bzw. K-N-/H-Typ hin. Die Klassifizierung und farbige Kodierung sind der darunter stehenden Tabelle zu entnehmen. Cx26 und Cx46, die in dieser Arbeit verwendet wurden, sind durch die doppelte Umrandung hervorgehoben. **Unten:** W- und R-Typ-Connexine

hexamerisieren in unterschiedlichen Kompartimenten. W-Typ-Connexine oligomerisieren bereits im ER bzw. ERGIC und werden als Connexon über den Golgi-Apparat zur Plasmamembran transportiert. R-Typ-Connexine hingegen oligomerisieren erst im TNG. Hierfür werden die Monomere durch Chaperone, wie beispielsweise ERp29 (gelb dargestellt), stabilisiert. Für Cx43 wurde die Interaktion mit ERp29 gezeigt und für Cx40 und Cx46 konnte die Oligomerisierung im TGN gezeigt werden (Aasen *et al.*, 2018). Die Abbildung wurde in Anlehnung an Koval *et al.*, 2014 erstellt und basiert auf den Ergebnissen vieler Wissenschaftler (Manthey *et al.*, 2001; Nagy *et al.*, 2003; Cottrell & Burt, 2005; Sun *et al.*, 2005; Gemel *et al.*, 2006; Koval, 2006; Kreuzberg *et al.*, 2006a; Kreuzberg *et al.*, 2006b; Locke *et al.*, 2007; Orthmann-Murphy *et al.*, 2007; Yum *et al.*, 2007; Rackauskas *et al.*, 2007a; Rackauskas *et al.*, 2007b; Ahn *et al.*, 2008; Gemel *et al.*, 2008; Orthmann-Murphy *et al.*, 2008; Palacios-Prado & Bukauskas, 2009; Lin *et al.*, 2010; Magnotti *et al.*, 2011a; Magnotti *et al.*, 2011b; Wasseff & Scherer, 2011; Gemel *et al.*, 2012; Beyer *et al.*, 2013; Tong *et al.*, 2013).

Die Schlüsselposition der Asparagin-Aminosäure in der E2-Domäne wurde in Experimenten mit hCx32 bestätigt. N175 im hCx32 nimmt eine homologe Position zu N176 bei hCx26 ein und bildet Wasserstoffbrückenbindungen zu K167, T176 und D178 des Kopf-an-Kopf-gedockten hCx32 aus (Nakagawa *et al.*, 2011; Gong *et al.*, 2013; Bai & Wang, 2014). Für die mit der Charcot-Marie-Tooth-Krankheit assoziierten Mutation N175D des hCx32 konnte gezeigt werden, dass Connexine mit dieser Mutation nicht in der Lage waren, Gap Junction-Kanäle zu bilden, während die Funktionalität der Halbkanäle dadurch nicht eingeschränkt war (Nakagawa *et al.*, 2011; Bai *et al.*, 2018). Selbst der Austausch einer einzelnen Aminosäure in diesem stark konservierten Bereich kann somit zu schwerwiegenden physiologischen Einschränkungen führen, da das Docking gestört ist und keine Gap Junction-Kanäle gebildet werden können.

Für das hCx46 sind bisher 55 Mutationen bekannt, die zu einem Katarakt führen. 26 Mutationen davon betreffen die extrazellulären Domänen, welche für das Docking der Connexone notwendig sind (Stand November 2018, http://cat-map.wustl.edu/). Obwohl die extrazellulären Domänen nur etwa 13 % des gesamten Connexins ausmachen, sind hier fast die Hälfte der Mutationen, die zu einem Katarakt führen, zu finden, was somit auch im hCx46 die Wichtigkeit dieser Region für die Proteinfunktion zeigt.

Die meisten Connexine können, basierend auf der E2-Sequenzhomologie, in zwei Gruppen, die **K-N-** und die **H**-Gruppe, eingeteilt werden (siehe Abbildung 2). Die zur K-N-Gruppe gehörenden Connexine tragen in der E2-Domäne die Sequenz ϕ(**K**/**R**)CxxxPCP**N**xVDC$\Omega\psi$S. Im Gegensatz dazu haben die zur H-Gruppe gehörigen Connexine die Sequenz ϕxCxxxPCP**H**xVDC$\Omega\psi$S an dieser Position. ϕ steht für eine hydrophobe, x für eine beliebige und Ω für eine aromatische Aminosäure. ψ beschreibt eine Aminosäure mit einer großen aliphatischen Seitenkette, wie Valin, Leucin oder Isoleucin (Bennett & Verselis, 1992; Niessen *et al.*, 2000; Neijssen *et al.*, 2005; Bedner *et al.*, 2006; Koval *et al.*, 2014). Für Connexone unterschiedlicher Gruppen ergibt sich dadurch an den benötigten Schlüsselstellen eine fehlende Kompatibilität zur Bildung von Wasserstoffbrückenbindungen, sodass

das Docking dieser Connexone miteinander nicht möglich ist (Milks *et al.*, 1988; Laird & Revel, 1990; Zhang & Nicholson, 1994; Sosinsky & Nicholson, 2005).

Nach dem Docking der Gap Junction-Kanäle können diese in cholesterinreichen Mikrodomänen der Zellmembran (Schubert *et al.*, 2002), sogenannten *lipid rafts*, integriert werden. Diese können wiederum beispielsweise durch Caveoline strukturiert werden, was die Regulation und Strukturierung der Gap Junctions beeinflusst (Schubert *et al.*, 2002; Langlois *et al.*, 2008; Hervé, 2012; Hervé *et al.*, 2012; Ampey *et al.*, 2016). Einen weiteren post-translationalen Regulationsmechanismus von Connexinen stellt die Phosphorylierung des C-Terminus dar, welche einige wichtige Aspekte im Connexin-Lebenszyklus beeinflussen kann, wie den Transport über den sekretorischen Stoffwechselweg, Gap Junction-Assemblierung, die Kanal-Leitfähigkeiten und die Degradation der Kanäle (Lampe & Lau, 2004; Solan & Lampe, 2005; Moreno & Lau, 2007; Thévenin *et al.*, 2013; Leybaert *et al.*, 2017).

Die Dauer des Connexin-Lebenszyklus unterscheidet sich zwischen den verschiedenen Isoformen. Die meisten Connexine besitzen eine Halbwertszeit von $1 - 5$ h (Fallon & Goodenough, 1981; Beardslee *et al.*, 1998; Berthoud *et al.*, 2004). Für das Schaf-Linsen-Connexin49 (oCx49), welches homolog zu hCx50 beim Menschen ist, wurden jedoch etwas längere Halbwertzeiten von bis zu 10 h nachgewiesen (Breidert *et al.*, 2005). Noch längere Halbwertszeiten von bis zu 90 h konnten *in vitro* für die Hühner-Linsen-Connexine cCx45,6 und cCx56, die homolog zu hCx46 und hCx50 sind, beobachtet werden (Jiang & Goodenough, 1998). Durch *Photobleaching*-Experimente konnte gezeigt werden, dass ältere Gap Junction-Kanäle aus der Plaquemitte heraus abgebaut werden, während sich neue Kanäle am Rand des Plaques durch das Docking der Halbkanäle formen (Lauf *et al.*, 2002).

Für die Degradation von Gap Junction-Kanälen und Connexinen werden je nach Oligomerisierungsgrad entweder der lysosomale oder der proteasomale Abbauweg verwendet (Falk *et al.*, 2014), was durch Inhibierungsstudien gezeigt werden konnte (Laing *et al.*, 1997; Musil *et al.*, 2000). Gap Junction-Kanäle können unter physiologischen Bedingungen nach dem Docking nicht wieder in zwei Halbkanäle gespalten werden (Goodenough & Gilula, 1974; Ghoshroy *et al.*, 1995). Daher erfolgt ihre Degradation durch die Internalisierung der vollständigen Kanäle von einer der beteiligten Zellen mittels spezieller großer Doppel-Membran-Vesikel, die Annular Junctions genannt werden, welche elektronenmikroskopisch nachgewiesen werden konnten (Larsen *et al.*, 1979; Larsen *et al.*, 1981; Mazet *et al.*, 1985). Bei der Annular Junction-Bildung sind Clathrine, Aktin-Filamente sowie Adapterproteine involviert, die die Endozytose katalysieren (Murray *et al.*, 1997; Piehl *et al.*, 2007; Baker *et al.*, 2008; Gumpert *et al.*, 2008; Nickel *et al.*, 2008; Kopanic *et al.*, 2015). Die Annular Junctions fusionieren mit dem Lysosom und werden dort durch die lysosomalen Proteine degradiert

(Gregory & Bennett, 1988; Naus *et al.*, 1993; Falk *et al.*, 2014). Neue Studien zeigen, dass endozytierte Annular Junctions auch komplett oder zum Teil recycelt werden können, indem die Connexone über ein Recycling-Endosom wieder zurück an die Zellmembran transportiert werden (Gilleron *et al.*, 2011; Gilleron *et al.*, 2012; Carette *et al.*, 2015). Das verdeutlicht die enorme Flexibilität der Zelle, die Gap Junction-Kanal- und Halbkanal-Expression und -Funktion zu steuern und somit die benötigten Kanaleigenschaften, die perfekt an die physiologischen Bedürfnisse der Zelle angepasst sind, zu erzeugen. Die Flexibilität der Zelle beschränkt sich nicht nur auf den Auf- und Abbau der Connexone und Gap Junction-Kanäle. Auch das Kombinieren verschiedener Connexin-Isoformen erlaubt es der Zelle, die Gap Junction-Kopplung auf ihre physiologischen Bedürfnisse abzustimmen. So ermöglicht das Bilden von heteromeren Connexonen und heterotypischen Gap-Junction-Kanälen der Zelle, beispielsweise eine spezifische Permeabilität für bestimmte Metaboliten zu kreieren (Zhong *et al.*, 2017).

1.3 Erforschung von heteromeren Connexonen und heterotypischen Kanälen

Heteromere Connexone und heterotypische Kanäle sind zum derzeitigen Zeitpunkt physiologisch und regulatorisch noch nicht vollständig verstanden, obwohl sie wahrscheinlich für die physiologischen Aufgaben und die Flexibilität der Zelle sehr wichtig sein könnten. Jedoch können nicht alle Connexin-Isoformen miteinander Gap Junction-Kanäle und -Halbkanäle bilden. Daher ist die Kompatibilität der Connexine und die resultierenden Kanaleigenschaften für die Forschung von großem Interesse.

Um die Kompatibilität verschiedener Connexin-Isoformen bezüglich der heterotypischen homomeren Gap Junction-Kanal-Bildung und somit die Kompatibilität während des Dockings der Connexone zu untersuchen, wurden die zu untersuchenden Connexine in Zellenlinien wie HeLa, SKHep1, N2A und RIN, die alle Connexin-defizient sind, rekombinant exprimiert (Bai *et al.*, 2018). Heterotypische homomere Kanäle können relativ einfach gezielt gebildet und analysiert werden, indem Zellen, die eine Connexin-Isoform exprimieren, neben markierten Zellen, die einen anderen Connexin-Typ exprimieren, kultiviert werden (siehe Abbildung 2). Die zwischen den verschieden markierten Zellen gebildeten Gap Junction-Kanäle können anschließend physiologisch charakterisiert werden. So konnten die Kompatibilität der Connexine bestimmt und bezüglich des Dockings in K-N- und H-Typ-Connexine gruppiert werden. Sehr viel komplexer ist es, die Kompatibilität und die spezifischen Kanaleigenschaften von heteromeren Connexonen aufzuklären, insbesondere wenn die stöchiometrische Connexin-Verteilung berücksichtigt werden soll.

Bei der Erforschung heteromerer Connexone und der Kompatibilität zur Bildung heteromerer Halbkanäle wurden bisher verschiedene Methoden verwendet, die sich in drei Bereiche gliedern lassen: biochemische, mikroskopische und elektrophysiologischen Methoden.

Mit biochemischen Methoden, wie etwa der Koimmunopräzipitation in Kombination mit Dichtegradienten-Zentrifugation oder Gelchromatographie zur Massen- bzw. Größenbestimmung, wurden beispielsweise Cx26 und Cx32 über eine Immunoaffinitäts-Chromatographie koimmunopräzipitiert (Diez *et al.*, 1999). Dafür wurden die in der Membran insertierten Connexine mit *cross-linkern*, wie DSP (3,3-Dithio-*bis*-(succinimidyl)propionat) und DTSSP (3,3-Dithio-*bis*-(sulfosuccinimidyl)propionat), verknüpft (Bevans *et al.*, 1998). Mit der Koimmunopräzipitation kann jedoch ausschließlich die räumliche Nähe zueinander nachgewiesen werden. Das heißt allerdings nicht, dass sich die Connexine in einem Connexon befunden haben müssen (Koval *et al.*, 2014). Auch benachbarte Connexone wären räumlich dicht genug beieinander, um ein Signal zu erzeugen.

Mikroskopische Methoden zur Detektion von heteromeren Connexonen, bei denen die Connexine unterschiedlich fluoreszenzmarkiert sind (immunzytochemisch oder direkt mittels *tag*), können ebenfalls nur die räumliche Nähe der untersuchten Connexine zueinander bestätigen. Da die Auflösungsgrenze bei klassischen lichtmikroskopischen Techniken, bedingt durch die Wellenlänge des sichtbaren Lichts, bei etwa 200 nm liegt (Abbe, 1873) und die Connexone (Cx26) lediglich einen Außendurchmesser von 9,2 nm haben (Maeda *et al.*, 2009; Maeda & Tsukihara, 2011), können selbst mit *super-resolution*-Mikroskopen, die 20 nm auflösen können (Betzig *et al.*, 2006; Bates *et al.*, 2007), keine sicheren Aussagen über die Connexin-Zusammensetzung eines Connexons getroffen werden.

Die FRET-Mikroskopie (*Fluorescence Resonance Energy Transfer* oder auch Förster-Resonanzenergietransfer), die auf dem Energie-Transfer zweier Fluorophore beruht, funktioniert nur bei Abständen bis zu 10 nm zwischen den Fluorophoren (Kenworthy & Edidin, 1998; Kenworthy, 2001). Mit der FRET-Technik wurde bei co-transfizierten Keratinozyten nachgewiesen, dass Cx26, Cx30 und Cx31 sowohl homomere als auch heteromere Connexone miteinander bilden (Di *et al.*, 2005).

Hochauflösende elektronenmikroskopische Aufnahmen zeigen, dass Cx36 und Cx45 in der Retina keine heteromeren Connexone formen, sondern dass sie nebeneinander Gap Junction-Plaques bilden. Für die Markierung wurden Antikörper, die an unterschiedlich große Gold-Partikel gekoppelt waren, verwendet (Rash *et al.*, 2012). Diese Technik erlaubt zwar die eindeutige Detektion von heteromeren Connexonen, ist jedoch *in vivo* nicht anwendbar und sehr aufwendig.

Die elektrophysiologischen Methoden, welche die Bestimmung der Gap Junction-Kanal-Leitfähigkeit und -Durchlässigkeit sowie Halbkanal-Leitfähigkeit ermöglichen (Harris, 2007), stellen den dritten Methodenbereich dar, der verwendet wird, um heteromere Connexone zu detektieren. So konnte eindeutig gezeigt werden, dass nur heteromere Connexone aus Cx26 und Cx32 permeabel für Inositol-Phosphate waren. Homomere Cx26- und Cx32- Kanäle hielten das Inositol-Phoshat zurück (Ayad *et al.*, 2006).

Da bereits homomere Kanäle unterschiedliche Leitfähigkeiten besitzen und diese durch die vielfältige Stöchiometrie heteromerer Kanäle vervielfacht werden, ist das elektrophysiologische Charakterisieren und Identifizieren von heteromeren Kanälen erschwert.

Der Nachweis von heteromeren Connexinen kann mehr oder weniger zuverlässig durch die beschriebenen Methoden erfolgen und erlaubt eine Klassifizierung in W- und R-Typ-Connexine. Jedoch kann bisher keine Aussage über die Connexin-Stöchiometrie getroffen werden, sodass die untersuchten Kanaleigenschaften meist auf Mischpopulationen beruhen. Für die Erforschung der Stöchiometrie von Gap Junction-Kanälen bedarf es einer neuen Methode, die während dieser Arbeit durch das Erstellen von Connexin-Konkatemeren entwickelt wurde.

1.4 Konkatemere

Der Begriff Konkatemer beschreibt ein Biopolymer, welches aus mehreren repetitiven DNA-Sequenzen oder Proteinuntereinheiten aufgebaut ist (Basu *et al.*, 2010). Für die Expression eines konkatemeren Proteins werden die proteinkodierenden Bereiche auf DNA-Ebene durch einen Linker miteinander verknüpft, der für ein flexibles meist 20-40 Aminosäuren langes Polypeptid kodiert (Kuryatov & Lindstrom, 2011). Um eine hohe Flexibilität des Linkers zu gewährleisten, werden bevorzugt *random coil*-bildende Aminosäuresequenzen als Linker verwendet (Steinbach & Akk, 2011).

Bei Eukaryonten sind die meisten kanalbildenden Membranproteine aus mehreren Untereinheiten aufgebaut, wodurch eine enorme Vielzahl an unterschiedlichen Kanälen durch die Kombination weniger Untereinheiten gebildet werden kann. Spannungsabhängige Natrium- und Calciumkanäle bestehen aus einem einzelnen Protein und bilden diesbezüglich eine Ausnahme (Yu & Catterall, 2003). Um Kanäle, die aus mehreren Untereinheiten aufgebaut sind, gezielt auf ihre Kanaleigenschaften zu untersuchen, ist es nötig, die Anzahl und die Position der Untereinheiten zu determinieren, um so Kanäle mit einer spezifischen Stöchiometrie zu generieren. Das wird durch die Bildung von Konkatemeren ermöglicht.

So wurde die Konkatemerisierung von Protein-Untereinheiten beispielsweise für die Erforschung von Acetylcholin- (ACh)- und γ-Aminobuttersäure- (GABA-) Rezeptoren oder ionotropen ATP-Rezeptor-Kanälen verwendet (Stoop *et al.*, 1999; Baumann *et al.*, 2001; Sigel *et al.*, 2009; Ahring *et al.*, 2018). Bei spannungssensitiven Kalium-Kanälen wurde diese Methode für kanalbildende Membranproteine erstmals eingesetzt, wodurch gezeigt werden konnte, dass heteromere Kanäle existieren, die andere Kanaleigenschaften aufweisen als die entsprechenden homomeren Kanäle (Isacoff *et al.*, 1990).

Die angeführten Beispiele zeigen, dass das Konkatemerisieren der Protein-Untereinheiten von kanalbildenden Membranproteinen ermöglicht, die Stöchiometrie und die damit verbundenen Kanaleigenschaften aufzuklären. Daher kann angenommen werden, dass die Konkatemerisierung von Connexinen geeignet ist, um die Kanaleigenschaften von heteromeren Connexonen und heteromeren heterotypischen Gap Junction-Kanälen mit einer definierten Stöchiometrie zu untersuchen.

1.5 Zielsetzung der Dissertation

In dieser Dissertation sollte das Oligomerisierungsverhalten von Connexinen, sowohl in Hinblick auf das Hexamerisieren von sechs Connexinen zu einem Connexon, als auch in Hinblick auf das Docking von zwei Connexonen zu einem Gap Junction-Kanal, analysiert werden.

Zur Analyse des Dockingverhaltens von Connexonen sollten die strukturellen und funktionellen Konsequenzen der Katarakt-assoziierten Mutation N188T des humanen Connexin46 (hCx46) auf das Docking mittels elektrophysiologischen und zellbiologischen Methoden in Verbindung mit Molekül-Dynamik-Simulationen untersucht werden. Dabei sollte ein besonderes Augenmerk auf die Interaktion zwischen den beiden Connexonen, verbunden mit der Analyse der gebildeten Wasserstoffbrückenbindungen, gelegt werden. Unterschiede zwischen dem hCx46-Wildtyp und der funktionseingeschränkten Mutante hCx46N188T sollten herausgearbeitet und erklärt werden. Ferner sollte untersucht werden, ob die Kanalfunktionalität der Mutante durch die Substitution einer strukturell ähnlichen Aminosäure wiederhergestellt werden kann. Um auf molekularer Ebene zu analysieren, wie die Patienten pathophysiologisch betroffen sind, die die Mutation zusammen mit Wildtyp hCx46 heterozygot exprimieren, sollte die Anzahl und die stöchiometrische Zusammensetzung mutierter Connexine innerhalb eines Connexons determiniert werden.

Hierfür sollten Connexine konkatemerisiert werden, was die stöchiometrische Connexin-Zusammensetzung in einem Connexon determinieren würde. Auf diese Weise sollte ein System für die Erforschung der spezifischen Metabolitenselektivität und Flussrichtung von heterotypischen Gap Junction-Kanälen und heteromeren Halbkanälen generiert werden. Das Bilden von Konkatemeren ist eine neue Herangehensweise für Connexine. 2013 wurde auf der Internationalen Gap Junction Konferenz (IGJC 2013) die Schwierigkeit der Konkatemerisierung von Connexinen im Vergleich zu Pannexinen diskutiert (http://www.kovallab.org/Igjc2013/files/roundtable_summaries.pdf). Bei Connexinen ragt der N-Terminus in die Pore, was bei Pannexinen nicht der Fall ist, weshalb die Bildung von Konkatemeren problematisch sein könnte. Für eine Machbarkeitsstudie sollten aus hCx46 und hCx26 dimere Konkatemere erstellt werden, die mit mikroskopischen Methoden, Funktionalitätsanalysen und elektrophysiologischen Techniken charakterisiert werden sollten.

Die Konkatemerisierung von Connexinen sollte außerdem eingesetzt werden, um das dominante Verhalten der hCx46N188T-Mutation auf das Docking der Connexone zu demonstrieren. Hierfür sollten Konkatemere aus dem Wildtyp und der Mutante analysiert werden, wodurch die heterozygote Expression imitiert wurde, um so pathophysiologische Auswirkungen auf molekularer Ebene zu erforschen. Mit Molekül-Dynamik-Simulationen sollten die physiologischen Experimente strukturbiologisch unterstützen werden.

1.6 Veröffentlichungen

Im Rahmen dieser Dissertation wurde das Oligomerisierungsverhalten von humanen Connexinen in Bezug auf die Connexin-Connexin-Interaktion von heteromeren Halbkanälen sowie heterotypischen Kanälen untersucht. Es sind währenddessen vier Manuskripte entstanden (siehe Anhang A-D), welche die funktionellen Konsequenzen der Katarakt-assoziierten Mutation N188T von humanem Connenxin46 (hCx46), Molekül-Dynamik-Simulationen für die Interaktion von hCx46-Gap Junctions, die Konkatemerisierung verschiedener Connexin-Isoformen zur Charakterisierung von heteromeren Gap Junction-Kanälen und -Halbkanälen sowie die Analyse der dominanten Eigenschaft der N188T-Mutation in hCx46 darstellen.

Anhang A: **The cataract related mutation N188T in human connexin46 (hCx46) revealed a critical role for residue N188 in the docking process of gap junction channels.** Veröffentlicht in *Biochimica et Biophysica Acta – Biomembranes* (Schadzek *et al.*, 2015).

Anhang B: **Data of the molecular dynamics simulations of mutations in the human connexin46 docking interface.** Veröffentlicht in *Data in Brief-Journal* (Schadzek *et al.*, 2016).

Anhang C: **Concatenation of Human Connexin26 (hCx26) and Human Connexin46 (hCx46) for the Analysis of Heteromeric Gap Junction Hemichannels and Heterotypic Gap Junction Channels.** Veröffentlicht im *International Journal of Molecular Sciences* (Schadzek *et al.*, 2018).

Anhang D: **Analysis of the dominant mutation N188T of human Connexin46 (hCx46) using concatenation and molecular dynamics simulation.** Veröffentlicht in *FEBS open bio*. (Schadzek *et al.*, 2019)

2. Ergebnisse

In Rahmen der vorliegenden Dissertation wurde das Oligomerisierungsverhalten von humanen Connexinen in Bezug auf die Connexon-Connexon-Interaktion von heterotypischen Kanälen sowie die Connexin-Connexin-Interaktion von heteromeren Halbkanälen und Gap Junction-Kanälen untersucht. Die Ergebnisse der Publikationen, die während dieser Arbeit entstanden sind (siehe Kapitel 1.6, Anhang A-D), werden nachfolgend zusammengefasst.

2.1 Die kataraktassoziierte Mutation N188T des humanen Connexin46 (hCx46) zeigte die Schlüsselrolle der Position N188 für die Connexon-Connexon-Interaktion von Gap Junction-Kanälen

Die Mutation N188T des humanen Connexin46 (hCx46) geht mit einem erblich bedingten grauen Star einher (Li *et al.*, 2004). Diese Mutation befindet sich in der zweiten extrazellulären Schleife, eine Region die für das Zusammenlagern (*Docking*) der Gap Junction-Halbkanäle zweier benachbarter Zellen wichtig ist. Um die Folgen der Mutation für die Protein-Protein-Interaktion zu verstehen, wurden sowohl die Mutante hCx46N188T als auch der Wildtyp (hCx46wt) in Eizellen des südafrikanischen Krallenfrosches (*Xenopus Leavis*) und in HeLa- Zellen exprimiert. Bei der Untersuchung der Halbkanäle in den Oozyten konnte zwischen der Mutante und dem Wildtyp kein Unterschied in Bezug auf deren elektrophysiologischen Eigenschaften festgestellt werden. Auch die analysierten Halbkanäle, die mit dem angehängten eGFP-Fluoreszenzprotein in HeLa-Zellen exprimiert wurden, zeigten beide die typische Ca^{2+}- und La^{3+}-Sensitivität. Diese Ergebnisse lassen vermuten, dass die Mutation weder die Proteinexpression noch den Transport zur Membran stört. Zellen, die hCx46wt-eGFP exprimierten, bildeten Gap Junction-Plaques, jedoch konnten in hCx46N188T-eGFP-exprimierenden Zellen kaum noch Plaques beobachtet werden (siehe Abbildung 3A). Auch wurde eine Reduzierung der Gap Junction-Plaqueanzahl festgestellt, wenn HeLa-Zellen gleiche Konzentration an hCx46wt-mCherry und hCx46N188T-eGFP co-exprimierten (siehe Abbildung 3B). Oder wenn eine Zelle hCx46wt-mCherry und ihre benachbarte Zelle hCx46N188T-eGFP exprimierte (siehe Abbildung 3C). In Farbstofftransferexperimenten waren Zellen, die hCx46N188T exprimierten, signifikant weniger gekoppelt als Zellen, die mit dem hCx46wt-Plasmid transfiziert wurden. Daher lässt sich vermuten, dass die N188T-Mutation von hCx46 die Connexon-Connexon-Interaktion negativ beeinflusst.
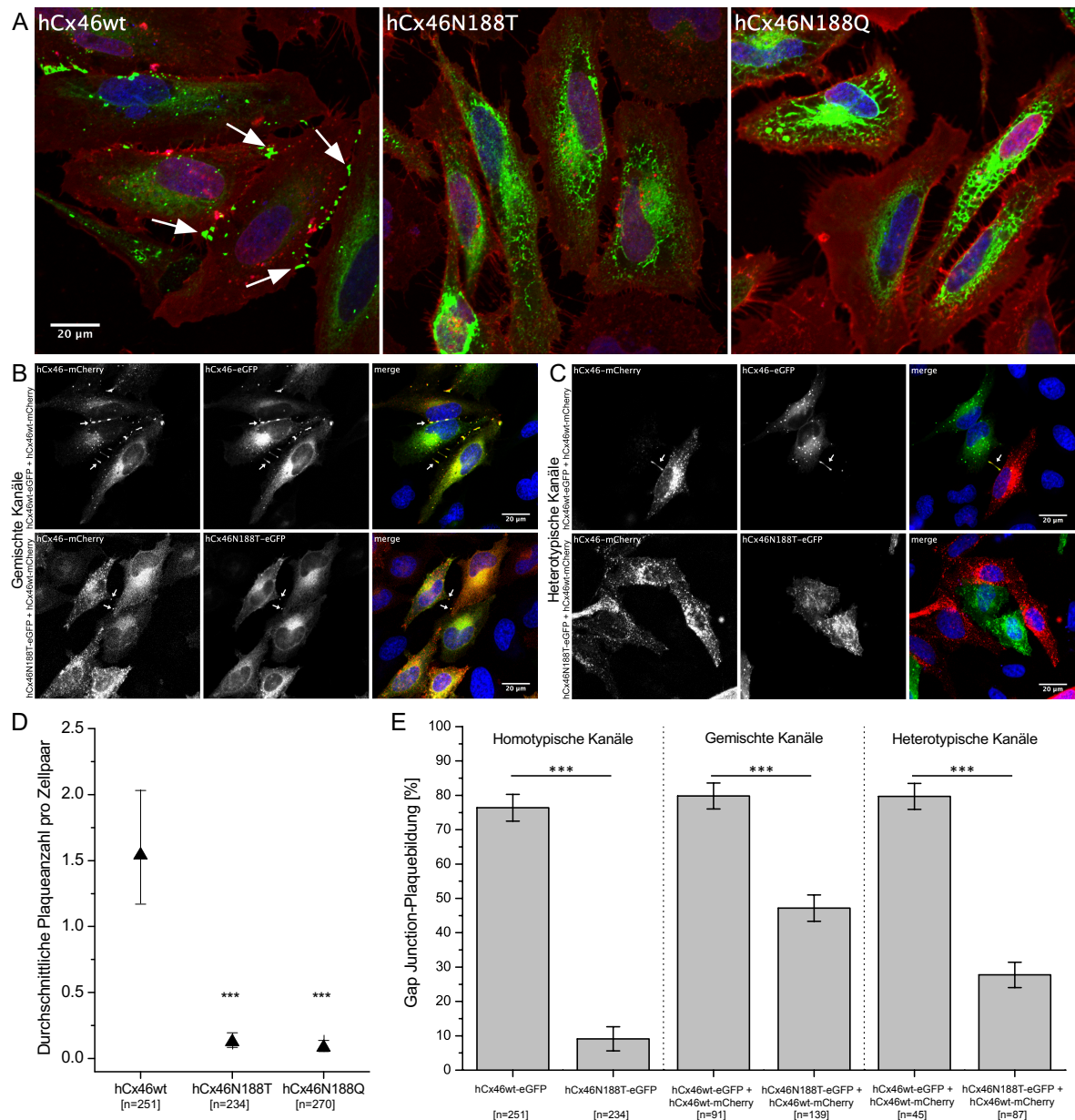
Abbildung 3: Die N188T-Mutation beeinträchtigt die Bildung von Gap Junction-Plaques. (**A**) Konfokale (CLSM) Aufnahmen von HeLa-Zellen, die 24 h nach der Transfektion fixiert und mit WGA-555 (rot, Membran) und Hoechst 33342 (blau, Zellkern) gefärbt wurden. Die Pfeile weisen auf Gap Junction-Plaques hin. Bei der Rettungsmutante N188Q waren wie bei hCx46N188T ebenfalls keine Plaques sichtbar. (**B**) Bei einer Co-Expression reduzierte die Mutation N188T die Plaquebildung im Vergleich zu hCx46wt. Hierfür wurde das Wildtyp-Connexin mit mCherry (rot) und das hCx46N188T mit eGFP (grün) markiert. Analysiert wurden Plaques bei denen sich das Signal von mCherry und eGFP überlagerte (merge; gelbe Plaques). (**C**) Die Ausbildung von heterotypischen Gap Junction-Plaques wurde durch diese Mutation deutlich gestört. (**D**) Für die Quantifizierung der durchschnittlichen Plaqueanzahl pro Zellpaar [n] wurde ein verallgemeinertes lineares Mischmodell mit Annahme einer Poisson-Verteilung zugrunde gelegt. Eine im Vergleich zu hCx46wt signifikant reduzierte Anzahl an Plaques konnte für hCx46N188T und hCx46N188Q beobachtet werden. (**E**) Die Quantifizierung der prozentualen Plaquebildungsrate zeigt, dass die N188T-Mutation in homotypischen, gemischten und heterotypischen Kanälen die Bildung von Gap Junction-Plaques behindert. Für den statistischen Vergleich wurde ein t-Test (*** $p \leq 0{,}001$) verwendet (modifiziert nach Schadzek *et al.*, 2015).

Diese Hypothese wird durch die Ergebnisse der Molekül-Dynamik-Simulationen von hCx46, basierend auf der Röntgenkristallstrukturanalyse von hCx26, unterstützt (siehe Abbildung 4). Dieses Modell zeigt, dass die Aminosäure N188 in hCx46 für die Connexon-Connexon-Interaktion immens wichtig ist. N188 bildet Wasserstoffbrücken zu den Aminosäuren R180, T189 und D191 des gegenüberliegenden hCx46 aus. Die Ergebnisse zeigen, dass die Mutation N188T das Andocken der gegenüberliegenden Connexone und somit auch die Bildung von Gap Junction-Kanälen verhindert.

Des Weiteren zeigten Versuche, bei denen Glutamin an der Position 188 (hCx46N188Q) anstelle von Asparagin eingebaut wurde, dass das Andocken der Connexone bereits durch diese kleine Modifikation gestört war. Glutamin (Q) ist eine Aminosäure, deren Seitenkette bei gleicher funktioneller Gruppe im Vergleich zu Asparagin (N) eine CH_2-Gruppe länger ist. Dies unterstreicht die Wichtigkeit der Aminosäure N188 für das Andocken der Connexone und die Bildung von Gap Junction-Kanälen.
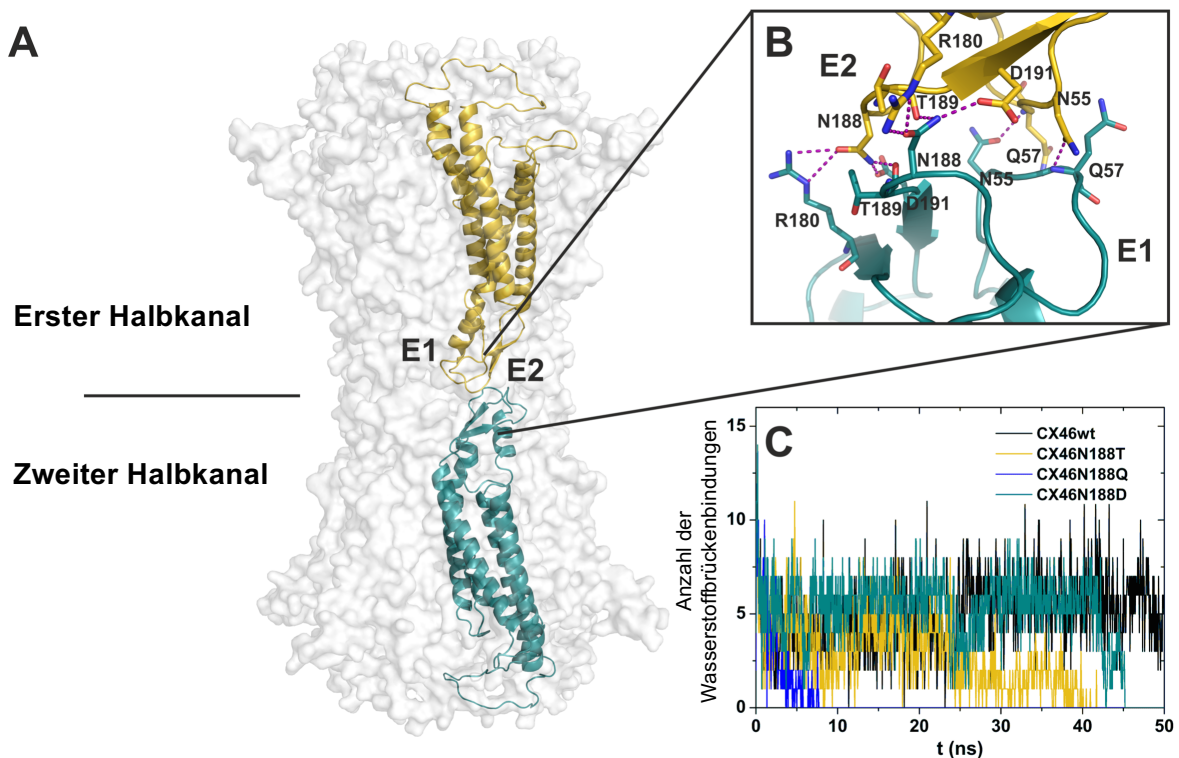

Abbildung 4: Molekül-Dynamik-Simulation von Kopf-an-Kopf-gedockten Connexinen. (**A**) Basierend auf der Röntgenkristallstruktur von hCx26 wurde ein homologes Modell erstellt. Die beiden Connexine (gold und cyan), die als Modell für die Connexon-Connexon-Interaktion über Wasserstoffbrückenbindungen dienen, sind vor dem transparenten Hintergrund eines Gap Junction-Kanals gezeigt. (**B**) Die gestrichelten lilafarbenen Linien stellen Wasserstoffbrückenbindungen im Interaktionsraum dar. (**C**) Die Anzahl der Wasserstoffbrücken-bindungen während der 50 ns langen Molekül-Dynamik-Simulation im Modellsystem für das Bindungsnetzwerk geht bei den drei getesteten Mutanten hCx46N188T, hCx46N188Q und hCx46N188D über die Simulationszeit auf null zurück. Nur hCx46wt bleibt über die gesamte Dauer stabil (modifiziert nach Schadzek *et al.*, 2015).

2.2 Daten der Molekül-Dynamik-Simulationen zeigen den Einfluss der Connexin-Connexin-Interaktion von Mutationen des humanen Connexin46 auf das Wasserstoffbrückenbindungsnetzwerk

Die Röntgenkristallstruktur des humanen Connexin26 (hCx26) diente als Vorlage für ein homologes Modell für hCx46. Zwei über Wasserstoffbrückenbindungen interagierende Connexin-Moleküle wurden als Ausgangssystem für die Molekül-Dynamik-Simulation verwendet. Hierfür wurde das Open-Source-Programm NAMD (*nanoscale molecular dynamics*) benutzt, welches erlaubt, Vorhersagen über das dynamische Molekülverhalten von hCx46wt und der kataraktassoziierten Mutante hCx46N188T, sowie zwei artifiziellen Mutanten, hCx46N188Q und hCx46N188D, zu treffen. Durch die artifizielle Mutante N188Q wurde mit Glutamin im Vergleich zu Asparagin eine um eine CH_2-Gruppe größere Aminosäure an der Position 188 eingefügt, die die gleiche funktionelle Gruppe wie der Wildtyp an dieser Position trägt. Bei der N188D-Mutation wurde das Asparagin durch die gleichgroße aber anders funktionalisierte Aminosäure Asparaginsäure ersetzt. Während der 50 ns umfassenden Simulation dissoziierte der Komplex der Kopf-an-Kopf-gedockten Connexine bei allen untersuchten Mutanten, nur hCx46wt blieb stabil. N188D brachte eine negative Ladung ein, was zu einer elektrostatischen Abstoßung mit der Aminosäure D191 führte. N188Q war zu groß, um mit der gegenüberliegenden E2-Domäne Wasserstoffbrückenbindungen auszubilden. Bei N188T führten die fehlenden Wasserstoffbrückenbindungen zum Dissoziieren der angedockten Moleküle (siehe Abbildung 5). Nur für den Wildtyp zeigen die Daten, dass ein hCx46-Molekül 5-7 Wasserstoffbrückenbindungen zu dem gegenüberliegenden Connexin ausbildete. Diese Wasserstoffbrückenbindungen waren für das Andocken und die Stabilisierung von Connexonen essentiell. Auch die Simulation eines ganzen Gap Junction-Kanals konnte zeigen, dass nur der hCx46wt Kanal stabil blieb, während der getestete hCx46N188Q-Kanal nach nur 4 ns Simulationszeit nicht mehr durch eine ausreichende Anzahl an Wasserstoffbrückenbindungen stabilisiert werden konnte.
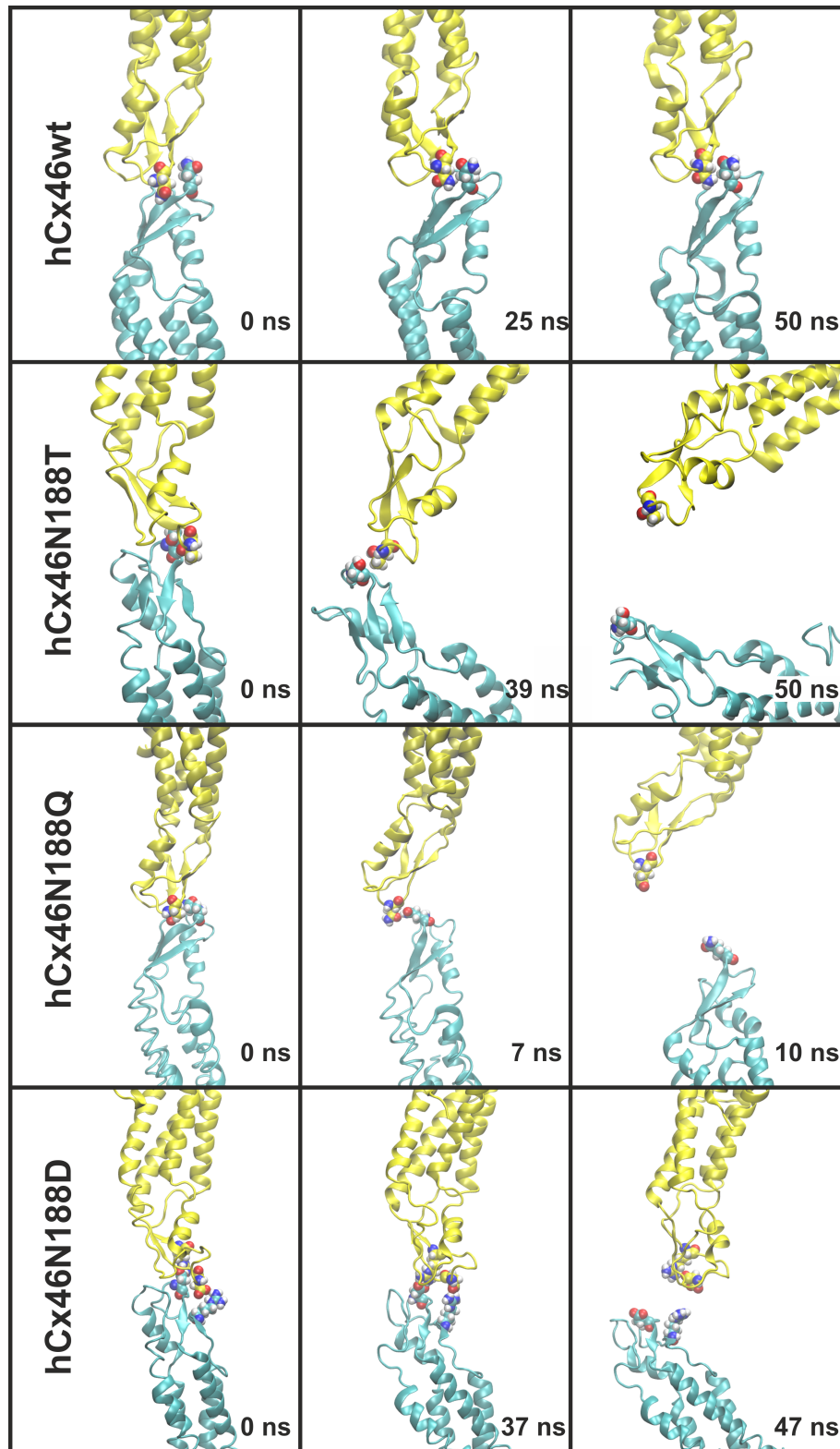
Abbildung 5: Ausschnitte aus der Molekül-Dynamik-Simulation von hCx46wt und den drei getesteten Mutanten hCx46N188T, hCx46N188Q und hCx46N188D. Nur hCx46wt blieb, im Gegensatz zu den Mutanten, über die gesamte Simulationsdauer stabil (aus Schadzek *et al.*, 2016).

2.3 Konkatemerisierung von humanem Connexin26 (hCx26) und humanem Connexin46 (hCx46) zur Analyse von heteromeren Gap Junction-Halbkanälen und heterotypischen Gap Junction-Kanälen

Connexine und die von ihnen gebildeten Gap Junction-Kanäle sind essentiell für die Zell-Zellkommunikation. Beim Menschen sind bisher 21 Isoformen bekannt (Söhl & Willecke, 2004), von denen in vielen Geweben mehrere Isoformen gleichzeitig exprimiert werden. Sind verschiedene Connexin-Isoformen an der Bildung eines Halbkanals beteiligt, wird dieser als heteromerer Kanal bezeichnet. Um die Kanalstöchiometrie zu determinieren, wurden Connexin-Konkatemere erstellt. Dies ist eine neue Herangehensweise, um heteromere Kanäle erforschbar zu machen. Zur Machbarkeitsprüfung wurden aus humanem Connexin26 (hCx26) und humanem Connexin46 (hCx46) Konkatemere erstellt.

Monomere (hCx46 und hCx26), homodimere (hCx46-hCx46 und hCx26-hCx26) sowie heterodimere (hCx46-hCx26 und hCx26-hCx46) Connexine wurden am C-Terminus mit GFP markiert und in HeLa-Zellen exprimiert. Konfokale Laser-Scanning-Mikrokopie zeigte, dass alle Konstrukte in der Lage waren, Gap Junction-Plaques auszubilden. Jedoch war die Plaquefläche bei den konkatemeren im Vergleich zu den monomeren Connexinen signifikant reduziert (siehe Abbildung 6). In Farbstofftransferexperimenten konnte gezeigt werden, dass die Konkatemere ebenso gut über Gap Junctions gekoppelt waren wie die untersuchten Monomere. Die Messung von Einzelkanälen mittels *inside-out patch-clamp*-Technik von in *Xenopus*-Eizellen exprimierten Connexonen ergab eine Leitfähigkeit von etwa 46 pS und 39 pS für die monomeren hCx46- und hCx26-Halbkanäle. Die homodimeren Connexone hatten eine geringere Leitfähigkeit von 25 pS für hCx46-hCx46, bzw. 33 pS für hCx26-hCx26. Dieses resultiert wahrscheinlich aus der Konkatemerisierung. Bei der Untersuchung der heteromeren Halbkanäle waren die beobachteten Leitfähigkeiten abhängig von der Reihenfolge der Connexine. Für hCx46-hCx26 wurden Leitfähigkeiten von 16 pS und 26 pS im Mittel gemessen, während das hCx26-hCx46-Konkatemer 20 pS und 31 pS als Leitfähigkeit aufwies (siehe Abbildung 7). Auch bei der Analyse der Gap Junction-Kanäle mittels *double-whole-cell patch-clamp*-Technik konnten für die monomeren und homodimeren hCx46-Kanäle ähnliche Leitfähigkeiten dokumentiert werden. Für die hCx26-Kanäle wichen die gemessenen Leitfähigkeiten voneinander ab. Selbiges wurde auch für die beiden heteromeren Kanäle festgestellt. Eine mögliche Erklärung hierfür könnte sein, dass die Konkatemerisierung des sehr kurzen C-Terminus von hCx26 zu strukturrelevanten Veränderungen des Kanals führte.
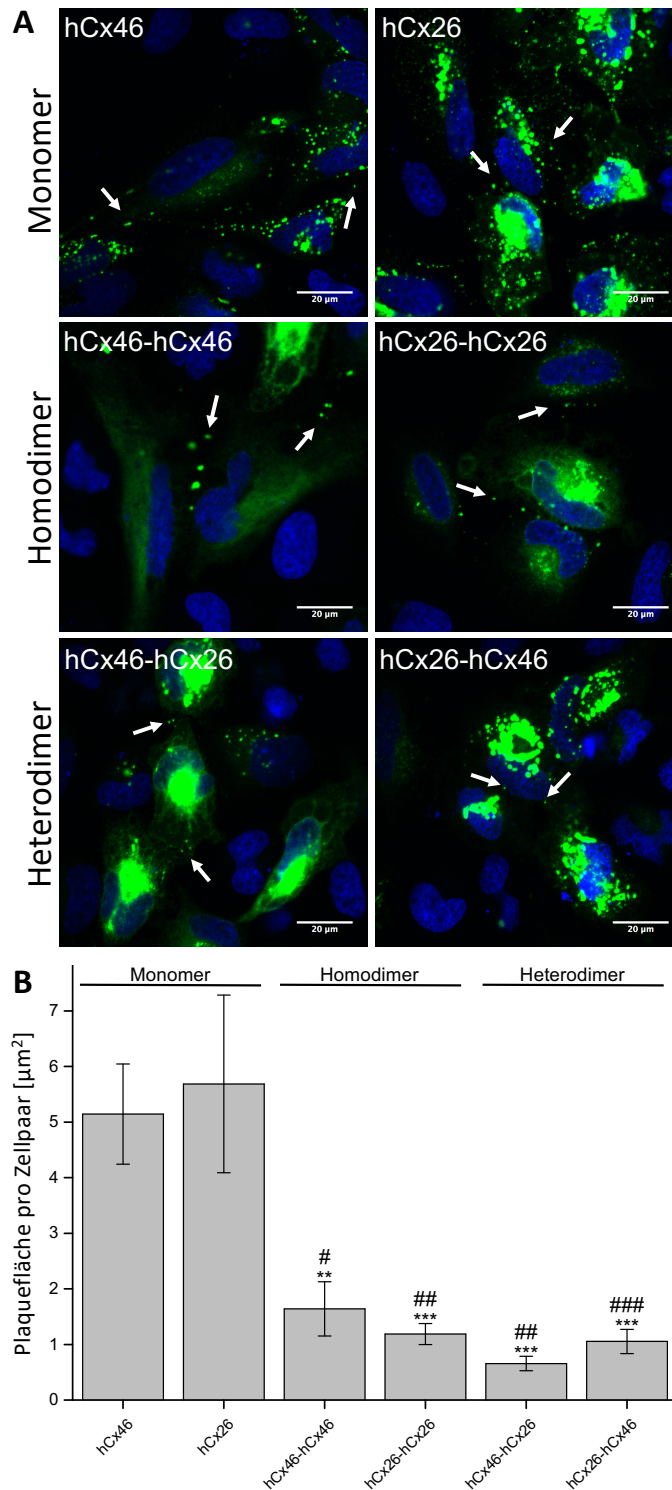
Abbildung 6: Connexin-Konkatemere bilden Gap Junction-Plaques. (**A**) Die Pfeile weisen auf Gap Junction-Plaques in den repräsentativen konfokalen Aufnahmen hin. (**B**) Die Quantifizierung ergab, dass die Konkatemerisierung zu einer reduzierten Plaquefläche pro Zellpaar führte. Die Plaquefläche wurde mit der Partikel-Analyse der ImageJ-Software ausgewertet und auf die Anzahl der transfizierten Zellpaare normalisiert. Für die statistische Auswertung wurde ein Ein-Weg-ANOVA-Test mit anschließendem Tukey-Test im Vergleich zu hCx46 (** $p \leq 0,01$, *** $p \leq 0,001$) und hCx26 (### $p \leq 0,001$) durchgeführt (modifiziert nach Schadzek *et al.*, 2018)
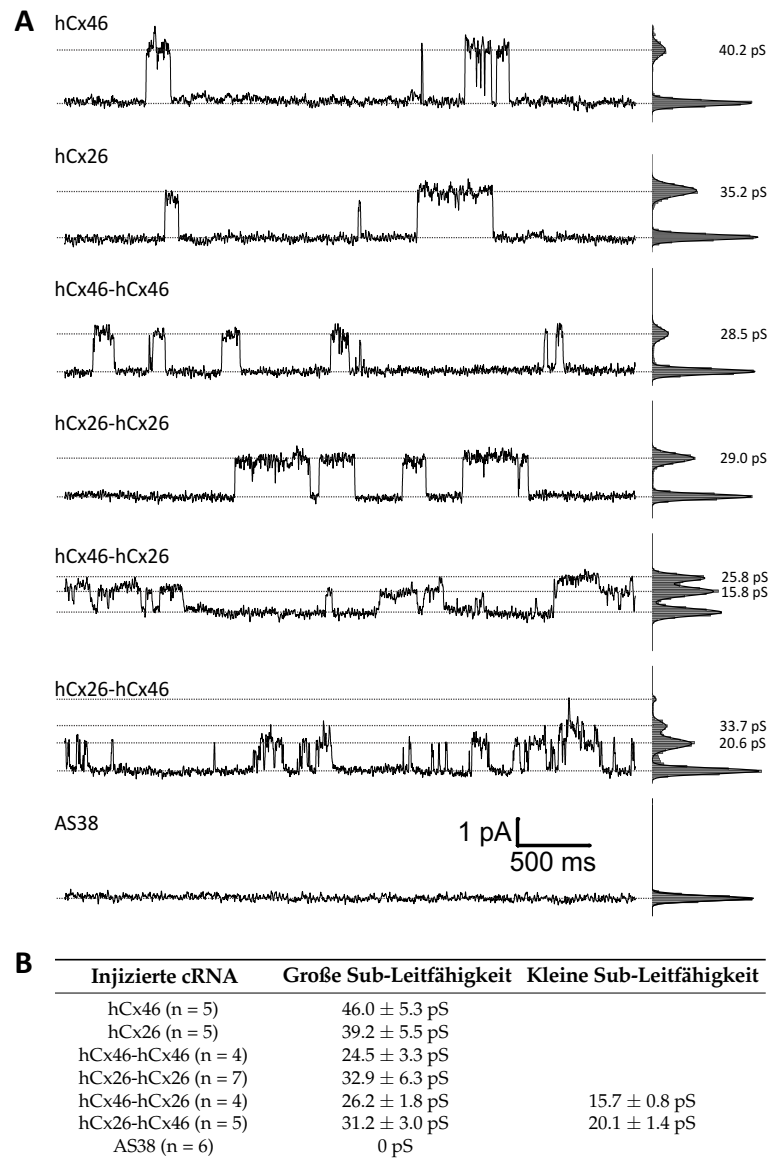
Abbildung 7: Analyse der Halbkanäle von konkatemerisierten Connexinen. *Xenopus*-Eizellen wurden mit der entsprechenden cRNA 24 h vor Versuchsbeginn injiziert. *Inside-out patch-clamp*-Messungen wurden nach dem Entfernen der Vitellinmembran in einem Cs^+-haltigen und Cl^--freien Medium durchgeführt, um die Oozyten-eigenen Kanäle zu blockieren. (**A**) Die Beispielmessungen zeigen die Einzelkanalströme während eines + 50 mV-Pulses in Ca^{2+}-freiem Badmedium. (**B**) Die gemessenen Halbkanal-Leitfähigkeiten (± Standartfehler, SEM) zeigen, dass es Abweichungen zwischen den monomeren und homodimeren Connexonen gibt. Die Anzahl der analysierten Oozyten ist mit n angegeben (modifiziert nach Schadzek *et al.*, 2018).

Bei Farbstoffaufnahmeexperimenten fiel auf, dass das hCx26-hCx26-Homodimer im Vergleich zu den anderen getesteten Konkatemeren und Monomeren eine signifikant höhere Ethidiumbromid-Aufnahme aufwies. Diese Ergebnisse lassen folgenden Schluss zu: Wegen des Linkers zwischen den Connexinen innerhalb eines Konkatemers sind die Eigenschaften der gebildeten Halbkanäle und Gap Junction-Kanäle möglicherweise nicht mit denen von natürlich gebildeten hetero-oligomerisierten Kanälen vergleichbar. Sollte das Entfernen des Linkers jedoch erfolgreich sein, so könnte diese

Methode für die Analyse der elektrischen und metabolischen Selektivität von Halbkanälen und Gap Junction-Kanälen verwendet werden und deren physiologische Bedeutung für das Gewebe erforscht werden.

2.4 Untersuchung der dominanten Eigenschaften der Mutation N188T in humanem Connexin46 (hCx46) mittels Connexin-Konkatemerisierung und Molekül-Dynamik-Simulationen

Aus der kataraktassoziierten Mutation N188T im humanen Connexin46 (hCx46N188T) wurden zusammen mit dem Wildtyp (hCx46wt) Konkatemere erzeugt, um den Effekt der Mutation auf Linsenfaserzellen, die sowohl hCx46N188T als auch hCx46wt exprimieren, zu untersuchen. Hierfür wurden die beiden Monomere, die homodimeren hCx46wt-hCx46wt- und hCx46N188T-hCx46N188T- sowie die heterodimeren hCx46wt-hCx46N188T- und hCx46N188T-hCx46wt-Konkatemere in HeLa-Zellen exprimiert. Durch Farbstoffaufnahmeexperimente konnte gezeigt werden, dass die Konkatemere, ebenso wie die Monomere, den Farbstoff Ca^{2+}- und La^{3+}-abhängig aufnehmen. Auch konnte dadurch, wie schon zuvor berichtet (Schadzek *et al.*, 2015), gezeigt werden, dass die Mutation keinen Einfluss auf die Expression, die Insertion in die Membran und die Funktion von Halbkanälen hat. Jedoch bildeten hCx46N188T und hCx46N188T-hCx46N188T im Gegensatz zu hCx46wt und hCx46wt-hCx46wt fast keine Gap Junction-Plaques zwischen den Zellen aus. Die beiden heteromeren Konkatemere bildeten signifikant weniger Plaques aus als die Wildtyp-Kanäle, wobei die Anzahl der ausgebildeten Plaques allerdings deutlich größer war als bei Zellen, die ausschließlich die Mutante exprimierten (siehe Abbildung 8). Sobald Gap Junction-Plaques sichtbar waren, waren die gebildeten Kanäle auch permeabel für Metaboliten, was mittels *Lucifer Yellow*-Farbstofftransferexperimenten gezeigt werden konnte.

Für die Molekül-Dynamik-Simulationen wurde die Röntgenkristallstruktur von Cx26 als Vorlage verwendet, um die Anzahl der zwischen den hCx46-Connexonen befindlichen Wasserstoffbrückenbindungen zu bestimmen. Die Position N188 spielt die Schlüsselrolle für die E2-E2-Interaktion, da pro gedocktem Connexin acht Wasserstoffbrückenbindungen zu R180, N189 und D191 ausgebildet werden können. Die E1-E1-Interaktion von hCx46 steuert pro gedocktem Connexin noch vier weitere Bindungen bei (2 × N55-Q57 & Q58=Q58). Durch die Mutation N188T fallen pro gedocktem Connexin sechs der E2-E2-Wasserstoffbrückenbindungen weg (nur zwischen T188 und T189 können Wasserstoffbrückenbindungen ausgebildet werden), sodass pro Connexin-Connexin-Interaktion nur noch sechs der ursprünglich zwölf Bindungen die Kopf-an-Kopf-gedockten Gap Junction-Kanäle stabilisieren könnten, was nicht genügt, um Gap Junction-Kanäle und somit Plaques zu bilden (siehe Abbildung 8 und Abbildung 9).
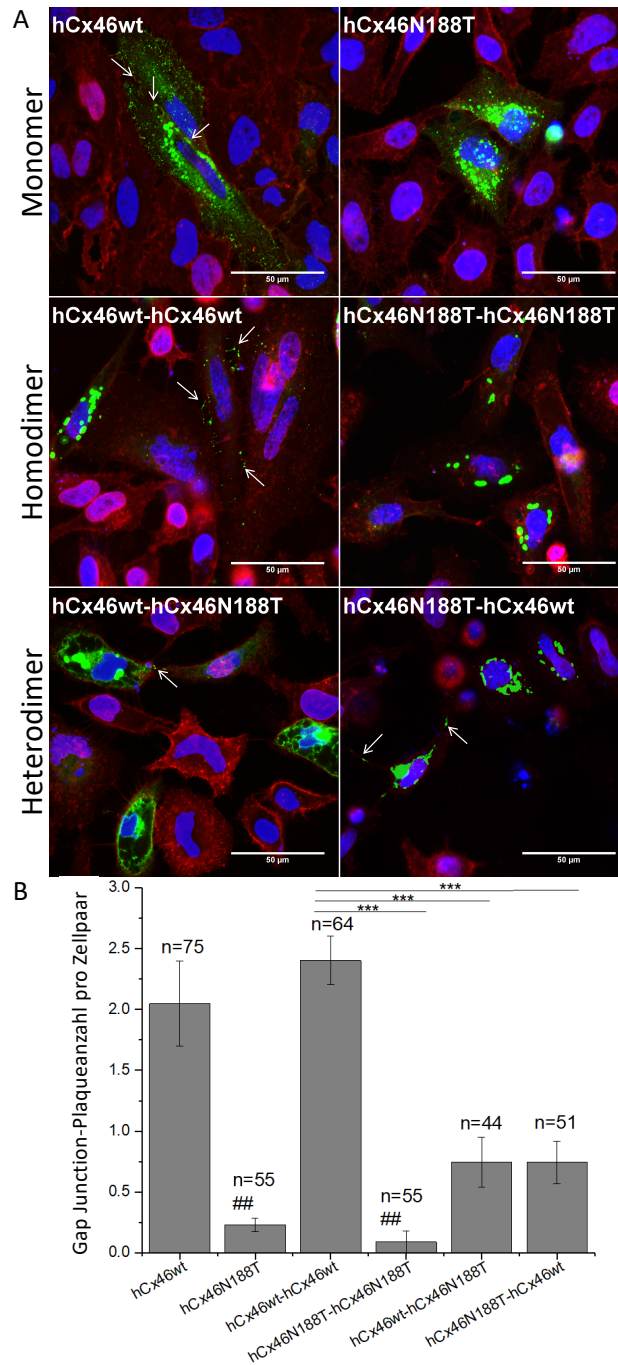
Abbildung 8: Die N188T-Mutation reduziert die Anzahl von Gap Junction-Plaques. (A) Die repräsentativen konfokalen Aufnahmen zeigen HeLa-Zellen, die eGFP-markierte hCx46wt- und hCx46N188T-Monomere sowie die homodimeren (hCx46wt-hCx46wt, hCx46N188T-hCx46N188T) und heterodimeren (hCx46wt-hCx46N188T, hCx46N188T-hCx46wt) Tandems exprimierten. Die Zellen wurden nach 24 h fixiert und mit WGA555 (rot, Membran) und Hoechst 33342 (blau, Zellkern) gefärbt. Die Pfeile weisen auf Gap Junction-Plaques hin. (B) Die Quantifizierung der Plaqueanzahl pro Zellpaar mittels ImageJ zeigte deutlich den Einfluss der N188T-Mutation auf die Anzahl der gebildeten Gap Junction-Plaques. Der statistische Vergleich erfolgte mittels t-Test im Vergleich zu hCx46wt (## $p \leq 0,01$) und hCx46wt-hCx46wt (*** $p \leq 0,001$). Die Anzahl der analysierten Zellpaare ist mit n angegeben (modifiziert nach Schadzek *et al.*, 2019).

In der 100 ns langen Molekül-Dynamik-Simulation konnten die Wildtypkanäle durchschnittlich 53 und die hCx46N188T-Kanäle 12 Wasserstoffbrückenbindungen ausbilden. Um den möglichen Einfluss des Bindungspartners in heteromeren Kanälen zu überprüfen, wurde sowohl die Interaktion zwischen Wildtyp-Wildtyp benachbart mit Mutante-Mutante als auch die Interaktion Wildtyp-Mutante benachbart mit Mutante-Wildtyp simuliert. Diese beiden Szenarien unterschieden sich nicht signifikant und erreichten durchschnittlich 31 bzw. 35 Wasserstoffbrückenbindungen für einen Gap Junction-Kanal. Die Reduktion der Anzahl der Wasserstoffbrückenbindungen für die Kanäle, die hCx46wt und hCx46N188T äquimolar enthielten, führte zu einer reduzierten Anzahl an Gap Junction-Kanälen zwischen den Zellen, was die negativ dominante Eigenschaft der N188T Mutation begründete.
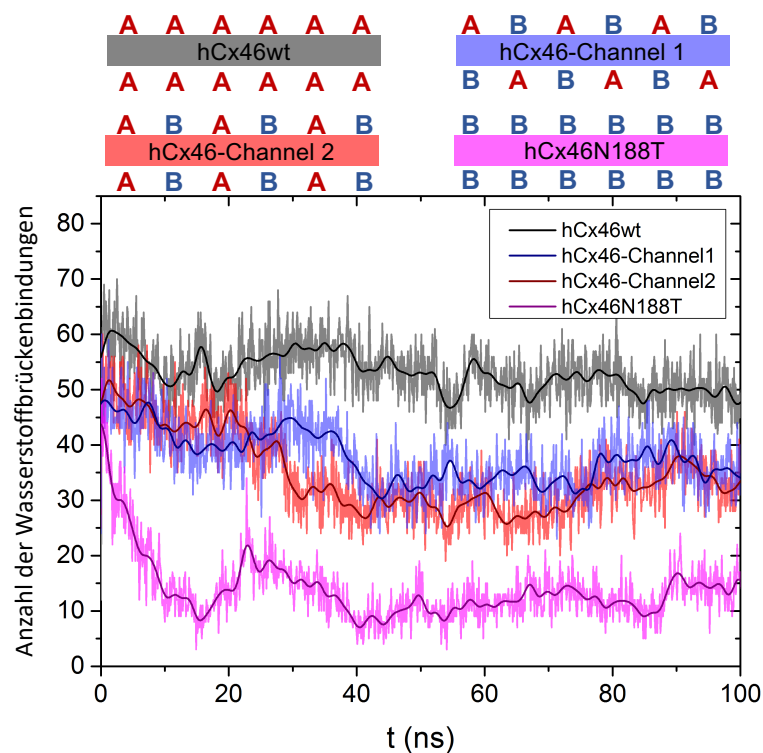

Abbildung 9: Anzahl der Wasserstoffbrückenbindungen zwischen den Connexonen. In einer Molekül-Dynamik-Simulation wurde die Anzahl der Wasserstoffbrückenbindungen für vier verschiedene Kanäle berechnet. Oben ist dargestellt, welches Connexin an welcher Stelle eines Gap Junction-Kanals simuliert wurde. Ein rotes A steht für ein hCx46wt, während ein blaues B ein hCx46N188T repräsentiert (modifiziert nach Schadzek *et al.*, 2019).

3. Diskussion und Ausblick

Beim Menschen, wie auch bei anderen Wirbeltieren, stellen Gap Junction-Kanäle die einzige direkte Verbindungsmöglichkeit zwischen benachbarten Zellen dar, welche den Austausch von Ionen, kleinen Signalmolekülen und Stoffwechselprodukten erlaubt und somit die Zell-Zell-Kommunikation ermöglicht (Kumar & Gilula, 1996; Harris, 2001). Um einen Gap Junction-Kanal zu formen, oligomerisieren sechs Connexine zu einem Connexon und zwei Connexone benachbarter Zellen docken aneinander und verbinden so die Zytoplasmen der Zellen.

Im Rahmen dieser Dissertation wurde zum einen die Connexon-Connexon-Interaktion von hCx46 und der kataraktassoziierten Mutation N188T analysiert (Publikationen in Anhang A und B) und zum anderen eine Technik entwickelt, um das Oligomerisierungsverhalten von heteromeren Kanälen und Halbkanälen untersuchen zu können (Publikation in Anhang C). Diese neue Technik wurde zusammen mit Molekül-Dynamik-Simulationen eingesetzt, um die dominante Eigenschaft der N188T-Mutation von hCx46 aufzuklären (Publikation in Anhang D).

3.1 Docking: Connexon-Connexon-Interaktion

Beim Docking von zwei benachbarten Connexonen ist die Interaktion der beiden extrazellulären Schleifen essentiell für die Bildung eines Gap Junction-Kanals (Harris, 2001). Cx46 ist, neben Cx43 und Cx50, eines der drei in der Linse vorkommenden Connexine, welches während der Entwicklung zu reifen Linsenfaserzellen zusammen mit Cx50 im Expressionslevel hochreguliert wird (Bassnett *et al.*, 2009; Berthoud & Ngezahayo, 2017). Obwohl Cx50 stärker exprimiert ist, konnte in Experimenten mit adulten Mauselinsen durch Gen-*knock-out* und *knock-in*-Versuche gezeigt werden, dass hauptsächlich Cx46 für die Bildung von Gap Junction-Kanälen zwischen reifen Linsenfaserzellen verantwortlich ist (Gong *et al.*, 1998; Baldo *et al.*, 2001; Martinez-Wittinghan *et al.*, 2004; White *et al.*, 2007).

In dieser Arbeit konnten erstmals die funktionellen Konsequenzen der kataraktassoziierten Mutation N188T im hCx46 aufgeklärt werden (Schadzek *et al.*, 2015). Es wurde bereits gezeigt, dass die in einer chinesischen Familie aufgetretene Mutation N188T im hCx46 zu einem erblich bedingten grauen Star führt (Li *et al.*, 2004). Die molekularen und biophysikalischen Konsequenzen der Mutation waren jedoch nicht bekannt. Da die Mutation in der zweiten extrazellulären Schleife von hCx46 lokalisiert ist und die extrazellulären Schleifen essentiell für das Docking sind, liegt es nahe, dass die Mutation die Connexon-Connexon-Interaktion beeinflussen könnte. Um die funktionellen Konsequenzen zu verstehen, wurde das Wildtyp-hCx46 sowie hCx46N188T in *Xenopus*-Eizellen und in HeLa-Zellen exprimiert. Die elektrophysiologische Charakterisierung zeigte, dass die hCx46N188T-Connexone ungehindert zur Plasmamembran transportiert und insertiert wurden.

Auch waren sie gleichermaßen funktionell wie der hCx46-Wildtyp (Anhang A). Dies deckt sich auch mit den Ergebnissen von Nakagawa *et al.*, 2011, die für hCx32N175Y zeigen konnten, dass diese Mutation nicht in der Lage war, Gap Junction-Kanäle auszubilden. Trotzdem bildete diese Mutante Connexone in der Membran. Obwohl diese nicht mikroskopisch visualisiert werden konnten, erlaubten sie eine Farbstoffaufnahme in die Zellen (Nakagawa *et al.*, 2011). Die hCx46N188T-Mutante zeigte in Farbstoffaufnahmeexperimenten mit Ethidiumbromid als Tracer vergleichbare Aufnahmeraten für Ca^{2+}-haltiges und Ca^{2+}-freies Medium wie die mit hCx46wt transfizierten HeLa-Zellen (Anhang D). Auch unterschieden sich die Halbkanäle nicht in ihrer Sensitivität zu La^{3+}, welches sowohl Halbkanäle als auch Gap Junction-Kanäle inhibiert (Pan *et al.*, 2007), was für die Anwesenheit funktioneller hCx46N188T-Connexone spricht.

Bei der Bildung von Gap Junction-Plaques fällt auf, dass die N188T-Mutante kaum Plaques zwischen benachbarten Zellen bildet (siehe Abbildung 3, Anhang A). Die hCx46wt-exprimierenden Zellen bildeten in über 75 % der Zellpaare Gap Junction-Plaques mit durchschnittlich 1,540 Plaques pro Zellpaar (95 % Konfidenzintervall [1,170 ; 2,030]). Im Gegensatz dazu bildeten nur etwa 10 % der hCx46N188T-exprimierenden Zellen Gap Junction-Plaques mit durchschnittlich 0,126 [0,085 ; 0,196] Plaques pro Zellpaar. Die Ergebnisse ließen sich auch mit den konkatemerisierten Connexinen (hCx46wt-hCx46wt und hCx46N188T-hCx46N188T) reproduzieren (siehe Abbildung 8, Anhang D), was darauf hindeutet, dass diese Mutation möglicherweise zu einer Störung der Connexon-Connexon-Interaktion führt, sodass keine Gap Junction-Plaques aus den in der Membran befindlichen Connexonen gebildet werden können.

Um die Interaktion zwischen den Connexonen zu verstehen, wurden Molekül-Dynamik-Simulationen, basierend auf der Röntgenkristallstruktur von hCx26, durchgeführt (Maeda *et al.*, 2009). Ein Sequenzalignment aller Connexinen zeigte, dass die meisten Connexine eine typische Aminosäuresequenz in der zweiten extrazellulären Schleife aufweisen. Man kann zwei Gruppen von Connexinen unterscheiden, die K-N- und H-Gruppe (Koval *et al.*, 2014). Durch die Analyse von heterotypischen Kanälen konnte die Connexin-Kompatibilität zwischen unterschiedlichen Connexin-Isoformen (H-Gruppe / K-N-Gruppe) aufgeklärt werden (White *et al.*, 1995). Innerhalb ihrer Gruppe können Connexone heterotypische Kanäle miteinander bilden (siehe Abbildung 2). In Domänen-Austausch-Experimenten mit Cx43 (H-Gruppe), Cx46 und Cx50 (beide K-N-Gruppe) konnte gezeigt werden, dass die zweite extrazelluläre Schleife wichtig ist für die Selektivität bei der Connexon-Connexon-Interaktion und somit für die Bildung von funktionalen Gap Junction-Kanälen (White *et al.*, 1994). Cx26 und Cx46 gehören beide zur K-N-Gruppe. Daher unterscheidet sich die Sequenzen von Cx26 und Cx46 in der zweiten extrazellulären Schleife nur marginal (Schadzek *et al.*, 2015), weshalb sich die Röntgenkristallstruktur von hCx26 hervorragend als Vorlage für das homologe Modell eignet.

Für die Molekül-Dynamik-Simulation dienten zwei Kopf-an-Kopf-interagierende Connexine als Modellsystem für das Docking von Connexonen (siehe Abbildung 4). Während der Simulation blieb nur das hCx46wt-Modell über die gesamte Zeitspanne von 50 ns stabil. Es wurde von durchschnittlich fünf Wasserstoffbrückenbindungen stabilisiert. Die über Wasserstoffbrückenbindungen interagierenden Connexine mit der Mutation hCx46N188T, sowie die zwei artifiziellen Mutationen hCx46N188Q und hCx46N188D dissoziierten während der Simulationszeit voneinander (siehe Abbildung 5 und Anhang B). N188Q sollte als „Rettungsmutante" die Funktionalität wiederherstellen. Asparagin (N) und Glutamin (Q) besitzen die gleiche funktionelle Gruppe, jedoch ist die Aminosäure Glutamin um eine CH_2-Gruppe länger. hCx46N188Q konnte, ebenso wie hCx46N188T, kaum Gap Junction-Plaques bilden und war in Farbstofftransferexperimenten nicht metabolisch gekoppelt. Im Gegensatz dazu waren die Halbkanäle in *Xenopus*-Oozyten funktionell. In der Molekül-Dynamik-Simulation konnten durch die Größe der Aminosäure und die damit verbundene abweichende räumliche Orientierung keine Wasserstoffbrückenbindungen zwischen den zweiten extrazellulären Schleifen ausgebildet werden. Bei der N188D Mutante wurde Asparagin durch die gleichgroße Asparaginsäure ersetzt. Durch das Einfügen einer negativen Ladung kam es jedoch in den Molekül-Dynamik-Simulationen zu einer elektrostatischen Repulsion mit D191, was zur Dissoziation der interagierenden Connexine führte (siehe Anhang B). Jedoch war in Molekül-Dynamik-Simulationen die Mutante N188D auch nicht durch das Einfügen der D191N Mutation stabilisierbar. Gong *et al.*, 2013 beschrieben, dass das Docking der Mutante hCx32N175D (homolog zu hCx46N188D) durch das Einfügen der hCx26D179N-Mutation (homolog zu hCx46D191N) stabilisiert werden konnte. Da die „Rettung" durch die zweite Mutation bei hCx46 nicht funktionierte, verdeutlicht dies, wie sensibel das Wasserstoffbrückenbindungsnetzwerk ist. Die zweite extrazelluläre Schleife im hCx46 ist im Vergleich zu hCx26 und hCx32 um eine Aminosäure kürzer (Maeda *et al.*, 2009), was die Flexibilität einschränken und somit das Docking störanfälliger machen könnte.

Eine ebenfalls in einer chinesischen Familie auftretende Mutation von hCx46N188I geht, wie auch die Mutation N188T, mit einem Katarakt einher (Zhang *et al.*, 2012). Dies verdeutlicht die Schlüsselrolle der Aminosäure Asparagin an der Position 188 des hCx46 für das Wasserstoffbrückenbindungsnetzwerk. Im statischen Modell, das die maximal mögliche Anzahl der Wasserstoffbrückenbindungen darstellt, bildet N188 zu R180 zwei und zu T189 und D191 jeweils eine Wasserstoffbrückenbindung aus (siehe Abbildung 4B). N176 in hCx26 ist die homologe Aminosäure zu N188 in hCx46 und bildet drei Wasserstoffbrückenbindungen zu K168, T177 und D179 aus (Maeda *et al.*, 2009; Gong *et al.*, 2013). Im hCx32 stellt die Aminosäure N175 die zentrale Position dar, die je eine Wasserstoffbrückenbindung zu K167, T176 und D178 ausbildet (Nakagawa *et al.*, 2011). Gong *et al.* (2013) zeigten, indem sie verschiedene Connexin-Mutationen in

homotypischen und heterotypischen Kanälen analysierten, dass bei hCx32 und hCx26 zwischen den beiden zweiten extrazellulären Schleifen vier von sechs Wasserstoffbrückenbindungen ausgeprägt sein mussten, um einen funktionalen Kanal zu formen. Neben den Wasserstoffbrückenbindungen zwischen den zweiten extrazellulären Schleifen werden die Connexone auch durch die Interaktion der ersten extrazellulären Schleifen stabilisiert. Bei hCx26 zeigte die Röntgenkristallstruktur, dass je Connexin-Connexin-Interaktion vier Wasserstoffbrückenbindungen zwischen N54, L56 und Q57 ausgebildet werden (Maeda *et al.*, 2009; Bai & Wang, 2014). Ein hCx26-Kanal wird von insgesamt 60 Wasserstoffbrückenbindungen (sechs Connexine, die jeweils vier Wasserstoffbrückenbindungen zwischen den ersten extrazellulären Schleifen und sechs zwischen den zweiten extrazellulären Schleifen der Kopf-an-Kopf interagierenden Connexine ausbilden) zusammengehalten (Nakagawa *et al.*, 2010; (Nakagawa *et al.,* 2011; Gong *et al.*, 2013). Beim hCx46 zeigte das statische Modell, dass zwischen den beiden ersten extrazellulären Schleifen ebenfalls vier Wasserstoffbrückenbindungen, jeweils eine zwischen N55 und Q57 und zwei zwischen Q58 und Q58, ausgebildet werden (siehe Abbildung 4B und Angang D). Ein hCx46-Kanal wird somit durch insgesamt 72 Wasserstoffbrückenbindungen stabilisiert. Dabei sind pro Kopf-an-Kopf-interagierendem Connexin-Paar vier Bindungen zwischen den ersten extrazellulären Schleifen (zwei zu dem gegenüberliegenden und zwei zum schräg gegenüberliegenden Connexin) und acht Wasserstoffbrückenbindungen zwischen den zweiten extrazellulären Schleifen vorhanden.

In Molekül-Dynamik-Simulationen mit einem ganzen Gap Junction-Kanal konnten für den hCx46wt-Kanal durchschnittlich 53 Wasserstoffbrückenbindungen während einer 100 ns langen Simulation ermittelt werden. Für hCx46N188T lag der Wert bei durchschnittlich 12 Wasserstoffbrückenbindungen pro Kanal (siehe Abbildung 9, Anhang D). Auch beim hCx46N188Q-Kanal sank die Anzahl der Wasserstoffbrückenbindungen innerhalb der ersten 4 ns Simulationszeit auf unter 10 Wasserstoffbrückenbindungen (Anhang B).

Die mangelnde Fähigkeit zur Bildung von ausreichend vielen Wasserstoffbrückenbindungen der N188T-Mutation führt zu direkten Auswirkungen auf die Gap Junction-Kanalbildung. Wenn ein Teil der Zellen hCx46wt und ein anderer Teil hCx46N188T exprimierte und daran die Plaquebildung von heterotypischen Kanälen untersucht wurde, so war eine deutliche Reduktion der Plaquebildung, verglichen mit nur hCx46wt-exprimierenden Zellen, zu beobachten (siehe Abbildung 3C). Auch wenn die Mutante zusammen mit dem Wildtyp co-exprimiert wurde, reduzierte sie die Plaquebildung (siehe Abbildung 3B). Vermutlich wurden heteromere Connexone gebildet, in denen die Mutante und der Wildtyp zusammen vorlagen. Diese heteromeren Connexone konnten folglich nicht mehr ausreichend durch Wasserstoffbrückenbindungen stabilisiert werden und führten so zu der festgestellten Verringerung der Plaqueanzahl.

Die Stammbaumanalyse der chinesischen Familie, bei der die N188T-Mutation auftrat, zeigte, dass alle Betroffenen, die einen Katarakt entwickelten, heterozygot für die Mutante waren. Das heißt, dass sie ein Allel besitzen, welches für das mutierte Connexin (hCx46N188T) kodiert, und ein zweites Allel für das Wildtyp-Connexin (Li *et al.*, 2004). Bei den meisten Betroffenen wurde der Katarakt operativ therapiert. Vor der Therapie variierte die verbliebene Sehkraft der Betroffenen zwischen 10 % und 50 %, was darauf hindeutet, dass die Auswirkungen der Mutation und damit die Schwere der Katarakt-Ausprägung variiert. Auch die in der Publikation von Li *et al.* (2004) gezeigte Analyse der Expressionsstärke der Mutante auf mRNA-Ebene unterstützt diese Vermutung. Durch die Mutation von Adenin zu Cytosin an der Position 563 der cDNA-Sequenz entsteht die Ale1-Schnittstelle, welche für die Analyse von fünf Generationen der chinesischen Familie verwendet wurde. Dabei konnte eine inhomogene Transkriptionsstärke des mutierten Connexin46 nachgewiesen werden. Weiterhin auffällig war, dass das Wildtyp-Connexin bei den meisten Betroffenen stärker exprimiert zu sein schien als die Mutante. Das von Li *et al.* (2004) publizierte DNA-Chromatogramm eines Betroffenen zeigt ebenfalls, dass die Adenin-Base an der Position 563, die zur Identifikation des Wildtyp-Connexins diente, häufiger vorlag (etwa 60 %) als die entsprechende Cytosin-Base der Mutante (40 %).

Wenn die Synthese und das *Trafficking* der Mutante sich nicht grundlegend von dem Verhalten des Wildtyps unterscheidet, kann von einer statistischen Verteilung der Mutante in Kanälen und Halbkanälen ausgegangen werden. Auf diese Weise wären sowohl Halbkanäle denkbar, die entweder nur aus dem Wildtyp, ausschließlich aus der Mutante oder aus dem Wildtyp und der Mutante aufgebaut wären. Die statistisch wahrscheinlichste Zusammensetzung wäre unter den beschriebenen Bedingungen die heteromere Bildung von Connexonen aus hCx46wt und hCx46N188T. Um gezielt heteromere Connexone dieser Art zu generieren und damit ein Modell für die heterozygoten Patienten zu entwickeln, wurden in dieser Arbeit Connexin-Konkatemere aus hCx46wt und hCx46N188T erstellt. Diese heterodimeren Konkatemere imitieren das Expressionsverhalten eines heterozygoten Patienten, der die Mutante genauso stark wie den Wildtyp exprimiert. Die Konkatemerisierung führt außerdem zu einer alternierenden Anordnung von hCx46wt und hCx46N188T in einem Connexon. In diesem Aufbau sind die Wasserstoffbrückenbindungen, die während des Dockingprozesses gebildet werden, gleichmäßig über den Kanal verteilt. Die Wildtyp-Connexine, die mehr Wasserstoffbrückenbindungen ausbilden können als die Mutante, sind wahrscheinlich bei einer alternierenden Reihenfolge besser in der Lage den Gap Junction-Kanal zu stabilisieren, als wenn die Wasserstoffbrückenbindungsverteilung einseitiger wäre. Das wäre zum Beispiel der Fall, wenn jeweils drei Wildtyp-Connexine und drei mutierte Connexine in einem Connexon nebeneinander liegen und bei der Kanalbildung ausschließlich Wildtyp an Wildtyp und Mutante an Mutante docken würden. Ob ein derartiger Kanal tatsächlich existieren kann und wie viel

instabiler er in dem Fall wäre, wurde bisher noch nicht untersucht. Da die stöchiometrische Verteilung der Connexone *in vivo* ebenfalls unbekannt ist und methodisch bisher nicht bestimmt werden kann, wurden eine alternierende Reihenfolge und eine gleich starke Expression von Mutante und Wildtyp angenommen, was durch die heterodimere Konkatemerisierung simuliert wurde. Die Konkatemerisierung und die daraus resultierende Verteilung der Connexine über das Connexon stellt somit ein methodisch realisierbares und statistisch legitimes erstes Modell für die hCx46N188T-heterozygoten Patienten dar.

Um die strukturbiologischen und molekularen Konsequenzen der Mutation zu untersuchen, wurden sowohl die Heterodimere hCx46wt-hCx46N188T und hCx46N188T-hCx46wt als auch die Homodimere hCx46wt-hCx46wt und hCx46N188T-hCx46N188T, sowie die beiden Monomere hCx46wt und hCx46N188T in HeLa-Zellen exprimiert und die gebildeten Halbkanäle und Gap Junction-Kanäle analysiert. In Farbstoffaufnahmeexperimenten mit Ethidiumbromid als Tracer konnte gezeigt werden, dass die Halbkanäle aller Konstrukte in die Membran insertiert wurden und die Farbstoffaufnahmerate unabhängig von der Mutation N188T war. Alle Halbkanäle waren sensitiv zu Ca^{2+}- und La^{3+}-Ionen. In Ca^{2+}-freiem Medium zeigten sie eine signifikant erhöhte Farbstoffaufnahmerate im Vergleich zu den Kontrollzellen, die mit GFP transfiziert wurden. Dies ist eine Gap Junction-typische Reaktion auf eine Reduktion der extrazellulären Ca^{2+}-Konzentration. So konnte für Cx26 mittels AFM-Topographie gezeigt werden, dass das Connexon in Ca^{2+}-freiem Medium geöffnet ist und 0,5 mM Ca^{2+} zum Verschließen der Pore führt (Müller *et al.*, 2002; Figueroa *et al.*, 2013). Nicht alle Connexin-Isoformen sind gleich sensitiv gegenüber Ca^{2+} (Nielsen *et al.*, 2012). So schließt beispielsweise 1,8 mM Ca^{2+} Cx43-Halbkanäle (Thimm *et al.*, 2005). Unter normalen physiologischen Bedingungen (2 mM im extrazellulären Raum (Clapham, 2007)) ist die Öffnungswahrscheinlichkeit von Halbkanälen stark reduziert, denn die Ca^{2+}-Bindung an das Connexon führt zu einer Reorganisation der spezifischen Interaktion innerhalb des Connexin-Proteins, was zum Schließen der Pore führt (Lopez *et al.*, 2016).

Wie oben bereits erwähnt, bilden Zellen so gut wie keine Gap Junction-Plaques, die das hCx46N188T-hCx46N188T oder das Monomer hCx46N188T exprimierten (siehe Abbildung 8). Wurde ein Connexon aus drei hCx46wt- und drei hCx46N188T-Connexinen gebildet, so wie es bei den heterodimeren Konkatemeren (hCx46wt-hCx46N188T und hCx46N188T-hCx46wt) der Fall war, wurden zwischen diesen Zellpaaren mehr Gap Junction-Plaques gebildet (nicht signifikant im Vergleich zu hCx46N188T-hCx46N188T). Jedoch war die Anzahl der Plaques bei den heterodimeren Konkatemeren signifikant geringer als bei den Zellen, die das Homodimer hCx46wt-hCx46wt exprimierten. In Farbstofftransferexperimenten mit Lucifer Yellow als Tracer zeigten sowohl die heterodimeren Konstrukte als auch die hCx46-Wildtyp-exprimierenden Zellen (Homodimer hCx46wt-hCx46wt und Monomer hCx46wt) eine zu den Kontrollzellen und

hCx46N188T-exprimierenden Zellen (Homodimer hCx46N188T-hCx46N188T und Monomer hCx46N188T) signifikant höhere Gap Junction-Kopplung. Die Funktionalität der Gap Junction-Kanäle scheint durch die Mutation hCx46N188T sowohl in Hinblick auf die Gap Junction-Plaquebildung als auch auf die Gap Junction-Kopplung beeinträchtigt zu werden.

In der Molekül-Dynamik-Simulation zeigten die Connexone, die abwechselnd hCx46wt und hCx46N188T enthielten, wie es bei den heterodimeren Konstrukten der Fall ist, durchschnittlich 31 bzw. 35 Wasserstoffbrückenbindungen, wenn sie entweder immer mit sich selbst oder immer hCx46wt mit hCx46N188T interagierten (siehe Abbildung 9), welches wesentlich mehr Wasserstoffbrückenbindungen sind als bei der Mutante allein. Im Gegensatz dazu wurde der hCx46wt-Kanal von durchschnittlich 53 Wasserstoffbrückenbindungen stabilisiert. Dies verdeutlicht, dass die Anzahl der Wasserstoffbrückenbindungen, die fürs Docking elementar sind, reduziert wird, sobald hCx46N188T an der Bildung eines Gap Junction-Kanals beteiligt ist, was zu einer Verringerung der Plaqueanzahl führt.

Zusammenfassend kann festgehalten werden, dass die Position N188 von hCx46 eine Schlüsselrolle für das Docking der Connexone darstellt. Durch die funktionale Analyse von konkatemerisiertem hCx46wt und hCx46N188T in Kombination mit den Daten der Molekül-Dynamik-Simulationen konnte der zuvor postulierte negativ-dominante Charakter der autosomalen Mutation N188T strukturbiologisch erfasst werden (Li *et al.*, 2004; Veitia, 2007). hCx46 Gap Junction-Kanäle beteiligen sich am Versorgungssystem der Linse, welches für die metabolische Homöostase und die Physiologie der avaskulären Linse notwendig ist (Mathias *et al.*, 2007). hCx46N188T reduziert die Anzahl der zwischen den Zellen gebildeten hCx46-Gap Junction-Kanäle, erschwert dadurch die metabolische Homöostase und begünstigt somit die Katarakt-Bildung.

3.2 Oligomerisierung: Connexin-Connexin-Interaktionen

In den meisten Zellen werden verschiedene Connexin-Isoformen zeitgleich exprimiert. Das Bilden von heteromeren Connexonen und heterotypischen Kanälen ermöglicht es der Zelle, die Gap Junction-Kopplung genauestens auf ihre physiologischen Bedürfnisse abzustimmen und dadurch eine metabolische Selektivität zu schaffen oder die Flussrichtung von Metaboliten zu steuern (White *et al.*, 1995; Desplantez *et al.*, 2015; Oh & Bargiello, 2015).

Um gezielt heteromere Connexone und heterotypische Kanäle untersuchen zu können, wurden erstmals Connexin-Konkatemere verwendet, wodurch die Stöchiometrie der Connexone determiniert werden kann. Dies kann zukünftig eine vielversprechende Methode sein, um die physiologischen

Konsequenzen der Hetero-Oligomerisierung von Connexinen in Halbkanälen und Gap Junction-Kanälen analysieren zu können (Anhang C).

In HeLa-Zellen wurden die GFP-markierten Monomere hCx46 und hCx26, Homodimere hCx46-hCx46 und hCx26-hCx26, sowie Heterodimere hCx46-hCx26 und hCx26-hCx46 exprimiert und analysiert. Die Konkatemere wurden, wie es von den Monomeren bekannt ist, zur Plasmamembran transportiert und waren außerdem in der Lage, Gap Junction-Plaques auszubilden. Jedoch waren die von den Konkatemeren gebildeten Plaques signifikant kleiner als die der Monomere (siehe Abbildung 6). Im Western Blot zeigte sich, dass das hCx46-hCx46-Tandem nach der Transfektion etwa 40 % weniger exprimiert war als das hCx46-Monomer. Dieses Resultat kann die mindestens dreifache Reduktion der Plaquefläche im Vergleich zu den Monomeren nur zum Teil erklären, weshalb die Ergebnisse vermuten lassen, dass durch die Konkatemerisierung zusätzlich zur Synthese auch der Transport zur Membran gestört ist. Interessant ist, dass sich die Gap Junction-Plaqueanzahl nicht zwischen dem hCx46-Monomer und dem hCx46-hCx46-Homodimer unterschied (Anhang D) und nur die Plaquefläche betroffen war.

In Farbstofftransferexperimenten zeigten alle getesteten hCx46/hCx26-Konkatemere eine Funktionalität, die mit der der Monomere vergleichbar war. Nur die Kontrollzellen zeigten eine signifikant reduzierte Kopplung. Diese Ergebnisse decken sich mit denen der hCx46N188T/hCx46wt-Konkatemere. Sobald auf konfokalen Aufnahmen deutliche Gap Junction-Plaques erkennbar waren, waren die gebildeten Kanäle funktional (Anhang D). Für das monomere hCx46 sind bereits ähnliche Farbstofftransfer-Raten beschrieben worden (Schlingmann *et al.*, 2012; Schlingmann *et al.*, 2013), was zumindest *in-vitro* auf eine ungestörte Funktionalität der Konkatemere hindeutet.

Die Röntgenkristallstruktur von hCx26 zeigt, dass der N-Terminus des Connexins in die Pore gefaltet ist (Maeda *et al.*, 2009; Maeda & Tsukihara, 2011) und dort einen spannungssensitiven Trichter bildet (Schlingmann *et al.*, 2012), weshalb N-terminal mit Fluoreszenzproteinen markierte Connexine zwar oligomerisieren, zur Membran transportiert werden und docken können, aber weder als Halbkanal noch als Gap Junction-Kanal funktional sind (Laird *et al.*, 2001; Contreras *et al.*, 2003). Das Dimerisieren der Connexine führt zu einem Protein mit acht hydrophoben Transmembrandomänen, bei dem der C-Terminus des ersten Connexins mit dem N-Terminus des zweiten Connexins über einen 19 Aminosäuren langen Linker verbunden ist. Der C-Terminus von hCx46 ist 207 Aminosäuren lang und hCx26 hat mit nur 10 Aminosäuren den kürzesten C-Terminus aller Connexine (Maeda *et al.*, 2009; Schadzek *et al.*, 2015). Daher kann vermutet werden, dass die Länge des C-Terminus eine höhere Flexibilität erlaubt, wenn der C-Terminus eines hCx46 mit dem N-Terminus des folgenden Connexins verbunden wird, als wenn das erste Connexin in einem

Tandem ein hCx26 ist. Welche Struktur der C-Terminus einnimmt, ist nicht vollständig verstanden. Jedoch zeigten experimentelle NMR-Daten, dass der C-Terminus hoch flexibel ist (Sorgen *et al.*, 2004). Daher kann angenommen werden, dass durch die Interaktion mit assoziierten Proteinen und die hohe Flexibilität des C-Terminus der C-Terminus des ersten Connexins trotz der mechanischen Einschränkungen durch die Konkatemerisierung nah genug an der Membran lokalisiert ist, um die richtige Faltung des folgenden konkatemerisierten N-Terminus zu ermöglichen.

Die Einzelkanal-Leitfähigkeiten, die mittels *inside-out patch-clamp*-Technik in *Xenopus*-Oozyten-Membranen gemessen wurden, zeigten Werte von etwa 46 pS und 39 pS für hCx46 und hCx26 (siehe Abbildung 7). Aus der Maus isolierte Linsenfaserzellen wiesen eine deutlich größere Leitfähigkeit von etwa 240 pS auf (Ebihara *et al.*, 2011). Ähnliche Leitfähigkeiten (250 - 300 pS) wurden auch für Cx46-Halbkanäle verzeichnet, die in *Xenopus*-Eizellen oder in N2A- bzw. HeLa-Zellen exprimiert wurden (Trexler *et al.*, 1996; Hu & Dahl, 1999; Trexler *et al.*, 2000; Srinivas *et al.*, 2005). Auch für Cx26 sind in der Literatur hohe Leitfähigkeiten von 320 pS (Mese *et al.*, 2011) und 400 pS (Sánchez *et al.*, 2010) verzeichnet. Solch hohe Leitfähigkeiten konnten nicht in den *inside-out patch-clamp*-Experimenten gemessen werden, weshalb davon ausgegangen werden muss, dass es sich bei den gemessenen Werten um Sub-Leitfähigkeiten handelt. Solche wurden bereits sowohl für Cx26 als auch für Cx46 von anderen Autoren publiziert (Oh *et al.*, 1999; Hopperstad *et al.*, 2000; Bao *et al.*, 2004; Gassmann *et al.*, 2009). Gaßmann *et al.* (2009) beschrieben für Cx26, dass die Leitfähigkeit 34 ± 8 pS mindestens mit dem Faktor zehn häufiger vorkam, als die beiden anderen Leitfähigkeiten 70 ± 8 pS und 165 ± 19 pS. Dies verdeutlicht, dass die Sub-Leitfähigkeiten wesentlich häufiger auftreten als die Hauptleitfähigkeit, weshalb eventuell nur Sub-Leitfähigkeiten in den *Xenopus*-Oozyten gemessen werden konnten.

Des Weiteren wurden die Messungen in Cl⁻-freiem Medium durchgeführt, um die Hintergrundströme der Oozyten-eigenen Kanäle zu minimieren. Die anstelle von Chlorid verwendeten Gegenionen waren Acetat- und Gluconat-Anionen, welche bedingt durch ihre Größe eine geringere Beweglichkeit durch die Kanäle haben, wodurch die Leitfähigkeit reduziert werden kann (Suchyna *et al.*, 1999; Slavi *et al.*, 2014).

Die gemessenen Leitfähigkeiten für die Homodimere waren mit 25 pS und 33 pS für hCx46-hCx46 bzw. hCx26-hCx26 im Vergleich zu den Monomeren geringer (siehe Abbildung 7B), was durch die artifiziellen Änderungen, die die Konkatemerisierung für die Connexine mit sich bringt, erklärt werden könnte. Trotz kleiner Abweichungen zu monomeren Connexinen erlaubt es die Konkatemerisierung, heteromere Gap Junction-Kanäle mit einer definierten Stöchiometrie zu erforschen. Dementsprechend konnten bei den heteromeren Connexonen jeweils zwei neue Leitfähigkeiten von etwa 16 pS und 26 pS für das hCx46-hCx26- sowie etwa 20 pS und 31 pS für

das hCx26-hCx46-Tandem gemessen werden. Die Leitfähigkeiten der untersuchten Homodimere (hCx46-hCx46 und hCx26-hCx26) unterschieden sich signifikant von denen, die für die heterodimeren Connexone (hCx46-hCx26 und hCx26-hCx46) festgestellt wurden, was beweist, dass beide Connexine eines Konkatemers an der Connexon-Bildung beteiligt sind. Wäre das nicht der Fall und würde beispielsweise immer nur das erste Connexin eines Tandems in der Membran eingebaut werden, würde zwischen dem hCx46-hCx46 und dem hCx46-hCx26 kein Unterschied zu erwarten sein.

Auch die Analyse der Plaqueanzahl in Zellen, die mit Konkatemeren aus hCx46N188T und hCx46wt transfiziert wurden, liefert einen deutlichen Beweis dafür, dass beide Connexine eines Konkatemers in die Membran insertiert sind und an der Plaquebildung beteiligt sind (siehe Abbildung 8 und Anhang D). Die Beobachtung, dass die konkatemerisierten Connexine als ein ganzes Verbundprotein mit allen acht Transmembrandomänen in die Plasmamembran insertiert werden, stimmt auch mit Experimenten von anderen Wissenschaftlern überein, welche Untereinheiten von anderen Membranproteinen, wie etwa Acetylcholin-, γ-Aminobuttersäure- (GABA) oder ionotropen ATP-Rezeptor-Kanälen, konkatemerisierten, um die Kanalstöchiometrie zu erforschen (Stoop *et al.*, 1999; Baumann *et al.*, 2001; Sigel *et al.*, 2009; Ahring *et al.*, 2018).

Die Ergebnisse der Einzelkanalmessungen mittels *inside-out patch-clamp*-Technik deuten darauf hin, dass trotz der Unterschiede zwischen den Homodimeren und Monomeren die Bildung von heterodimeren Halbkanälen zu einer weitgreifenden Veränderung der Leitfähigkeit (zwei beobachtete Leitfähigkeiten) und der Offenwahrscheinlichkeit führt, wodurch die Erforschung von heteromere Kanälen ermöglicht wird. Um die biophysikalischen Kanaleigenschaften durch die Konkatemerisierung nicht zu verfälschen, wäre es wünschenswert, die verbundenen N- und C-Termini nach dem Einbau der Connexone in die Membran wieder voneinander trennen zu können. Ein solches System wurde für die Erforschung von PanX1-Kanälen verwendet, indem konkatemerisierte Untereinheiten durch eine TEV-Endoprotease *in-vitro* voneinander getrennt wurden (Chiu *et al.*, 2017).

Um die Leitfähigkeit der Gap Junction-Kanäle zu bestimmen, wurden *dual-whole-cell patch-clamp*-Experimente mit N2A-Zellen, die die verschiedenen Monomere, Homodimere und Heterodimere exprimierten, durchgeführt. Die Monomere formten Gap Junction-Kanäle mit einer maximalen Leitfähigkeit von etwa 200 pS für hCx46 und 140 pS für hCx26. Ähnliche Leitfähigkeiten konnten für diese Connexine bereits in anderen Expressionssystemen erzielt werden (Oh *et al.*, 1999; Slavi *et al.*, 2016). Neben der Hauptleitfähigkeit für Gap Junction-Kanäle konnten auch Sub-Leitfähigkeiten festgestellt werden, unter anderem auch etwa 20 pS für hCx46 und etwa 17 pS für hCx26, was mit den in den Oozyten gemessenen Werten von ca. 40 pS und 35 pS übereinstimmt.

Wird die Leitfähigkeit (G) des Halbkanals halbiert, so erhält man die Leitfähigkeit für den Gap Junction-Kanal, da der Widerstand (R) eines Gap Junction-Kanals im Vergleich zum Halbkanal doppelt so groß ist und somit G=1/R gilt (Sáez *et al.*, 2005). Durch das Konkatemerisieren von hCx46 wird die maximale Gap Junction-Kanal-Leitfähigkeit nicht beeinflusst (siehe Anhang C). Bei hCx26 hat das hCx26-hCx26-Konkatemer im Vergleich zum Monomer (138 pS) eine etwas größere maximale Leitfähigkeit von etwa 180 pS, was verdeutlicht, dass die Konkatemerisierung die biophysikalischen Kanaleigenschaften beeinflusst. Die untersuchten heterodimeren Kanäle wiesen, wie auch die Halbkanäle, deutliche Änderungen in den Kanaleigenschaften (z.B. die maximale Leitfähigkeit oder die Kanalaktivität) auf und unterschieden sich klar von den aus homodimeren und monomeren Connexinen gebildeten Gap Junction-Kanälen. Daher wird angenommen, dass solche Änderungen eher an der Hetero-Oligomerisierung der Connexine liegen als an der Konkatemerisierung. Jedoch wäre für den abschließenden Beweis dieser These das Spalten des Linkers, der die Connexine im Konkatemer miteinander verknüpft, nötig.

Bei den *dual-whole-cell patch-clamp*-Experimenten zeigten hCx26-hCx26 und hCx26-hCx46 Kanäle im Vergleich zu dem Monomer hCx26 und dem Heterodimer hCx46-hCx26 eine höhere Kanalaktivität, das heißt schnellerer Wechsel zwischen den geöffneten und geschlossenen Zuständen, und eine erhöhte maximale Leitfähigkeit, was durch den kurzen C-Terminus von hCx26 und den dadurch einhergehenden Mangel an Flexibilität erklärbar ist. Dies führt eventuell zu einem Kanal, dessen Pore nicht mehr vollständig verschließbar ist. War das erste Connexin eines Tandems ein hCx46, konnte das nicht beobachtet werden.

Bei Farbstoffaufnahme-Experimenten zeigte nur hCx26-hCx26, verglichen mit den anderen Tandems und den Monomeren, eine in Ca^{2+}-freiem Medium signifikant erhöhte Ethidiumbromid-Aufnahme. Jedoch war auch die Aufnahme des Tracers im Ca^{2+}-haltigen Medium erhöht (nicht signifikant), was dafür spricht, dass die Pore von hCx26-hCx26 entweder größer ist (eventuell mehr als sechs Connexine in einem Kanal) oder, was wahrscheinlicher ist, dass es durch die Konkatemerisierung des kurzen C-Terminus mit dem N-Terminus zu einer Pore kommt, die nicht vollständig verschlossen werden kann.

Extrazelluläre La^{3+}-Ionen sind dafür bekannt, Gap Junction-Halbkanäle zu blockieren (Contreras *et al.*, 2002; Retamal *et al.*, 2007; Brokamp *et al.*, 2012). Jedoch ist die genaue Wirkweise von La^{3+} bisher nicht geklärt. Zudem wurde für Cx26 eine La^{3+}-Insensitivität bereits beschrieben (Jara *et al.*, 2012). Diese zeigte sich auch in den Farbstoffaufnahme-Experimenten mit dem hCx26-Monomer. Bei den heterodimeren Konkatemeren wurde auch die Tendenz der La^{3+}-Insensitivität abhängig von der Reihenfolge der Connexine beobachtet. So reagierten die Halbkanäle von hCx46-hCx26 tendenziell insensitiver auf La^{3+}-Ionen als die hCx26-hCx46-Heterodimere. Der beobachtete Trend

der La^{3+}-Insensitivität könnte mit der Anzahl an freien N-Termini korrelieren. Durch den langen C-Terminus von hCx46 im hCx46-hCx26-Konkatemer besitzt der folgende N-Terminus von hCx26 die notwendige Bewegungsfreiheit. Somit hat ein hCx46-hCx26 Halbkanal drei fast frei bewegliche hCx26-N-Termini und drei freie hCx46 N-Termini. Beim hCx26-hCx46-Tandem hingegen sind die an den kurzen C-Terminus von hCx26 gebundenen N-Termini stark in ihrer Bewegungsfreiheit eingeschränkt, wodurch die bei hCx26 beobachtete Insensitivität zu La^{3+} verloren geht.

Das hCx46-Monomer oder das hCx46-hCx46-Homodimer reagierten, wie erwartet, sensitiv auf den Gap Junction-Inhibitor La^{3+}. Auch die hCx46wt- und hCx46N188T-exprimierenden HeLa-Zellen zeigten in *whole-cell patch-clamp*-Experimenten die erwartete La^{3+}-Sensitivität (Anhang A), wodurch sich der Einfluss von La^{3+} auf die hCx46-Halbkanäle bestätigte.

Bezüglich der Hetero-Oligomerisierung von Connexinen zu Connexonen werden in der Literatur zwei verschiedene, sich nicht gegenseitig ausschließende, Motive beschrieben: Zum einen der Übergang von der zytoplasmatischen Schleife (CL) zur dritten Transmembran-Domäne (TM3) und zum anderen eine Region innerhalb der ersten Transmembran-Domäne (TM1) stellen wichtige Bereiche der Aminosäuresequenz für die Hetero-Oligomerisierung dar (Martínez *et al.*, 2011; Jara *et al.*, 2012; Koval *et al.*, 2014).

Das TM1-Motiv wurde bei Cx26 gefunden, da Mutationen in diesem Bereich (V37-A40: VVAA) mit einer Verschlechterung der Oligomerisierung einhergehen (Jara *et al.*, 2012). Die Proteine können über diese Stelle dimerisieren, was einen Zwischenschritt bei der Oligomerisierung zu einem Hexamer darstellt. Viele der zur β-Gruppe gehörenden Connexine tragen das VVAA-Motiv in der TM1. Connexine der α-Gruppe sind in dem homologen Bereich weniger stark konserviert. Das ebenfalls in dieser Arbeit verwendete hCx46 hat an der Stelle des TM1-Motivs beispielsweise die Aminosäuresequenz GAAA (G38-A41). Bei den zur α-Gruppe gehörenden Connexinen Cx40 und Cx50 ist die homologe Sequenz GTAA, während Cx43 dort die Sequenz GTAV aufweist, sodass sich diese Connexine durch das GxAx-Motive (x: beliebige Aminosäure) innerhalb des TM1 deutlich von den zur β-Gruppe gehörenden Connexinen unterscheiden.

Die meisten α-Connexine haben in dem CL-TM3-Motiv eine Asparagin (R)- oder Lysin-Aminosäure und werden daher als R-Typ bezeichnet (Smith *et al.*, 2012; Koval *et al.*, 2014). Im Gegensatz dazu tragen die zur β-Gruppe gehörenden Connexine an dieser Position zwei aufeinanderfolgende Tryptophan (W)-Aminosäuren und werden daher W-Typ genannt (Lagree *et al.*, 2003; Smith *et al.*, 2012). Es wurde gezeigt, dass das R- und W-Typ-Motiv, welches sich am Übergang der zytoplasmatischen Domäne zur Membrandomäne befindet, nicht direkt an der Connexin-Connexin-Interaktion beteiligt ist, also die Oligomerisierung nur indirekt beeinflusst (Maeda *et al.*, 2009; Smith

et al., 2012). Maeda *et al.* (2009) konnten zeigen, dass Connexine an den Übergängen von TM2 und TM4 zu den extrazellulären Schleifen konservierte Domänen besitzen, die über ionische Wechselwirkungen oder Wasserstoffbrückenbindungen direkt an der Stabilisierung der oligomerisierten Hexamere beteiligt sind.

R- und W-Typ-Connexine oligomerisieren in unterschiedlichen Kompartimenten. W-Typ-Connexine hexamerisieren im Endoplasmatischen Retikulum (ER) (Maza *et al.*, 2005; Das *et al.*, 2009). Für das am besten bekannte R-Typ-Connexin Cx43 wurde gezeigt, dass es mit dem Chaperon ERp29 über die zweite extrazelluläre Schleife (E2) interagiert und somit die Oligomerisierung im ER zunächst verhindert (Das *et al.*, 2009). Es oligomerisiert erst im Trans-Golgi-Netzwerk (TGN) nach dem Entfernen des ERp29-Moleküls (Musil & Goodenough, 1993; Maza *et al.*, 2005; Smith *et al.*, 2012). Das während dieser Arbeit verwendete hCx46 gehört zu den R-Typ-Connexinen und oligomerisiert im TGN (Koval *et al.*, 1997). Das hCx26 hingegen besitz zwei aufeinanderfolgende Tryptophan-Aminosäuren im CL-TM3-Motiv und ist daher ein W-Typ-Connexin.

Bezüglich dieser beiden Klassifizierungen anhand des TM1-Motivs und anhand des CL-TM3-Motivs gehören hCx46 und hCx26 zu unterschiedlichen Klassen, die nicht miteinander oligomerisieren können sollten. Die Experimente mit den heterodimeren Tandems zeigen jedoch, dass diese beiden Connexine miteinander oligomerisieren können und somit das Oligomerisierungsverhalten nicht direkt von den Connexinen bestimmt sein kann sondern indirekt kontrolliert wird, indem Hilfsproteine oder Chaperone, wie beispielsweise das zuvor beschriebene ERp29, die Oligomerisierung steuern.

Abschließend kann festgehalten werden, dass die Expression von Connexin-Konkatemeren zur Verkleinerung der Plaquefläche führt. Jedoch können konkatemerisierte Connexine zur Membran transportiert werden und bilden dort sowohl funktionale Halbkanäle als auch Gap Junction-Kanäle. Die Methode kann verwendet werden, um Connexone und Kanäle mit einer definierten Connexin-Stöchiometrie zu untersuchen. Selbst wenn Zellen im Gewebe nur zwei Connexin-Isoformen exprimieren, können schon zwei Homomere und zwölf verschiedene Heteromere also insgesamt 14 verschiedene Connexone gebildet werden. Daraus resultieren 196 unterschiedliche Möglichkeiten, einen Gap Junction-Kanal zu bilden (Harris, 2001). Viele Zellen exprimieren jedoch mehr als zwei Connexin-Isoformen, was die Möglichkeit, verschiedene Kanäle zu bilden, wiederum vervielfacht. Dies verdeutlicht die Vielfalt und Varianz der möglichen gebildeten Halbkanäle und Gap Junction-Kanäle im Co-Expressionssystem. Daher ist es von großem Vorteil, die Kanalstöchiometrie durch gezielte Konkatemerisierung determinieren zu können. Wegen des eingefügten Linkers zwischen den Connexinen stimmen die biophysikalischen Kanaleigenschaften nicht exakt mit denen von hetero-oligomerisierten Kanälen und Halbkanälen überein. Wenn jedoch das Entfernen des Linkers

erfolgreich sein sollte, kann diese Methode zukünftig uneingeschränkt eingesetzt werden, um die elektrische und metabolitenabhängige Selektivität von heteromeren Gap Junction-Kanälen und -Halbkanälen zu untersuchen und die physiologische Bedeutung für ein Gewebe detailliert zu charakterisieren.

3.3 Ausblick

Die Gap Junction-abhängige Zell-Zell-Kommunikation ist die Grundvoraussetzung für das Überleben bzw. die Existenz von multizellulären Organismen (Kelly *et al.*, 2015). So gut wie jedes Gewebe exprimiert mindestens eine von den beim Menschen bekannten 21 Connexin-Genen (Gray *et al.*, 2013). Störungen dieser Zell-Zell-Kommunikation gehen mit vielen, je nachdem welches Connexin betroffen ist, schwerwiegenden, teilweise letalen Krankheiten einher (Srinivas *et al.*, 2018). Um Therapieansätze und Modellsysteme zur Behandlung zu finden, ist das Verständnis der Molekülfunktion unerlässlich.

In dieser Arbeit konnten erstmals die funktionellen Konsequenzen der kataraktassoziierten Mutation N188T von hCx46 dargestellt und dadurch das Docking von hCx46-Gap Junction-Kanälen präziser verstanden werden. Durch die Konkatemerisierung von hCx46wt und hCx46N188T konnte die dominante Eigenschaft dieser Mutation belegt werden. Die während dieser Arbeit entwickelte neue Technik der Connexin-Konkatemerisierung erlaubt es, die Kanalstöchiometrie von Gap Junction-Kanälen und Connexonen zu determinieren. Das Konkatemerisieren von hCx26 und hCx46 hat zu funktionalen Halbkanälen und Gap Junction-Kanälen geführt, deren biophysikalische Eigenschaften durch das Einfügen eines Linkers verändert wurden.

Daher sollte zukünftig das Entfernen des Linkers zwischen den beiden Connexinen eines Tandems ein primäres Ziel sein, um ein Modellsystem zu erhalten, welches die biophysikalischen Eigenschaften von natürlich hetero-oligomerisierten Kanälen und Halbkanälen widerspiegelt. Hierfür wäre ein nicht invasives und von außen steuerbares System von Vorteil. Ein geeignetes System könnte eine opto-genetisch aktivierbare Protease sein, die den Linker, der die beiden Connexine verbindet, spaltet. Durch die Co-Expression von I-PhoCl-HCVp (Protease Inhibitor-*photocleavable protein*-Hepatitis C-Virus-Protease) und einem $Panx1^{HCV}$, einem Pannexin1, bei dem die natürliche Caspase3-Substrat-Sequenz durch eine Hepatitis C-Virus-Protease-Substrat-Sequenz ersetzt wurde, konnte ein opto-genetisch aktivierbares Pannexin1 erzeugt werden (Zhang *et al.*, 2017). Wenn dieses Ziel erreicht ist und die biophysikalischen Eigenschaften der homotypischen Kanäle bzw. Halbkanäle den natürlichen entsprechen, dann könnte die Kanalstöchiometrie noch genauer determiniert werden.

Bisher wurden zwei Connexine konkatemerisiert. Um die Kanalstöchiometrie noch genauer zu determinieren, sollten bei der Weiterentwicklung zunächst drei Connexine konkatemerisiert werden. Somit könnten Kanäle und Halbkanäle analysiert werden, die aus bis zu drei verschiedenen Untereinheiten bestehen. Ziel sollte es sein, Connexin-Hexamere zu exprimieren, die ein Connexon formen, um so die Halbkanalstöchiometrie komplett zu determinieren und damit die Auswirkungen von verschiedenen Connexin-Anordnungen innerhalb eines Connexons untersuchbar zu machen. Die gerichtete Leitfähigkeit für einzelne Metaboliten könnte auf diese Weise erforscht werden.

Um einen Gap Junction-Kanal mit einer definierten Stöchiometrie zu erhalten, sollte die Kompatibilität der extrazellulären Schleifen zueinander berücksichtigt werden. In Domänen-Austausch-Experimenten mit H-Gruppen und K-N-Gruppen wurde die Selektivität der Connexon-Connexon-Interaktion gezeigt (White *et al.*, 1994; Martínez *et al.*, 2011). Dies könnte jedoch genutzt werden, um zwei Hexamere definiert und verdrehsicher zu paaren. Bestünde ein Connexon aus fünf K-N-Typ-Connexinen und einem H-Typ-Connexin, so sollten die Connexone nur in einer Orientierung miteinander interagieren können.

Literaturverzeichnis

Aasen, T., Johnstone, S., Vidal-Brime, L., Lynn, K.S. & Koval, M. (2018). Connexins: Synthesis, Post-Translational Modifications, and Trafficking in Health and Disease. *International journal of molecular sciences*, **19**, 1296.

Abascal, F. & Zardoya, R. (2013). Evolutionary analyses of gap junction protein families. *Biochimica et biophysica acta*, **1828**, 4–14.

Abbe, E. (1873). *Beiträge zur Theorie des Mikroskops und der mikroskopischen Wahrnehmung*. Universitätsbibliothek Johann Christian Senckenberg, Archiv für mikroskopische Anatomie, 9, S. 413-468.

Ahn, M., Lee, J., Gustafsson, A., Enriquez, A., Lancaster, E., Sul, J.-Y., Haydon, P.G., Paul, D.L., Huang, Y., Abrams, C.K. & Scherer, S.S. (2008). Cx29 and Cx32, two connexins expressed by myelinating glia, do not interact and are functionally distinct. *Journal of neuroscience research*, **86**, 992–1006.

Ahring, P.K., Liao, V.W.Y. & Balle, T. (2018). Concatenated nicotinic acetylcholine receptors: A gift or a curse? *The Journal of general physiology*, **150**, 453–473.

Alexander, D.B. & Goldberg, G.S. (2003). Transfer of biologically important molecules between cells through gap junction channels. *Current medicinal chemistry*, **10**, 2045–2058.

Ampey, B.C., Morschauser, T.J., Ramadoss, J. & Magness, R.R. (2016). Domain-Specific Partitioning of Uterine Artery Endothelial Connexin43 and Caveolin-1. *Hypertension (Dallas, Tex. : 1979)*, **68**, 982–988.

Ayad, W.A., Locke, D., Koreen, I.V. & Harris, A.L. (2006). Heteromeric, but not homomeric, connexin channels are selectively permeable to inositol phosphates. *The Journal of biological chemistry*, **281**, 16727–16739.

Bai, D. & Wang, A.H. (2014). Extracellular domains play different roles in gap junction formation and docking compatibility. *The Biochemical journal*, **458**, 1–10.

Bai, D., Yue, B. & Aoyama, H. (2018). Crucial motifs and residues in the extracellular loops influence the formation and specificity of connexin docking. *Biochimica et biophysica acta*, **1860**, 9–21.

Baker, S.M., Kim, N., Gumpert, A.M., Segretain, D. & Falk, M.M. (2008). Acute internalization of gap junctions in vascular endothelial cells in response to inflammatory mediator-induced G-protein coupled receptor activation. *FEBS letters*, **582**, 4039–4046.

Baldo, G.J., Gong, X., Martinez-Wittinghan, F.J., Kumar, N.M., Gilula, N.B. & Mathias, R.T. (2001). Gap junctional coupling in lenses from alpha(8) connexin knockout mice. *The Journal of general physiology*, **118**, 447–456.

Bao, L., Sachs, F. & Dahl, G. (2004). Connexins are mechanosensitive. *American journal of physiology. Cell physiology*, **287**, C1389–95.

Bassnett, S., Wilmarth, P.A. & David, L.L. (2009). The membrane proteome of the mouse lens fiber cell. *Molecular vision*, **15**, 2448–2463.

Basu, A., Mazor, S. & Casey, J.R. (2010). Distance measurements within a concatamer of the plasma membrane Cl^-/HCO_3^- exchanger, AE1. *Biochemistry*, **49**, 9226–9240.

Bates, M., Huang, B., Dempsey, G.T. & Zhuang, X. (2007). Multicolor super-resolution imaging with photo-switchable fluorescent probes. *Science (New York, N.Y.)*, **317**, 1749–1753.

Baumann, S.W., Baur, R. & Sigel, E. (2001). Subunit arrangement of gamma-aminobutyric acid type A receptors. *The Journal of biological chemistry*, **276**, 36275–36280.

Beardslee, M.A., Laing, J.G., Beyer, E.C. & Saffitz, J.E. (1998). Rapid turnover of connexin43 in the adult rat heart. *Circulation research*, **83**, 629–635.

Bedner, P., Niessen, H., Odermatt, B., Kretz, M., Willecke, K. & Harz, H. (2006). Selective permeability of different connexin channels to the second messenger cyclic AMP. *The Journal of biological chemistry*, **281**, 6673–6681.

Bennett, M.V.M. & Verselis, V.K.V. (1992). Biophysics of gap junctions. *Seminars in cell biology*, **3**, 29–47.

Berthoud, V.M. & Beyer, E.C. (2009). Oxidative stress, lens gap junctions, and cataracts. *Antioxidants & redox signaling*, **11**, 339–353.

Berthoud, V.M. & Ngezahayo, A. (2017). Focus on lens connexins. *BMC cell biology*, **18**, 6.

Berthoud, V.M., Minogue, P.J., Laing, J.G. & Beyer, E.C. (2004). Pathways for degradation of connexins and gap junctions. *Cardiovascular research*, **62**, 256–267.

Betzig, E., Patterson, G.H., Sougrat, R., Lindwasser, O.W., Olenych, S., Bonifacino, J.S., Davidson, M.W., Lippincott-Schwartz, J. & Hess, H.F. (2006). Imaging intracellular fluorescent proteins at nanometer resolution. *Science (New York, N.Y.)*, **313**, 1642–1645.

Bevans, C.G., Kordel, M., Rhee, S.K. & Harris, A.L. (1998). Isoform composition of connexin channels determines selectivity among second messengers and uncharged molecules. *The Journal of biological chemistry*, **273**, 2808–2816.

Beyer, E.C. & Berthoud, V.M. (2008). Chapter 1: The Family of Connexin Genes. In: *Connexins: A Guide* (edited by A. Harris & D. Locke). Humana Press.

Beyer, E.C., Lin, X. & Veenstra, R.D. (2013). Interfering amino terminal peptides and functional implications for heteromeric gap junction formation. *Frontiers in pharmacology*, **4**, 67.

Beyer, E.C., Paul, D.L. & Goodenough, D.A. (1987). Connexin43: a protein from rat heart homologous to a gap junction protein from liver. *The Journal of cell biology*, **105**, 2621–2629.

Breidert, S., Jacob, R., Ngezahayo, A., Kolb, H.-A. & Naim, H.Y. (2005). Trafficking pathways of Cx49-GFP in living mammalian cells. *Biological chemistry*, **386**, 155–160.

Brink, P.R., Valiunas, V., Gordon, C., Rosen, M.R. & Cohen, I.S. (2012). Can gap junctions deliver? *Biochimica et biophysica acta*, **1818**, 2076–2081.

Brokamp, C., Todd, J., Montemagno, C. & Wendell, D. (2012). Electrophysiology of single and aggregate Cx43 hemichannels. *PloS one*, **7**, e47775.

Carette, D., Gilleron, J., Denizot, J.-P., Grant, K., Pointis, G. & Segretain, D. (2015). New cellular mechanisms of gap junction degradation and recycling. *Biology of the cell / under the auspices of the European Cell Biology Organization*, **107**, 218–231.

Chan, D.K. & Chang, K.W. (2014). GJB2-associated hearing loss: systematic review of worldwide prevalence, genotype, and auditory phenotype. *The Laryngoscope*, **124**, E34–53.

Chiu, Y.-H., Jin, X., Medina, C.B., Leonhardt, S.A., Kiessling, V., Bennett, B.C., Shu, S., Tamm, L.K., Yeager, M., Ravichandran, K.S. & Bayliss, D.A. (2017). A quantized mechanism for activation of pannexin channels. *Nature communications*, **8**, 14324.

Clapham, D.E. (2007). Calcium signaling. *Cell*, **131**, 1047–1058.

Cole, N.B., Smith, C.L., Sciaky, N., Terasaki, M., Edidin, M. & Lippincott-Schwartz, J. (1996). Diffusional mobility of Golgi proteins in membranes of living cells. *Science (New York, N.Y.)*, **273**, 797–801.

Contreras, J.E., Sáez, J.C., Bukauskas, F.F. & Bennett, M.V.L. (2003). Gating and regulation of connexin 43 (Cx43) hemichannels. *Proceedings of the National Academy of Sciences of the United States of America*, **100**, 11388–11393.

Contreras, J.E., Sánchez, H.A., Eugenin, E.A., Speidel, D., Theis, M., Willecke, K., Bukauskas, F.F., Bennett, M.V.L. & Sáez, J.C. (2002). Metabolic inhibition induces opening of unapposed connexin 43 gap junction hemichannels and reduces gap junctional communication in cortical astrocytes in culture. *Proceedings of the National Academy of Sciences of the United States of America*, **99**, 495–500.

Cottrell, G.T. & Burt, J.M. (2005). Functional consequences of heterogeneous gap junction channel formation and its influence in health and disease. *Biochimica et biophysica acta*, **1711**, 126–141.

Cruciani, V. & Mikalsen, S.-O. (2006). The vertebrate connexin family. *Cellular and molecular life sciences : CMLS*, **63**, 1125–1140.

Das, S., Smith, T.D., Sarma, J.D., Ritzenthaler, J.D., Maza, J., Kaplan, B.E., Cunningham, L.A., Suaud, L., Hubbard, M.J., Rubenstein, R.C. & Koval, M. (2009). ERp29 restricts Connexin43 oligomerization in the endoplasmic reticulum. *Molecular biology of the cell*, **20**, 2593–2604.

Desplantez, T., Grikscheit, K., Thomas, N.M., Peters, N.S., Severs, N.J. & Dupont, E. (2015). Relating specific connexin co-expression ratio to connexon composition and gap junction function. *Journal of molecular and cellular cardiology*, **89**, 195–202.

Dhein, S. (2004). Pharmacology of gap junctions in the cardiovascular system. *Cardiovascular research*, **62**, 287–298.

Di, W.-L., Gu, Y., Common, J.E.A., Aasen, T., O'Toole, E.A., Kelsell, D.P. & Zicha, D. (2005). Connexin interaction patterns in keratinocytes revealed morphologically and by FRET analysis. *Journal of cell science*, **118**, 1505–1514.

Diez, J.A., Ahmad, S. & Evans, W.H. (1999). Assembly of heteromeric connexons in guinea-pig liver en route to the Golgi apparatus, plasma membrane and gap junctions. *European journal of biochemistry / FEBS*, **262**, 142–148.

Donaldson, P., Kistler, J. & Mathias, R.T. (2001). Molecular solutions to mammalian lens transparency. *News in physiological sciences : an international journal of physiology produced jointly by the International Union of Physiological Sciences and the American Physiological Society*, **16**, 118–123.

Eastman, S.D., Chen, T.H.-P., Falk, M.M., Mendelson, T.C. & Iovine, M.K. (2006). Phylogenetic analysis of three complete gap junction gene families reveals lineage-specific duplications and highly supported gene classes. *Genomics*, **87**, 265–274.

Ebihara, L., Tong, J.-J., Vertel, B., White, T.W. & Chen, T.-L. (2011). Properties of connexin 46 hemichannels in dissociated lens fiber cells. *Investigative ophthalmology & visual science*, **52**, 882–889.

Falk, M.M. & Gilula, N.B. (1998). Connexin membrane protein biosynthesis is influenced by polypeptide positioning within the translocon and signal peptidase access. *The Journal of biological chemistry*, **273**, 7856–7864.

Falk, M.M., Kells, R.M. & Berthoud, V.M. (2014). Degradation of connexins and gap junctions. *FEBS letters*, **588**, 1221–1229.

Falk, M.M., Kumar, N.M. & Gilula, N.B. (1994). Membrane insertion of gap junction connexins: polytopic channel forming membrane proteins. *The Journal of cell biology*, **127**, 343–355.

Fallon, R.F. & Goodenough, D.A. (1981). Five-hour half-life of mouse liver gap-junction protein. *The Journal of cell biology*, **90**, 521–526.

Figueroa, V., Sáez, P.J., Salas, J.D., Salas, D., Jara, O., Martínez, A.D., Sáez, J.C. & Retamal, M.A. (2013). Linoleic acid induces opening of connexin26 hemichannels through a PI3K/Akt/Ca(2+)-dependent pathway. *Biochimica et biophysica acta*, **1828**, 1169–1179.

Foote, C.I., Zhou, L., Zhu, X. & Nicholson, B.J. (1998). The pattern of disulfide linkages in the extracellular loop regions of connexin 32 suggests a model for the docking interface of gap junctions. *The Journal of cell biology*, **140**, 1187–1197.

Friend, D.S. & Gilula, N.B. (1972). Variations in tight and gap junctions in mammalian tissues. *The Journal of cell biology*, **53**, 758–776.

Gassmann, O., Kreir, M., Ambrosi, C., Pranskevich, J., Oshima, A., Röling, C., Sosinsky, G., Fertig, N. & Steinem, C. (2009). The M34A mutant of Connexin26 reveals active conductance states in pore-suspending membranes. *Journal of structural biology*, **168**, 168–176.

Gemel, J., Lin, X., Collins, R., Veenstra, R.D. & Beyer, E.C. (2008). Cx30.2 can form heteromeric gap junction channels with other cardiac connexins. *Biochemical and biophysical research communications*, **369**, 388–394.

Gemel, J., Lin, X., Veenstra, R.D. & Beyer, E.C. (2006). N-terminal residues in Cx43 and Cx40 determine physiological properties of gap junction channels, but do not influence heteromeric assembly with each other or with Cx26. *Journal of cell science*, **119**, 2258–2268.

Gemel, J., Nelson, T.K., Burt, J.M. & Beyer, E.C. (2012). Inducible coexpression of connexin37 or connexin40 with connexin43 selectively affects intercellular molecular transfer. *The Journal of membrane biology*, **245**, 231–241.

Ghoshroy, S., Goodenough, D.A. & Sosinsky, G.E. (1995). Preparation, characterization, and structure of half gap junctional layers split with urea and EGTA. *The Journal of membrane biology*, **146**, 15–28.

Gilleron, J., Carette, D., Chevallier, D., Segretain, D. & Pointis, G. (2012). Molecular connexin partner remodeling orchestrates connexin traffic: from physiology to pathophysiology. *Critical reviews in biochemistry and molecular biology*, **47**, 407–423.

Gilleron, J., Carette, D., Fiorini, C., Dompierre, J., Macia, E., Denizot, J.-P., Segretain, D. & Pointis, G. (2011). The large GTPase dynamin2: A new player in connexin 43 gap junction endocytosis, recycling and degradation. *The international journal of biochemistry \& cell biology*, **43**, 1208–1217.

Gong, X., Baldo, G.J., Kumar, N.M., Gilula, N.B. & Mathias, R.T. (1998). Gap junctional coupling in lenses lacking alpha3 connexin. *Proceedings of the National Academy of Sciences of the United States of America*, **95**, 15303–15308.

Gong, X.-Q., Nakagawa, S., Tsukihara, T. & Bai, D. (2013). A mechanism of gap junction docking revealed by functional rescue of a human-disease-linked connexin mutant. *Journal of cell science*, **126**, 3113–3120.

Goodenough, D.A. & Gilula, N.B. (1974). The splitting of hepatocyte gap junctions and zonulae occludentes with hypertonic disaccharides. *The Journal of cell biology*, **61**, 575–590.

Görlich, D. & Rapoport, T.A. (1993). Protein translocation into proteoliposomes reconstituted from purified components of the endoplasmic reticulum membrane. *Cell*, **75**, 615–630.

Gray, K.A., Daugherty, L.C., Gordon, S.M., Seal, R.L., Wright, M.W. & Bruford, E.A. (2013). Genenames.org: the HGNC resources in 2013. *Nucleic acids research*, **41**, D545–52.

Gregory, W.A. & Bennett, M.V. (1988). Gap junctions in goldfish preoptic ependyma: regional variation in cellular differentiation. *Brain research*, **470**, 205–216.

Gumpert, A.M., Varco, J.S., Baker, S.M., Piehl, M. & Falk, M.M. (2008). Double-membrane gap junction internalization requires the clathrin-mediated endocytic machinery. *FEBS letters*, **582**, 2887–2892.

Harris, A.L. (2001). Emerging issues of connexin channels: biophysics fills the gap. *Quarterly reviews of biophysics*, **34**, 325–472.

Harris, A.L. (2007). Connexin channel permeability to cytoplasmic molecules. *Progress in biophysics and molecular biology*, **94**, 120–143.

Harris, A.L. (2018). Electrical coupling and its channels. *The Journal of general physiology*, jgp.201812203.

Hervé, J.-C. (2012). The communicating junctions, composition, structure and characteristics. *Biochimica et biophysica acta*, **1818**, 1803–1806.

Hervé, J.-C., Derangeon, M., Sarrouilhe, D., Giepmans, B.N.G. & Bourmeyster, N. (2012). Gap junctional channels are parts of multiprotein complexes. *Biochimica et biophysica acta*, **1818**, 1844–1865.

Hopperstad, M.G., Srinivas, M. & Spray, D.C. (2000). Properties of gap junction channels formed by Cx46 alone and in combination with Cx50. *Biophysical journal*, **79**, 1954–1966.

Hu, X. & Dahl, G. (1999). Exchange of conductance and gating properties between gap junction hemichannels. *FEBS letters*, **451**, 113–117.

Isacoff, E.Y., Jan, Y.N. & Jan, L.Y. (1990). Evidence for the formation of heteromultimeric potassium channels in Xenopus oocytes. *Nature*, **345**, 530–534.

Jara, O., Acuña, R., García, I.E., Maripillán, J., Figueroa, V., Sáez, J.C., Araya-Secchi, R., Lagos, C.F., Perez-Acle, T., Berthoud, V.M., Beyer, E.C. & Martínez, A.D. (2012). Critical role of the first transmembrane domain of Cx26 in regulating oligomerization and function. *Molecular biology of the cell*, **23**, 3299–3311.

Jiang, J.X. & Goodenough, D.A. (1998). Phosphorylation of lens-fiber connexins in lens organ cultures. *European journal of biochemistry / FEBS*, **255**, 37–44.

Jordan, K., Solan, J.L., Dominguez, M., Sia, M., Hand, A., Lampe, P.D. & Laird, D.W. (1999). Trafficking, assembly, and function of a connexin43-green fluorescent protein chimera in live mammalian cells. *Molecular biology of the cell*, **10**, 2033–2050.

Kelly, J.J., Simek, J. & Laird, D.W. (2015). Mechanisms linking connexin mutations to human diseases. *Cell and tissue research*, **360**, 701–721.

Kelly, S.C., Ratajczak, P., Keller, M., Purcell, S.M., Griffin, T. & Richard, G. (2006). A novel GJA 1 mutation in oculo-dento-digital dysplasia with curly hair and hyperkeratosis. *European journal of dermatology : EJD*, **16**, 241–245.

Kenworthy, A.K. (2001). Imaging protein-protein interactions using fluorescence resonance energy transfer microscopy. *Methods (San Diego, Calif.)*, **24**, 289–296.

Kenworthy, A.K. & Edidin, M. (1998). Distribution of a glycosylphosphatidylinositol-anchored protein at the apical surface of MDCK cells examined at a resolution of. *The Journal of cell biology*, **142**, 69–84.

Kleopa, K.A., Abrams, C.K. & Scherer, S.S. (2012). How do mutations in GJB1 cause X-linked Charcot-Marie-Tooth disease? *Brain research*, **1487**, 198–205.

Kopanic, J.L., Schlingmann, B., Koval, M., Lau, A.F., Sorgen, P.L. & Su, V.F. (2015). Degradation of gap junction connexins is regulated by the interaction with Cx43-interacting protein of 75 kDa (CIP75). *The Biochemical journal*, **466**, 571–585.

Koval, M. (2006). Pathways and control of connexin oligomerization. *Trends in cell biology*, **16**, 159–166.

Koval, M., Harley, J.E., Hick, E. & Steinberg, T.H. (1997). Connexin46 is retained as monomers in a trans-Golgi compartment of osteoblastic cells. *The Journal of cell biology*, **137**, 847–857.

Koval, M., Molina, S.A. & Burt, J.M. (2014). Mix and match: Investigating heteromeric and heterotypic gap junction channels in model systems and native tissues. *FBBS Letters*, **588**, 1193–1204.

Kreuzberg, M.M., Schrickel, J.W., Ghanem, A., Kim, J.-S., Degen, J., Janssen-Bienhold, U., Lewalter, T., Tiemann, K. & Willecke, K. (2006a). Connexin30.2 containing gap junction channels decelerate impulse propagation through the atrioventricular node. *Proceedings of the National Academy of Sciences of the United States of America*, **103**, 5959–5964.

Kreuzberg, M.M., Willecke, K. & Bukauskas, F.F. (2006b). Connexin-mediated cardiac impulse propagation: connexin 30.2 slows atrioventricular conduction in mouse heart. *Trends in cardiovascular medicine*, **16**, 266–272.

Kronengold, J., Trexler, E.B., Bukauskas, F.F., Bargiello, T.A. & Verselis, V.K. (2003). Single-channel SCAM identifies pore-lining residues in the first extracellular loop and first transmembrane domains of Cx46 hemichannels. *The Journal of general physiology*, **122**, 389–405.

Kumar, N.M. & Gilula, N.B. (1996). The gap junction communication channel. *Cell*, **84**, 381–388.

Kuryatov, A. & Lindstrom, J. (2011). Expression of functional human α6β2β3* acetylcholine receptors in Xenopus laevis oocytes achieved through subunit chimeras and concatamers. *Molecular pharmacology*, **79**, 126–140.

Lagree, V., Brunschwig, K., Lopez, P., Gilula, N.B., Richard, G. & Falk, M.M. (2003). Specific amino-acid residues in the N-terminus and TM3 implicated in channel function and oligomerization compatibility of connexin43. *Journal of cell science*, **116**, 3189–3201.

Laing, J.G., Tadros, P.N., Westphale, E.M. & Beyer, E.C. (1997). Degradation of connexin43 gap junctions involves both the proteasome and the lysosome. *Experimental cell research*, **236**, 482–492.

Laird, D.W. & Revel, J.P. (1990). Biochemical and immunochemical analysis of the arrangement of connexin43 in rat heart gap junction membranes. *Journal of cell science*, **97 (Pt 1)**, 109–117.

Laird, D.W., Jordan, K., Thomas, T., Qin, H., Fistouris, P. & Shao, Q. (2001). Comparative analysis and application of fluorescent protein-tagged connexins. *Microscopy research and technique*, **52**, 263–272.

Lampe, P.D. & Lau, A.F. (2004). The effects of connexin phosphorylation on gap junctional communication. *The international journal of biochemistry \& cell biology*, **36**, 1171–1186.

Langlois, S., Cowan, K.N., Shao, Q., Cowan, B.J. & Laird, D.W. (2008). Caveolin-1 and -2 interact with connexin43 and regulate gap junctional intercellular communication in keratinocytes. *Molecular biology of the cell*, **19**, 912–928.

Larsen, W.J., Tung, H.N. & Polking, C. (1981). Response of granulosa cell gap junctions to human chorionic gonadotropin (hCG) at ovulation. *Biology of reproduction*, **25**, 1119–1134.

Larsen, W.J., Tung, H.N., Murray, S.A. & Swenson, C.A. (1979). Evidence for the participation of actin microfilaments and bristle coats in the internalization of gap junction membrane. *The Journal of cell biology*, **83**, 576–587.

Lauf, U., Giepmans, B.N.G., Lopez, P., Braconnot, S., Chen, S.-C. & Falk, M.M. (2002). Dynamic trafficking and delivery of connexons to the plasma membrane and accretion to gap junctions in living cells. *Proceedings of the National Academy of Sciences of the United States of America*, **99**, 10446–10451.

Leybaert, L., Lampe, P.D., Dhein, S., Kwak, B.R., Ferdinandy, P., Beyer, E.C., Laird, D.W., Naus, C.C., Green, C.R. & Schulz, R. (2017). Connexins in Cardiovascular and Neurovascular Health and Disease: Pharmacological Implications. *Pharmacological reviews*, **69**, 396–478.

Li, C., Meng, Q., Yu, X., Jing, X., Xu, P. & Luo, D. (2012). Regulatory effect of connexin 43 on basal Ca2+ signaling in rat ventricular myocytes. *PloS one*, **7**, e36165.

Li, Y., Wang, J., Dong, B. & Man, H. (2004). A novel connexin46 (GJA3) mutation in autosomal dominant congenital nuclear pulverulent cataract. *Molecular vision*, **10**, 668–671.

Lin, X., Gemel, J., Glass, A., Zemlin, C.W., Beyer, E.C. & Veenstra, R.D. (2010). Connexin40 and connexin43 determine gating properties of atrial gap junction channels. *Journal of molecular and cellular cardiology*, **48**, 238–245.

Locke, D., Jamieson, S., Stein, T., Liu, J., Hodgins, M.B., Harris, A.L. & Gusterson, B. (2007). Nature of Cx30-containing channels in the adult mouse mammary gland. *Cell and tissue research*, **328**, 97–107.

Lopez, W., Ramachandran, J., Alsamarah, A., Luo, Y., Harris, A.L. & Contreras, J.E. (2016). Mechanism of gating by calcium in connexin hemichannels. *Proceedings of the National Academy of Sciences of the United States of America*, **113**, E7986–E7995.

Maeda, S. & Tsukihara, T. (2011). Structure of the gap junction channel and its implications for its biological functions. *Cellular and molecular life sciences : CMLS*, **68**, 1115–1129.

Maeda, S., Nakagawa, S., Suga, M., Yamashita, E., Oshima, A., Fujiyoshi, Y. & Tsukihara, T. (2009). Structure of the connexin 26 gap junction channel at 3.5 A resolution. *Nature*, **458**, 597–602.

Magnotti, L.M., Goodenough, D.A. & Paul, D.L. (2011a). Functional heterotypic interactions between astrocyte and oligodendrocyte connexins. *Glia*, **59**, 26–34.

Magnotti, L.M., Goodenough, D.A. & Paul, D.L. (2011b). Deletion of oligodendrocyte Cx32 and astrocyte Cx43 causes white matter vacuolation, astrocyte loss and early mortality. *Glia*, **59**, 1064–1074.

Manthey, D., Banach, K., Desplantez, T., Lee, C.G., Kozak, C.A., Traub, O., Weingart, R. & Willecke, K. (2001). Intracellular domains of mouse connexin26 and -30 affect diffusional and electrical properties of gap junction channels. *The Journal of membrane biology*, **181**, 137–148.

Martin, P.E., Easton, J.A., Hodgins, M.B. & Wright, C.S. (2014). Connexins: sensors of epidermal integrity that are therapeutic targets. *FEBS letters*, **588**, 1304–1314.

Martin, P.E., Errington, R.J. & Evans, W.H. (2001). Gap junction assembly: multiple connexin fluorophores identify complex trafficking pathways. *Cell communication \& adhesion*, **8**, 243–248.

Martinez-Wittinghan, F.J., Sellitto, C., White, T.W., Mathias, R.T., Paul, D. & Goodenough, D.A. (2004). Lens gap junctional coupling is modulated by connexin identity and the locus of gene expression. *Investigative ophthalmology & visual science*, **45**, 3629–3637.

Martínez, A.D., Maripillán, J., Acuña, R., Minogue, P.J., Berthoud, V.M. & Beyer, E.C. (2011). Different domains are critical for oligomerization compatibility of different connexins. *The Biochemical journal*, **436**, 35–43.

Mathias, R.T., Kistler, J. & Donaldson, P. (2007). The lens circulation. *The Journal of membrane biology*, **216**, 1–16.

Mathias, R.T., White, T.W. & Gong, X. (2010). Lens gap junctions in growth, differentiation, and homeostasis. *Physiological reviews*, **90**, 179–206.

Maza, J., Sarma, Das, J. & Koval, M. (2005). Defining a minimal motif required to prevent connexin oligomerization in the endoplasmic reticulum. *The Journal of biological chemistry*, **280**, 21115–21121.

Mazet, F., Wittenberg, B.A. & Spray, D.C. (1985). Fate of intercellular junctions in isolated adult rat cardiac cells. *Circulation research*, **56**, 195–204.

Mese, G., Sellitto, C., Li, L., Wang, H.-Z., Valiunas, V., Richard, G., Brink, P.R. & White, T.W. (2011). The Cx26-G45E mutation displays increased hemichannel activity in a mouse model of the lethal form of keratitis-ichthyosis-deafness syndrome. *Molecular biology of the cell*, **22**, 4776–4786.

Milks, L.C., Kumar, N.M., Houghten, R., Unwin, N. & Gilula, N.B. (1988). Topology of the 32-kd liver gap junction protein determined by site-directed antibody localizations. *The EMBO journal*, **7**, 2967–2975.

Moreno, A.P. & Lau, A.F. (2007). Gap junction channel gating modulated through protein phosphorylation. *Progress in biophysics and molecular biology*, **94**, 107–119.

Murray, S.A., Williams, S.Y., Dillard, C.Y., Narayanan, S.K. & McCauley, J. (1997). Relationship of cytoskeletal filaments to annular gap junction expression in human adrenal cortical tumor cells in culture. *Experimental cell research*, **234**, 398–404.

Musil, L.S. & Goodenough, D.A. (1993). Multisubunit assembly of an integral plasma membrane channel protein, gap junction connexin43, occurs after exit from the ER. *Cell*, **74**, 1065–1077.

Musil, L.S., Le, A.C., VanSlyke, J.K. & Roberts, L.M. (2000). Regulation of connexin degradation as a mechanism to increase gap junction assembly and function. *The Journal of biological chemistry*, **275**, 25207–25215.

Müller, D.J., Hand, G.M., Engel, A. & Sosinsky, G.E. (2002). Conformational changes in surface structures of isolated connexin 26 gap junctions. *The EMBO journal*, **21**, 3598–3607.

Nagy, J.I., Ionescu, A.-V., Lynn, B.D. & Rash, J.E. (2003). Coupling of astrocyte connexins Cx26, Cx30, Cx43 to oligodendrocyte Cx29, Cx32, Cx47: Implications from normal and connexin32 knockout mice. *Glia*, **44**, 205–218.

Nakagawa, S., Gong, X.-Q., Maeda, S., Dong, Y., Misumi, Y., Tsukihara, T. & Bai, D. (2011). Asparagine 175 of connexin32 is a critical residue for docking and forming functional heterotypic gap junction channels with connexin26. *The Journal of biological chemistry*, **286**, 19672–19681.

Nakagawa, S., Maeda, S. & Tsukihara, T. (2010). Structural and functional studies of gap junction channels. *Current opinion in structural biology*, **20**, 423–430.

Naus, C.C., Hearn, S., Zhu, D., Nicholson, B.J. & Shivers, R.R. (1993). Ultrastructural analysis of gap junctions in C6 glioma cells transfected with connexin43 cDNA. *Experimental cell research*, **206**, 72–84.

Neijssen, J., Herberts, C., Drijfhout, J.W., Reits, E., Janssen, L. & Neefjes, J. (2005). Cross-presentation by intercellular peptide transfer through gap junctions. *Nature*, **434**, 83–88.

Nicholson, B.J. (2003). Gap junctions - from cell to molecule. *Journal of cell science*, **116**, 4479–4481.

Nicholson, S.M. & Bruzzone, R. (1997). Gap junctions: getting the message through. *Current biology : CB*, **7**, R340–4.

Nickel, B.M., DeFranco, B.H., Gay, V.L. & Murray, S.A. (2008). Clathrin and Cx43 gap junction plaque endoexocytosis. *Biochemical and biophysical research communications*, **374**, 679–682.

Nielsen, M.S., Nygaard Axelsen, L., Sorgen, P.L., Verma, V., Delmar, M. & Holstein-Rathlou, N.-H. (2012). Gap junctions. *Comprehensive Physiology*, **2**, 1981–2035.

Niessen, H., Harz, H., Bedner, P., Krämer, K. & Willecke, K. (2000). Selective permeability of different connexin channels to the second messenger inositol 1,4,5-trisphosphate. *Journal of cell science*, **113 (Pt 8)**, 1365–1372.

Oh, S. & Bargiello, T.A. (2015). Voltage regulation of connexin channel conductance. *Yonsei medical journal*, **56**, 1–15.

Oh, S., Rubin, J.B., Bennett, M.V., Verselis, V.K. & Bargiello, T.A. (1999). Molecular determinants of electrical rectification of single channel conductance in gap junctions formed by connexins 26 and 32. *The Journal of general physiology*, **114**, 339–364.

Orthmann-Murphy, J.L., Abrams, C.K. & Scherer, S.S. (2008). Gap junctions couple astrocytes and oligodendrocytes. *Journal of molecular neuroscience : MN*, **35**, 101–116.

Orthmann-Murphy, J.L., Freidin, M., Fischer, E., Scherer, S.S. & Abrams, C.K. (2007). Two distinct heterotypic channels mediate gap junction coupling between astrocyte and oligodendrocyte connexins. *The Journal of neuroscience : the official journal of the Society for Neuroscience*, **27**, 13949–13957.

Palacios-Prado, N. & Bukauskas, F.F. (2009). Heterotypic gap junction channels as voltage-sensitive valves for intercellular signaling. *Proceedings of the National Academy of Sciences of the United States of America*, **106**, 14855–14860.

Pan, F., Mills, S.L. & Massey, S.C. (2007). Screening of gap junction antagonists on dye coupling in the rabbit retina. *Visual neuroscience*, **24**, 609–618.

Pfeffer, S.R. & Rothman, J.E. (1987). Biosynthetic protein transport and sorting by the endoplasmic reticulum and Golgi. *Annual review of biochemistry*, **56**, 829–852.

Phelan, P. (2005). Innexins: members of an evolutionarily conserved family of gap-junction proteins. *Biochimica et biophysica acta*, **1711**, 225–245.

Piehl, M., Lehmann, C., Gumpert, A., Denizot, J.-P., Segretain, D. & Falk, M.M. (2007). Internalization of large double-membrane intercellular vesicles by a clathrin-dependent endocytic process. *Molecular biology of the cell*, **18**, 337–347.

Rackauskas, M., Kreuzberg, M.M., Pranevicius, M., Willecke, K., Verselis, V.K. & Bukauskas, F.F. (2007a). Gating properties of heterotypic gap junction channels formed of connexins 40, 43, and 45. *Biophysical journal*, **92**, 1952–1965.

Rackauskas, M., Verselis, V.K. & Bukauskas, F.F. (2007b). Permeability of homotypic and heterotypic gap junction channels formed of cardiac connexins mCx30.2, Cx40, Cx43, and Cx45. *American journal of physiology. Heart and circulatory physiology*, **293**, H1729–36.

Rash, J.E., Kamasawa, N., Davidson, K.G.V., Yasumura, T., Pereda, A.E. & Nagy, J.I. (2012). Connexin composition in apposed gap junction hemiplaques revealed by matched double-replica freeze-fracture replica immunogold labeling. *The Journal of membrane biology*, **245**, 333–344.

Retamal, M.A. & Sáez, J.C. (2014). Hemichannels; from the molecule to the function. *Frontiers in physiology*, **5**, 411.

Retamal, M.A., Froger, N., Palacios-Prado, N., Ezan, P., Sáez, P.J., Sáez, J.C. & Giaume, C. (2007). Cx43 hemichannels and gap junction channels in astrocytes are regulated oppositely by proinflammatory cytokines released from activated microglia. *The Journal of neuroscience : the official journal of the Society for Neuroscience*, **27**, 13781–13792.

Revel, J.P. & Karnovsky, M.J. (1967). Hexagonal array of subunits in intercellular junctions of the mouse heart and liver. *The Journal of cell biology*, **33**, C7–C12.

Sáez, J.C., Berthoud, V.M., Branes, M.C., Martínez, A.D. & Beyer, E.C. (2003). Plasma membrane channels formed by connexins: their regulation and functions. *Physiological reviews*, **83**, 1359–1400.

Sáez, J.C., Retamal, M.A., Basilio, D., Bukauskas, F.F. & Bennett, M.V.L. (2005). Connexin-based gap junction hemichannels: gating mechanisms. *Biochimica et biophysica acta*, **1711**, 215–224.

Sánchez, H.A., Mese, G., Srinivas, M., White, T.W. & Verselis, V.K. (2010). Differentially altered Ca2+ regulation and Ca2+ permeability in Cx26 hemichannels formed by the A40V and G45E mutations that cause keratitis ichthyosis deafness syndrome. *The Journal of general physiology*, **136**, 47–62.

Scemes, E., Spray, D.C. & Meda, P. (2009). Connexins, pannexins, innexins: novel roles of "hemi-channels". *Pflügers Archiv : European journal of physiology*, **457**, 1207–1226.

Schadzek, P., Stahl, Y., Preller, M. & Ngezahayo, A. (2019) Analysis of the dominant mutation N188T of human connexin46 (hCx46) using concatenation and molecular dynamics simulation. *FEBS open bio*, DOI 10.1002/2211-5463.12624.

Schadzek, P., Hermes, D., Stahl, Y., Dilger, N. & Ngezahayo, A. (2018). Concatenation of Human Connexin26 (hCx26) and Human Connexin46 (hCx46) for the Analysis of Heteromeric Gap Junction Hemichannels and Heterotypic Gap Junction Channels. *International journal of molecular sciences*, **19**, 2742.

Schadzek, P., Schlingmann, B., Schaarschmidt, F., Lindner, J., Koval, M., Heisterkamp, A., Ngezahayo, A. & Preller, M. (2016). Data of the molecular dynamics simulations of mutations in the human connexin46 docking interface. *Data in Brief*, **7**, 93–99.

Schadzek, P., Schlingmann, B., Schaarschmidt, F., Lindner, J., Koval, M., Heisterkamp, A., Preller, M. & Ngezahayo, A. (2015). The cataract related mutation N188T in human connexin46 (hCx46) revealed a critical role for residue N188 in the docking process of gap junction channels. *Biochimica et biophysica acta*, **1858**, 57–66.

Schlingmann, B., Schadzek, P., Busko, S., Heisterkamp, A. & Ngezahayo, A. (2012). Cataract-associated D3Y mutation of human connexin46 (hCx46) increases the dye coupling of gap junction channels and suppresses the voltage sensitivity of hemichannels. *Journal of bioenergetics and biomembranes*, **44**, 607–614.

Schlingmann, B., Schadzek, P., Hemmerling, F., Schaarschmidt, F., Heisterkamp, A. & Ngezahayo, A. (2013). The role of the C-terminus in functional expression and internalization of rat connexin46 (rCx46). *Journal of bioenergetics and biomembranes*, **45**, 59–70.

Schubert, A.-L., Schubert, W., Spray, D.C. & Lisanti, M.P. (2002). Connexin family members target to lipid raft domains and interact with caveolin-1. *Biochemistry*, **41**, 5754–5764.

Segretain, D. & Falk, M.M. (2004). Regulation of connexin biosynthesis, assembly, gap junction formation, and removal. *Biochimica et biophysica acta*, **1662**, 3–21.

Sigel, E., Kaur, K.H., Lüscher, B.P. & Baur, R. (2009). Use of concatamers to study GABAA receptor architecture and function: application to delta-subunit-containing receptors and possible pitfalls. *Biochemical Society transactions*, **37**, 1338–1342.

Slavi, N., Rubinos, C., Li, L., Sellitto, C., White, T.W., Mathias, R. & Srinivas, M. (2014). Cx46 Gap Junctions Provide a Pathway for the Delivery of Glutathione to the Lens Nucleus. *The Journal of biological chemistry*, **289**, 32694–32702.

Slavi, N., Wang, Z., Harvey, L., Schey, K.L. & Srinivas, M. (2016). Identification and Functional Assessment of Age-Dependent Truncations to Cx46 and Cx50 in the Human Lens. *Investigative ophthalmology & visual science*, **57**, 5714–5722.

Smith, T.D., Mohankumar, A., Minogue, P.J., Beyer, E.C., Berthoud, V.M. & Koval, M. (2012). Cytoplasmic amino acids within the membrane interface region influence connexin oligomerization. *The Journal of membrane biology*, **245**, 221–230.

Solan, J.L. & Lampe, P.D. (2005). Connexin phosphorylation as a regulatory event linked to gap junction channel assembly. *Biochimica et biophysica acta*, **1711**, 154–163.

Sorgen, P.L., Duffy, H.S., Sahoo, P., Coombs, W., Delmar, M. & Spray, D.C. (2004). Structural changes in the carboxyl terminus of the gap junction protein connexin43 indicates signaling between binding domains for c-Src and zonula occludens-1. *The Journal of biological chemistry*, **279**, 54695–54701.

Sosinsky, G.E. & Nicholson, B.J. (2005). Structural organization of gap junction channels. *Biochimica et biophysica acta*, **1711**, 99–125.

Söhl, G. & Willecke, K. (2003). An update on connexin genes and their nomenclature in mouse and man. *Cell communication \& adhesion*, **10**, 173–180.

Söhl, G. & Willecke, K. (2004). Gap junctions and the connexin protein family. *Cardiovascular research*, **62**, 228–232.

Srinivas, M., Kronengold, J., Bukauskas, F.F., Bargiello, T.A. & Verselis, V.K. (2005). Correlative studies of gating in Cx46 and Cx50 hemichannels and gap junction channels. *Biophysical journal*, **88**, 1725–1739.

Srinivas, M., Verselis, V.K. & White, T.W. (2018). Human diseases associated with connexin mutations. *Biochimica et biophysica acta. Biomembranes*, **1860**, 192–201.

Steinbach, J.H. & Akk, G. (2011). Use of concatemers of ligand-gated ion channel subunits to study mechanisms of steroid potentiation. *Anesthesiology*, **115**, 1328–1337.

Stoop, R., Thomas, S., Rassendren, F., Kawashima, E., Buell, G., Surprenant, A. & North, R.A. (1999). Contribution of individual subunits to the multimeric P2X(2) receptor: estimates based on methanethiosulfonate block at T336C. *Molecular pharmacology*, **56**, 973–981.

Suchyna, T.M., Nitsche, J.M., Chilton, M., Harris, A.L., Veenstra, R.D. & Nicholson, B.J. (1999). Different ionic selectivities for connexins 26 and 32 produce rectifying gap junction channels. *Biophysical journal*, **77**, 2968–2987.

Sun, J., Ahmad, S., Chen, S., Tang, W., Zhang, Y., Chen, P. & Lin, X. (2005). Cochlear gap junctions coassembled from Cx26 and 30 show faster intercellular Ca2+ signaling than homomeric counterparts. *American journal of physiology. Cell physiology*, **288**, C613–23.

Thévenin, A.F., Kowal, T.J., Fong, J.T., Kells, R.M., Fisher, C.G. & Falk, M.M. (2013). Proteins and mechanisms regulating gap-junction assembly, internalization, and degradation. *Physiology*, **28**, 93–116.

Thimm, J., Mechler, A., Lin, H., Rhee, S. & Lal, R. (2005). Calcium-dependent open/closed conformations and interfacial energy maps of reconstituted hemichannels. *The Journal of biological chemistry*, **280**, 10646–10654.

Thomas, T., Jordan, K. & Laird, D.W. (2001). Role of cytoskeletal elements in the recruitment of Cx43-GFP and Cx26-YFP into gap junctions. *Cell communication \& adhesion*, **8**, 231–236.

Thomas, T., Jordan, K., Simek, J., Shao, Q., Jedeszko, C., Walton, P. & Laird, D.W. (2005). Mechanisms of Cx43 and Cx26 transport to the plasma membrane and gap junction regeneration. *Journal of cell science*, **118**, 4451–4462.

Tong, J.-J., Sohn, B.C.H., Lam, A., Walters, D.E., Vertel, B.M. & Ebihara, L. (2013). Properties of two cataract-associated mutations located in the NH2 terminus of connexin 46. *American journal of physiology. Cell physiology*, **304**, C823–32.

Trexler, E.B., Bennett, M.V., Bargiello, T.A. & Verselis, V.K. (1996). Voltage gating and permeation in a gap junction hemichannel. *Proceedings of the National Academy of Sciences of the United States of America*, **93**, 5836–5841.

Trexler, E.B., Bukauskas, F.F., Kronengold, J., Bargiello, T.A. & Verselis, V.K. (2000). The first extracellular loop domain is a major determinant of charge selectivity in connexin46 channels. *Biophysical journal*, **79**, 3036–3051.

Unger, V.M., Kumar, N.M., Gilula, N.B. & Yeager, M. (1999). Three-dimensional structure of a recombinant gap junction membrane channel. *Science (New York, N.Y.)*, **283**, 1176–1180.

Van Norstrand, D.W., Asimaki, A., Rubinos, C., Dolmatova, E., Srinivas, M., Tester, D.J., Saffitz, J.E., Duffy, H.S. & Ackerman, M.J. (2012). Connexin43 mutation causes heterogeneous gap junction loss and sudden infant death. *Circulation*, **125**, 474–481.

Veitia, R.A. (2007). Exploring the molecular etiology of dominant-negative mutations. *The Plant cell*, **19**, 3843–3851.

Wasseff, S.K. & Scherer, S.S. (2011). Cx32 and Cx47 mediate oligodendrocyte:astrocyte and oligodendrocyte:oligodendrocyte gap junction coupling. *Neurobiology of disease*, **42**, 506–513.

White, T.W., Bruzzone, R., Wolfram, S., Paul, D.L. & Goodenough, D.A. (1994). Selective interactions among the multiple connexin proteins expressed in the vertebrate lens: the second extracellular domain is a determinant of compatibility between connexins. *The Journal of cell biology*, **125**, 879–892.

White, T.W., Gao, Y., Li, L., Sellitto, C. & Srinivas, M. (2007). Optimal lens epithelial cell proliferation is dependent on the connexin isoform providing gap junctional coupling. *Investigative ophthalmology & visual science*, **48**, 5630–5637.

White, T.W., Paul, D.L., Goodenough, D.A. & Bruzzone, R. (1995). Functional analysis of selective interactions among rodent connexins. *Molecular biology of the cell*, **6**, 459–470.

Willecke, K., Eiberger, J., Degen, J., Eckardt, D., Romualdi, A., Güldenagel, M., Deutsch, U. & Söhl, G. (2002). Structural and functional diversity of connexin genes in the mouse and human genome. *Biological chemistry*, **383**, 725–737.

Yen, M.R. & Saier, M.H. (2007). Gap junctional proteins of animals: the innexin/pannexin superfamily. *Progress in biophysics and molecular biology*, **94**, 5–14.

Yu, F.H. & Catterall, W.A. (2003). Overview of the voltage-gated sodium channel family. *Genome biology*, **4**, 207.

Yum, S.W., Zhang, J., Valiunas, V., Kanaporis, G., Brink, P.R., White, T.W. & Scherer, S.S. (2007). Human connexin26 and connexin30 form functional heteromeric and heterotypic channels. *American journal of physiology. Cell physiology*, **293**, C1032–48.

Zhang, J.T. & Nicholson, B.J. (1994). The topological structure of connexin 26 and its distribution compared to connexin 32 in hepatic gap junctions. *The Journal of membrane biology*, **139**, 15–29.

Zhang, W., Lohman, A.W., Zhuravlova, Y., Lu, X., Wiens, M.D., Hoi, H., Yaganoglu, S., Mohr, M.A., Kitova, E.N., Klassen, J.S., Pantazis, P., Thompson, R.J. & Campbell, R.E. (2017). Optogenetic control with a photocleavable protein, PhoCl. *Nature methods*, **14**, 391–394.

Zhang, X., Wang, L., Wang, J., Dong, B. & Li, Y. (2012). Coralliform cataract caused by a novel connexin46 (GJA3) mutation in a Chinese family. *Molecular vision*, **18**, 203–210.

Zhong, G., Akoum, N., Appadurai, D.A., Hayrapetyan, V., Ahmed, O., Martínez, A.D., Beyer, E.C. & Moreno, A.P. (2017). Mono-Heteromeric Configurations of Gap Junction Channels Formed by Connexin43 and Connexin45 Reduce Unitary Conductance and Determine both Voltage Gating and Metabolic Flux Asymmetry. *Frontiers in physiology*, **8**, 346.

Zhou, X.W., Pfahnl, A., Werner, R., Hudder, A., Llanes, A., Luebke, A. & Dahl, G. (1997). Identification of a pore lining segment in gap junction hemichannels. *Biophysical journal*, **72**, 1946–1953.

Zimmer, D.B., Green, C.R., Evans, W.H. & Gilula, N.B. (1987). Topological analysis of the major protein in isolated intact rat liver gap junctions and gap junction-derived single membrane structures. *The Journal of biological chemistry*, **262**, 7751–7763.

Anhang A: Publikation Schadzek *et al.*, 2015

Die kataraktassoziierte Mutation N188T des humanen Connexin46 (hCx46) zeigte die Schlüsselrolle der Position N188 für die Connexon-Connexon-Interaktion von Gap Junction-Kanälen

The cataract related mutation N188T in human connexin46 (hCx46) revealed a critical role for residue N188 in the docking process of gap junction channels

Patrik Schadzek, Barbara Schlingmann, Frank Schaarschmidt, Julia Lindner, Michael Koval, Alexander Heisterkamp, Matthias Preller, Anaclet Ngezahayo

Beitrag zur Publikation: Ich habe zusammen mit A.N. und B.S. die Experimente geplant. Ich habe zusammen mit B.S. die meisten Experimente durchgeführt, die Daten ausgewertet und interpretiert. Ich habe fast alle Abbildungen erstellt und das Manuskript zusammen mit A.N. und B.S. geschrieben.

CrossMark

The cataract related mutation N188T in human connexin46 (hCx46) revealed a critical role for residue N188 in the docking process of gap junction channels

Patrik Schadzek [a,1], Barbara Schlingmann [a,b,1], Frank Schaarschmidt [c], Julia Lindner [a], Michael Koval [b,d], Alexander Heisterkamp [e], Matthias Preller [f,g,*], Anaclet Ngezahayo [a,h,**]

[a] *Institute of Biophysics, Leibniz University Hannover, Germany*
[b] *Division of Pulmonary, Allergy and Critical Care and Sleep Medicine, Department of Medicine and Department of Cell Biology, Emory School of Medicine, Atlanta, GA, USA*
[c] *Institute of Biostatistics, Leibniz University Hannover, Germany*
[d] *Department of Cell Biology, Emory University, Atlanta, GA, USA*
[e] *Institut für Quantenoptik, Leibniz Universität Hannover, Deutschland*
[f] *Institute for Biophysical Chemistry, Hannover Medical School (MHH), Hannover, Germany*
[g] *Center for Structural Systems Biology, German Electron Synchrotron (DESY), Hamburg, Germany*
[h] *Center for System Neurosciences (ZSN), Hannover, Germany*

ARTICLE INFO

ABSTRACT

The mutation N188T in human connexin46 (hCx46) correlates with a congenital nuclear pulverulent cataract. This mutation is in the second extracellular loop, a domain involved in docking of gap junction hemichannels. To analyze the functional consequences of this mutation, we expressed hCx46N188T and the wild type (hCx46wt) in *Xenopus* oocytes and HeLa cells. In *Xenopus* oocytes, hemichannels formed by hCx46wt and hCx46N188T had similar electrical properties. Additionally, a Ca^{2+} and La^{3+} sensitive current was observed in HeLa cells expressing eGFP-labeled hCx46wt or eGFP-labeled hCx46N188T. These results suggest that the N188T mutation did not alter apparent expression and the membrane targeting of the protein. Cells expressing hCx46wt-eGFP formed gap junction plaques, but plaques formed by hCx46N188T were extremely rare. A reduced plaque formation was also found in cells cotransfected with hCx46N188T-eGFP and mCherry-labeled hCx46wt as well as in cocultured cells expressing hCx46N188T-eGFP and hCx46wt-mCherry. Dye transfer experiments in cells expressing hCx46N188T revealed a lower transfer rate than cells expressing hCx46wt. We postulate that the N188T mutation affects intercellular connexon docking. This hypothesis is supported by molecular modeling of hCx46 using the crystal structure of hCx26 as a template. The model indicated that N188 is important for hemichannel docking through formation of hydrogen bonds with the residues R180, T189 and D191 of the opposing hCx46. The results suggest that the N188T mutation hinders the docking of the connexons to form gap junction channels. Moreover, the finding that a glutamine substitution (hCx46N188Q) could not rescue the docking emphasizes the specific role of N188.

© 2015 Elsevier B.V. All rights reserved.

1. Introduction

Gap junctions are cell–cell channels that bind the cytoplasmic spaces of adjacent cells. They are permeable to ions and molecules as large as 1–2 kDa [1–4] and therefore allow an ionic and metabolic homeostasis between cells in tissues. In vertebrates, gap junctions are formed by connexins. Six connexins oligomerize to form a hemichannel, also called a connexon. A gap junction channel is composed of two connexons that dock with each other in a head-to-head interaction. The interacting hemichannels are provided by the respective interacting cells. The membrane topology of the connexins is highly conserved. They belong to a family of tetraspan transmembrane proteins with intracellular N- and C-termini, four transmembrane domains (TM1–TM4), two extracellular

loops (E1 and E2) and a cytoplasmic loop (CL) between the transmembrane domains TM2 and TM3 [5–8].

Like other membrane proteins, connexins are thought to follow the classical secretory pathway, starting with the cotranslational insertion into the membrane of the endoplasmic reticulum (ER) and passing through the Golgi apparatus before being delivered to the plasma membrane [9]. En route to the plasma membrane, connexins oligomerize to form connexons. It has been shown that depending on the connexin isoform, oligomerization can occur in the ER, in the ER–Golgi intermediate or in the trans-Golgi network [1–4,10–12]. Oligomerization of hCx46 was found to occur predominantly in the trans-Golgi network [1–8,11]. In the plasma membrane, connexons of adjacent cells can dock to each other to form gap junction channels. Within the plane of the plasma membrane, multiple gap junction channels form so called gap junction plaques [5–9,13,14] which can be easily observed by immunostaining for connexins [9,15] or in cells expressing connexins tagged with fluorescent proteins such as eGFP [1–4,10–12,16].

Several studies suggest a crucial role of the E2 domain in connexon–connexon docking to form functional gap junction channels between adjacent cells [17–20]. Based on the sequence of E2, connexins can be classified into a K–N group (bold residue in the sequence) with the sequence ϕ(**K/R**)CXXXPCP**N**XVDC$\Omega\psi$S or an H group with the sequence ϕ**X**CXXXPCP**H**XVDC$\Omega\psi$S, where ϕ represents a hydrophobic residue, X is any residue, Ω refers to aromatic residues and ψ indicates a residue with a large aliphatic side chain [1–4,21]. Connexons composed of connexins belonging to different groups do not dock to each other [1–8, 21]. In order to dock, hydrogen bonds and salt bridges between specific residues within the E2 loops of the interacting connexons of adjacent cells are essential [5–9,20]. In particular, the analysis of the crystal structure of hCx26 revealed the central role of the asparagine residue at position 176. Each N176 in a connexon of an interacting cell is engaged in three hydrogen bonds, with a lysine at position 168, a threonine at position 177 and an aspartic acid residue at position 179 in the E2 domain of a hCx26 connexin in the connexon of the adjacent cells to stabilize the complex [1–4,9–12,22,23]. The importance of a similar asparagine residue was also shown for hCx32. For hCx32, the homologous asparagine residue is located at position 175, and the interacting lysine, threonine and aspartic acid residues are found at positions 167, 176 and 178, respectively (Fig. 1). The mutant hCx32N175D, which correlates with Charcot–Marie–Tooth disease, was shown to be unable to form gap junction channels despite still forming functional hemichannels [1–8,10–12,24,25].

The mutation found at position 188 in the second extracellular loop domain of lens connexin46 has been linked to an autosomal dominant zonular pulverulent cataract [1–9,11,13,14,26], but the molecular consequences of this mutation have not yet been analyzed. In this report, we combine structural modeling, electrophysiology, cell imaging, and dye transfer experiments to show that the N188T mutation in hCx46 alters the function of gap junction channels by inhibiting the formation of gap junction channels without impairing hemichannel function. Furthermore, amino acid substitution experiments with the structurally similar amino acid glutamine and homology modeling with charged aspartate revealed that the asparagine at position 188 is functionally conserved and plays a central role for the docking process of gap junction hemichannels.

2. Materials and methods

2.1. Molecular biology

The vector pGEMHE hCx46wt was used for in vitro transcription. pEGFP N1 hCx46wt was used for fluorescence imaging and dye transfer experiments [5–9,13–15,27]. These plasmids were used as templates for further site-directed mutagenesis steps. The N188T and N188Q mutations were introduced using the primers described in Table 1. For cotransfection and coculture experiments the eGFP of the pEGFP N1 hCx46 plasmid was replaced by mCherry using the restriction enzymes BamHI and MfeI. A proofreading DNA Polymerase (Phusion, Thermo Fisher Scientific, Waltham, MA, USA) was used to amplify the mCherry insert. Cloning and introduction of the mutations were verified by sequencing (Seqlab, Göttingen, Germany).

Escherichia coli XL10-Gold (Stratagene, Waldbronn, Germany) was used to host the gene-containing plasmids. Plasmids for transfection of HeLa cells and cRNA for expression of the hCx46 variants in *Xenopus* oocytes were obtained as described previously [9,15,16,27].

2.2. Characterization of gap junction plaque formation

For the characterization of gap junction plaque formation, the average number of gap junction plaques per cell pair was quantified for each hCx46 variant. Dye transfer experiments were performed to determine the degree of dye coupling. HeLa cells were used to analyze gap junction plaque formation and function. Cells were transfected with the different
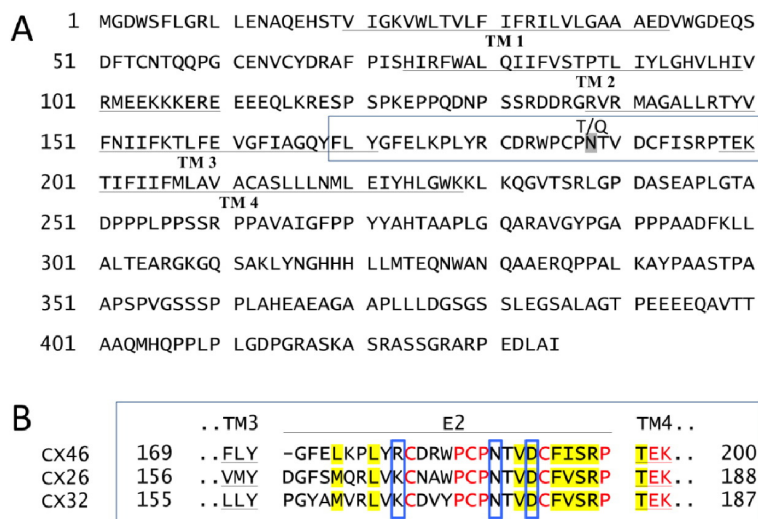

Fig. 1. (A) Amino acid sequence of hCx46. The four transmembrane domains are underlined. The site-directed amino acid replacement at position 188 in the second extracellular loop is indicated as bold letters above the wild-type amino acid, which is marked with a gray box. (B) Alignment analysis of the second extracellular loop domain of hCx46, hCx26 and hCx32, adapted from Ref. [22,24]. Color-coding: red: residues highly conserved among all connexin members; yellow: homologous residues; blue box: residues mediating inter-connexon interactions such as HBs.

Table 1
Primers used for site-directed mutagenesis and restriction enzyme cloning.

Primer	5′–3′ sequence
Mut N188T pGEMHE/pEGFP F	GGCCCTGCCCCACCACGGTGGACTG
Mut N188T pGEMHE/pEGFP R	CAGTCCACCGTGGTGGGGCAGGGCC
Mut N188Q pGEMHE/pEGFP F	CTGGCCCTGCCCCCAGACGGTGGACTGCT
Mut N188Q pGEMHE/pEGFP R	AGCAGTCCACCGTCTGGGGGCAGGGCCAG
mCherry BamHI F	GATTGGATCCCATGGTGAGCAAGGGCGAG
mCherry MfeI R	GGATCAATTGAACTGCAGCCGGGCG

eGFP-labeled hCx46 variants for fluorescence imaging and dye transfer experiments. Transfection and cultivation of HeLa cells were performed as previously described [1–4,10–12,16–20,27].

For quantification of plaque formation, HeLa cells expressing the different hCx46 variants were fixed with 3.7% formaldehyde 24 h after transfection. The nuclei of the transfected cells were stained with Hoechst 33342 (1 μg/ml; Sigma Aldrich), and the cell membranes were stained with Alexa 555-conjugated Wheat Germ Agglutinin (5 μg/ml; Molecular Probes, Eugene, OR, USA) to improve cell visualization. The fluorescence images were acquired as previously described [16,27]. Gap junction plaque quantification for the different hCx46 variants was performed in a double-blinded randomized fashion. For each transfection, six coverslips were evaluated. Four images of different regions of a coverslip were analyzed using ImageJ (http://rsbweb.nih.gov/ij/docs/menus/analyze.html#plot).

Using R-2.15.2 (R Core Team, 2012), the number of plaques per cell pair was analyzed in a generalized linear mixed model with log-link and assuming a Poisson distribution. The differences between the different hCx46 variants were estimated as fixed effects, the nesting of observations was accounted for by a hierarchical structure of two random effects, namely for the transfection and the repeated coverslips nested within transfection. Based on the estimates of the fitted model (on the log scale), multiplicity-adjusted tests and simultaneous 95% confidence intervals (CI) for the differences of the mutants to the hCx46wt were computed [1–4,21,28]. Back-transformation of these confidence intervals results in intervals for the ratio of expected plaque numbers among the hCx46 variants. Additionally, asymptotic 95% confidence intervals for the expected number of plaques per cell pair were computed for each hCx46 variant. The number of counted cell pairs for each variant is given by [n].

Dye transfer experiments were performed with Lucifer yellow (LY) (1 mg/ml) as previously described [16,27]. Results are given as the average ratio ± SEM of the sum of coupled pairs to the sum of tested pairs [n] for at least three transfection experiments. The significance of the difference was evaluated using Student's t-test.

To analyze the dominate-negative effect of the N188T mutation, HeLa cells were cotransfected with an eGFP-labeled hCx46N188T and hCx46wt-mCherry. For cotransfection, both plasmids were mixed before adding them to the transfection mixture. As control experiment, hCx46-eGFP and hCx46-mCherry coexpressing cells were used. Staining and data acquisition was performed as described above. Only cotransfected cell pairs were evaluated.

To measure formation of heterotypic gap junction channels, HeLa cells were transfected with plasmids containing the eGFP-labeled hCx46wt or hCx46N188T. Another batch of cells was transfected with the plasmid coding for the mCherry-labeled hCx46wt. After an expression time of 24 h, the cells expressing the eGFP-labeled variant were cocultivated for an additional 24 h with the hCx46-mCherry expressing cells. Staining and data acquisition were performed as described above. Only cell pairs, which were formed from one eGFP-labeled and one mCherry-labeled cell, were analyzed.

2.3. Characterization of hemichannel function in Xenopus oocytes

To investigate hemichannel function, two-electrode voltage-clamp experiments were performed in *Xenopus* oocytes expressing hemichannels of the different hCx46 variants. The expression of the hCx46 variants in *Xenopus* oocytes was performed as previously described [27,29]. The oocytes were injected with 23 nl of a solution containing the cRNA of the variant of interest (500 ng/μl) and the antisense oligonucleotide targeting the *Xenopus* oocyte endogenous Cx38 (400 ng/μl). The antisense oligonucleotide (AS38) (C*T*GACTGCTCGTCTGTCCACAC*A*G*; * indicates phosphorothioate modifications) was purchased from Eurofins MWG Operon (Ebersberg, Germany). For the control oocytes, 23 nl of AS38 (400 ng/μl) was injected.

The recordings of the macroscopic currents with two-electrode voltage-clamp technique (TEV) were performed on single *Xenopus* oocytes 12–36 h after cRNA injection, as described previously [27]. From a holding potential of −90 mV, test voltage pulses ranging from −90 mV to +30 mV were applied for 3 s in 10 mV steps. The data acquisition and analysis were performed as previously described [29]. For the steady-state current voltage plots (I(V)), the amplitude of the steady-state currents at the end of each voltage pulse was measured and plotted against the corresponding voltage. The activation parameters of the hemichannels were estimated by fitting the macroscopic conductance for the different voltage pulses with a Boltzmann equation $(G(V) = 1 / (1 + EXP(V_{1/2} - V) / zF/RT))$ as previously described [27]. Data points of the I(V) and the G(V) plot are given as averages ± SEM of at least five oocytes.

2.4. Formation of hemichannels in HeLa cell

Formation of hemichannels in HeLa cells was analyzed using the whole cell configuration of the patch-clamp technique. The cells transiently transfected with plasmids containing the hCx46wt-eGFP, hCx46N188T-eGFP and eGFP constructs were seeded on glass coverslips for 24–48 h. The cells were then transferred in a superfusion chamber containing 500 μl bath solution composed of (in mM) 140 NaCl, 5 KCl, 2 CaCl$_2$, 1 MgCl$_2$, 5 glucose, 10 HEPES (pH: 7.4). The perfusion chamber was mounted on a Ti-E fluorescence inverted microscope (Nikon GmbH, Düsseldorf, Germany), which allowed cells expressing the molecule of interest to be identified. For imaging, the microscope was equipped with a monochromator polychrome V (FEI, Munich, Germany), a CCD camera Orca-Flash 4 (Hamamtsu Photonics Deutschland GmbH, Herrsching am Ammersee, Germany) and the software NIS-Elements AR (Nikon). A whole-cell configuration was established using an EPC 10 USB Double (HEKA Elektronik Dr. Schulze GmbH, Lambrect/Pfalz, Germany) coupled to PulseMaster software (Heka Elektronik). The patch-pipette filling solution was composed of (in mM) 125 K-Gluconat, 15 CsCl, 0.2 CaCl$_2$, 2.5 MgATP, 2 Na$_2$ATP, 0.1 cAMP, 0.5 EGTA, 5 glucose, 10 HEPES (pH: 7.25). The cells were clamped at a − 60 mV. Membrane currents were elicited by a voltage pulse between −90 and +50 mV for 500 ms in 10 mV steps. To activate the hemichannels, a Ca^{2+}-free bath solution containing 15 mM TEA-Cl was applied. The hemichannels were closed by addition of 250 μM La^{3+}. The perfusion system allowed the bath solution to be changed from the control solution to the Ca^{2+}-free solution and La^{3+} containing Ca^{2+}-free solution within 30 s.

2.5. Structural modeling and molecular dynamics simulations

A structural model of hCx46 was generated using MODELLER [30] and the high-resolution crystal structure of hCx26 (PDB ID: 2ZW3) [22] was used as a template. The MODELLER objective function and the discrete optimized protein energy (DOPE) were used for the evaluation and selection of the models. The CL loop conformation, which is missing in the template structure, was subsequently optimized. The gap junction channel of hCx46 was constructed by superposition of the hCx46 connexins on the hCx26 connexin chains in the connexon derived from the X-ray structure [22]. A two-fold symmetry operation was used to build the second hemichannel. A dimer pair of interacting hCx46 monomers of opposing hemichannels was selected as the model system

for molecular dynamics simulations, and residue N188 in both monomers was replaced with either threonine, glutamine or aspartic acid. The four simulation systems – hCx46wt, hCx46N188T, hCx46N188Q and hCx46N188D – were immersed individually in a cubic box filled with explicit TIP3P water molecules [31], and the net charge was neutralized by adding Na^+ counter ions. To keep disulfide bridges stable, patches were implemented between residues C54–C192, C61–C186, and C65–C181 of hCx46, which correlate with the disulfide bridges C53–C180, C60–C174, and C64–C169 in hCx26. All molecular dynamics simulations were conducted using NAMD 2.9 [32] and the CHARMM27 force field [33]. A 12 Å cutoff was used for non-bonded short-range interactions, and long-range electrostatics were treated with the particle-mesh Ewald method [34]. Temperature and pressure were maintained at 310 K and 101.3 kPa using Langevin dynamics and the Langevin piston method. The simulation time step was 1 fs. Each simulation system was first energy minimized and subsequently equilibrated for approximately 5 ns – during which the systems converged towards a backbone RMSD of 5–7 Å – prior to production runs. Molecular dynamics (MD) simulations were conducted for 50 ns each at the Computer Cluster of the Norddeutscher Verbund für Hoch- und Höchstleistungsrechnen (HLRN).

3. Results

Mutations in the human lens connexin46 (hCx46) correlate with various forms of cataract [35]. The recently described A → C replacement at position 563 in the cDNA sequence of hCx46 causes an amino acid exchange at position 188 (Fig. 1) from asparagine to threonine (N188T). This mutation was found to be associated with an autosomal dominant congenital nuclear pulverulent cataract [26], but the functional consequences are not yet known.

Using site-directed mutagenesis, we generated the hCx46N188T mutant. The mutant as well as hCx46wt was expressed in *Xenopus* oocytes, and the formation of voltage-activated hemichannels was studied using the two-electrode voltage-clamp (TEV) technique. In further experiments, hCx46wt and hCx46N188T were C-terminally labeled with eGFP or mCherry and expressed in HeLa cells, allowing us to characterize the formation of gap junction plaques via confocal microscopy and dye transfer experiments.

hCx46 and its orthologs rat Cx46, chicken Cx56 and bovine Cx44 are known to form voltage-activated hemichannels when expressed in *Xenopus* oocytes [36–40]. We therefore examined whether the N188T mutation of hCx46 alters the formation of voltage-activated hemichannels (Fig. 2A).

Hemichannels formed by hCx46wt opened at depolarizing voltage pulses above −50 mV (Fig. 2B). TEV measurements with oocytes expressing hCx46N188T revealed similar results (Fig. 2B). The activation parameters for hCx46wt and hCx46N188T hemichannels were estimated by fitting the macroscopic conductance for the different voltage pulses with a Boltzmann equation (Fig. 2C). Analysis of the biophysical properties gave similar characteristics for the hemichannels formed by hCx46wt and hCx46N188T (Fig. 2C). Half-activation voltages of −20.06 ± 3.48 mV and −18.20 ± 2.42 mV were observed for hCx46wt and hCx46N188T hemichannels, respectively (Table 2). The hCx46wt and hCx46N188T hemichannels also showed similar apparent gating charges z of 1.88 ± 0.20 for hCx46wt and 1.92 ± 0.15 for hCx46N188T (Table 2). This indicates that the formation and function of the hemichannels are not affected by the mutation.

To investigate the effect of the mutation on the formation of gap junction channels, we expressed the mutant and wild type hCx46, both labeled with eGFP, in HeLa cells for further analysis. Using confocal microscopy, we analyzed the ability of the wild type and mutant hCx46 constructs to form gap junction plaques (Fig. 3A). Quantification of gap junction plaques in cell pairs expressing the wild type showed that 76.4% of the cell pairs expressing eGFP hCx46wt formed gap junction plaques (Fig. 3B) with an average of 1.540 plaques per cell pair (95% confidence interval (CI) [1.170, 2.030]) (Fig. 3C). In contrast, HeLa cell pairs expressing the mutant N188T gap junction plaques were observed in only 9.1% of the evaluated cell pairs (Fig. 3B) and an average of 0.126 plaques per cell pair (95% CI [0.085, 0.196]) was found (Fig. 3C). These
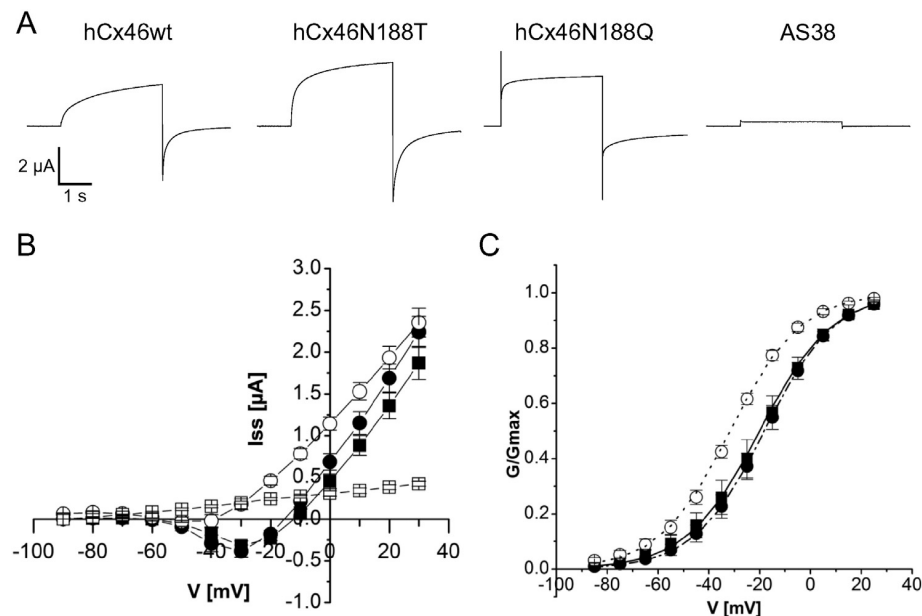

Fig. 2. The hCx46 variants formed connexons when expressed in *Xenopus* oocytes. *Xenopus* oocytes injected with cRNA encoding for the hCx46 variants were investigated by TEV from a holding potential of −90 mV, voltage pulses between −90 mV and +30 mV were applied for 3 s in 10 mV steps. (A) Example of current induced by depolarizing voltage pulses to +30 mV in oocytes expressing the corresponding variants. (B) The current–voltage I(V) plots of current elicited in oocytes, which were injected with cRNA for hCx46wt (■), hCx46N188T (●), hCx46N188Q (○), and AS38 (□) (negative control). The amplitudes of the steady state currents, measured at the end of the voltage pulse, are plotted against the corresponding voltages. The results shown are averages of at least five different oocytes for each variant. The error bars represent the SEM. (C) The conductance–voltage (G(V)) plots of the hCx46wt (■), hCx46N188T (●), and hCx46N188Q (○) hemichannels expressed in *Xenopus* oocytes. For each experiment, the conductance was normalized to the maximum conductance of each experiment and fitted to the Boltzmann equation. The data points represent the averages of at least five experiments for each variant.

Table 2
The activation parameters were estimated by Boltzmann fitting of the normalized G(V) data points of the experiments. The results are given as averages ± SEM of at least 5 oocytes for each connexin variant.

	$V_{1/2}$ [mV]	z
hCx46wt	−20.06 ± 3.48	1.88 ± 0.20
hCx46N188T	−18.20 ± 2.42	1.92 ± 0.15
hCx46N188Q	−31.68 ± 1.38	2.03 ± 0.15

findings lead to the conclusion that the N188T mutation in hCx46 inhibits the formation of gap junction plaques.

To investigate whether the observed gap junction plaques contain functional gap junction channels, dye transfer experiments were performed using Lucifer yellow (LY). Of the tested cell pairs expressing hCx46wt, 40.7% ± 2.8% were able to transfer LY. In contrast, only 15.7% ± 5.6% of the tested cell pairs expressing hCx46N188T showed transfer of LY, which is significantly different from cells expressing wild type hCx46. In non-transfected HeLa cells (control), the rate of dye transfer was 12.9% ± 3.8% (Fig. 3D). The level of dye transfer in cells expressing hCx46N188T was similar to dye transfer between untransfected cell pairs. Based on plaque quantification (Fig. 3A, B, C), it was assumed that the hCx46N188T mutation affected the capacity of the protein to form gap junction channels. This assumption is consistent with dye transfer experiments (Fig. 3D). However, the transport of hCx46N188T protein to the membrane appeared to be unaffected because hCx46N188T formed gap junction hemichannels in *Xenopus* oocytes similar to those formed by wild type hCx46 (Fig. 2).

It is noteworthy, that the absence of the gap junction plaques was not related to a loss of connexons in the plasma membrane. Indeed using the patch clamp, we found Ca^{2+} and La^{3+} sensitive current in single HeLa cells expressing the hCx46wt-eGFP and hCx46N188T-eGFP, respectively, which was not observed in cells expressing eGFP alone (Fig. 4). Additionally we observed that cells expressing hCx46wt-eGFP and hCx46N188T-eGFP were depolarized by suppression of external Ca^{2+}. In the presence of external Ca^{2+}, a membrane potential varying between −49 mV and −60 mV was found. The removal of external Ca^{2+} induced a depolarization to voltages between −27 mV and −45 mV. The application of La^{3+} repolarized the cells to the original values. The removal of external Ca^{2+} did not affect the membrane potential of the cells expressing the eGFP alone.

The mutation did not only impair the formation of gap junction plaques by hCx46N188T, it affected hCx46wt gap junction plaque formation as well. Cotransfection of HeLa cells with both eGFP-labeled hCx46N188T and mCherry-labeled hCx46wt correlated with a reduction in formation of gap junction plaques when compared to cells expressing eGFP- or mCherry-labeled hCx46wt only (Fig. 5A, C). Additionally, we also found a reduction of gap junction formation when we cocultured cells expressing mCherry-labeled hCx46wt with eGFP-labeled hCx46N188T cells to allow the formation of heterotypic hCx46wt-hCx46N188T channels (Fig. 5B, C).

The N188T mutation replaces an asparagine with threonine. Asparagine contains a carboxamide group as a side chain, whereas threonine contains a hydroxyl group. To investigate whether the removal of the carboxamide side chain is responsible for a loss in the ability of hCx46N188T to form gap junction channels, we reintroduced a
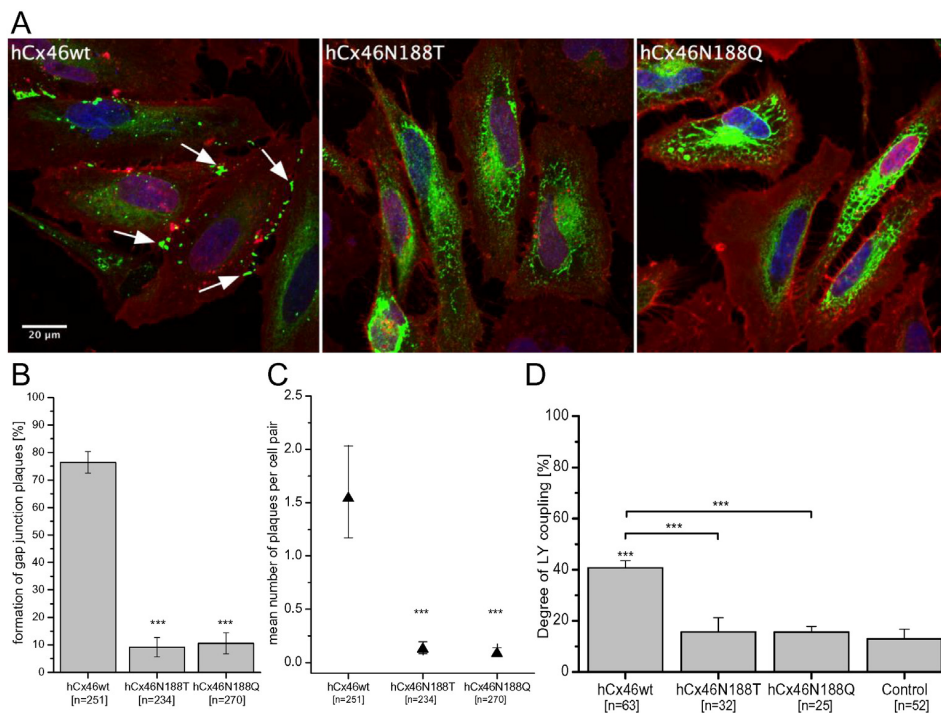

Fig. 3. hCx46N188T and hCx46N188Q show impaired gap junction plaque formation. Cells were transfected with the different eGFP-labeled hCx46 variants. 24 h after transfection, cells were fixed and stained with Hoechst (blue, nuclei) and WGA-Alexa555 (red, membranes). Further analysis was conducted using a laser-scanning confocal microscope. (A) Representative micrographs of cell pairs expressing the different eGFP-labeled hCx46 variants (green). The arrows indicate gap junction plaques. (B) Analysis of gap junction plaque formation. The diagram shows the percentage of cell pairs, which formed gap junction plaques. The number of tested cell pairs for each variant is represented as n. The error bars represent SEM. For statistical comparison between the mutants and the wild type Student's t-test was applied (*** p ≤ 0.001). (C) Quantification of the mean number of gap junction plaques per cell pair. The number of plaques per cell pair [n] was analyzed in a generalized linear mixed model with a log-link and assumption of the Poisson distribution. The differences between the two mutants and the wild type were tested by multiplicity-adjusted tests (*** p ≤ 0.001). Error bars represent 95% asymptotic confidence intervals for the mean number of plaques per cell pair. Cell pairs expressing hCx46N188T and hCx46N188Q show a significant decrease in the number of gap junction plaques per cell pair compared to the wild type. (D) Functional testing of gap junction coupling in HeLa cells expressing the different hCx46 variants. LY diffusion in cells was tested as described in Section 2. Quantification of the degree of dye coupling is given as the ratio of the sum of coupled pairs to the sum of the tested pairs for each hCx46 variant [n]. The results are shown as the average of at least three transfection experiments for each variant. The error bars represent the SEM. Student's t-test was applied for statistical comparisons between the non-transfected cells (control) and the hCx46 variants as well as between hCx46wt and the mutants (*** p ≤ 0.001).

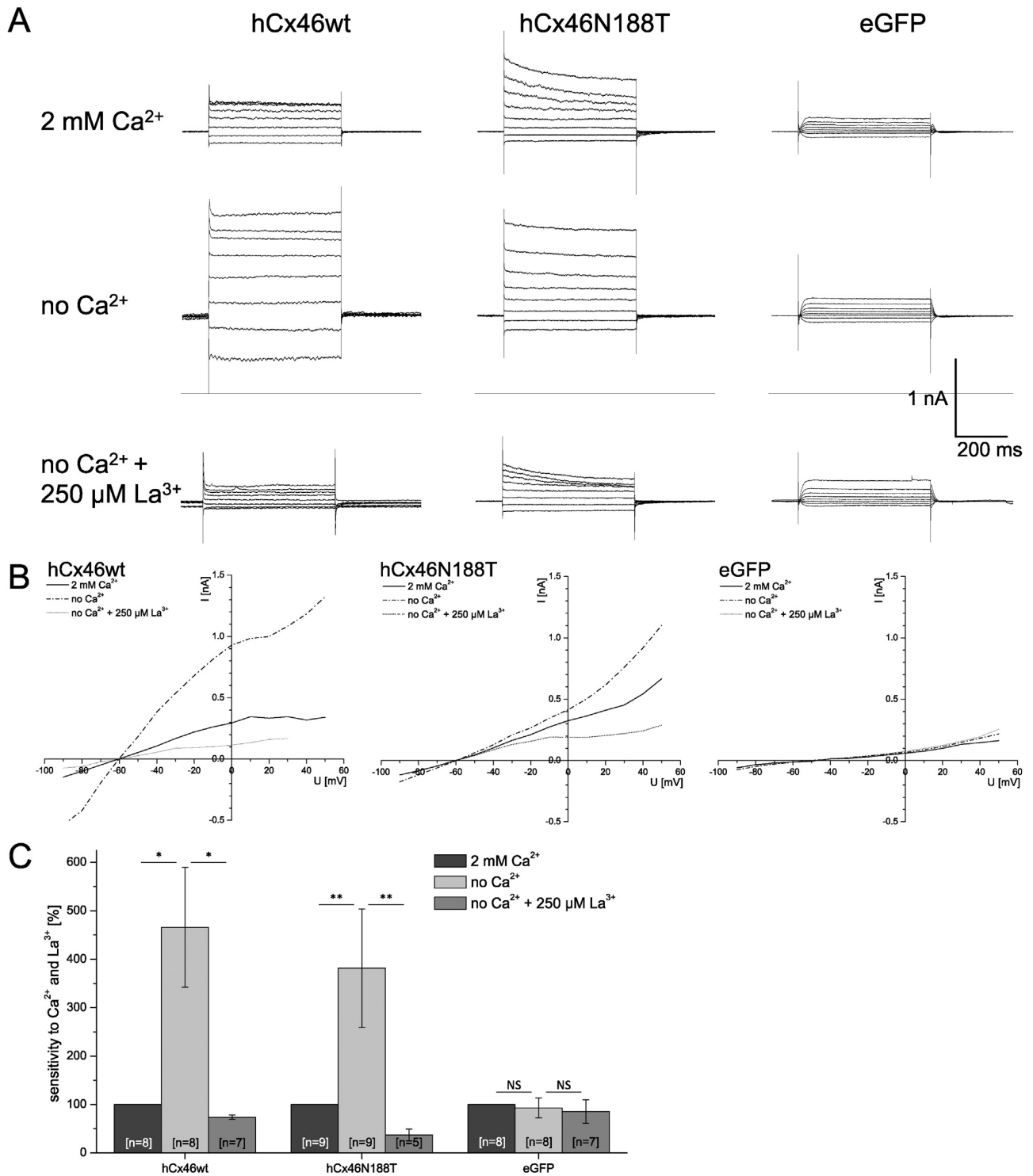**Fig. 4.** hCx46wt and hCx46N188T formed hemichannels in single HeLa cells. (A) Currents elicited by depolarizing voltage pulses from a holding potential of −60 mV stepped from −90 mV to +50 mV under whole-cell configuration in cells expressing hCx46wt-eGFP, hCx46N188T-eGFP and eGFP in the presence of external 2 mM Ca^{2+}, without external Ca^{2+} and in the presence of external 250 μM La^{3+}. (B) The corresponding current–voltage plot. (C) The sensitivity of the current to external Ca^{2+} and La^{3+}. The currents evoked by a depolarization to +40 mV in the absence of external Ca^{2+} and in the presence of La^{3+} are given as a percentage of the currents measured in the presence of external Ca^{2+}. The error bars represent SEM for n experiments as given for the treatments. For statistical comparison of the sensitivity to extracellular Ca^{2+} and La^{3+}, the Student's t-test was applied (* p ≤ 0.05; ** p ≤ 0.01).

carboxamide group by insertion of a glutamine residue. We analyzed whether the reintroduction of the carboxamide group by generation of the hCx46N188Q mutant could restore the function of the protein. Expression of eGFP-labeled hCx46N188Q in HeLa cells revealed that with respect to plaque formation and dye transfer coupling,

reintroduction of the carboxamide group was not sufficient to restore the docking function of the protein (Fig. 3). Only 10.6% of the cell pairs expressing hCx46N188Q formed plaques with an average of only 0.084 plaques per cell pair (95% CI [0.052, 0.136]) (Fig. 3A, B, C). Dye transfer experiments revealed that only 15.6 ± 2.3% of all tested cell
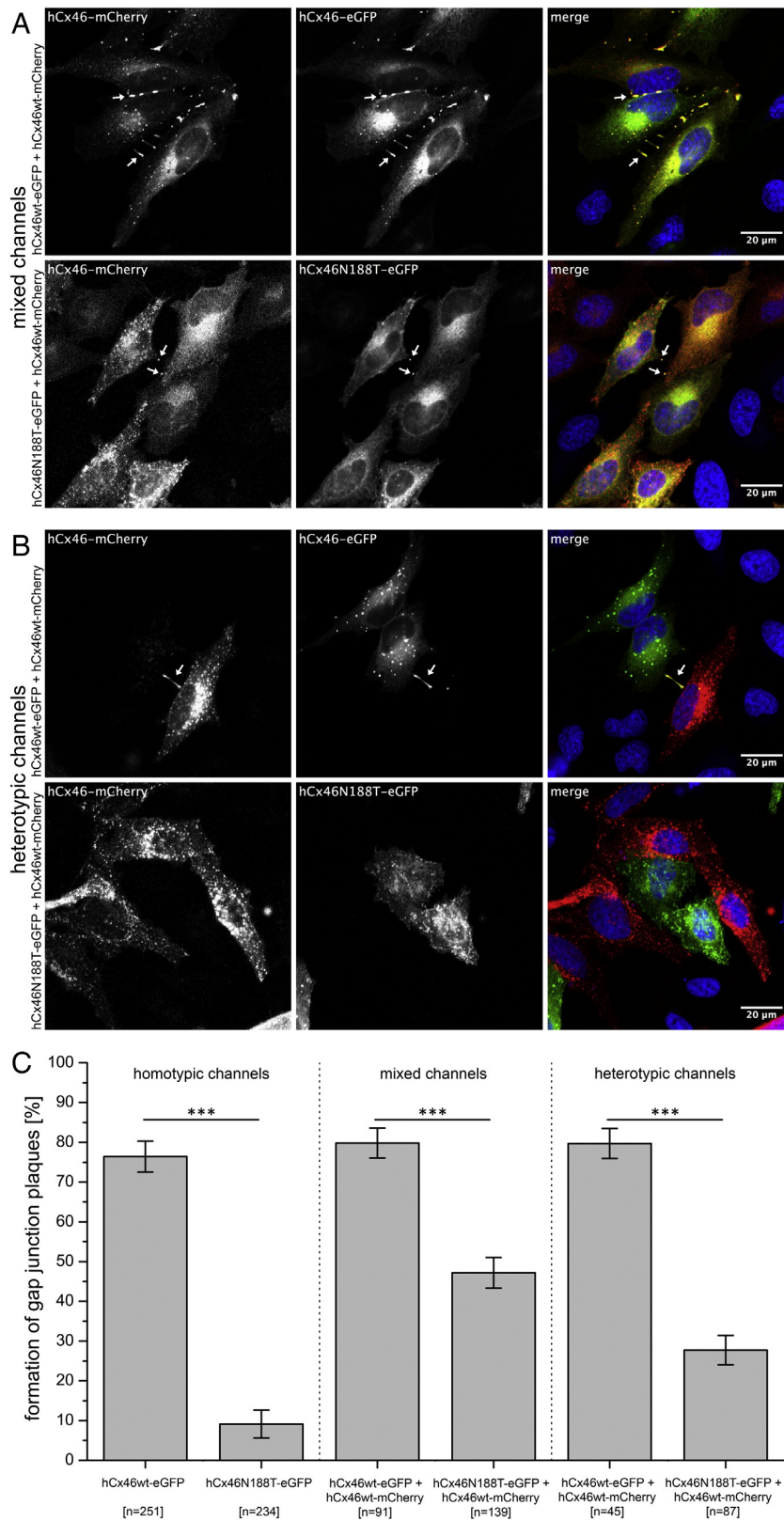
Fig. 5. hCx46N188T reduced the capacity of hCx46 to form gap junction plaques when coexpressed in the same cell or when allowed to form heterotypic gap junction channels. (A and B) Fluorescence micrographs of cells transfected with the corresponding hCx46 variants. The arrows indicate gap junction plaques. (C) Quantification of cell pairs forming gap junction plaques. The diagram shows the percentage of cell pairs, which formed gap junction plaques. The number of analyzed cell pairs for each variant is represented as n. The error bars represent SEM. For statistical comparison between the mutants and the wild type Student's t-test was applied (*** p ≤ 0.001). No statistical significant between the hCx46wt-eGFP and the cultured or cotransfected hCx46wt-eGFP/hCx46wt-mCherry cells could be observed. (note that the data for hCx46wt-eGFP and hCx46N188T-eGFP are the same as in Fig. 3B).

pairs were dye-coupled, which is not significantly different from controls (Fig. 3D). However, in *Xenopus* oocytes, hCx46N188Q formed voltage-activated hemichannels (Fig. 2), suggesting that the asparagine residue at position 188 plays a critical role for the docking process.

Alignment analysis of hCx46 with the crystallized hCx26 (PDB ID: 2ZW3) shows that Cx46, along with Cx26 and Cx32, belongs to the K/R–N group [21]. The residue N188 is positioned in the E2 domain, which comprises 26 amino acid residues, from residue G172 to P197 [22,24]. Using homology modeling of hCx46, with hCx26 as a template, we found high similarity in the properties of the E2 domains of hCx46 and hCx26 with respect to hydrophobicity and 3D structure. For hCx26, residue N176 was shown to form hydrogen bonds with residues K168, T177 and D179 in the E2 domain of the opposing hCx26 [24,25]. Our modeling of hCx46 suggests that residue N188 of hCx46 may play a similar critical function in the docking process of opposing connexons in adjacent cells (Figs. 1 and 6).

The structural model predicts that N188 of one hCx46 connexin within a connexon will form hydrogen bonds with the amino acid residues R180, T189 and D191 of the hCx46 in the counterpart connexon in the adjacent cell (Fig. 6B). This appears to stabilize the binding interface between the connexons. To assess whether the interface is stable over time, we performed molecular dynamics (MD) simulations of a fully solvated hCx46wt dimer of opposing connexins. The dimer remained intact throughout the entire 50 ns MD simulations (Fig. 6; Supplementary Materials S3, S6, S10). The complexes were stabilized by an average of 5 hydrogen bonds (Fig. 6). In contrast, substitution of the N188 residue with threonine, as found in the cataract-related N188T mutation, disrupted the tight network of hydrogen bonds in E2. The N188T mutation led to a kinking of the monomers relative to each other during the simulations, with a decrease in the angle between the two monomers from about 150° to 60°, and finally to the dissociation of the complex within 30 ns simulation time (Fig. 6C; Supplemental Materials S1A, S3, S7). These findings suggest an impaired docking capacity of the mutated hCx46 connexons in gap junction channels (Supplementary materials). MD simulation with the structurally similar amino acid glutamine at position 188 indicated that the longer glutamine residue could not replace the asparagine residue, despite its similar physicochemical properties

(Fig. 6C, Supplementary materials S1B, S2, S8). The N188Q mutations of the two interacting connexins sterically interfered with each other and consequently pushed the two monomers away from each other, thus hampering proper docking. The complex dissociated within the first 10 ns of the MD trajectories (Supplemental Materials S1B, S8, S12). The introduction of an aspartate at position 188 (hCx46N188D) sterically matched the interaction space between the two connexins perfectly and hydrogen bonds between N188D and R180 were formed (Supplemental Material S1C). However, the N188D mutation introduced a negative charge, which seems to cause an electrostatic repulsion with D191, interfering with the ability of the connexins to interact, likely causing the complex to dissociate within 40 ns as in the MD simulation (Fig. 6C; Supplemental Materials S1C, S2, S4, S9). This finding is similar to that found for hCx32, where an aspartate at position 175 impaired hemichannel docking indicating that N175 of hCx32 and N188 hCx46 are functionally similar. Taken together, the results of the present report indicate that the asparagine at position 188 in hCx46 is specifically required for docking of the hCx46 connexon in gap junction channels. Even a minor change like the N188Q mutation did not allow a proper docking as showed by the MD simulation of the hCx46N188Q connexins (Supplementary Materials S2, S8) or by the MD simulation of the entire hCx46N188Q gap junction channels (Supplemental Material S11).

4. Discussion

The N188T mutation of hCx46 has been shown to cause an autosomal dominant zonular pulverulent cataract [26]. The present report examines how the exchange of an asparagine residue in the second extracellular loop of hCx46 by a threonine residue (N188T), affects gap junction formation and functionality. Formation of gap junction channels requires the docking of the extracellular domains of interacting connexons in adjacent cells [17]. The interaction between two opposing connexons involves both the E1 and E2 domains [23]. However, domain swap with Cx46, Cx43 and Cx50 showed that the E2 domain is important for the selectivity in the docking process and formation of functional gap junction hemichannels [41]. Moreover, it has
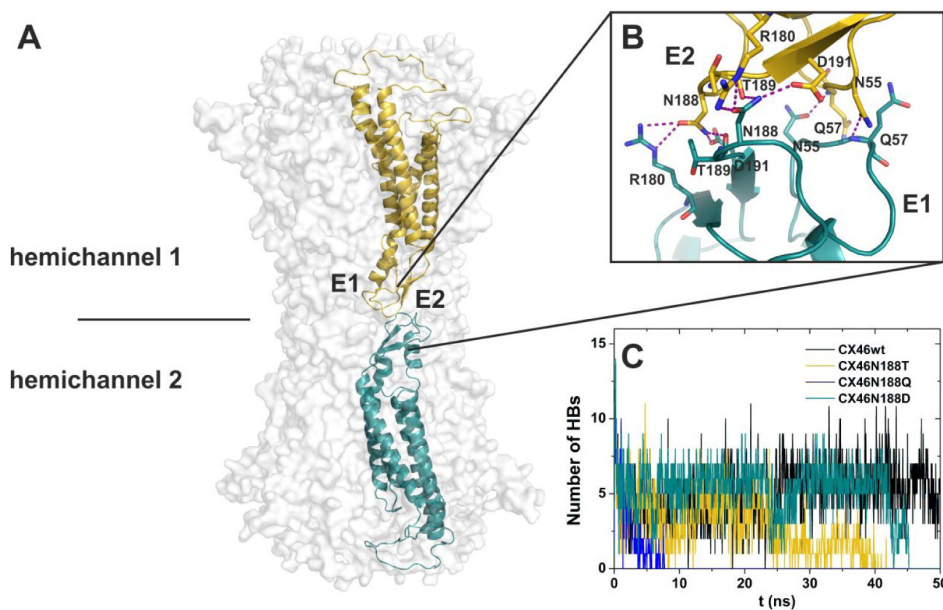

Fig. 6. Structural features of the human connexin46 (hCx46). (A) Homology model of the hCx46 gap junction channel. The two connexon hemichannels are shown in transparent surface representation with the two interacting connexins of each connexon shown as ribbons in gold and cyan, respectively. (B) Close-up view of the binding area between the two connexins (gold and cyan). A tight network of hydrogen bonds (dashed lines, purple) is formed between the amino acid residues of the interacting extracellular loops E1 and E2. (C) Diagram showing the number of hydrogen bonds (HBs) as a function of time along the MD simulations. Note the consistent average number of five HBs, stabilizing the hCx46wt dimer (black), whereas three mutants (blue, gold and cyan) dissociate and lose all HBs at different time points.

been shown that there are key hydrogen bonds (HBs) in the second extracellular loop domain that are required for proper docking and the formation of functional gap junction channels [22,24,25]. The analysis of the structure of crystallized hCx26 showed that residue N176 in the E2 of a connexin in the connexon of one cell formed three hydrogen bonds, with K168, T177 and D179, of the counterpart hCx26 in the connexon of the neighboring cell [22,24]. A homology model showed that this hydrogen bond model could be applied to hCx32. The central residue in hCx32 is N175, which would interact with K167, T176, and D178 [24,25]. Alignment analysis of hCx26, hCx32 and hCx46 revealed that within the sequence of the second extracellular loop, residue N188 of hCx46 has a similar functional position to N176 in hCx26 and N175 in hCx32, predicting similar interactions between N188 in hCx46 and R180, T189 and D191 (Fig.1) [21,24]. Therefore, we postulate that N188 plays a crucial role in the docking process of hCx46 connexons in adjacent cells. Gong et al. found that four to six hydrogen bonds between the hCx32 or hCx26 variants are required for the formation of stable gap junction channels [24]. Wild type hCx26 and hCx32 were found to form six hydrogen bonds between two connexins [24,25]. For hCx46, an average of five hydrogen bonds maintained the interaction of two interacting hCx46 monomers during MD simulations (Fig. 6C, Supplementary Materials S2, S3, S6, S10). In addition, our simulations predict that replacement of the N188 residue with a T residue, as in hCx46N188T, suppresses hydrogen bonding with R180, thereby reducing the possibility of proper docking between the connexons (Fig. 6; Supplementary Materials S2, S3, S7). By considering only two opposing connexins in the MD simulations, it is not possible to capture all possible interactions that are present in the gap junction channels for example interactions between connexin molecules within a hemichannel. To analyze the extent of the limitations of our model system, we performed MD simulations of the entire hCx46 gap junction channel and the N188Q channel. We found a close resemblance in the behavior and observed effects for the two-connexin models and the gap junction channels (Supplementary Materials S2–S11).

The X-ray structure of hCx26 indicates additional formation of hydrogen bonds between the conserved E1 residues N54, L56 and Q57 with the corresponding residues in the opposing connexin [22,42]. Our modeling showed that the homologous residues in hCx46 N55, T55 and Q57 also form hydrogen bonds. However these E1-E1 interactions were not affected by the mutations in E2 (Fig. 6; Supplementary Material S1). Our predictions agree very well with the quantification of plaque formation between cells expressing hCx46N188T in comparison to cells expressing hCx46wt (Fig. 3). Whereas more than 75% of the cell pairs expressing hCx46wt formed gap junction plaques with an average 1.54 gap junction plaques per cell pair, only about 10% cells expressing hCx46N188T were found to form gap junction plaques and an average of 0.13 plaques per cell pair was found (Fig. 3B and C). The reduced numbers of gap junction plaques also correlated with a reduction in dye transfer ability in HeLa cells expressing hCx46N188T as compared to cells expressing hCx46wt (Fig. 3B and D). It can be argued that the cells expressing hCx46N188T were not able to target the molecule to the plasma membrane. This argument can even be correlated with the observation that the protein appeared to be more localized to intracellular organelles in comparison with hCx46wt (Fig. 3A). However, electrophysiological experiments in *Xenopus* oocytes (Fig. 2) indicate that targeting of hCx46wt connexons and those formed by hCx46N188T was not notably different (Fig. 2). Moreover, whole cell patch-clamp experiments identified a Ca^{2+} and La^{3+} sensitive current in single HeLa cells expressing hCx46wt-eGFP or hCx46N188T-eGFP, which was not found in cells expressing eGFP (Fig. 4). The data shows clearly that like hCx46wt, hCx46N188T formed hemichannels, which were transported to the cell plasma membrane. Confocal microscopy and dye transfer experiments showed that the mutant was not able to form functional gap junction plaques (Fig. 3), but electrophysiological characterization (Figs. 2, 4) showed functional hemichannels, suggesting that hCx46N188T is inserted into the plasma membrane as

unapposed connexons. The presence of unapposed hCx46N188T connexons, as shown by electrophysiological experiments (Figs. 2, 4), agrees very well with the observation made by Nakagawa et al. [25]. They found that hCx32N175Y, which was not able to form gap junction channels, was mostly found in the cytoplasm. However, the mutant was also able to form connexons in the membrane, and although they were not visualized by microscopy, these connexons allowed dye uptake into the cells.

It is striking that the N188T mutation has further consequences for formation of gap junction channels. As shown in Fig. 5, when cotransfected with wild type hCx46, mutant hCx46N188T reduced the formation of gap junction plaques suggesting formation of heteromeric connexons in which the wild type and the mutants were mixed, and thus could not stably dock. Similarly, we found a reduced formation of gap junction plaques between cells expressing hCx46wt and those expressing hCx46N188T in coculture. These results of cotransfection and cocultivation suggest that whenever cells express the mutated isoform, the formation of gap junctions will be impaired. This suggests that the N188T mutation has a dominant negative effect of hCx46 gap junction channel formation and is likely to be the reason for this dominant form of cataract.

The carboxamide side chain of N188 in hCx46 appears to be essential for the docking of the connexons. The replacement of the asparagine at position 188 with threonine clearly disrupted the docking. However, we found that the reintroduction of a carboxamide group of a glutamine (hCx46N188Q) could not restore the docking function (Figs. 3 and 6; Supplementary Materials S1B, S2, S5, S8, S11). MD simulations indicated that the glutamine mutation at position 188 sterically hindered the stable positioning of connexins of interacting connexons (Fig. 6C; Supplementary Materials S1B, S2, S5, S8, S11). This modeling agrees very well with the analysis of plaque formation and dye transfer experiments, which showed reduced plaque formation and reduced probability of dye coupling by hCx46N188Q compared to hCx46wt (Fig. 3). The homology modeling approach presented by Nakagawa et al. [25] suggests that a spatiotemporally constrained network of hydrogen bonds is required for the docking process. A decrease in the number of possible hydrogen bonds due to longer or bulkier residues at positions 168 and 176 of Cx26 in interacting hemichannels would lead to the disruption of hemichannel interactions [25]. For hCx46, the comparable positions are R180 and N188 (Fig. 1B). Although the asparagine residue at position 180 of hCx46 is longer than the lysine residue at position 168 of hCx26, docking of hCx46 can still take place (Supplementary Materials S2, S3, S6, S10). However, the bulky glutamine at position 188 hindered connexon docking (Figs. 2, and 6C, Supplementary Materials S1B, S8, S11). The aspartate residue at position 188 does not sterically influence the molecule, but it introduced a charge, which suppresses the hydrogen bonds with T189 and D191 of the counterpart connexin. The MD simulation showed a docking stability for the hCx46N188D variant longer than that observed for the hCx46N188T (Fig. 6C, Supplementary Materials S1C, S2, S4, S9). Gong et al. reported that Cx32N175D could dock to Cx26D179N, suggesting a functional rescue by reciprocal charge mutations for the Cx32/Cx26 complex [22,24]. Our MD simulation showed that the mutant generated by Gong et al. formed stable complex. In case of hCx46N188D and hCx46D191 however, the MD simulation showed that the complex was not stable, it dissociated during the 50 ns of simulation time (Supplementary Material S12). This finding shows that a careful analysis of each member of the connexin family is needed for a better understanding of the interactions.

5. Conclusion

The present report shows clearly that the N188T mutation in the E2 domain of hCx46 does not alter the synthesis of the protein and did not hinder its oligomerization into connexons or the trafficking and insertion of hCx46N188T connexons into the plasma membrane. In addition, the electrophysiological characteristics of the hemichannels were not

affected (Fig. 2, Table 2). However, the docking of the connexons in adjacent cells to form gap junction channels was impaired. As indicated by our homology model, the asparagine residue at position 188 with its specific physico-chemical properties and stereo-geometry is critical for the fine-tuned docking of connexons in adjacent cells and cannot be replaced by structurally similar amino acids.

Supplementary data to this article can be found online at http://dx.doi.org/10.1016/j.bbamem.2015.10.001.

Transparency Document

The Transparency document associated with this article can be found, in the online version.

References

[1] J. Neijssen, C. Herberts, J.W. Drijfhout, E. Reits, L. Janssen, J. Neefjes, Cross-presentation by intercellular peptide transfer through gap junctions, Nat. 434 (2005) 83–88.

[2] P. Bedner, H. Niessen, B. Odermatt, M. Kretz, K. Willecke, H. Harz, Selective permeability of different connexin channels to the second messenger cyclic AMP, J. Biol. Chem. 281 (2006) 6673–6681.

[3] M.V.M. Bennett, V.K.V. Verselis, Biophysics of gap junctions, Semin. Cell Biol. 3 (1992) 29–47.

[4] H. Niessen, H. Harz, P. Bedner, K. Krämer, K. Willecke, Selective permeability of different connexin channels to the second messenger inositol 1,4,5-trisphosphate, J. Cell Sci. 113 (Pt 8) (2000) 1365–1372.

[5] D.W. Laird, J.P. Revel, Biochemical and immunochemical analysis of the arrangement of connexin43 in rat heart gap junction membranes, J. Cell Sci. 97 (Pt 1) (1990) 109–117.

[6] L.C. Milks, N.M. Kumar, R. Houghten, N. Unwin, N.B. Gilula, Topology of the 32-kd liver gap junction protein determined by site-directed antibody localizations, Embo J. 7 (1988) 2967–2975.

[7] G.E. Sosinsky, B.J. Nicholson, Structural organization of gap junction channels, Biochim. Biophys. Acta 1711 (2005) 99–125.

[8] J.T. Zhang, B.J. Nicholson, The topological structure of connexin 26 and its distribution compared to connexin 32 in hepatic gap junctions, J. Membr. Biol. 139 (1994) 15–29.

[9] D.W. Laird, The gap junction proteome and its relationship to disease, Trends Cell Biol. 20 (2009) 92–101.

[10] J.A. Diez, S. Ahmad, W.H. Evans, Assembly of heteromeric connexons in guinea-pig liver en route to the Golgi apparatus, plasma membrane and gap junctions, Eur. J. Biochem. 262 (1999) 142–148.

[11] M. Koval, J.E. Harley, E. Hick, T.H. Steinberg, Connexin46 is retained as monomers in a trans-Golgi compartment of osteoblastic cells, J. Cell Biol. 137 (1997) 847–857.

[12] L.S. Musil, D.A. Goodenough, Multisubunit assembly of an integral plasma membrane channel protein, gap junction connexin43, occurs after exit from the ER, Cell 74 (1993) 1065–1077.

[13] A. Forge, D. Becker, S. Casalotti, J. Edwards, N. Marziano, G. Nevill, Gap junctions in the inner ear: comparison of distribution patterns in different vertebrates and assessment of connexin composition in mammals, J. Comp. Neurol. 467 (2003) 207–231.

[14] N.S. McNutt, R.S. Weinstein, The ultrastructure of the nexus. A correlated thin-section and freeze-cleave study, J. Cell Biol. 47 (1970) 666–688.

[15] D. Begandt, A. Bader, L. Gerhard, J. Lindner, L. Dreyer, B. Schlingmann, A. Ngezahayo, Dipyridamole-related enhancement of gap junction coupling in the GM-7373 aortic endothelial cells correlates with an increase in the amount of connexin43 mRNA and protein as well as gap junction plaques, J. Bioenerg. Biomembr. 45 (2013) 409–419.

[16] B. Schlingmann, P. Schadzek, F. Hemmerling, F. Schaarschmidt, A. Heisterkamp, A. Ngezahayo, The role of the C-terminus in functional expression and internalization of rat connexin46 (rCx46), J. Bioenerg. Biomembr. 45 (2013) 59–70.

[17] A.L. Harris, Emerging issues of connexin channels: biophysics fills the gap, Q. Rev. Biophys. 34 (2001) 325–472.

[18] J. Kronengold, E.B. Trexler, F.F. Bukauskas, T.A. Bargiello, V.K. Verselis, Single-channel SCAM identifies pore-lining residues in the first extracellular loop and first transmembrane domains of Cx46 hemichannels, J. Gen. Physiol. 122 (2003) 389–405.

[19] X.W. Zhou, A. Pfahnl, R. Werner, A. Hudder, A. Llanes, G. Dahl, Identification of a pore lining segment in gap junction hemichannels, Biophys. J. 72 (1997) 1946–1953.

[20] C.I. Foote, L. Zhou, X. Zhu, B.J. Nicholson, The pattern of disulfide linkages in the extracellular loop regions of connexin 32 suggests a model for the docking interface of gap junctions, J. Cell Biol. 140 (1998) 1187–1197.

[21] M. Koval, S.A. Molina, J.M. Burt, Mix and Match: Investigating Heteromeric and Heterotypic Gap Junction Channels in Model Systems and Native Tissues, FBBS Letters, 2014.

[22] S. Maeda, S. Nakagawa, M. Suga, E. Yamashita, A. Oshima, Y. Fujiyoshi, T. Tsukihara, Structure of the connexin 26 gap junction channel at 3.5 Å resolution, Nature 458 (2009) 597–602.

[23] S. Maeda, T. Tsukihara, Structure of the gap junction channel and its implications for its biological functions, Cell. Mol. Life Sci. 68 (2011) 1115–1129.

[24] X.-Q. Gong, S. Nakagawa, T. Tsukihara, D. Bai, A mechanism of gap junction docking revealed by functional rescue of a human-disease-linked connexin mutant, J. Cell Sci. 126 (2013) 3113–3120.

[25] S. Nakagawa, X.-Q. Gong, S. Maeda, Y. Dong, Y. Misumi, T. Tsukihara, D. Bai, Asparagine 175 of connexin32 is a critical residue for docking and forming functional heterotypic gap junction channels with connexin26, J. Biol. Chem. 286 (2011) 19672–19681.

[26] Y. Li, J. Wang, B. Dong, H. Man, A novel connexin46 (GJA3) mutation in autosomal dominant congenital nuclear pulverulent cataract, Mol. Vis. 10 (2004) 668–671.

[27] B. Schlingmann, P. Schadzek, S. Busko, A. Heisterkamp, A. Ngezahayo, Cataract-associated D3Y mutation of human connexin46 (hCx46) increases the dye coupling of gap junction channels and suppresses the voltage sensitivity of hemichannels, J. Bioenerg. Biomembr. 44 (2012) 607–614.

[28] T. Hothorn, F. Bretz, P. Westfall, Simultaneous inference in general parametric models, Biom. J. 50 (2008) 346–363.

[29] W.J. Walter, C. Zeilinger, W. Bintig, H.-A. Kolb, A. Ngezahayo, Phosphorylation in the C-terminus of the rat connexin46 (rCx46) and regulation of the conducting activity of the formed connexons, J. Bioenerg. Biomembr. 40 (2008) 397–405.

[30] A. Sali, T.L. Blundell, Comparative protein modelling by satisfaction of spatial restraints, J. Mol. Biol. 234 (1993) 779–815.

[31] W.L. Jorgensen, J. Chandrasekhar, J.D. Madura, R.W. Impey, M.L. Klein, Comparison of simple potential functions for simulating liquid water, J. Chem. Phys. 79 (1983) 926–935.

[32] J.C. Phillips, R. Braun, W. Wang, J. Gumbart, E. Tajkhorshid, E. Villa, C. Chipot, R.D. Skeel, L. Kalé, K. Schulten, Scalable molecular dynamics with NAMD, J. Comput. Chem. 26 (2005) 1781–1802.

[33] A.D. MacKerell, D. Bashford, M. Bellott, R.L. Dunbrack, J.D. Evanseck, M.J. Field, S. Fischer, J. Gao, H. Guo, S. Ha, D. Joseph-McCarthy, L. Kuchnir, K. Kuczera, F.T. Lau, C. Mattos, S. Michnick, T. Ngo, D.T. Nguyen, B. Prodhom, W.E. Reiher, et al., All-atom empirical potential for molecular modeling and dynamics studies of proteins, J. Phys. Chem. B 102 (1998) 3586–3616.

[34] T.A. Darden, L.G. Pedersen, Molecular modeling: an experimental tool, Environ. Health Perspect. 101 (1993) 410–412.

[35] V.M. Berthoud, E.C. Beyer, Oxidative stress, lens gap junctions, and cataracts, Antioxid. Redox Signal. 11 (2009) 339–353.

[36] E.C. Beyer, Gap junctions, Int. Rev. Cytol. 137C (1993) 1–37.

[37] L. Ebihara, V.M. Berthoud, E.C. Beyer, Distinct behavior of connexin56 and connexin46 gap junctional channels can be predicted from the behavior of their hemi-gap-junctional channels, Biophys. J. 68 (1995) 1796–1803.

[38] V.K. Gupta, V.M. Berthoud, N. Atal, J.A. Jarillo, L.C. Barrio, E.C. Beyer, Bovine connexin44, a lens gap junction protein: molecular cloning, immunologic characterization, and functional expression, Invest. Ophthalmol. Vis. Sci. 35 (1994) 3747–3758.

[39] A. Ngezahayo, C. Zeilinger, I. Todt, I. Marten, H.A. Kolb, Inactivation of expressed and conducting rCx46 hemichannels by phosphorylation, Pflugers Arch. 436 (1998) 627–629.

[40] D.L. Paul, L. Ebihara, L.J. Takemoto, K.I. Swenson, D.A. Goodenough, Connexin46, a novel lens gap junction protein, induces voltage-gated currents in nonjunctional plasma membrane of *Xenopus* oocytes, J. Cell Biol. 115 (1991) 1077–1089.

[41] T.W. White, R. Bruzzone, S. Wolfram, D.L. Paul, D.A. Goodenough, Selective interactions among the multiple connexin proteins expressed in the vertebrate lens: the second extracellular domain is a determinant of compatibility between connexins, J. Cell Biol. 125 (1994) 879–892.

[42] D. Bai, A.H. Wang, Extracellular domains play different roles in gap junction formation and docking compatibility, Biochem. J. 458 (2014) 1–10.

Anhang B: Publikation Schadzek *et al.*, 2016

Daten der Molekül-Dynamik-Simulationen zeigen den Einfluss der Connexin-Connexin-Interaktion von Mutationen des humanen Connexin46 auf das Wasserstoffbrückenbindungsnetzwerk

Data of the molecular dynamics simulations of mutations in the human connexin46 docking interface

Patrik Schadzek, Barbara Schlingmann, Frank Schaarschmidt, Julia Lindner, Michael Koval, Alexander Heisterkamp, Anaclet Ngezahayo, Matthias Preller

Beitrag zur Publikation: Ich habe die erste Version des Manuskripts erstellt, die Daten ausgewertet und zusammen mit A.N. das Manuskript fertig geschrieben.

Contents lists available at ScienceDirect

Data in Brief

journal homepage: www.elsevier.com/locate/dib

ELSEVIER

CrossMark

Data Article

Data of the molecular dynamics simulations of mutations in the human connexin46 docking interface

Patrik Schadzek [a], Barbara Schlingmann [a,b],
Frank Schaarschmidt [c], Julia Lindner [a], Michael Koval [b,d],
Alexander Heisterkamp [e], Anaclet Ngezahayo [a,f,*],
Matthias Preller [g,h,**]

[a] Institute of Biophysics, Leibniz University Hannover, Germany
[b] Division of Pulmonary, Allergy and Critical Care and Sleep Medicine, Department of Medicine
and Department of Cell Biology, Emory School of Medicine, Atlanta, GA, USA
[c] Institute of Biostatistics, Leibniz University Hannover, Germany
[d] Department of Cell Biology, Emory University, Atlanta, GA, USA
[e] Institut für Quantenoptik, Leibniz Universität Hannover, Deutschland
[f] Center for System Neurosciences (ZSN), Hannover, Germany
[g] Institute for Biophysical Chemistry, Hannover Medical School (MHH), Hannover, Germany
[h] Center for Structural Systems Biology, German Electron Synchrotron (DESY), Hamburg, Germany

ARTICLE INFO

ABSTRACT

The structure of hCx26 derived from the X-ray analysis was used to generate a homology model for hCx46. Interacting connexin molecules were used as starting model for the molecular dynamics (MD) simulation using NAMD and allowed us to predict the dynamic behavior of hCx46wt and the cataract related mutant hCx46N188T as well as two artificial mutants hCx46N188Q and hCx46N188D. Within the 50 ns simulation time the docked complex composed of the mutants dissociate while hCx46wt remains stable. The data indicates that one hCx46 molecule forms 5–7 hydrogen bonds (HBs) with the counterpart

connexin of the opposing connexon. These HBs appear essential for a stable docking of the connexons as shown by the simulation of an entire gap junction channel and were lost for all the tested mutants.

The data described here are related to the research article entitled "The cataract related mutation N188T in human connexin46 (hCx46) revealed a critical role for residue N188 in the docking process of gap junction channels" (Schadzek et al., 2015) [1].

Specifications Table

Subject area	*Computational Biology*
More specific subject area	*Molecular dynamics simulation of the connexin docking interface*
Type of data	*Figure, diagram, videos*
How data was acquired	*Homology modelling using MODELLER* [2] *and the crystal structure of hCx26 (PDB ID: 2ZW3)* [3]; *hCx46 connexins were superimposed on the hCx26 connexins chains in the connexon derived from the X-ray structure* [3]. *The molecular dynamics simulation of interacting hCx46 connexins was performed using NAMD 2.9* [4] *and the CHARMM27 force field* [5]
Data format	*Analyzed*
Experimental factors	*The interacting hCx46 connexins were placed in a cubic box filled with TIP3P water* [6] *and Na^+-Ions; the disulfide bridges were created by patches. Temperature (310 K) and pressure (101.3 kPa) were maintained constant. The system was equilibrated for 5 ns and the dynamic was followed for 50 ns at steps of 1 fs*
Experimental features	*Simulation of connexin-connexin docking interaction*
Data source location	Institute for Biophysical Chemistry, Hannover Medical School (MHH), Hannover, Germany; Center for Structural Systems Biology, German Electron Synchrotron (DESY), Hamburg, Germany
Data accessibility	*The data is with this article*

Value of the data

- The data allow a prediction of the dynamic behavior of hCx46 molecules during docking process by molecular dynamics simulation.
- The hydrogen bonds formed by N188 of hCx46 within a connexon with residues R180, T189 and D191 of the counterpart connexin in the connexon of the adjacent cell appear to be crucial for the interacting connexin molecules to form a stable complex.
- hCx46 formed 5–7 HBs with the opposing connexins in the counterpart connexon of the adjacent cell, which stabilize the docked complex and the formation of a gap junction channel.
- Crystallization of connexins is still very difficult. However, the presented data for hCx46 shows that the structure of hCx26 derived from the X-ray analysis can be used to predict the molecular dynamic behaviors of other connexins.

1. Data

In this Data article we share molecular dynamics simulation data of Cx46 molecules. In our data we simulated the influence of different N188 mutation of hCx46.

2. Experimental design, materials and methods

2.1. Structural modeling and molecular dynamics simulations

To produce the data, a structural model of hCx46 was generated using MODELLER [2], and the high-resolution crystal structure of hCx26 (PDB ID: 2ZW3) [3] was taken as a template. Both connexins belong to the K/R-N group [7] and have a high sequence homology in the second extracellular loop E2, the essential region for connexon docking. Therefore the usage of hCx26 as template for this region seems to be acceptable. The MODELLER objective function and the discrete optimized protein energy (DOPE) were used for the evaluation and selection of the models. The CL loop conformation, which is missing in the template structure, was subsequently optimized. The gap junction channel of hCx46 was constructed by superposition of the hCx46 connexins on the hCx26 connexin chains in the connexon derived from the X-ray structure [3]. A two-fold symmetry operation was used to build the second hemichannel. A pair of interacting hCx46 molecules of opposing hemichannels was selected as the model system for molecular dynamics simulations, and for the different mutants in which the aspargine residue at position 188 was replaced by either threonine, glutamine or aspartic acid. The four simulations – hCx46wt, hCx46N188T, hCx46N188Q and hCx46N188D – were immersed individually in a cubic box filled with explicit TIP3P water molecules [6], and the net charge was neutralized by adding Na$^+$ counter ions. To keep disulfide bridges stable, patches were implemented between residues C54 - C192, C61 - C186, and C65 - C181 of hCx46, which correlate with the disulfide bridges C53 - C180, C60 - C174, and C64 - C169 in hCx26. All molecular dynamics simulations were conducted using NAMD 2.9 [4] and the CHARMM27 force field [5]. A 12 Å cutoff was used for non-bonded short-
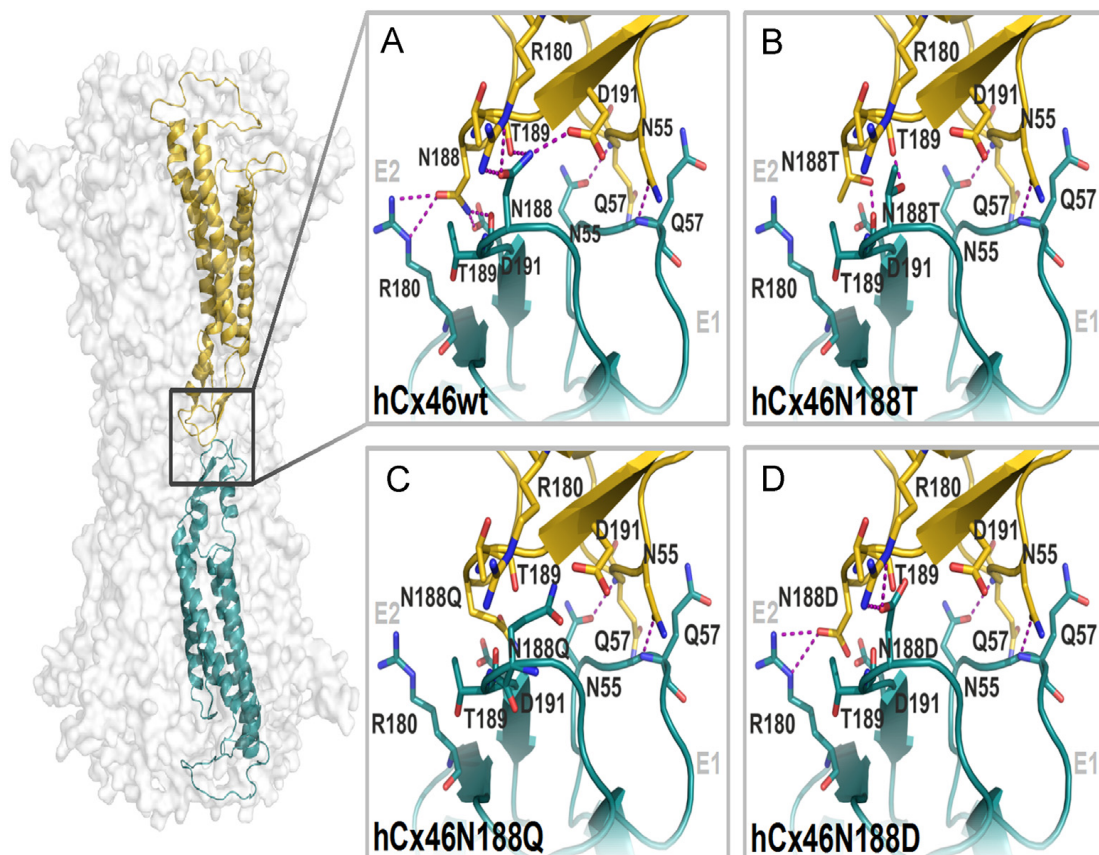

Fig. 1. Binding interface and HBs network of the wild type (A) and the three mutants, hCx46N188T (B), hCx46N188Q (C) and hCx46N188D (D). The three N188 mutations disturb the HB network to varying degrees.
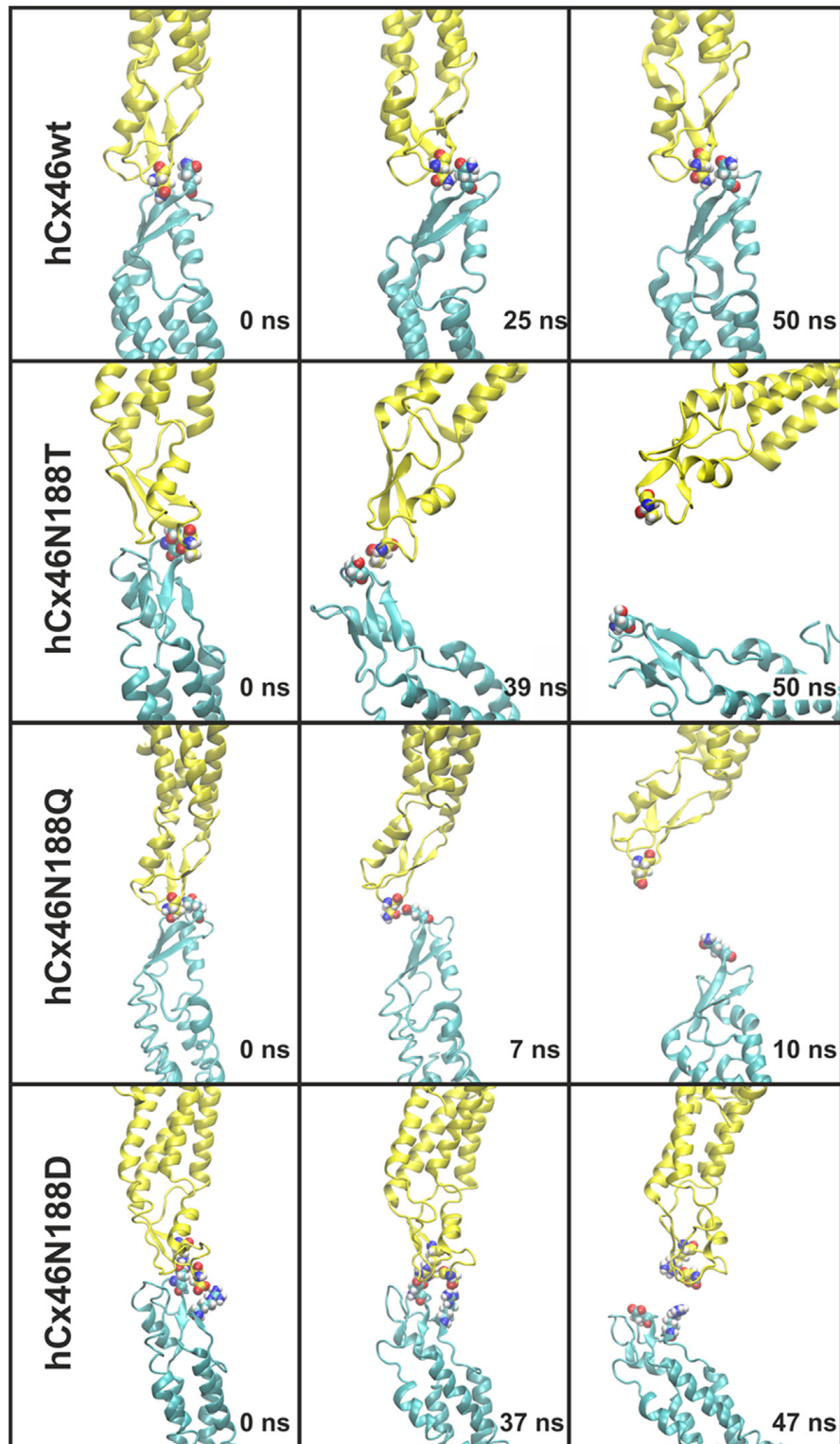
Fig. 2. Snapshots from the molecular dynamics simulations of hCx46wt and the three mutants.

range interactions, and long-range electrostatics were treated with the particle-mesh Ewald method [8]. Temperature and pressure were maintained at 310 K and 101.3 kPa using Langevin dynamics and the Langevin piston method. The simulation time step was 1 fs. Each simulation system was first energy minimized and subsequently equilibrated for approximately 5 ns – during which the systems converged towards a backbone RMSD of 5–7 Å - prior to production runs. Molecular dynamics (MD) simulations were conducted for 50 ns each at the Computer Cluster of the Norddeutscher Verbund für Hoch- und Höchstleistungsrechnen (HLRN). Simulations of the entire hCx46wt and hCx46N188Q gap junction channels were prepared and treated analogously to the above described procedure.

2.2. Molecular dynamics simulation of interacting hCx46 connexins

The data shows the influence of the N188T mutation compared to the wild type, molecular dynamics simulations were performed over 50 ns simulation time. The artificial mutation N188Q reintroduces a carboxamide group at position 188 but is bulkier. In the second artificial mutation N188D, the asparagine residue is replaced by the equally sized aspartic acid residue. Fig. 1 shows the data of the HB network surrounding residues N188, T188, Q188 and D188, [1] which got disrupted in all the mutants, leading to a destabilization of the complex during the MD simulation (Fig. 2, movies of the molecular dynamics simulation: supplementary material S1–S4). Furthermore, monitoring the angles between the interacting connexins along the simulation time for the wild type and the N188T mutant showed a stable angle of about 170° between the hCx46wt monomers, while the hCx46N188T monomers bent relative to each other, reducing the angle to about 60° during the trajectory (Fig. 3).

Supplementary material related to this article can be found online at http://dx.doi.org/10.1016/j. dib.2016.01.067.

2.3. N188D introduces a negative charge

The data of the artificial mutation N188D introduces a negative charge that seems to cause an electrostatic repulsion. Fig. 4 shows the electrostatic surface potential of the molecules of wild type connexin compared to the N188D mutation (blue areas symbolize positive charges, white areas indicate neutral regions and red colored areas represent negatively charged regions) as well as the repulsion after 20 ns simulation time (long arrows).

Furthermore, we tested the effect of reciprocal charge mutations N188D and D191N on our Cx46 model system during MD simulations (see supplementary video S5) since our data shows that the residue N188 forms a hydrogen bond with D191. Despite the reported rescue function of such reciprocal charge mutations for the Cx32/Cx26 complex [4,9], the Cx46 complex dissociated within 50 ns in our simulations.
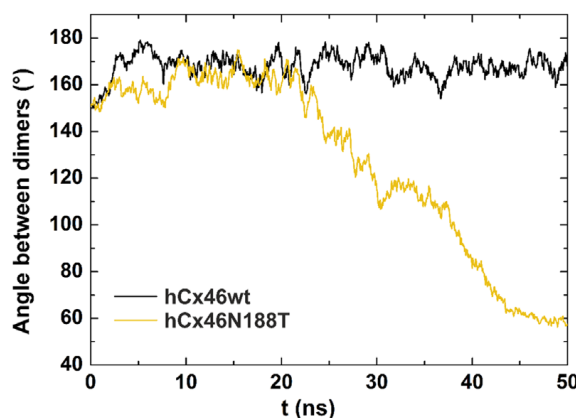

Fig. 3. Diagram depicting the angle between the interacting connexins along the simulation time for hCx46wt (black) and hCx46N188T (gold). While the N188T mutation leads to a kinking of the connexins relative to each other and finally to the dissociation of the complex, hCx46wt connexins remain rather constant with an angle around 170°.
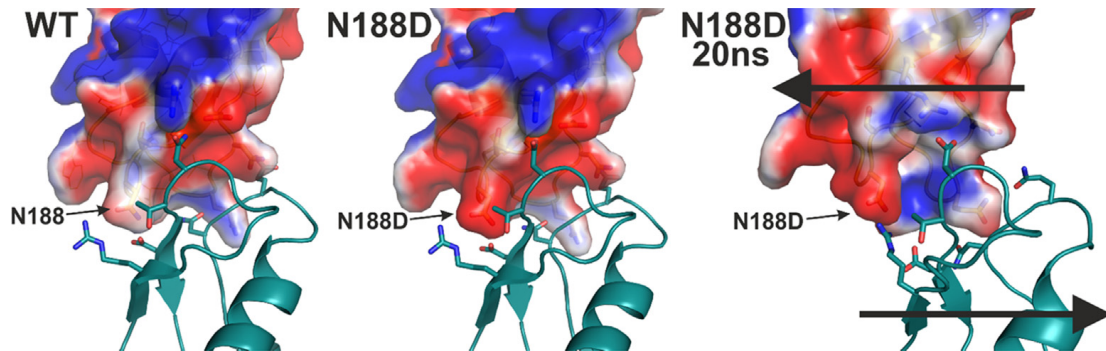
Fig. 4. The snapshot sequence shows the electrostatic repulsion of the hCx46N188D mutation with D191 (long arrows). Blue areas symbolize a positive charge, white a neutral charge and the red colored area is negatively charged.
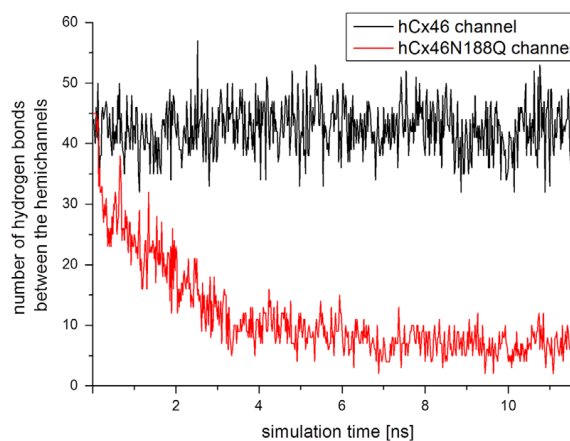

Fig. 5. The number of HBs between the hemichannels composed of hCx46wt (black) and hCx46N188Q (red). According to Gong et al. [9], the stability of a gap junction channel is achieved if an average of 18 HBs is achieved. For the hCx46N188Q channel the number of HBs is reduced to less than 10 within the first 3 ns leading to the dissociation of the complex. The supplemental movie S7 shows the dissociation. In comparison, movie S6 shows that hCx46wt hemichannels form a stable complex.

Supplementary material related to this article can be found online at http://dx.doi.org/10.1016/j. dib.2016.01.067.

2.4. Data from a model of whole gap junction channels

Simulations were performed for the entire hCx46wt and hCx46N188Q gap junction channels (see movies in the supplementary material S6 and S7). The data shows that hCx46wt connexons interact through an average of 40 HBs in the simulations. These HBs stabilize the whole gap junction channel complex along the trajectory (movie S6). For the hCx46N188Q connexins, the connexons formed also about 40 HBs at the beginning of the simulation. However, the number of HBs decreased rapidly within the first 3–4 ns of simulation and the channel complex started to dissociate (Fig. 5 and movie S7). Nevertheless, after 10 ns complete dissociation of the channel was not achieved and an average of 5 HBs were still detectable.

Supplementary material related to this article can be found online at http://dx.doi.org/10.1016/j. dib.2016.01.067.

Acknowledgments

Appendix A.   Supplementary material

Supplementary data associated with this article can be found in the online version at http://dx.doi.org/10.1016/j.dib.2016.01.067.

References

[1] P. Schadzek, B. Schlingmann, F. Schaarschmidt, J. Lindner, M. Koval, A. Heisterkamp, M. Preller, A. Ngezahayo, The cataract related mutation N188T in human connexin46 (hCx46) revealed a critical role for residue N188 in the docking process of gap junction channels, Biochim. Biophys. Acta (2015), http://dx.doi.org/10.1016/j.bbamem.2015.10.001.
[2] A. Sali, T.L. Blundell, Comparative protein modelling by satisfaction of spatial restraints, J Mol. Biol. 234 (1993) 779–815.
[3] S. Maeda, S. Nakagawa, M. Suga, E. Yamashita, A. Oshima, Y. Fujiyoshi, T. Tsukihara, Structure of the connexin 26 gap junction channel at 35 A resolution, Nature 458 (2009) 597–602.
[4] J.C. Phillips, R. Braun, W. Wang, J. Gumbart, E. Tajkhorshid, E. Villa, C. Chipot, R.D. Skeel, L. Kalé, K. Schulten, Scalable molecular dynamics with NAMD, J Comput. Chem. 26 (2005) 1781–1802.
[5] A.D. MacKerell, D. Bashford, M. Bellott, R.L. Dunbrack, J.D. Evanseck, M.J. Field, S. Fischer, J. Gao, H. Guo, S. Ha, D. Joseph-McCarthy, L. Kuchnir, K. Kuczera, F.T. Lau, C. Mattos, S. Michnick, T. Ngo, D.T. Nguyen, B. Prodhom, W.E. Reiher, et al., All-atom empirical potential for molecular modeling and dynamics studies of proteins, J Phys. Chem. B 102 (1998) 3586–3616.
[6] W.L. Jorgensen, J. Chandrasekhar, J.D. Madura, R.W. Impey, M.L. Klein, Comparison of simple potential functions for simulating liquid water, J. Chem. Phys. 79 (1983) 926–935.
[7] M. Koval, S.A. Molina, J.M. Burt, Mix and match: investigating heteromeric and heterotypic gap junction channels in model systems and native tissues, FBBS Lett. (2014).
[8] T.A. Darden, L.G. Pedersen, Molecular modeling: an experimental tool, Environ. Health Perspect. 101 (1993) 410–412.
[9] X.-Q. Gong, S. Nakagawa, T. Tsukihara, D. Bai, A mechanism of gap junction docking revealed by functional rescue of a human-disease-linked connexin mutant, J Cell Sci. 126 (2013) 3113–3120.

Anhang C: Publikation Schadzek *et al.*, 2018

Konkatemerisierung von humanem Connexin26 (hCx26) und humanem Connexin46 (hCx46) zur Analyse von heteromeren Gap Junction-Halbkanälen und heterotypischen Gap Junction-Kanälen

Concatenation of Human Connexin26 (hCx26) and Human Connexin46 (hCx46) for the Analysis of Heteromeric Gap Junction Hemichannels and Heterotypic Gap Junction Channels

Patrik Schadzek, Doris Hermes, Yannick Stahl, Nadine Dilger, Anaclet Ngezahayo

Beitrag zur Publikation: Ich habe zusammen mit A.N. die Experimente geplant. Ich habe die meisten Experimente durchgeführt, die alle Daten ausgewertet und interpretiert. Ich habe alle Abbildungen erstellt und das Manuskript zusammen mit A.N. geschrieben.

Article

Concatenation of Human Connexin26 (hCx26) and Human Connexin46 (hCx46) for the Analysis of Heteromeric Gap Junction Hemichannels and Heterotypic Gap Junction Channels

Patrik Schadzek [1] iD**, Doris Hermes** [1,2] iD**, Yannick Stahl** [1] iD**, Nadine Dilger** [1] **and Anaclet Ngezahayo** [1,3,*]

[1] Institut für Biophysik, Leibniz Universität Hannover, Herrenhäuser Straße 2, 30419 Hannover, Germany; p.schadzek@biophysik.uni-hannover.de (P.S.); hermes@em.mpg.de (D.H.); yannick.stahl1@googlemail.com (Y.S.); n.dilger@biophysik.uni-hannover.de (N.D.)
[2] Department of Clinical Neurophysiology, University of Göttingen, Robert-Koch Str. 40, D-37075 Göttingen, Germany
[3] Zentrum für Systemische Neurowissenschaften Stiftung Tierärztliche Hochschule Hannover, Bünteweg 2, 30559 Hannover, Germany
[*] Correspondence: ngezahayo@biophysik.uni-hannover.de; Tel.: +49-511-762-4568

check for updates

Abstract: Gap junction channels and hemichannels formed by concatenated connexins were analyzed. Monomeric (hCx26, hCx46), homodimeric (hCx46-hCx46, hCx26-hCx26), and heterodimeric (hCx26-hCx46, hCx46-hCx26) constructs, coupled to GFP, were expressed in HeLa cells. Confocal microscopy showed that the tandems formed gap junction plaques with a reduced plaque area compared to monomeric hCx26 or hCx46. Dye transfer experiments showed that concatenation allows metabolic transfer. Expressed in *Xenopus* oocytes, the inside-out patch-clamp configuration showed single channels with a conductance of about 46 pS and 39 pS for hemichannels composed of hCx46 and hCx26 monomers, respectively, when chloride was replaced by gluconate on both membrane sides. The conductance was reduced for hCx46-hCx46 and hCx26-hCx26 homodimers, probably due to the concatenation. Heteromerized hemichannels, depending on the connexin-order, were characterized by substates at 26 pS and 16 pS for hCx46-hCx26 and 31 pS and 20 pS for hCx26-hCx46. Because of the linker between the connexins, the properties of the formed hemichannels and gap junction channels (e.g., single channel conductance) may not represent the properties of hetero-oligomerized channels. However, should the removal of the linker be successful, this method could be used to analyze the electrical and metabolic selectivity of such channels and the physiological consequences for a tissue.

Keywords: oligomerization; concatenated connexins; gap junction; channel stoichiometry; heteromeric connexons; human connexin46; human connexin26; inside-out patch-clamp configuration; dual whole-cell patch-clamp; dye transfer

1. Introduction

Gap junction channels (GJC) are formed between adjacent cells by docking of two hemichannels. The hemichannels are formed by oligomerization of connexins (Cx). Connexins are membrane proteins encoded by a gene family which in the human genome comprises 21 members [1]. In many tissues, different connexins are concurrently expressed and the formation of heteromeric connexons and heterotypic gap junction channels has been postulated. It is assumed that by forming heteromeric

connexons and heterotypic gap junction channels, the cells in a tissue could achieve a rectification of gap junctions as it is observed in tissue [2,3]. Using expression systems such as the *Xenopus* oocytes, the formation of heterotypic gap junction channels could be unequivocally demonstrated by coupling two oocytes expressing two different connexins [4]. With such experiments, it was possible to specify which connexins were able to form heterotypic gap junction channels with each other. In combination with molecular biology and protein modeling, it was possible to classify the connexins into two different groups depending on some residues found in the second extracellular loop (EL2). One group is represented by Cx26 and named K-N group with the sequence ϕ(K/R)CXXXPCPNXVDC$\Omega\psi$S and a second group is represented by Cx43 called H group with the sequence ϕXCXXXPCPHXVDC$\Omega\psi$S. In the sequences, ϕ represents a hydrophobic residue, X is any residue, Ω an aromatic residue, and ψ indicates a residue with a large aliphatic side chain [5–10]. Within a group the connexins formed compatible connexons. An asparagine residue in position 168 of Cx26 or in a homologous position in other connexins belonging to the K-N group was shown to form hydrogen bonds and was therefore essential for the docking between hemichannels of this group [11–13]. The analysis of hCx26, for which a crystal structure was generated, revealed that each asparagine residue at position 176 (N176) in a hemichannel formed three hydrogen bonds with a lysine residue at position 168 (K168), a threonine residue at position 177 (T177), and an aspartic acid residue at position 179 (D179) in the E2 domain of the counterpart hCx26 in the hemichannel of the adjacent cell [6–9,11,14–18]. For hCx32 and hCx46, homologous N residues to N176 were described [12,13,19,20]. For hCx32, the central N residue was N175, which interacted with K167, T176, and D178. For hCx46, the N188 formed corresponding hydrogen bonds with R180, T189, and D191. The importance of N176 and K168 for the docking interaction was recently demonstrated by Karademir et al. (2016) [21]. The authors showed that by adapting the homologous residues, heterotypic docking between Cx26 and Cx40 connexons could be achieved.

With respect to oligomerization in connexons, the first transmembrane domain (TM1) and the transition between the cytoplasmic loop (CL) and the third transmembrane domain (TM3) were identified as the critical regions [10,22,23]. Analyzing Cx26 mutants, the sequence V37-A40 (VVAA) of the wild type Cx26 was identified as an important motive for Cx26 oligomerization. However, as stated in Jara et al. (2012), the motive did not determine hetero-oligomerization of connexins [10,22,23]. Concerning the hetero-oligomerization of different connexin types within a connexon, the compatibility between connexins was mostly related to the amino acid residues in the region of the transition between the cytoplasmic loop (CL) and the third transmembrane domain (TM3) [10]. According to the sequence of these regions, the connexins were classified into the R-type connexins, which contain a conserved arginine or lysine motif in this region, and the W-type connexins with a di-tryptophan motif. In compliance to this classification, only connexins belonging to the same type can hetero-oligomerize. However, even if the motif in this region is important for the oligomerization, it was proposed that indirect mechanisms associated with the motif were necessary to achieve the discrimination between connexins that do not belong to the same type. Cx43 proteins, for example, are maintained as monomers in the endoplasmic reticulum (ER) by the chaperone protein ERp29, which is associated with the second extracellular loop, thereby avoiding oligomerization. After the transport to the trans-Golgi network, the Cx43 proteins are separated from ERp29 for oligomerization [24]. Therefore, it was suggested that the sequence did not per se hinder the oligomerization between connexins belonging to different types. The sequence was rather an element involved in recruiting quality control proteins like ERp29 that in turn regulated the oligomerization.

Concatenation of subunits of the GABA, Ach, and $P_{2\times7}$ ionotropic receptors has been used to analyse the architecture of these membrane channels [25–28]. In these studies, it was shown that concatenated proteins were completely inserted in the cell membrane. In the present report, we concatenated hCx26 and hCx46 (Figure 1). Cx26 and Cx46 are concurrently expressed in trachea and alveolar epithelium type 1 and 2 cells [29,30]. With respect to the docking they belong to the K-N group. Therefore, they form hemichannels that can dock to each other. But with respect to the oligomerization

behavior, Cx26 belongs to the W-type while Cx46 belongs to the R-type so that they are not supposed to oligomerize [10]. The analysis of the formed gap junction channels with imaging methods and functional assays, as well as electrophysiological characterization, showed that the concatenated proteins were able to form functional hemichannels and gap junction channels. Although aspects of the channels e.g., single channel conductance might be affected by concatenation, aspects such as docking of hetero-oligomerized connexins in variable and clearly determined stoichiometry could be analyzed using concatenation of connexins. For an accurate analysis of the biophysical properties of the concatenated channels, it would be desirable to cleave the linkers of the concatenated connexins in a connexon to reintroduce the full C- and N-terminal flexibility (and thus the natural functionality), as it was done for the concatenated pannexin1 [31].
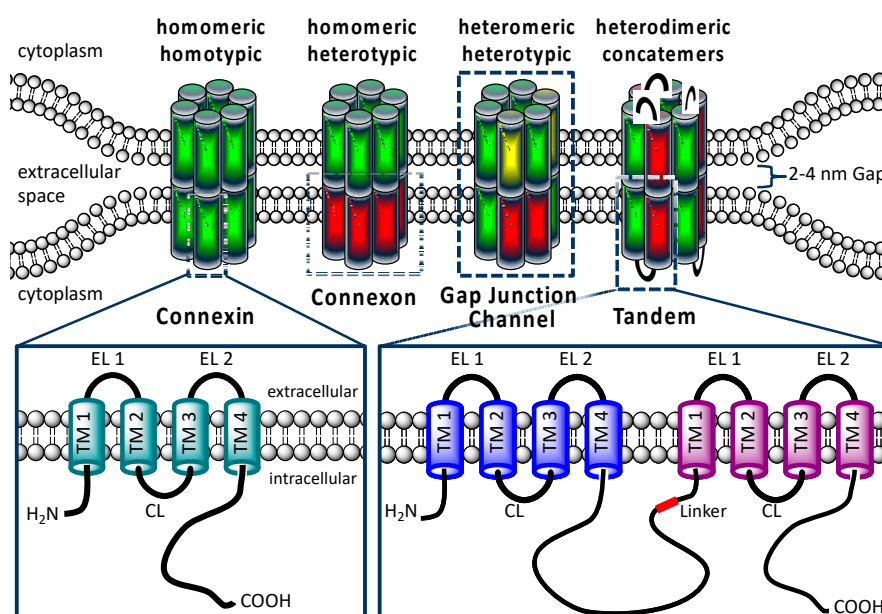

Figure 1. Structural organization of connexins and gap junctions. A gap junction channel is composed of two hemichannels or connexons, which consist of six connexins. Connexins have four transmembrane domains (TM), two extracellular loops (EL), one cytoplasmatic loop (CL), as well an intracellularly localized N- and C-terminus. Homomeric connexons and homotypic gap junction channels are formed by a single connexin isoform. In the postulated heteromeric connexons and heterotypic gap junction channels, different connexin isoforms are expected. The lower right pictogram shows the constructed concatemeric connexins as heterodimeric tandem.

2. Results

2.1. Gap Junction Plaques Formed by Concatenated Variants of hCx26 and hCx46

Molecular cloning was used to generate concatenated hCx26-hCx26-GFP (green fluorescent protein), hCx46-hCx46-GFP, hCx26-hCx46-GFP, and hCx46-hCx26-GFP. In order to concatenate two neighboring connexins, a 19-amino acid long linker was inserted into the sequence. The linker, which was used between the connexin and the GFP tag, was 23 amino acids long (Table 1).

Table 1. The amino acid linkers (one-letter code) between the two concatenated connexins and between the connexin and the GFP tag. The GFP tag was always located at the C-terminus.

Linker	Amino Acid Sequence
Cx-Cx	GGNLQSTVPR ATTLYTKVV
Cx-GFP	GGNLQSTVPR AHPAFLYKVV RSR

The concatenated constructs, as well as hCx26-GFP and hCx46-GFP, were expressed in HeLa cells to analyze their capacity to form gap junction plaques. Confocal laser scanning microscopy showed that the GFP labeled constructs formed gap junction plaques between neighboring cells (Figure 2A and Figure S1 in the Supplemental Materials). Compared to the expressed monomeric hCx26-GFP or hCx46-GFP, the dimeric connexins formed gap junction plaques with a reduced surface, suggesting a possible reduction of the protein synthesis for both heterodimeric and homodimeric tandems (Figure 2B). Moreover, western blotting of the hCx46 monomer and hCx46-hCx46 homodimer seems to corroborate the suggestion (Figure 2C). When quantifying the protein amount of the hCx46 monomer and the hCx46-hCx46 homodimer using an anti-Cx46 antibody, cells expressing the homodimer showed a reduction of about 40% of the relative hCx46 amount compared to cells expressing the monomeric hCx46.
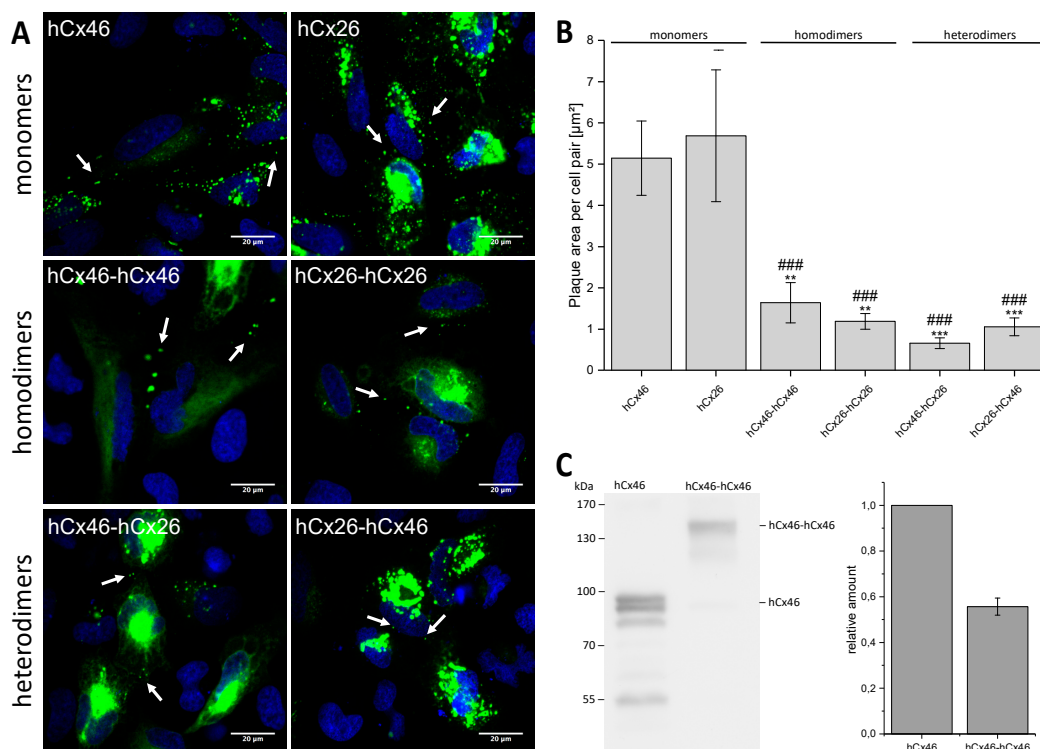

Figure 2. Expression of the GFP-labeled monomeric and concatemeric connexins in HeLa cells. (**A**) Representative micrographs of cell pairs expressing GFP-labeled hCx46, hCx26, hCx46-hCx46, hCx26-hCx26, hCx46-hCx26, and hCx26-hCx46 are shown. The cells were imaged 24 h after transfection using a confocal laser scanning microscope. The nuclei (blue) were stained with Hoechst 33342. Gap junction plaques are indicated by arrows. Gap junction plaques were found in HeLa cells expressing hCx46, hCx26, and the four different tandems. In cells expressing the tandems, a trend to accumulate the proteins in intracellular organelles was observed. (**B**) Quantification of the gap junction plaque area formed by the monomers and the four different tandems in HeLa cells. The plaque area was calculated using the particle analyzer of ImageJ and normalized to the number of transfected cell pairs. At least three transfections were performed per construct. The results are given as average plaque area per cell pair [μm^2]. Error bars represent the SEM. The data were evaluated by a one-way ANOVA and a post-hoc Tukey test (** $p \leq 0.01$, *** $p \leq 0.001$) in comparison to hCx46 and hCx26 (### $p \leq 0.001$). (**C**) Quantification of the relative protein amount in HeLa cells expressing the monomeric hCx46-GFP or the homodimeric hCx46-hCx46-GFP. An anti-Cx46 antibody was used for the western blotting. For the quantification, four independent replicates were analyzed by using the gel analyzer tool of the FiJi software [32]. The data was normalized to the intensity of the hCx46 monomer.

To test the physiological functionality of the built gap junction channels, dye transfer experiments with the monomeric and the tandem connexins in all variations were performed in HeLa and N2A cells (Figure 3). HeLa cells, transfected with either a GFP-labelled monomeric connexin or a homo- or heterodimeric tandem, showed a degree of Lucifer Yellow dye coupling of about 45%, while mock-transfected HeLa cells showed a significantly reduced degree of dye coupling (11%). When using AMCA (7-amino-4-methyl-3-coumarinylacetic acid) as tracer dye in Neuro2A (N2A) cells, expressing the untagged homo- or heterodimeric tandems or the monomeric variants together with soluble GFP (IRES-GFP plasmids), a dye transfer rate between 32% and 46% could be observed, while N2A cells expressing only the soluble GFP showed a significantly reduced dye coupling ability of about 5%. Interestingly, the concatenation did not alter the formation of the functionally coupled gap junction channels.
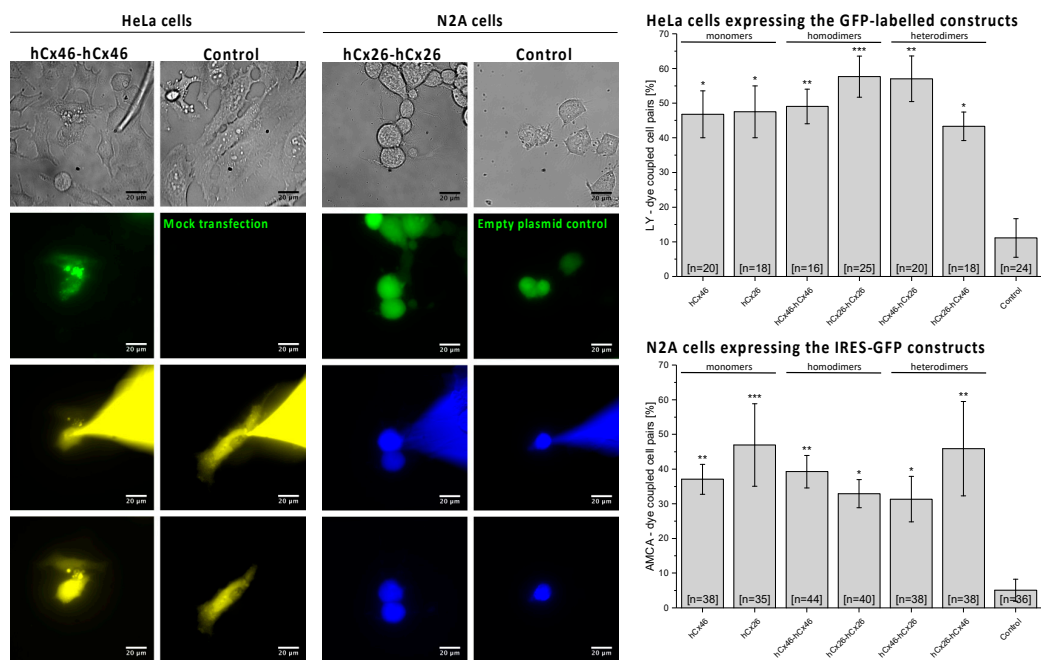

Figure 3. Analyzing the gap junction functionality by dye transfer experiments. A whole-cell patch-clamp configuration with a pipette solution containing 1 mg/mL Lucifer yellow was established on a HeLa cell pair expressing GFP-labelled monomeric hCx26 or hCx46 or one of the concatemeric variants. Mock transfected cells were used as control. The first row of the micrographs shows the phase contrast images of example experiments. In the second row, the GFP fluorescence signal before a dye transfer experiment is shown. The third and fourth rows show the fluorescence signal of the tracer dye 5 min and 10 min after establishment of the whole cell configuration. For the sake of clarity, the image in the fourth row was taken after removal of the dye filled capillary. Likewise, the experiments were performed with N2A cells. The cells were transfected with IRES-GFP constructs resulting in the expression of untagged constructs in the membrane and GFP in the cytosol. As control, cells expressing only GFP were used. The experiments were performed with a pipette solution containing 1 mg/mL AMCA, which could easily be distinguished from GFP under the fluorescence microscope. The cells were considered as coupled if the fluorescence intensity, which was measured in the unpatched cell of a cell pair after 10 min, was at least twice as bright as the background, which was measured at the beginning of the experiment. The probability of coupling (bar diagrams) was estimated as ratio of the sum of coupled cell pairs per the sum of tested pairs. The results are given as average. Error bars represent the SEM. The data were evaluated by a one-way ANOVA and post-hoc Tukey test (* $p \leq 0.05$, ** $p \leq 0.01$, *** $p \leq 0.01$) in comparison to the control cells.

2.2. Single Channel Activity of Connexons

Cx46 is known to form gap junction hemichannels when expressed in *Xenopus* oocytes [33–35]. Therefore, *Xenopus* oocytes were used as expression system to measure the single channel activity of connexons formed by the single connexins, as well as the variant tandems. In inside-out patch-clamp experiments, we found that the open probability *p* of channels composed of the monomeric connexins, as well as the homodimers and heterodimers, was increased by suppression of Ca^{2+} on both side of the channels (Figure 4). Moreover, we observed that all configurations were sensitive to the gap junction channel inhibitor carbenoxolone (CBX). With respect to CBX, the Cx26 connexons were less sensitive to the agent than the hCx46 connexons (Figure 4). The insensitivity to CBX was even more pronounced for the hCx26-hCx26 homodimer, while the hCx46-hCx46 heterodimeric hemichannels were almost completely closed by CBX (Figure 4B). For the hemichannels formed by the heterodimers in either configuration, the sensitivity to CBX was more similar to that observed for hCx46 connexons than that of hCx26 connexons. For a further characterization of the hemichannels, we analyzed the single channel conductance in absence of Ca^{2+} (Figure 4A). Under our experimental conditions, in which the chloride was completely replaced by gluconate at both sides of the membrane, a single channel conductance of 46.0 ± 5.3 pS and 39.2 ± 5.5 pS was found for hCx46 and hCx26, respectively. For the homodimers, the conductance was reduced to 24.5 ± 3.3 pS and 32.9 ± 6.3 pS for hCx46-hCx46 and hCx26-hCx26, respectively. For the heterodimers, two substates were observed for each configuration: A conductance of 15.7 ± 0.8 pS and 26.2 ± 1.8 pS for hCx46-hCx26, and 20.1 ± 1.4 pS and 31.2 ± 3.0 pS for the hCx26-hCx46 configuration (Table 2, Figure 4). The changes in conductance are also related to the concatenation. A successful cleavage of the linker to separate the connexins in the channels is needed in order to evaluate changes solely caused by hetero-oligomerization of the connexins within a channel.
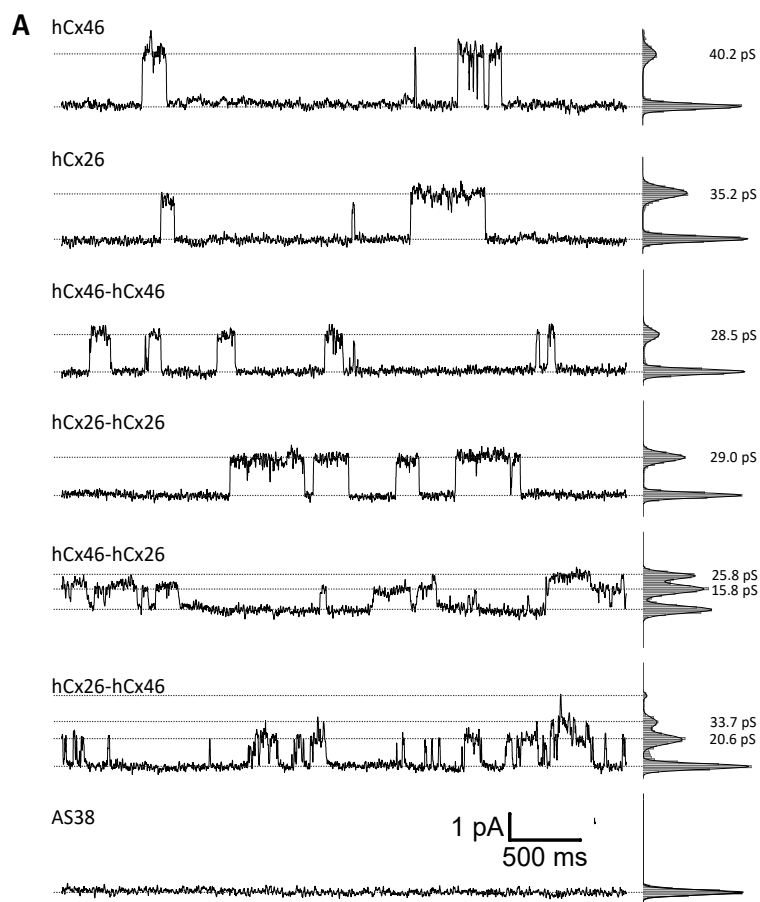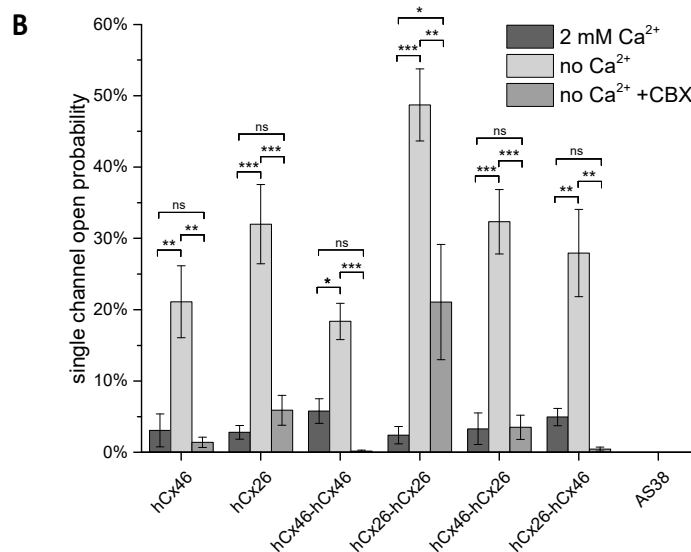
Figure 4. *Cont.*

Int. J. M

Figure 4. Analysis of single hemichannels formed by concatemeric connexins. The stripped membrane of *Xenopus* oocytes, which were injected with hCx46, hCx26, or the four different concatemeric constructs, as well as the AS38 (control) cRNA 24 h before, was used to perform the inside-out patch-clamp recordings. The measurements were performed in presence of Cs^+ and in absence of Cl^- on both sides of the membrane. (**A**) Examples of single channel currents elicited by a depolarizing voltage pulse of +50 mV in absence of Ca^{2+} in the bath solution are shown. (**B**) The open probability of all measured single channels was analyzed. The error bars represent the SEM. The data were evaluated by a one-way ANOVA followed by a Tukey test (* $p \leq 0.05$, ** $p \leq 0.01$, *** $p \leq 0.001$, ns: not significant). The statistical comparison showed that the presence of Ca^{2+} or carbenoxolone (CBX) in the bath solution significantly reduced the open probability of all tested variants.

Table 2. Conductance states of the hemichannels expressed in *Xenopus* oocytes as measured in inside out patch-clamp configuration. n gives the number of analyzed oocytes.

Injected cRNA	Large Substates $\pm$ SEM	Small Substates $\pm$ SEM
hCx46 (n = 5)	46.0 ± 5.3 pS	
hCx26 (n = 5)	39.2 ± 5.5 pS	
hCx46-hCx46 (n = 4)	24.5 ± 3.3 pS	
hCx26-hCx26 (n = 7)	32.9 ± 6.3 pS	
hCx46-hCx26 (n = 4)	26.2 ± 1.8 pS	15.7 ± 0.8 pS
hCx26-hCx46 (n = 5)	31.2 ± 3.0 pS	20.1 ± 1.4 pS
AS38 (n = 6)	0 pS	

2.3. Dye Uptake through Hemichannels

Using ethidium bromide (Etd), we observed the dye uptake by HeLa cells expressing hemichannels formed by the different variants in order to clarify how the constructed tandems could affect the function of the channels. First, we found that the cells expressing the monomers or the tandems in different variations did not differ from mock cells in their capacity to absorb ethidium bromide as long as external Ca^{2+} was present (Figure 5). The dye uptake in presence of external Ca^{2+} was therefore considered as background uptake. Specific hemichannel uptake of the dye was initialized when the cells were superfused with a Ca^{2+}-free external solution (Figure 5). To determine a possible mechanical effect on the dye uptake, the cells were first superfused with a 2 mM Ca^{2+}-containing solution. In cells expressing the homodimeric hCx26-hCx26, a tendency to increase the rate of dye uptake during the perfusion with the Ca^{2+}-containing solution was observed. However, this mechanical sensitivity of the channel was not statistically significant when analyzed by a two-way ANOVA and a post-hoc Tukey test. For cells expressing the GFP control or the other

variants, the tendency to respond to a mechanical stimulus was not observed (Figure 5). For all variants, the ethidium bromide uptake was accelerated by the superfusion of the cells with Ca^{2+}-free external solution compared to cells expressing the GFP control (Figure 5A,B and Figure S2: Table in the Supplemental Materials). In the context of low external Ca^{2+}, only the hCx26-hCx26 homodimer showed an increased rate of dye uptake compared to the monomeric hCx26 and hCx46, as well as the hCx46-hCx46 homodimer and both heterodimers (S2). These changes in the ethidium bromide dye uptake rate seems to be an artifact due to the concatenation. For hCx46 however, the hCx46-hCx46 homodimer as well as the hCx46 monomer showed a comparable rate of dye uptake, and this uptake rate of hCx46 was also measured for the heterodimers in either order. Additionally, dye uptake by hemichannels in all variants except for the hCx26 monomer (and the GFP control cells) was significantly reduced by the superfusion with a La^{3+}-containing medium. When using a two-way ANOVA and a post-hoc Tukey test for the comparison of the different variants, neither the perfusion with the Ca^{2+}-containing solution nor the perfusion with a Ca^{2+}-free and La^{3+}-containing solution showed a significant difference to another variant or the GFP expressing control cells. Only the perfusion with the Ca^{2+}-free solution led to significant differences, as described above (S2).
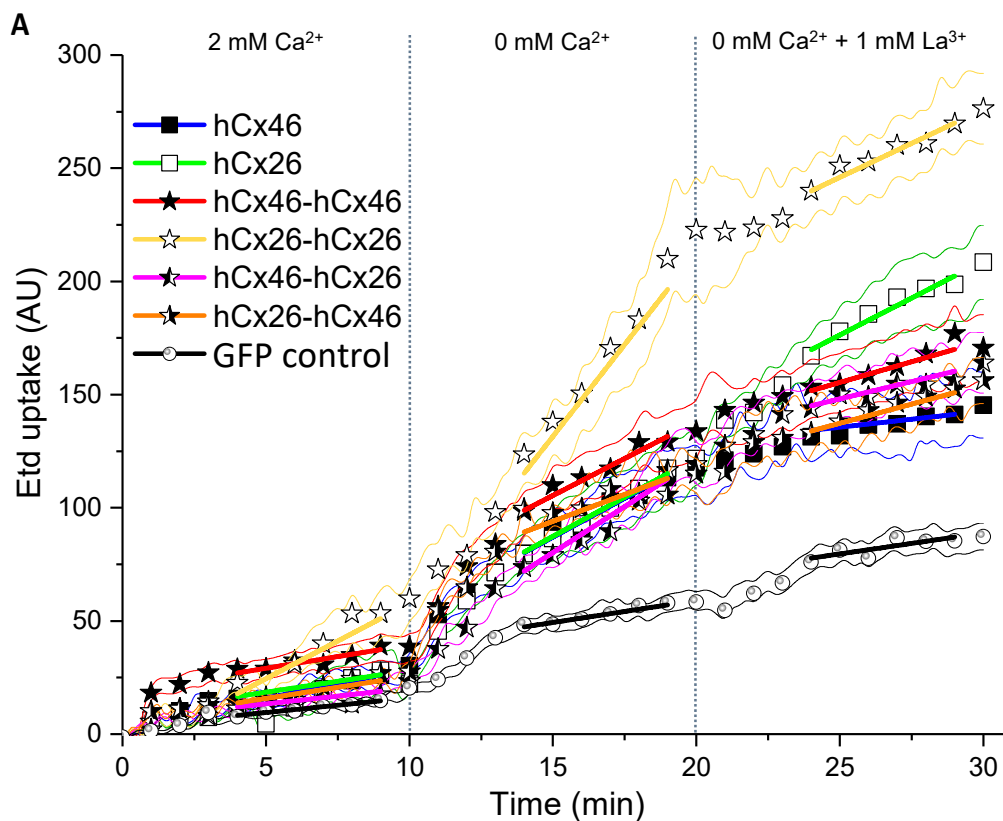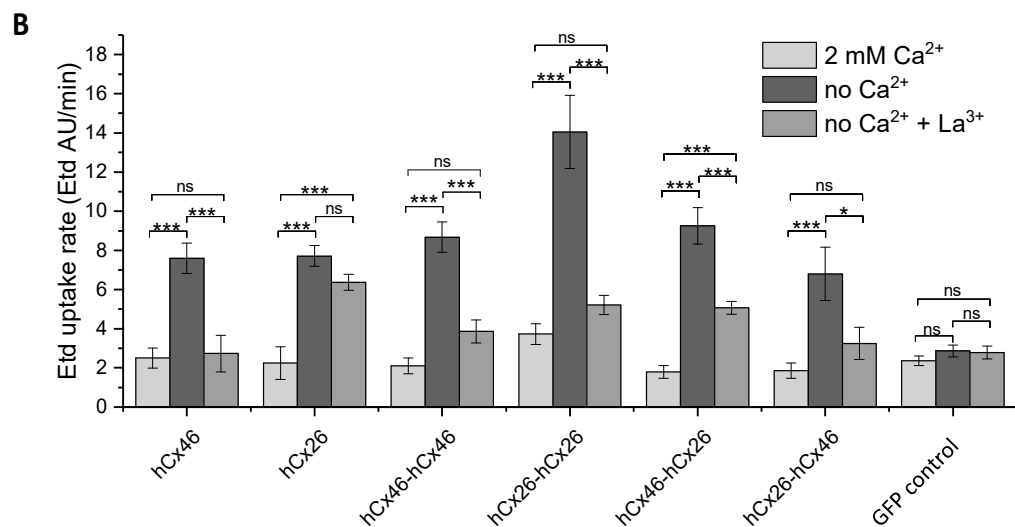
Figure 5. *Cont.*

B

Figure 5. Dye uptake through hemichannels using ethidium bromide. HeLa cells were grown on coverslips to a confluency of about 40–50% and transfected with IRES-GFP-plasmids. The GFP allowed the identification of transfected cells by fluorescent microscopy. (**A**) Time course of dye uptake experiments by cells expressing the different variants when perfused with bath solutions containing 2 mM Ca^{2+}, no Ca^{2+}, and no Ca^{2+} but 1 mM La^{3+}. The fine lines show the SEM spread for all measured points. The symbols indicate the average for data points measured every 1 min. The solid lines indicate the part of the curves that was used to estimate the dye uptake rate. (**B**) Quantification of the dye uptake rate (Etd AU/min) for all tested variants and the backbone control in absence or presence of Ca^{2+} or La^{3+}. The error bars represent the SEM. The data were evaluated by a one-way ANOVA and a post-hoc Tukey test (* $p \leq 0.05$, *** $p \leq 0.001$, ns: not significant).

2.4. Activity of Single Gap Junction Channels

The activity of single gap junction channels was analyzed by dual whole-cell patch-clamp experiments [36,37] applied on N2A cells expressing hCx26 and hCx46, as well as the different dimeric variants. Compared to HeLa cells, which were used for the analysis of gap junction plaques, N2A cells did not form a monolayer, which offered the advantage of an easy identification of unambiguous cell pairs suitable for the dual whole-cell patch-clamp experiments. Moreover, probably due to their round morphology, the cells formed small gap junction plaques with less gap junction channels allowing a better observation of single gap junction channel activity (Figure 6).

Cells expressing the different variants were found to form gap junction channels with a total macroscopic conductance of up to 1000 pS. In some of these cell pairs, it was possible to follow the closing and opening of single gap junction channels at different transjunctional voltages, and to estimate the conductance of the single gap junction channels in dependency of the expressed variant. Although multiple simultaneously opened channels were recorded, it was possible to follow the opening and closing of single gap junction channels (Figure 6).

Considering the clear opening and closing of the single channels, maximal conductance levels of 202 pS, 198 pS, 138 pS, 184 pS, 137 pS, and 371 pS were estimated for the Cx46 monomer, Cx46-Cx46 homodimer, Cx26 monomer, Cx26-Cx26 homodimer, Cx46-Cx26 heterodimer, and Cx26-Cx46 heterodimer, respectively. The mean of the large conductance ± SEM of these variants is given in Table 3. Besides these large conductance levels, low subconductance states were observed (Figure 6 and Figure S3 in the Supplemental Materials). However, because of the rapid flickering, a clear estimation of the numeric values was not possible.
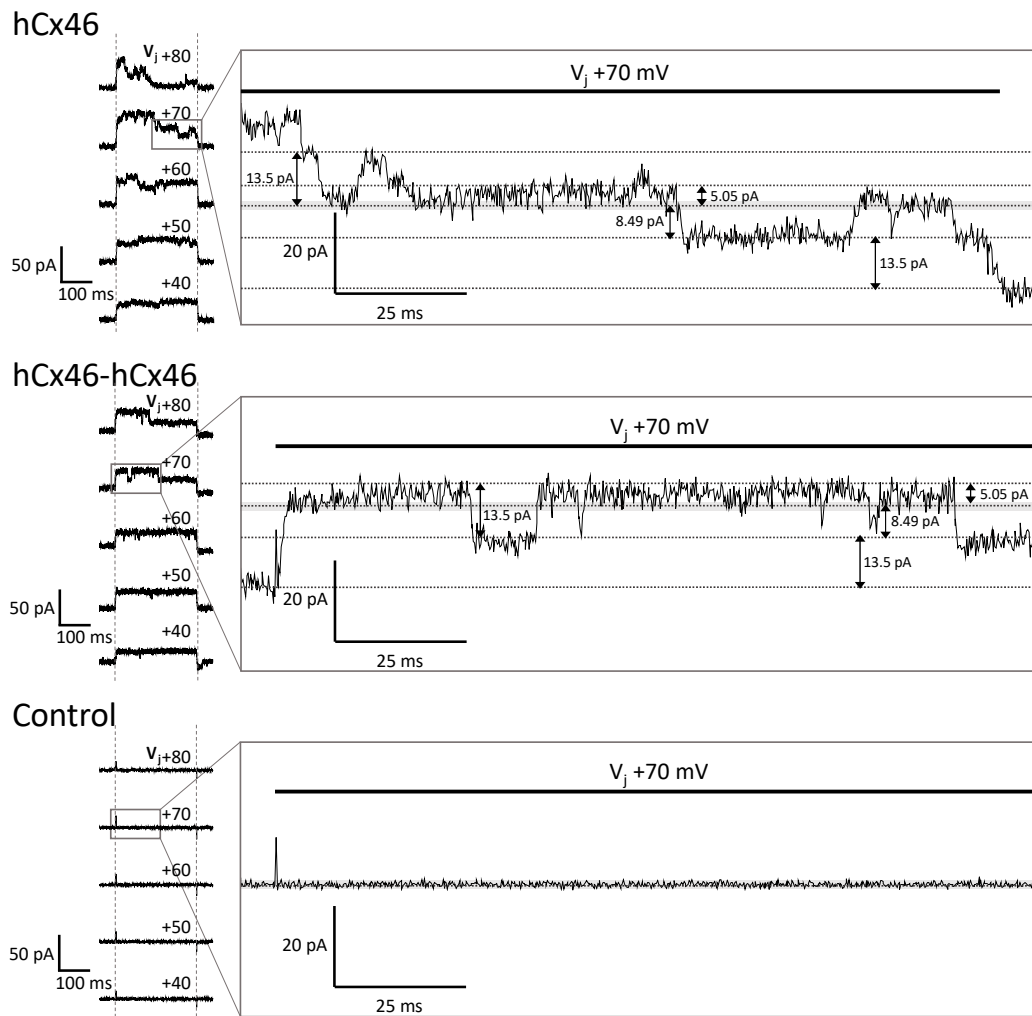
Figure 6. Recordings of dual whole-cell patch-clamp experiments. N2A cells were cultured and transfected with the different IRES-GFP-plasmids. As control, cells expressing only soluble GFP in the cytosol were used. Twenty-four hours post transfection, the dual whole-cell patch-clamp experiments were performed. The resting membrane potential was set to −40 mV for both cells. One cell of a cell pair was alternatingly stepped from −120 mV to +60 mV, while the junctional currents were recorded in the other cell. The junctional currents (ΔI2) recorded during the 250 ms-long voltage pulses at different transjunctional potentials are shown above the current responses. Magnification of the Vj +70 mV traces of the hCx46 monomer, as well as of the hCx46-hCx46 homodimer, showed several simultaneously open channels, with a large conductance of ~193 pS (13.5 pA step), and low conductance of ~72 pS (5.05 pA step) and ~121 pS (8.49 pA step). Similar steps were observed for Cx46 by other authors [38–41]. The control cells showed only the background noise, which was below 2 pA (grey band), indicating that the fluctuations of about 5 pA were conducting substates.

Table 3. Large conductance states of the gap junction channels expressed in transfected N2A cell pairs. n gives the number of analyzed cell pairs for each variant.

Expressed Variant	Large Conductance $\pm$ SEM
hCx46 (n = 7)	175.5 $\pm$ 5.7 pS
hCx26 (n = 7)	182.8 $\pm$ 1.0 pS
hCx46-hCx46 (n = 14)	193.5 $\pm$ 2.4 pS
hCx26-hCx26 (n = 9)	125.1 $\pm$ 4.0 pS
hCx46-hCx26 (n = 18)	110.5 $\pm$ 8.5 pS
hCx26-hCx46 (n = 11)	281.2 $\pm$ 24.7 pS
GFP control (n = 8)	0 pS

3. Discussion

In cells, different connexin isoforms are concurrently expressed. The formation of heteromeric connexons and heterotypic channels with a variable stoichiometry offers the cell a mode for fine tuning the gap junction coupling, thereby producing a flux rectification and selectivity [3,4]. The goal of the present report was to test whether concatenated connexins form heteromeric connexons and heterotypic gap junction channels with clearly determined stoichiometry (Figure 1). This could be a promising method to study the physiological consequences of the hetero-oligomerization of connexins in hemichannels and gap junction channels.

By expressing GFP labeled hCx46 and hCx26 monomers, hCx46-hCx46 and hCx26-hCx26 homodimers, as well as hCx46-hCx26 and hCx26-hCx46 heterodimers in HeLa cells, we found that the monomers as well as the homodimers and heterodimers were transported to the cell membrane and were able to form gap junction plaques (Figure 2A). However, as shown for the hCx46 monomer and the hCx46-hCx46 homodimer, the concatenation reduced the quantity of the produced protein. This might contribute to the reduction of the gap junction plaque area formed by the tandems (Figure 2B). The results suggest that concatenation might induce changes in the synthesis or the trafficking of the proteins to the membrane. Furthermore, a tendency to retain the proteins in the ER and Golgi apparatus was observed in cells expressing the hCx46-hCx46 tandem compared to cells expressing the hCx46 monomer (Figure 2; cells expressing the hCx26 per se showed a higher intracellular signal, which limited the possibility to compare trafficking of homomers and dimers). Although this trend was not statistically significant, it could indicate a possible concatenation-related problem with protein trafficking. Nevertheless, the different tandem proteins as well as the monomers formed functional gap junction channels, as demonstrated by the dye transfer experiments (Figure 3). Consequently, the concatenation of connexins might be helpful for the analysis of hetero-oligomerization of connexins and, inter alia, opens the possibility to prospectively study metabolite selectivity, which could not be predicted so far. Oligomerization, trafficking to the membrane, and the assembly to gap junction plaques were not affected when GFP was coupled to the N-terminus. However, the fusion of a fluorescent protein tag to the N-terminus of a connexin has been shown to block the channel conductance of hemichannels and gap junction channels [42,43]. The mechanism responsible for this is still a matter of speculation. The crystal structure of Cx26 led to the prediction that the N-termini folded in the pore of the channel [11]. We can assume that the hydrophilic GFP subunits coupled to the N-termini might stay in the cytosol. They might hinder the correct folding of the N-terminus or form a lid on the cytosolic mouth of the channel. In case of the concatenated connexins, the hydrophobic transmembrane domains of the two linked connexins led to the formation of a protein with eight transmembrane domains. How the connexin C-terminus is structured is not fully understood. However, experimental data showed that the C-terminus is highly flexible [44] and interacts with cytoskeleton-associated proteins to structure the gap junction plaques in the cell membrane, suggesting that the C-terminus does not form a barrel like GFP [45]. We therefore assume that, by interacting with these associated proteins and in combination with the high flexibility, the C-terminus of the first connexin of the concatemer could be close enough to the membrane to

allow a correct structure formation of the linked N-terminus of the following connexin. However, the NMR (nuclear magnetic resonance) data also showed disorders in the C-termini that can be affected by binding to partners. Additionally, the NMR data showed the capability of dimerization in some parts of the C-termini [44]. Consequently, it is possible that the concatenation, even if it is compatible with the formation of hemichannels and gap junction channels, may affect the properties of the channels e.g., single channel conductance. Therefore, concatenation offers the possibility to form hemichannels with a determined stoichiometry and gap junction channels with manageable variabilities. However, a tool for the removal of the linker between the connexins after formation of the hemichannels is still needed to allow an exploitation of the potentialities of the method.

Considering the single channel conductance, the inside-out patch-clamp analysis of connexons formed in the membrane of *Xenopus* oocytes showed conductance values of about 46 pS and 39 pS for hCx46 and hCx26 monomers, respectively. In isolated lens fibers (Cx46) of rodents, a conductance of about 240 pS was measured [46]. Similarly, for Cx46 hemichannels expressed in *Xenopus* oocytes, HeLa, or N2A cells, main conductance levels of 250–300 pS could be identified [47–50]. For Cx26 expressed in *Xenopus* oocytes, HeLa, or N2A cells, a main conductance of 320 pS [51] and even a higher conductance above 400 pS was found [52]. In our inside-out patch-clamp experiments, we could not identify these large conductance values. However, the conductance values presented in this report of about 39 pS and 46 pS for hemichannels composed of hCx26 and hCx46 monomers are similar to measured subconductance states of these channels that were published by other authors [38–41]. For Cx26, Gaßmann et al. (2009) reported three conductance states with $G_1 = 34 \pm 8$ pS, $G_2 = 70 \pm 8$ pS, and $G_3 = 165 \pm 19$ pS. G_1 represents the vast majority of the detected events [39]. Moreover, the conductance values were measured after the replacement of chloride by the less mobile gluconate and acetate ions on both sides of the membrane. This allowed silencing the background currents and thereby isolating specific currents that were only observed in patches from oocytes expressing connexons (Figure 4). It is known that the replacement of chloride by less mobile ions leads to lower conductance values [53,54]. We therefore assume that the measurement of hemichannels formed by hCx46 and hCx26 monomers in our experimental conditions, where chloride was replaced by gluconate and acetate ions, only allowed the recording of substates with a low conductance.

The conductance values measured for the hCx46-hCx46 (24.5 $\pm$ 3.3 pS) and hCx26-hCx26 (32.9 $\pm$ 6.3 pS) homodimers were slightly lower than the conductance values found for the hemichannels formed by the respective monomers. Although the shown differences are comparably slight, concatenation-related artifacts might need to be suppressed by successfully removing the linker between the proteins within the hemichannels to reveal the properties of heteromerization-related changes. However, by allowing the generation of channels with a defined stoichiometry, concatenation could allow studying the aspects of heterodimerization of connexins. Correspondingly, we found that heterodimerization of hCx26 and hCx46 introduced two new substates with ~16 pS and ~26 pS for hCx46-hCx26, and ~20 pS and ~31 pS for hCx26-hCx46. The conductance of hemichannels formed by hCx46-hCx46 or hCx26-hCx26 homodimers was clearly different to that of hemichannels formed by hCx46-hCx26 or hCx26-hCx46 heterodimers, respectively. This result suggests that both parts of the concatenated connexins participated in the hemichannels. Further non-published data showed that concatenation of the hCx46 and the hCx46N188T mutant, which did not form gap junction plaques [13], reduced the formation of gap junction plaques compared to the homodimer hCx46-hCx46, suggesting that in concatenated form the hCx46N188T participated to formation of gap junction channels. The observation that concatenated connexins are inserted in the membrane as whole is an agreement with other experiments in which subunits of membrane proteins such as Ach, GABA, or ATP ionotropic receptors channels were concatenated [25–28]. As for the changes in conductance observed in the present report, the results indicate that the formation of heterodimeric hemichannels would change the conductance and opening properties of the channels in comparison to the respective homomeric hemichannels. A separation of the two connexins in a concatemer is desirable for the analysis of the biophysical properties of the channel.

Dual whole-cell patch-clamp experiments were performed to analyze the corresponding gap junction channels. The hCx46 and hCx26 homomers formed gap junction channels with a maximal conductance of ~200 pS for hCx46 and ~140 pS for hCx26. In other expression systems, similar conductance values were found for the gap junction channels formed by these connexins [41,55]. Beside these main conductance levels, other open substates and other residual substates with conductance values of about 20 pS for Cx46 and 17 pS for hCx26 were observed, suggesting that the conductance values (40 pS for hCx46 and 35 pS for hCx26) observed in the membrane of oocytes might represent the residual substates of the hemichannels. The concatenation of hCx46 did not change the maximal conductance of the channels (Figure 6). For hCx26, the concatenation resulted in channels with a slightly increased maximal conductance of about 180 pS. Similar to the hemichannels, the analysis of gap junction channels formed by the heterodimers revealed changes in the channel properties compared to the homodimers. Therefore, these changes, such as the strong increase of the maximal conductance, might be more related to heteromerization than to the concatenation. To confirm this hypothesis, a cleavage of the linker between the connexins in a concatemer is necessary.

The comparison of the electrophysiological data obtained from hCx46-hCx26 and hCx26-hCx46 heterodimers showed some unexpected variability with respect to hemichannels and gap junction channel activity, as well as to conductance states. The hCx26-hCx46 showed a higher activity as hemichannels and as gap junction channels in comparison to homodimers. In the case of gap junction channels, we found that channels formed by hCx26-hCx46 had a more elevated conductance (371 pS) than the channels composed of hCx46-hCx26 (137 pS). It shows that the concatenation might affect some properties of the channels, especially the electrical conductance, in a way that we cannot explain. We presume that this might be related to the short C-terminus of Cx26, which might affect the following N-terminus of Cx46. In their model, Maeda et al. (2009) suggested that the N-termini form a voltage-sensitive funnel in the cytoplasmic mouth of the pore [11]. In our experiments with the tandems, three N-termini were free while the other three termini were linked to the C-termini of the preceding molecule. If the C-terminus of Cx46 is linked, the length of this terminus may allow more flexibility to the linked N-terminus than if the C-terminus is given by Cx26, which is very short. The observation that the homodimer hCx26-hCx26 formed hemichannels and gap junction channels with more activity, as well as gap junction channels with higher conductance levels than those of the Cx26 homomers, is compatible with this presumption. Additionally, the presumed model could explain the difference in the trend of insensitivity to the inhibition by La^{3+}. Using ethidium bromide, Jara et al. (2012) already showed a degree of insensitivity of Cx26 hemichannels to La^{3+} [22]. This insensitivity was transferred to the hemichannels formed by hCx46-hCx26 heteromers and did not affect the hCx26-hCx46 heteromers (Figure 5). This trend might be related to the number of free N-termini. Because the C-terminus of Cx46 in hCx46-hCx26 is long, the N-terminus of the following hCx26 has more freedom to move. As result, we have three N-termini of hCx26, which are almost free to interact with the completely free N-termini of hCx46. In hCx26-hCx46, three N-termini of hCx46 are linked to the short C-termini of hCx26, thereby limiting the interaction of these N-termini with the free N-termini of hCx26. At that point, the concatenation limits the bearing of the information shown in this report. However, it will be a valuable method if the cleavage of the linker is successful. An increase of the conductance would be a good indication of a successful removal of the linker.

Using different methods, in this report we showed that concatenation could be a technique to understand the consequences of formation of heteromeric gap junction hemichannels, as well as of heterotypic gap junction channels built between cells. Concerning the oligomerization of connexins, two critical motifs, which were not mutually exclusive, have been identified: The end of the first transmembrane domain (TM1) and the transition between the cytoplasmic loop (CL) and the third transmembrane domain (TM3) [10,22,23]. The motif in TM1 which was found to be critical for the oligomerization of Cx26 was not important for hetero-oligomerization [10,22,23]. On the other side, the amino acid dendrogram showed that the compatibility of different connexin isoforms to hetero-oligomerize into a connexon was related to a motif situated at the transition region between CL

and TM3 [10]. According to the sequence of these regions, the connexins were classified between the R-type connexins, which contain a conserved arginine or lysine residue, and the W-type connexins with a di-tryptophan motif. According to this classification, connexins belonging to different types do not oligomerize.

In our experiments, we showed that Cx26 (W-type) and Cx46 (R-type), which are also different in the TM1 region, could form heteromeric connexons with each other. Thereby, our results support the assumption that the control of hetero-oligomerization is not regulate by the TM1 [10,22,23]. Moreover, the residues R and W of the connexins in the transition between the cytoplasmic loop (CL) and the third transmembrane domain (TM3) are indirect control and not an intrinsic property of the connexins that regulate the hetero-oligomerization. Our results show the importance of indirect controls for hetero-oligomerization above the sequences in the different parts of the connexins.

4. Materials and Methods

4.1. Molecular Cloning

In order to express various concatemers in HeLa cells, as well as in N2A cells and in *Xenopus laevis* oocytes, the multisite gateway cloning system with three different destination plasmids was used.

For the transfection of the cell lines, the destination plasmids pEF-I-GFP GX, which has an IRES element between the gateway cassette and the reporter GFP, and the psDEST47 were used. pEF-I-GFP GX [56] was a gift from John Brigande (Addgene plasmid # 45443). psDEST47 was created by using a "reverse" BP-cloning reaction with the expression clone pcDNA-DEST47-GFP-GFP and the pDONR221 linearized with EcoNI. pcDNA-DEST47-GFP-GFP [57] was a gift from Patrick Van Oostveldt (Addgene plasmid # 36139). The psDEST47 was transformed into ccdB survival *Escherichia coli* BD3.1 cells and selected on ampicillin- and chloramphenicol-containing LB-Agar plates. The purified psDEST47, which is similar to the commercially available pcDNA™-DEST47 vector (#12281010, Thermo Fisher Scientific, Waltham, MA, USA), was used to create a C-terminally GFP-labeled fusion protein via the LR-cloning reaction.

The vector psGEMHE-GW was used for in vitro transcription to produce the cRNA for the *Xenopus* oocytes. The vector was created by restriction enzyme cloning with XbaI and HindIII using the pGEMHE [35] as backbone. As insert the gateway cassette was amplified with the attR1-ccdB-attR2 XbaI F and attR1-ccdB-attR2 HindIII R primers (see Table 4). *Escherichia coli* BD3.1 cells (invitrogen, Carlsbad, CA, USA) were used to host the three different destination vectors.

Table 4. Primers used for restriction enzyme cloning to produce the destination vector psGEMHE-GW and for the BP-cloning to generate the various Entry clones.

Primer	5′-3′ Sequence
attR1-ccdB-attR2 XbaI F	CTTCATCTAGACACGCTCGAGATCACAAGTTTGTAC
attR1-ccdB-attR2 HindIII R	CTTCGAAGCTTTTACATCTCGAGCACCACTTTGTACAAG
GW_BP-cloning hCx46 attB1 F	GGGGACAAGTTTGTACAAAAAAGCAGGCTCCATGGGCGACTGGAGCTTTCTGG
GW_BP-cloning hCx46 attB2 R	GGGGACCACTTTGTACAAGAAAGCTGGGTGGGCCCGCGGTACCGTCGAC
GW_BP-cl. hCx46 stop attB2 R	GGGGACCACTTTGTACAAGAAAGCTGGGTTCTAGATGGCCAAGTCCTCCGGT
GW_BP-cloning hCx46 attB5r R	GGGGACAACTTTTGTATACAAAGTTGTGGCCCGCGGTACCGTCG
GW_BP-cloning hCx46 attB5 F	GGGGACAACTTTGTATACAAAAGTTGTAATGGGCGACTGGAGCTTTCTGG
GW_BP-cloning hCx26 attB1 F	GGGGACAAGTTTGTACAAAAAAGCAGGCTTAATGGATTGGGGCACGCT
GW_BP-cloning hCx26 attB2 R	GGGGACCACTTTGTACAAGAAAGCTGGGTGGGCCCGCGGTACCG
GW_BP-cl. hCx26 stop attB2 R	GGGGACCACTTTGTACAAGAAAGCTGGGTTCTAAACTGGCTTTTTTGACTTCCCAGAAC
GW_BP-cloning hCx26 attB5r R	GGGGACAACTTTTGTATACAAAGTTGTGGCCCGCGGTACCG
GW_BP-cloning hCx26 attB5 F	GGGGACAACTTTGTATACAAAAGTTGTAATGGATTGGGGCACGCT

The various Entry vectors were built by amplifying hCx46 or hCx26 with the primers listed in Table 4 with a proofreading DNA polymerase (Phusion, Thermo Fisher Scientific, Waltham, MA, USA) followed by the BP-clonase reaction (Thermo Fisher Scientific, Waltham, MA, USA) with the donor plasmids pDONR™221, pDONR™221 P1-P5r, and pDONR™221 P5-P2 (Thermo Fisher Scientific, Waltham, MA, USA). For the psGEMHE-GW and the pEF-I-GFP GX plasmids, the stop attB2 R primers

were used. *Escherichia coli* MachI (Thermo Fisher Scientific, Waltham, MA, USA) was used to host the ten different Entry plasmids. The purified Entry and destination plasmids were used to perform the multisite LR reaction (LR clonase II plus, Thermo Fisher Scientific, Waltham, MA, USA). *Escherichia coli* MachI was used to host the 18 different expression clones (three different destination plasmids, each with monomeric hCx46 and hCx26, homodimeric hCx46-hCx46 and hCx26-hCx26, as well as the heterodimeric hCx46-hCx26 and hCx26-hCx46). The BP-clonase II and LR-clonase II plus reactions were successfully performed in a total volume of only 2.5 μL. Restriction enzyme cloning and gateway cloning were verified by sequencing (Seqlab, Göttingen, Germany).

4.2. Cell Culture

HeLa cells (DSMZ no.: ACC 57, Leibniz Institute DSMZ-German Collection of Microorganisms and Cell Cultures, Braunschweig, Germany) were cultured in DMEM/Ham's F12 (1:1) medium (FG 4815, Biochrom, Berlin, Germany) supplemented with 10% fetal calf serum (Biochrom), 1 mg/mL penicillin, and 0.1 mg/mL streptomycin (Biochrom). The mouse neuroblastoma cells N2A, abbreviation for Neuro-2A (DSMZ no.: ACC 148), were cultured in DMEM with 1.0 g/L D-glucose (FG 0415, Biochrom) supplemented with 10% heat inactivated fetal calf serum (Biochrom), 1x non-essential amino acids (Biochrom), 1 mg/mL penicillin, and 0.1 mg/mL streptomycin (Biochrom). The cells were cultured in a humidified atmosphere with 5% CO_2 at 37 °C. Every two to three days the cell culture medium was renewed.

4.3. Quantification of the Expression Behavior

To analyze the formation of gap junctions, 7×10^4 HeLa cells were seeded on collagen I-coated glass coverslips with a diameter of 1 cm into a well of a 24-well plate 24 h before transfection to reach a confluency of about 70–80%. Prior to the transfection, the cell culture medium was replaced by 500 μL OptiMEM I medium (Thermo Fisher Scientific). The transfection was performed as described before [13,58,59]. In brief, per well, 500 ng purified plasmid and 1.5 μL FuGene HD (Promega, Mannheim, Germany) transfection reagent were incubated in 25 μL OptiMEM I medium for 15 min at room temperature and added to the prepared cells. After 4–6 h, the transfection medium was exchanged to the penicillin- and streptomycin-free culture medium.

For the quantification of the expression behavior, the psDEST47 constructs were used, which resulted in C-terminally labeled GFP fusion proteins. The cells were fixed 24 h after transfection with 3.7% formaldehyde. The nuclei of the cells were stained with Hoechst 33342 (1 μg/mL; Sigma Aldrich, St. Louis, MO, USA) and the cell membranes were stained with Alexa 555-conjungated Wheat Germ Agglutinin (5 μg/mL; Molecular Probes, Eugene, OR, USA) to improve the visibility of the cell-cell contact regions. The cells were imaged with a confocal Nikon Eclipse TE2000-E C1 laser scanning microscope (Nikon, Düsseldorf, Germany) as described previously [13,58,59]. For each variant, at least five different transfections and coverslips were evaluated. Four images were taken of different regions of each coverslip.

To analyze the plaque area per cell pair, the micrographs were evaluated using FiJi [32]. The resulting plaque areas per cell pair of the concatemers were evaluated in comparison to the monomeric hCx46 and hCx26 by using a one-way ANOVA, followed by a Tukey test and are given as mean ± SEM.

4.4. Western Blot

HeLa cells were grown to about 80% confluence in a 100 mm diameter cell culture plate. The cells were transfected with the psDEST47 hCx46 or the psDEST47 hCx46-hCx46 plasmids and cultivated for further 24 h. For the transfection of a 100 mm diameter cell culture plate, 5 μg plasmid DNA and 15 μL FuGene HD were used (details are described above in Section 4.3). For the protein isolation, the cells were washed twice with ice-cold PBS and were removed from the culture plate with a cell scraper in presence of 1 mL ice-cold PBS. After a centrifugation step at $750 \times g$ for 3 min at 4 °C, the pellet

was resuspended in 50 μL RIPA buffer containing 25 mM Tris HCl pH 7.6, 150 mM NaCl, 1% nonidet P-40, 1% sodium desoxycholate, 0.1% SDS, freshly added 0.5% protease inhibitor cocktail (Roche, Waiblingen, Germany), 10 mM NaF, 1 mM PMSF, and 1 mM Na_3VO_4. After an incubation for 15 min on ice, a centrifugation at $14,000 \times g$ for 15 min at 4 °C was used to separate the protein solution from the cell debris. A Bradford assay (Sigma Aldrich) was used to determine the protein concentration of the supernatant using BSA as standard. $1 \times$ Laemmli buffer (13 mM Tris HCl, 10 mM DTT, 2% glycerol, 0.4% SDS, 0.002% Bromphenol Blue, pH 6.8) was added to the protein solution and incubated for 10 min at 70 °C. Next, 100 μg protein per lane were separated in a 5% SDS-polyacrylamide stacking gel and a 10% separation gel. The proteins were transferred to a nitrocellulose membrane using a semi-dry blot (transfer buffer: 25 mM Tris HCL, pH 8.3, 192 mM glycine, 0.1% SDS, and 20% methanol). Afterwards, the membrane was blocked with 5% non-fat dry milk powder in PBS containing 0.1% Tween 20 (PBS-T) for 2 h at room temperature. Anti-Cx46 antibody (sc-365394, Santa Cruz Biotechnology, Heidelberg, Germany) was diluted 1:1000 in PBS-T and applied to the membranes for an overnight incubation at 4 °C. After washing, the secondary anti-mouse antibody (A9044, Sigma Aldrich) was diluted 1:100,000 and applied for 1 h at room temperature. For the detection, the SuperSignal West chemiluminescent reagent (Thermo Fisher Scientific) was used. The blot was imaged with a CCD camera system (Intas Science Imaging, Göttingen, Germany). For the quantification, four independent replicates were analyzed by using the gel analyzer tool of the FiJi software [32]. Data are displayed normalized to the intensity of the hCx46 monomer.

4.5. Dye Transfer Experiments

To test the functionality of the formed gap junction channels, dye transfer experiments with Lucifer Yellow and 7-amino-4-methyl-3-coumarinylacetic acid (AMCA) in HeLa and N2A cells were performed, respectively. HeLa cells were prepared and transfected with the different psDEST47-plasmids as described above in Section 4.3. As control, mock transfected HeLa cells were used. For the dye transfer experiments with the N2A cells, the cells were transfected with the different pEF-I-GFP GX-plasmids. For control experiments, the N2A cells were transfected with the empty destination vector pEF-I-GFP GX. Coverslips with transfected cells were transferred to a perfusion chamber containing 400 μL of a bath medium consisting of (in mM) 140 NaCl, 5 KCl, 10 HEPES, 10 glucose, 1 $MgCl_2$, and 2 $CaCl_2$ at pH 7.4 and osmolarity (π) of 295 mosmol/L. The chamber was mounted on an inverted fluorescence microscope (Ti-E, Nikon GmbH, Duesseldorf, Germany) equipped with a Polychrome V monochromator (T.I.L.L. Photonics GmbH, Planegg, Germany), a CCD Orca-Flash 4.0 camera (Hamamatsu Photonics Deutschland GmbH, Herrsching, Germany), and the NIS-Elements AR 4.4 software (Nikon GmbH).

For the dye transfer experiments, a whole-cell patch-clamp configuration was established on one cell of a transfected cell pair using an EPC 10 USB double patch-clamp amplifier (HEKA Elektronik Dr. Schulze GmbH, Lambrecht/Pfalz, Germany) coupled to the PatchMaster 2.9 software (HEKA Elektronik Dr. Schulze GmbH). For the pipette filling solution used for the HeLa cells, 1 mg/mL Lucifer Yellow (LY) lithium salt (Biotium, Hayward, CA, USA) was diluted in a pipette medium containing (in mM) 145 K gluconate, 5 KCl, 10 HEPES, 2.5 MgATP, 5 glucose, 0.5 Na_2ATP, 1 EGTA, and 0.2 $CaCl_2$ at pH 7.4 and π 295 mosmol/L. For the experiments with N2A cells, the LY was replaced by 1 mg/mL AMCA (Sigma Aldrich, St. Louis, MO, USA). The Polychrome V was used to excite the GFP-labeled connexin variants at 488 nm, LY at 410 nm, and AMCA at 350 nm. For each dye transfer experiment, micrographs of the GFP and LY or AMCA fluorescence were taken before the whole-cell configuration was established, during the experiment, and after 10 min with prior removal of the LY or AMCA containing pipette. For each variant, the degree of dye coupling was estimated as the ratio of the number of coupled pairs to the total number of tested pairs expressing the particular variant. The results are given as mean values $\pm$ SEM. The significance of the difference was evaluated by a one-way ANOVA and a post-hoc Tukey test (*** for $p \leq 0.001$, ** for $p \leq 0.01$, and * for $p \leq 0.05$).

4.6. Expression in Xenopus Oocytes

For the in vitro transcription, the mMESSAGE mMACHINE® T7 (Thermo Fisher Scientific, Waltham, MA, USA) and the PeaI-linearized (Thermo Fisher Scientific) psGEMHE vectors were used to generate the artificial cRNA. The cRNA was purified by a phenol/chloroform extraction and an isopropanol precipitation.

Xenopus laevis oocytes were harvested from an anaesthetized female frog. After mechanical disruption of the tissue, the oocytes were separated by an incubation (1 h at room temperature) in 190–240 U/mL collagenase type II (Worthington, Berlin, Germany) containing oocyte control medium composed of (in mM) 88 NaCl, 1 KCl, 10 Tris-HCl, and 0.82 $MgCl_2$ (pH 7.4 and π 180 mosmol/L). During the tissue digestion with collagenase, the tissue was shaken at 100 rpm. After the collagenase treatment, the oocytes were washed with oocyte control medium supplemented with 2 mM $CaCl_2$. The oocytes were stored and used for injection for up to three days after isolation.

Stage V and stage VI oocytes were injected with 23 nL of an aqueous solution containing 1 µg/µL connexin mRNA and 400 ng/µL antisense to the endogenous Cx38 (AS38) using the Nanoliter Injector (World Precision Instruments, Berlin, Germany). The antisense DNA (AS38) with the sequence C*T*GACTGCTCGTCTGTCCACAC*A*G* (* indicates phosphorothioate modification) was purchased from Microsynth AG (Balgach, Switzerland). The injected oocytes were incubated at 16 °C in the Ca^{2+}-containing oocyte medium and used for the measurement of single channels 18 to 48 h post injection.

4.7. Single Channel Recordings of the Connexons

For the recording of the single channels, the vitelline membrane of a connexin expressing oocyte was mechanically removed. The oocyte was incubated for at least 3 min in a stripping solution containing (in mM) 88 NaCl, 1 KCl, 10 Tris-HCl, 0.82 $MgCl_2$, 2 $CaCl_2$, and 200 D-mannitol (pH 7.4 and π 444 mosmol/L) to release the vitelline membrane from the oocyte membrane. The released vitelline membrane was removed using two Dumont no. 5 forceps (Manufactures D'Outils Dumont SA, Montignez, Switzerland) under a LEICA GZ4 binocular (Leica Mikrossysteme Vertrieb GmbH, Wetzlar, Germany). The stripped oocyte was transferred into a perfusion chamber containing 400 µL of a control bath solution consisting of (in mM) 88 Na gluconate, 1 K gluconate, 10 Tris, 2 Ca acetate, 0.82 Mg acetate, and 20 Cs acetate (pH 7.4 and π 220 mosmol/L) and mounted on an inverted fluorescence microscope described in Section 4.4. The patch-clamp experiments were performed using an EPC 10 USB double patch-clamp amplifier (HEKA Elektronik Dr. Schulze GmbH). The data were recorded with filter 1 (Bessel) at 10 kHz and filter 2 (I_Bessel) at 1 kHz. The patch pipettes were made from PG150T-7.5 glass capillaries (Clark Electromedical Instruments, Pangbourne, UK). Filled with the pipette filling solution composed of (in mM) 80 Na gluconate, 20 Cs acetate, and 10 HEPES (pH 7.4 and π 220 mosmol/L) the pipettes had an electrical resistance of about 5 MΩ. The reference electrode was filled with K gluconate solution to avoid problems related to Ag/AgCl junction [60].

Three minutes after the formation of a gigaseal, the inside-out patch-clamp configuration [61] was established. To measure the single channels, test voltage pulses between −70 mV and 60 mV were applied for 20 s in 10 mV steps. Between the voltage pulses, the membrane was clamped at 0 mV for 30 s. Thereafter, the bath solution was changed to a Ca^{2+}-free solution composed of (in mM) 88 Na gluconate, 1 K gluconate, 10 Tris, 0.82 Mg acetate, and 20 Cs acetate at pH 7.4 and π 220 mosmol/L. After application of the test voltages, the membrane was perfused with a Ca^{2+}-free solution supplied with 100 µM carbenoxolone (CBX) and the voltage pulses were applied again.

For the data analysis and the example curves, the data were filtered with the digital filter at 100 Hz in the FitMaster 2.90 software (HEKA Elektronik Dr. Schulze GmbH). The software was also used to generate an amplitude histogram, which was fitted using a multi Gaussian fit to calculate the single channel conductance states. The single channel open probability was estimated by using the single channel event detection tool of the FitMaster software. Simultaneous opening of channels was rarely observed. If it was observed this event was excluded in the calculation of the single channel

open probability. For the calculation, only the +40 mV to +60 mV traces, which had an unambiguous signal-to-noise ratio, were used. A measurement time of at least 4 min for at least four injected oocytes of each variant was used for the estimation. For the comparison of the data a one-way ANOVA followed by a Tukey test was used.

4.8. Dye Uptake through Hemichannels

The hemichannel activity was analyzed by measuring the ethidium bromide (Etd) uptake slightly modified from Schalper et al. (2008) [62]. A day before the experiment, subconfluent HeLa cells grown on collagen I-coated coverslips were transfected with the pEF-I-GFP variants. For the control group experiments, the empty destination plasmid pEF-I-GFP GX was used to transfect the cells. A coverslip with transfected cells was placed in a perfusion chamber with a chamber volume of approximately 400 μL mounted on an inverse Nikon Ti-E fluorescence microscope, as described in Section 4.4. The ISMATEC REGIO ICC peristaltic pump (Cole-Parmer GmbH, Wertheim, Germany) controlled by the software ISMATEC® Pump Control (Cole-Parmer GmbH) allowed the constant exchange of the medium with a flow rate of 1 mL/min. Prior to the experiment, the GFP fluorescence of the transfected cells was used to define the regions of interest (ROIs) for the Etd uptake measurement.

During the first 10 min of a 30-min long dye uptake experiment, the cells in the chamber were perfused with a prewarmed (37 °C) bath solution composed of (in mM) 121 NaCl, 5.4 KCl, 25 HEPES, 0.8 $MgCl_2$, 5.5 glucose, 6 $NaHCO_3$, 2 $CaCl_2$, and 5 μM ethidium bromide (pH 7.4 and π 296 mosmol/L). After 10 min, the medium was exchanged for additional 10 min to a Ca^{2+}- and Mg^{2+}-free solution, which was consisting of (in mM) 121 NaCl, 5.4 KCl, 25 HEPES, 5.5 glucose, 6 $NaHCO_3$, and 5 μM ethidium bromide (pH 7.4 and π 295 mosmol/L). In the last 10 min of a dye uptake experiment, 1 mM La^{3+} was added to the Ca^{2+}/Mg^{2+}-free solution. Before starting an experiment, regions of interest (ROIs) were selected in a fluorescent micrograph of the cells taken by an Orca flash 4.0 CCD camera (Hamamatsu Photonics Germany, Herrsching am Ammersee, Germany). During the entire experiment, fluorescent images were taken every 15 s with an exposure time of 700 ms. The images were used to assess the changes of the fluorescence intensity of the ROIs during an experiment. For the recording of the images and the measurement of fluorescence intensity in the ROIs, the NIS-Elements AR 4.4 software (Nikon GmbH) was used. The dye uptake rate (Etd AU/min) was calculated with OriginPro 2017 (OriginLab Corporation, Northampton, MA, USA) from minute 4–9, 14–19, and 24–29, respectively (stationary rate). The results are given as mean values $\pm$ SEM. The significance of the difference was evaluated by a one-way ANOVA and a post-hoc Tukey test (*** for $p \leq 0.001$, ** for $p \leq 0.01$, and * for $p \leq 0.05$). For the comparison between the groups a two-way ANOVA followed by a Tukey test was used.

4.9. Dual Whole-Cell Patch-Clamp Experiments

For the dual whole-cell patch-clamp experiments, approximately 3×10^4 N2A cells were cultured on a collagen I-coated coverslip in a well of a 24-well plate and were transfected as described above with the pEF-I-GFP variants, which resulted in the separate expression of the different connexin-variants and GFP as the reporter. For the control experiments, the N2A cells were transfected with the empty pEF-I-GFP destination vector. The coverslip with the transfected cells was transferred into a perfusion chamber filled with 400 μL of a bath solution composed of (in mM) 121 NaCl, 5.4 KCl, 25 HEPES, 0.8 $MgCl_2$, 5.5 glucose, 6 $NaHCO_3$, 2 $CaCl_2$ and mounted on the inverse Nikon Ti-E fluorescence microscope described in Section 4.4. The patch pipettes were filled with a pipette solution containing (in mM) 125 K gluconate, 15 CsCl, 0.2 $CaCl_2$, 2.5 $MgCl_2$, 1 MgATP, 5 glucose, 0.5 EGTA, 4 Na_2ATP, 0.1 cAMP, and 10 HEPES (pH 7.4 and π 295 mosmol/L). The patch pipettes were made from 40A502 glass capillaries (Kimble Chase Life Science and Research Products, Rockwood, TN, USA). Filled with the pipette solution the pipettes had an electrical resistance of 2–5 MΩ.

Dual whole-cell patch-clamp experiments were performed with the EPC 10 USB double patch-clamp amplifier described in Section 4.6. After establishing a whole-cell configuration on

both cells of a cell pair, both cells were clamped at -40 mV. For the measurements, one cell of the cell pair (cell 1) was alternatingly stepped from -120 mV to $+60$ mV (V_1) for a duration of 250 ms, while the junctional currents were recorded in the other cell (cell 2), which was maintained at -40 mV (V_2). The transjunctional voltage gradient ($V_j = V_2 - V_1$) was calculated.

5. Conclusions

In summary, the present paper shows that the expression of concatenated connexins leads to a reduced plaque area between cells. However, concatenation of connexins was compatible with trafficking of the hemichannels to the membrane and the formation of functional gap junction hemichannels in the cell membrane and gap junction channels between cells. It could be used to generate hemichannels and gap junction channels with a determined stoichiometry. Because of the linker between the connexins, the properties of the formed hemichannels and gap junction channels (e.g., single channel conductance) do not represent the properties of hetero-oligomerized channels. However, should the removal of the linker be successful, this method could be used to analyze the electrical and metabolic selectivity of such channels and the physiological consequences for a tissue.

Abbreviations

ACh	acetylcholine
AMCA	7-amino-4-methyl-3-coumarinylacetic acid
ANOVA	analysis of variance
AS38	antisence38 oligonucleotide, against *Xenopus laevis* Cx38
CBX	carbenoxolone
CL	cytoplasmatic loop
Cx	connexin
EL1	first extracellular loop
EL2	second extracellular loop
ER	endoplasmatic reticulum
Etd	ethidium bromide
GABA	γ-aminobutyric acid
GJC	gap junction channel
hCx	human connexin
LY	lucifer Yellow
N2A	neuro-2A, mouse neuroblastoma cell line
ns	not significant
ROIs	regions of interest
SEM	standard error of the mean
TM	transmembrane domain

References

1. Söhl, G.; Willecke, K. Gap junctions and the connexin protein family. *Cardiovasc. Res.* **2004**, *62*, 228–232. [CrossRef] [PubMed]
2. Desplantez, T.; Grikscheit, K.; Thomas, N.M.; Peters, N.S.; Severs, N.J.; Dupont, E. Relating specific connexin co-expression ratio to connexon composition and gap junction function. *J. Mol. Cell. Cardiol.* **2015**, *89*, 195–202. [CrossRef] [PubMed]
3. Oh, S.; Bargiello, T.A. Voltage regulation of connexin channel conductance. *Yonsei Med. J.* **2015**, *56*, 1–15. [CrossRef] [PubMed]
4. White, T.W.; Paul, D.L.; Goodenough, D.A.; Bruzzone, R. Functional analysis of selective interactions among rodent connexins. *Mol. Biol. Cell* **1995**, *6*, 459–470. [CrossRef] [PubMed]
5. Bai, D.; Wang, A.H. Extracellular domains play different roles in gap junction formation and docking compatibility. *Biochem. J.* **2014**, *458*, 1–10. [CrossRef] [PubMed]
6. Neijssen, J.; Herberts, C.; Drijfhout, J.W.; Reits, E.; Janssen, L.; Neefjes, J. Cross-presentation by intercellular peptide transfer through gap junctions. *Nature* **2005**, *434*, 83–88. [CrossRef] [PubMed]
7. Bedner, P.; Niessen, H.; Odermatt, B.; Kretz, M.; Willecke, K.; Harz, H. Selective permeability of different connexin channels to the second messenger cyclic AMP. *J. Biol. Chem.* **2006**, *281*, 6673–6681. [CrossRef] [PubMed]
8. Bennett, M.V.M.; Verselis, V.K.V. Biophysics of gap junctions. *Semin. Cell Biol.* **1992**, *3*, 29–47. [CrossRef]
9. Niessen, H.; Harz, H.; Bedner, P.; Krämer, K.; Willecke, K. Selective permeability of different connexin channels to the second messenger inositol 1,4,5-trisphosphate. *J. Cell Sci.* **2000**, *113*, 1365–1372. [PubMed]
10. Koval, M.; Molina, S.A.; Burt, J.M. Mix and match: Investigating heteromeric and heterotypic gap junction channels in model systems and native tissues. *FBBS Lett.* **2014**, *588*, 1193–1204. [CrossRef] [PubMed]
11. Maeda, S.; Nakagawa, S.; Suga, M.; Yamashita, E.; Oshima, A.; Fujiyoshi, Y.; Tsukihara, T. Structure of the connexin 26 gap junction channel at 3.5 A resolution. *Nature* **2009**, *458*, 597–602. [CrossRef] [PubMed]
12. Nakagawa, S.; Gong, X.-Q.; Maeda, S.; Dong, Y.; Misumi, Y.; Tsukihara, T.; Bai, D. Asparagine 175 of connexin32 is a critical residue for docking and forming functional heterotypic gap junction channels with connexin26. *J. Biol. Chem.* **2011**, *286*, 19672–19681. [CrossRef] [PubMed]
13. Schadzek, P.; Schlingmann, B.; Schaarschmidt, F.; Lindner, J.; Koval, M.; Heisterkamp, A.; Preller, M.; Ngezahayo, A. The cataract related mutation N188T in human connexin46 (hCx46) revealed a critical role for residue N188 in the docking process of gap junction channels. *Biochim. Biophys. Acta* **2016**, *1858*, 57–66. [CrossRef] [PubMed]
14. Laird, D.W. The gap junction proteome and its relationship to disease. *Trends Cell Biol.* **2009**, *20*, 92–101. [CrossRef] [PubMed]
15. Diez, J.A.; Ahmad, S.; Evans, W.H. Assembly of heteromeric connexons in guinea-pig liver en route to the Golgi apparatus, plasma membrane and gap junctions. *Eur. J. Biochem.* **1999**, *262*, 142–148. [CrossRef] [PubMed]
16. Koval, M.; Harley, J.E.; Hick, E.; Steinberg, T.H. Connexin46 is retained as monomers in a trans-Golgi compartment of osteoblastic cells. *J. Cell Biol.* **1997**, *137*, 847–857. [CrossRef] [PubMed]
17. Musil, L.S.; Goodenough, D.A. Multisubunit assembly of an integral plasma membrane channel protein, gap junction connexin43, occurs after exit from the ER. *Cell* **1993**, *74*, 1065–1077. [CrossRef]
18. Maeda, S.; Tsukihara, T. Structure of the gap junction channel and its implications for its biological functions. *Cell. Mol. Life Sci.* **2011**, *68*, 1115–1129. [CrossRef] [PubMed]
19. Schadzek, P.; Schlingmann, B.; Schaarschmidt, F.; Lindner, J.; Koval, M.; Heisterkamp, A.; Ngezahayo, A.; Preller, M. Data of the molecular dynamics simulations of mutations in the human connexin46 docking interface. *Data Brief* **2016**, *7*, 93–99. [CrossRef] [PubMed]
20. Bai, D.; Yue, B.; Aoyama, H. Crucial motifs and residues in the extracellular loops influence the formation and specificity of connexin docking. *Biochim. Biophys. Acta* **2018**, *1860*, 9–21. [CrossRef] [PubMed]
21. Karademir, L.B.; Aoyama, H.; Yue, B.; Chen, H.; Bai, D. Engineered Cx26 variants established functional heterotypic Cx26/Cx43 and Cx26/Cx40 gap junction channels. *Biochem. J.* **2016**, *473*, 1391–1403. [CrossRef] [PubMed]

22. Jara, O.; Acuña, R.; García, I.E.; Maripillán, J.; Figueroa, V.; Sáez, J.C.; Araya-Secchi, R.; Lagos, C.F.; Perez-Acle, T.; Berthoud, V.M.; et al. Critical role of the first transmembrane domain of Cx26 in regulating oligomerization and function. *Mol. Biol. Cell* **2012**, *23*, 3299–3311. [CrossRef] [PubMed]

23. Martínez, A.D.; Maripillán, J.; Acuña, R.; Minogue, P.J.; Berthoud, V.M.; Beyer, E.C. Different domains are critical for oligomerization compatibility of different connexins. *Biochem. J.* **2011**, *436*, 35–43. [CrossRef] [PubMed]

24. Das, S.; Smith, T.D.; Sarma, J.D.; Ritzenthaler, J.D.; Maza, J.; Kaplan, B.E.; Cunningham, L.A.; Suaud, L.; Hubbard, M.J.; Rubenstein, R.C.; et al. ERp29 restricts Connexin43 oligomerization in the endoplasmic reticulum. *Mol. Biol. Cell* **2009**, *20*, 2593–2604. [CrossRef] [PubMed]

25. Ahring, P.K.; Liao, V.W.Y.; Balle, T. Concatenated nicotinic acetylcholine receptors: A gift or a curse? *J. Gen. Physiol.* **2018**, *150*, 453–473. [CrossRef] [PubMed]

26. Baumann, S.W.; Baur, R.; Sigel, E. Subunit arrangement of gamma-aminobutyric acid type A receptors. *J. Biol. Chem.* **2001**, *276*, 36275–36280. [CrossRef] [PubMed]

27. Sigel, E.; Kaur, K.H.; Lüscher, B.P.; Baur, R. Use of concatamers to study GABAA receptor architecture and function: Application to delta-subunit-containing receptors and possible pitfalls. *Biochem. Soc. Trans.* **2009**, *37*, 1338–1342. [CrossRef] [PubMed]

28. Stoop, R.; Thomas, S.; Rassendren, F.; Kawashima, E.; Buell, G.; Surprenant, A.; North, R.A. Contribution of individual subunits to the multimeric P2X(2) receptor: Estimates based on methanethiosulfonate block at T336C. *Mol. Pharmacol.* **1999**, *56*, 973–981. [CrossRef] [PubMed]

29. Isakson, B.E.; Olsen, C.E.; Boitano, S. Laminin-332 alters connexin profile, dye coupling and intercellular Ca^{2+} waves in ciliated tracheal epithelial cells. *Respir. Res.* **2006**, *7*, 105. [CrossRef] [PubMed]

30. Oviedo-Orta, E.; Kwak, B.R.; Evans, W.H. *Connexin Cell Communication Channels*; CRC Press: Boca Raton, FL, USA, 2013.

31. Chiu, Y.-H.; Jin, X.; Medina, C.B.; Leonhardt, S.A.; Kiessling, V.; Bennett, B.C.; Shu, S.; Tamm, L.K.; Yeager, M.; Ravichandran, K.S.; et al. A quantized mechanism for activation of pannexin channels. *Nat. Commun.* **2017**, *8*, 14324. [CrossRef] [PubMed]

32. Schindelin, J.; Arganda-Carreras, I.; Frise, E.; Kaynig, V.; Longair, M.; Pietzsch, T.; Preibisch, S.; Rueden, C.; Saalfeld, S.; Schmid, B.; et al. Fiji: An open-source platform for biological-image analysis. *Nat. Methods* **2012**, *9*, 676–682. [CrossRef] [PubMed]

33. Paul, D.L.; Ebihara, L.; Takemoto, L.J.; Swenson, K.I.; Goodenough, D.A. Connexin46, a novel lens gap junction protein, induces voltage-gated currents in nonjunctional plasma membrane of Xenopus oocytes. *J. Cell Biol.* **1991**, *115*, 1077–1089. [CrossRef] [PubMed]

34. Ngezahayo, A.; Zeilinger, C.; Todt, I.; Marten, I.; Kolb, H.A. Inactivation of expressed and conducting rCx46 hemichannels by phosphorylation. *Pflugers Arch.* **1998**, *436*, 627–629. [CrossRef] [PubMed]

35. Walter, W.J.; Zeilinger, C.; Bintig, W.; Kolb, H.-A.; Ngezahayo, A. Phosphorylation in the C-terminus of the rat connexin46 (rCx46) and regulation of the conducting activity of the formed connexons. *J. Bioenerg. Biomembr.* **2008**, *40*, 397–405. [CrossRef] [PubMed]

36. Neyton, J.; Trautmann, A. Single-channel currents of an intercellular junction. *Nature* **1985**, *317*, 331–335. [CrossRef] [PubMed]

37. Ngezahayo, A.; Altmann, B.; Kolb, H.A. Regulation of ion fluxes, cell volume and gap junctional coupling by cGMP in GFSHR-17 granulosa cells. *J. Membr. Biol.* **2003**, *194*, 165–176. [CrossRef] [PubMed]

38. Bao, L.; Sachs, F.; Dahl, G. Connexins are mechanosensitive. *Am. J. Physiol. Cell Physiol.* **2004**, *287*, 1389–1395. [CrossRef] [PubMed]

39. Gaßmann, O.; Kreir, M.; Ambrosi, C.; Pranskevich, J.; Oshima, A.; Röling, C.; Sosinsky, G.; Fertig, N.; Steinem, C. The M34A mutant of Connexin26 reveals active conductance states in pore-suspending membranes. *J. Struct. Biol.* **2009**, *168*, 168–176. [CrossRef] [PubMed]

40. Hopperstad, M.G.; Srinivas, M.; Spray, D.C. Properties of gap junction channels formed by Cx46 alone and in combination with Cx50. *Biophys. J.* **2000**, *79*, 1954–1966. [CrossRef]

41. Oh, S.; Rubin, J.B.; Bennett, M.V.; Verselis, V.K.; Bargiello, T.A. Molecular determinants of electrical rectification of single channel conductance in gap junctions formed by connexins 26 and 32. *J. Gen. Physiol.* **1999**, *114*, 339–364. [CrossRef] [PubMed]

42. Contreras, J.E.; Sáez, J.C.; Bukauskas, F.F.; Bennett, M.V.L. Gating and regulation of connexin 43 (Cx43) hemichannels. *Proc. Natl. Acad. Sci. USA* **2003**, *100*, 11388–11393. [CrossRef] [PubMed]

43. Laird, D.W.; Jordan, K.; Thomas, T.; Qin, H.; Fistouris, P.; Shao, Q. Comparative analysis and application of fluorescent protein-tagged connexins. *Microsc. Res. Tech.* **2001**, *52*, 263–272. [CrossRef]

44. Sorgen, P.L.; Duffy, H.S.; Sahoo, P.; Coombs, W.; Delmar, M.; Spray, D.C. Structural changes in the carboxyl terminus of the gap junction protein connexin43 indicates signaling between binding domains for c-Src and zonula occludens-1. *J. Biol. Chem.* **2004**, *279*, 54695–54701. [CrossRef] [PubMed]

45. Leithe, E.; Mesnil, M.; Aasen, T. The connexin 43 C-terminus: A tail of many tales. *Biochim. Biophys. Acta* **2018**, *1860*, 48–64. [CrossRef] [PubMed]

46. Ebihara, L.; Tong, J.-J.; Vertel, B.; White, T.W.; Chen, T.-L. Properties of connexin 46 hemichannels in dissociated lens fiber cells. *Investig. Ophthalmol. Vis. Sci.* **2011**, *52*, 882–889. [CrossRef] [PubMed]

47. Trexler, E.B.; Bennett, M.V.; Bargiello, T.A.; Verselis, V.K. Voltage gating and permeation in a gap junction hemichannel. *Proc. Natl. Acad. Sci. USA* **1996**, *93*, 5836–5841. [CrossRef] [PubMed]

48. Trexler, E.B.; Bukauskas, F.F.; Kronengold, J.; Bargiello, T.A.; Verselis, V.K. The first extracellular loop domain is a major determinant of charge selectivity in connexin46 channels. *Biophys. J.* **2000**, *79*, 3036–3051. [CrossRef]

49. Hu, X.; Dahl, G. Exchange of conductance and gating properties between gap junction hemichannels. *FEBS Lett.* **1999**, *451*, 113–117. [CrossRef]

50. Srinivas, M.; Kronengold, J.; Bukauskas, F.F.; Bargiello, T.A.; Verselis, V.K. Correlative studies of gating in Cx46 and Cx50 hemichannels and gap junction channels. *Biophys. J.* **2005**, *88*, 1725–1739. [CrossRef] [PubMed]

51. Mese, G.; Sellitto, C.; Li, L.; Wang, H.-Z.; Valiunas, V.; Richard, G.; Brink, P.R.; White, T.W. The Cx26-G45E mutation displays increased hemichannel activity in a mouse model of the lethal form of keratitis-ichthyosis-deafness syndrome. *Mol. Biol. Cell* **2011**, *22*, 4776–4786. [CrossRef] [PubMed]

52. Sánchez, H.A.; Mese, G.; Srinivas, M.; White, T.W.; Verselis, V.K. Differentially altered Ca^{2+} regulation and Ca^{2+} permeability in Cx26 hemichannels formed by the A40V and G45E mutations that cause keratitis ichthyosis deafness syndrome. *J. Gen. Physiol.* **2010**, *136*, 47–62. [CrossRef] [PubMed]

53. Slavi, N.; Rubinos, C.; Li, L.; Sellitto, C.; White, T.W.; Mathias, R.; Srinivas, M. Cx46 Gap Junctions Provide a Pathway for the Delivery of Glutathione to the Lens Nucleus. *J. Biol. Chem.* **2014**, *289*, 32694–32702. [CrossRef] [PubMed]

54. Suchyna, T.M.; Nitsche, J.M.; Chilton, M.; Harris, A.L.; Veenstra, R.D.; Nicholson, B.J. Different ionic selectivities for connexins 26 and 32 produce rectifying gap junction channels. *Biophys. J.* **1999**, *77*, 2968–2987. [CrossRef]

55. Slavi, N.; Wang, Z.; Harvey, L.; Schey, K.L.; Srinivas, M. Identification and Functional Assessment of Age-Dependent Truncations to Cx46 and Cx50 in the Human Lens. *Investig. Ophthalmol. Vis. Sci.* **2016**, *57*, 5714–5722. [CrossRef] [PubMed]

56. Gubbels, S.P.; Woessner, D.W.; Mitchell, J.C.; Ricci, A.J.; Brigande, J.V. Functional auditory hair cells produced in the mammalian cochlea by in utero gene transfer. *Nature* **2008**, *455*, 537–541. [CrossRef] [PubMed]

57. Dieriks, B.; Van Oostveldt, P. Spatiotemporal behavior of nuclear cyclophilin B indicates a role in RNA transcription. *Int. J. Mol. Med.* **2012**, *29*, 1031–1038. [CrossRef] [PubMed]

58. Schlingmann, B.; Schadzek, P.; Busko, S.; Heisterkamp, A.; Ngezahayo, A. Cataract-associated D3Y mutation of human connexin46 (hCx46) increases the dye coupling of gap junction channels and suppresses the voltage sensitivity of hemichannels. *J. Bioenerg. Biomembr.* **2012**, *44*, 607–614. [CrossRef] [PubMed]

59. Schlingmann, B.; Schadzek, P.; Hemmerling, F.; Schaarschmidt, F.; Heisterkamp, A.; Ngezahayo, A. The role of the C-terminus in functional expression and internalization of rat connexin46 (rCx46). *J. Bioenerg. Biomembr.* **2013**, *45*, 59–70. [CrossRef] [PubMed]

60. Raynauld, J.P.; Laviolette, J.R. The silver-silver chloride electrode: A possible generator of offset voltages and currents. *J. Neurosci. Methods* **1987**, *19*, 249–255. [CrossRef]

61. Hamill, O.P.; Marty, A.; Neher, E.; Sakmann, B.; Sigworth, F.J. Improved patch-clamp techniques for high-resolution current recording from cells and cell-free membrane patches. *Pflugers Arch.* **1981**, *391*, 85–100. [CrossRef] [PubMed]
62. Schalper, K.A.; Palacios-Prado, N.; Retamal, M.A.; Shoji, K.F.; Martínez, A.D.; Sáez, J.C. Connexin hemichannel composition determines the FGF-1-induced membrane permeability and free $[Ca^{2+}]i$ responses. *Mol. Biol. Cell* **2008**, *19*, 3501–3513. [CrossRef] [PubMed]

Anhang D: Publikation Schadzek *et al.*, 2019

Untersuchung der dominanten Eigenschaften der Mutation N188T in humanem Connexin46 (hCx46) mittels Connexin-Konkatemerisierung und Molekül-Dynamik-Simulationen

Analysis of the dominant mutation N188T of human connexin46 (hCx46) using concatenation and molecular dynamics simulation

Patrik Schadzek, Yannick Stahl, Matthias Preller, Anaclet Ngezahayo

Beitrag zur Publikation: Ich habe zusammen mit A.N. die Experimente geplant. Ich habe die meisten Experimente durchgeführt, alle Daten ausgewertet und interpretiert. Ich habe alle Abbildungen erstellt und das Manuskript zusammen mit A.N. geschrieben.

Analysis of the dominant mutation N188T of human connexin46 (hCx46) using concatenation and molecular dynamics simulation

Patrik Schadzek[1] (iD), Yannick Stahl[1] (iD), Matthias Preller[2,3] (iD) and Anaclet Ngezahayo[1,4] (iD)

1 Institute of Cell Biology and Biophysics, Department of Cell Physiology and Biophysics, Leibniz University Hannover, Germany
2 Institute for Biophysical Chemistry, Hannover Medical School (MHH), Germany
3 Centre for Structural Systems Biology, DESY-Campus, Hamburg, Germany
4 Center for System Neurosciences (ZSN), Hannover, Germany

Connexins (Cx) are proteins that form cell-to-cell gap junction channels. A mutation at position 188 in the second extracellular loop (E2) domain of hCx46 has been linked to an autosomal dominant zonular pulverulent cataract. As it is dominantly inherited, it is possible that the mutant variant affects the co-expressed wild-type Cx and/or its interaction with other cellular components. Here, we proposed to use concatenated hCx46wt-hCx46N188T and hCx46N188T-hCx46wt to analyze how hCx46N188T affected co-expressed hCx46wt to achieve a dominant inheritance. Heterodimer hCx46wt-hCx46N188T formed fewer gap junction plaques compared to homodimer hCx46wt-hCx46wt, while the hCx46N188T-hCx46N188T homodimer formed almost no gap junction plaques. Dye uptake experiments showed that hemichannels of concatenated variants were similar to hemichannels of monomers. Molecular dynamics simulations revealed that for docking, the N188 of a protomer was engaged in hydrogen bonds (HBs) with R180, N189, and D191 of the counterpart protomer of the adjacent hemichannel. T188 suppressed the formation of HBs between protomers. Molecular dynamics simulations of an equimolar hCx46wt/hCx46N188T gap junction channel revealed a reduced number of HBs between protomers, suggesting reduction of gap junction channels between lens fibers co-expressing the variants.

Connexins (Cx) are proteins that form cell-to-cell gap junction channels. The gap junction channels allow exchange of ions and small metabolites between cells in a tissue leading, thereby to formation of synchronized physiological units within a tissue [1]. To form a gap junction channel, hemichannels within the membrane of adjacent cells dock to each other generating a cell-to-cell pore that allows diffusion of small metabolites up to 1–2 kDa between the cytoplasmic space of the interacting cells. Upon docking the gap junction, channels are assembled in gap junction plaques, which might contain more than thousand channels [2]. A hemichannel is composed of six Cx subunits that oligomerize along the traffic pathway between the endoplasmic reticulum and the trans-Golgi network [3–6]. They are inserted in the membrane where they form hemichannels. Cx are protein products of a related gene family, which in humans contains 21 members [7]. The expression pattern of Cx is regulated according to the tissue and the developmental and metabolic state [8]. In the lens, the isoforms

Abbreviations

Cx, connexin; E1, first extracellular loop; E2, second extracellular loop; Edt, ethidium bromide; HB, hydrogen bond; hCx, human connexin; LY, Lucifer yellow; MD, molecular dynamics; ns, not significant; wt, wild-type.

Cx43, Cx46, and Cx50 are expressed. Cx43 forms gap junction channels in the epithelial cell monolayer that covers the anterior surface of the lens. In the lens bulk, the gap junctions between the lens fibers are formed by Cx46 and Cx50 [9]. These gap junction channels are involved in the lens internal circulation system that is essential for the homeostasis of this avascular tissue [10]. Mutations that change the function of Cx46 and Cx50 are associated with cataracts (summarized in [9]), which stress the importance of gap junction channels in the lens. However, the functional link between mutation of the Cx and the phenotypic consequence is not always understood.

The mutation found at position 188 in the second extracellular loop (E2) domain of Cx46 has been linked to an autosomal dominant zonular pulverulent cataract [11]. As dominantly inherited, it is possible that the mutant variant affects the co-expressed wild-type (wt) Cx and/or its interaction with other cellular components [9]. Recent results showed that the Cx46N188T could oligomerize in connexons, which were trafficked to and inserted in the membrane in similar manner as connexons formed by the wt variant. However, it was found that the mutant was not able to form gap junction plaques, suggesting that the docking was affected. Structural modeling and molecular dynamics (MD) simulations of a human Cx46 (hCx46) model, using the crystallized Cx26 [12] as template, indicate that N188 in a protomer within a connexon of one cell forms hydrogen bonds (HB) with residues R180, T189, and D191 of the counterpart protomer within the connexon in the adjacent cell to stabilize the docked hCx46 gap junction channel. Mutation of the asparagine to T188 led to a decrease in the number of HBs and destabilized the favorable interaction between the connexons [13]. In multimeric protein complex, mutated subunits might oligomerize with wts and cause thereby the mutated phenotype [14]. The mutant might not affect the trafficking to and the insertion in the membrane. We proposed to use concatenated hCx46wt-hCx46N188T and hCx46N188T-hCx46wt to analyze how hCx46N188T affected co-expressed hCx46wt to achieve a dominant inheritance. Concatenation was shown to be a good technique that allows to gain insight in the architecture of multimeric membrane proteins such as acetyl choline or γ-aminobutyric acid receptors as well as K^+ channels or Cx [15–21].

In combination with MD simulation, the results of concatenated heterodimers (hCx46wt-hCx46N188T and hCx46N188T-hCx46wt) suggest that the presence of the hCx46N188T in hemichannels reduces the HBs between the hemichannels of adjacent lens fibers, thereby lowering the number of gap junction channels between the cells.

Materials and methods

Molecular biology

For the transfection of the HeLa cells, the destination plasmid pEF-I-GFP GX, which allowed the co-expression of untagged Cx together with a GFP, and the psDEST47 were used. pEF-I-GFP GX [22] was a gift from John Brigande (Addgene plasmid # 45443, Watertown, MA, USA). psDEST47 was created by using a 'reverse' BP-cloning reaction with the expression clone pcDNA-DEST47-GFP-GFP and the pDONR221 linearized with EcoNI. pcDNA-DEST47-GFP-GFP [23] was a gift from Patrick Van Oostveldt (Addgene plasmid # 36139). The psDEST47 was transformed into *Escherichia coli* BD3.1 cells and selected on ampicillin and chloramphenicol containing LB-Agar plates. The purified psDEST47 was used to create a C-terminally GFP-labeled fusion protein via the LR-cloning reaction. For the molecular cloning, the multisite Gateway Pro kit was used (Thermo Fisher Scientific, Waltham, MA, USA). To generate the various Entry plasmids for the gateway cloning, the hCx46 and hCx46N188T [13] genes were used as template for the PCR (Phusion; Thermo Fisher Scientific) with the primers listed in Table 1 followed by the BP-Clonase reaction (Thermo Fisher Scientific). The attB2 R stop primer was used for the pEF-I-GFP GX plasmids. The ten Entry plasmids were transformed into *E. coli* MachI cells. The twelve expression clones were generated by LR-cloning (LR Clonase II plus; Thermo Fisher Scientific) with the purified Entry vectors and the aforementioned destination plasmids followed by a transformation into *E. coli* MachI cells. All gateway reactions were performed in a total volume of 2.5 μL. The cloning was verified by sequencing (Seqlab, Göttingen, Germany).

Cell culture

For the cultivation of HeLa cells (DSMZ no.: ACC 57, Leibniz Institute DSMZ—German Collection of Microorganisms and Cell Cultures, Braunschweig, Germany), Dulbecco's modified Eagle's medium/Ham's F12 (1 : 1) medium (FG 4815; Biochrom, Berlin, Germany) supplemented with 10% fetal bovine serum (Biochrom), 1 mg·mL^{-1} penicillin, and 0.1 mg·mL^{-1} streptomycin (Biochrom) was used. HeLa cells were cultured in a humidified atmosphere with 5% CO_2 at 37 °C. Every 2–3 days, the medium was renewed.

Transfection

For the transfection of one well of a 24-well plate, 500 ng plasmid and 1.5 μL FuGene HD (Promega, Mannheim, Germany) were incubated in 25 μL OptiMEM I medium (Thermo Fisher Scientific) for 15 min at RT and added to the HeLa cells, which were washed with 500 μL OptiMEM

P. Schadzek *et al.*   Impaired docking of hCx46wt-hCx46N188T connexons

Table 1. Primers used for the PCR to generate the entry clones by BP-cloning.

Primer	5′–3′ sequence
GW_BP-cloning hCx46 attB1 F	GGGGACAAGTTTGTACAAAAAAGCAGGCTCCATGGGCGACTGGAGCTTTCTGG
GW_BP-cloning hCx46 attB2 R	GGGGACCACTTTGTACAAGAAAGCTGGGTGGGCCCGCGGTACCGTCGAC
GW_BP-cl. hCx46 stop attB2 R	GGGGACCACTTTGTACAAGAAAGCTGGGTTCTAGATGGCCAAGTCCTCCGGT
GW_BP-cloning hCx46 attB5r R	GGGGACAACTTTTGTATACAAAGTTGTGGCCCGCGGTACCGTCG
GW_BP-cloning hCx46 attB5 F	GGGGACAACTTTGTATACAAAAGTTGTAATGGGCGACTGGAGCTTTCTGG

I medium prior transfection. After 4–6 h, the medium was exchanged to the antibiotic-free culture medium.

Quantification of the gap junction plaques

A day prior to imaging, 7×10^4 HeLa cells were grown on collagen-I-coated coverslips and transfected with the psDEST47 plasmids. The cells were fixed with 3.7 % formaldehyde and stained with Hoechst 33342 (1 μg·mL^{-1}; Sigma-Aldrich, St. Louis, MO, USA) and Alexa 555-conjugated Wheat Germ Agglutinin (5 μg·mL^{-1}; Molecular Probes, Eugene, OR, USA) to improve the visibility of the cell-cell contact regions. For the imaging, a confocal Nikon Eclipse TE2000-E C1 laser scanning microscope (Nikon GmbH, Düsseldorf, Germany) was used as described previously [13,24,25]. For each variant, at least 50 cell pairs were analyzed from at least four different transfections. The number of gap junction plaques was evaluated by using FIJI [26]. The data are given as mean ± SEM and evaluated using Student's *t*-test.

Dye uptake

A day prior the dye uptake experiment, subconfluent HeLa cells grown on collagen-I-coated coverslips (10 mm) were transfected with the pEF-I-GFP plasmids. The GFP fluorescence was used to define the ROIs in which ethidium bromide (Etd) dye uptake was followed. A coverslip was placed in a chamber containing 400 μL bath solution composed of (in mM) 121 NaCl, 5.4 KCl, 25 HEPES, 0.8 MgCl$_2$, 5.5 glucose, 6 NaHCO$_3$, 2 CaCl$_2$, pH 7.4. The chamber was mounted on an inverted fluorescence microscope Nikon Ti-E (Nikon GmbH) equipped with a monochromator Polychrome V (TILL I.D. GmbH, Planegg, Germany) and a CCD camera Orca Flash 4.0 (Hamamatsu Photonics Deutschland GmbH, Herrsching, Germany). After determination of ROIs, the cells were perfused with a prewarmed (37 °C) bath solution containing 5 μM Etd, at a flow rate of 1 mL·min^{-1}. Ten minutes after the beginning of the experiment, a Ca^{2+}- and Mg^{2+}-free bath solution with Etd was applied for 10 min, followed by a Ca^{2+}- and Mg^{2+}-free bath solution containing Etd and 1 mM La^{3+} for further 10 min. Fluorescence images were taken every 15 s during the whole experiment (30 min). The rate of Etd uptake for each experimental section was estimated by evaluating the change in fluorescence intensity in the cells between 4–9 min, 14–19 min,

and 24–29 min, respectively. The results are given as mean values ± SEM. The significance of the difference was evaluated by an ANOVA and a post hoc Tukey test (*** for $P \leq 0.001$ and * for $P \leq 0.05$).

Dye transfer experiments

Dye transfer experiments were performed with Lucifer yellow (LY, 1 mg·mL^{-1}) using the whole-cell patch-clamp technique as previously described [24,25]. The dye coupling is given as average ratio of the sum of tested pairs (*n*) for at least four transfections for each variant. To evaluate the significance of the difference, Student's *t*-test was used.

Structural modeling and molecular dynamics simulations

All-atom structural models of hCx46 gap junction channels were generated as described earlier [13]. The amino acid asparagine 188 was mutated to threonine without disturbing the backbone geometry, and the structures were prepared and optimized using the Protein Preparation Wizard and Macromodel of the Schrödinger Suite 2018-1 (Schrödinger Release 2018-1: Maestro, Protein Preparation Wizard, Epik, Macromodel, Schrödinger, LLC, New York, NY, USA). Mixed gap junction channels of wt and N188T mutated Cx were prepared in two arrangements, channel 1 with alternating hCx46wt and hCx46N188T Cx per hemichannel and differing types of Cx binding each other at the connexon interface, while channel 2 featured identical types of Cx of the hemichannels facing each other at the binding interface. The TIP3P water model [27] was used to immerse the gap junction channels in a rectangular water box, extending up to 10 Å from the proteins, and Cl$^-$ anion was added to keep the net system charge neutral. Each system comprised a total of ~ 210 000 atoms. MD simulations were performed with NAMD2.12 [28] and the CHARMM36 all-atom additive force field [29]. Simulations were conducted in a NpT ensemble with a constant temperature of 310 K and pressure at 1 atm using Langevin dynamics and the Langevin piston method. The RATTLE algorithm was used to constrain all covalent bonds. Velocity Verlet integration was used with a time step of 2 fs. Long-range electrostatics was treated using the particle-mesh Ewald method [30] and a short-range cutoff of 12 Å

was used for nonbonded interactions. The solvated and neutralized gap junction channel systems were initially energy minimized and subsequently equilibrated at 310 K and 1 atm. After reaching a converged root mean square deviation of the protein backbone atoms, 100-ns MD production runs for each channel were carried out.

Results

An adenine–cytosine (A → C) replacement at position 563 in the coding sequence of hCx46 causes an exchange of amino acid residue asparagine to threonine at position 188 (N188T). This mutation is associated with an autosomal dominant congenital nuclear pulverulent cataract [11]. We transfected hCx46wt and hCx46N188T as well as concatenated hCx46wt-hCx46wt, hCx46N188T-hCx46N188T, hCx46wt-hCx46N188T, and hCx46N188T-hCx46wt in HeLa cells and analyzed the functional consequences of the mutation on the gap junction hemichannels and cell-cell coupling gap junction channels that may contain both Cx isoforms in combination with MD simulations.

For the analysis of the gap junction plaque number, the GFP-labeled variants were expressed in HeLa cells. Although the transfection efficiency of about 20–30% for all observed variants did not differ, the number of the formed gap junction plaques differed strongly (Fig. 1). Cells expressing the monomer hCx46wt and the homodimer hCx46wt-hCx46wt formed the most plaques (Fig. 1). By counting, we found an average number of about two gap junction plaques per cell pair expressing hCx46 monomer. A slight (not significant) increase to about 2.4 gap junction plaques per cell pair was observed for cells expressing the homodimer hCx46wt-hCx46wt (Fig. 1). Although the individual area of the plaques formed by the concatenated Cx was reduced, the number of gap junction plaques was not affected by the concatenation. In our previous study ([21]), we showed that the concatenated Cx are able to do the trafficking of hemichannels to the membrane and the formation of functional channels between cells. On the other side, in agreement with previous results ([13]), here we found that hCx46N188T rarely formed gap junction plaques (Fig. 1). Likewise, gap junction plaques between cells expressing the homodimer hCx46N188T-hCx46N188T were extremely rare (Fig. 1). A quantification showed an average of about 0.2 gap junction plaques between two adjacent cell expressing the hCx46N188T monomers. For cells expressing the homodimeric hCx46N188T, an average of about 0.1 gap junction plaques was counted (Fig. 1). For the heterodimers, the probability to form gap junction plaques was strongly increased in comparison with the homodimer hCx46N188T-hCx46N188T but clearly decreased

compared to the hCx46wt-hCx46wt homodimer. It is possible that the presence of the hCx46N188T either as homomer or as tandem in any combination strongly reduced the presence of the protein in the membrane. As for the hCx46N188T homomer, previous results showed that when expressed in *Xenopus* oocytes or HeLa cells, hCx46N188T caused a voltage dependent current comparable in amplitude with the current caused by the hCx46wt [13]. Moreover, by analyzing the dye uptake capacity of the cells expressing the monomers composed of hCx46wt and hCx46N188T, or the homodimers hCx46wt-hCx46wt and hCx46N188T-hCx46N188T or the heterodimers hCx46wt-hCx46N188T and hCx46N188T-hCx46wt, we found a similar dye uptake rate before and after reducing external Ca^{2+} in cells expressing either variant (Fig. 2).

At the cell-to-cell gap junction level, the dye transfer experiments showed that the gap junction plaques whether they were formed by hCx46wt, hCx46wt-hCx46wt homodimers, hCx46wt-hCx46N188T, or hCx46N188T-hCx46wt contained gap junction channels that allowed the transfer of LY from one cell to the adjacent cell (Fig. 3). LY transfer was observed in about 50% of the cell pairs. In contrast, in cells expressing the monomeric hCx46N188T and the homodimeric hCx46N188T-hCx46N188T, the probability of dye transfer did not significantly exceed that of control cells, which were MOCK transfected. Dye transfer was observed in about 10% of these cell pairs (Fig 3). The 10% of dye coupling in MOCK transfected cells is mostly related to a background which is not affected by gap junction inhibitors such as carbenoxolone.

Previously, we analyzed the stability of the interaction in a structural model of docked hCx46 Cx, derived from the crystal structure of hCx26, *in silico* [12]. We could show that the hCx46N188T mutation destabilized the Cx interaction, which indicated that the docking of mutated connexons of adjacent cells might be affected [31]. In the present report, we extended our study by classical MD simulations, including hexamers composed of either hCx46wt, hCx46N188T, or alternating hCx46wt and hCx46N188T protomers. Monitoring the number of interactions along the MD trajectories showed an average of 53 HBs of the hCx46wt connexons interacting with a second hCx46wt connexon. The overall number of stabilizing HBs between hCx46N188T hexamers markedly decreased in the first 40 ns of the simulations and reached a plateau around an average of 12 HBs over the 100-ns simulation time (Fig 4). For both gap junction channels with hCx46wt and hCx46N188T building the connexons, a reduction in the number of HBs was observed as compared to hCx46wt, which fluctuated around 31–35 HBs between the docked connexons (Fig. 4). These results
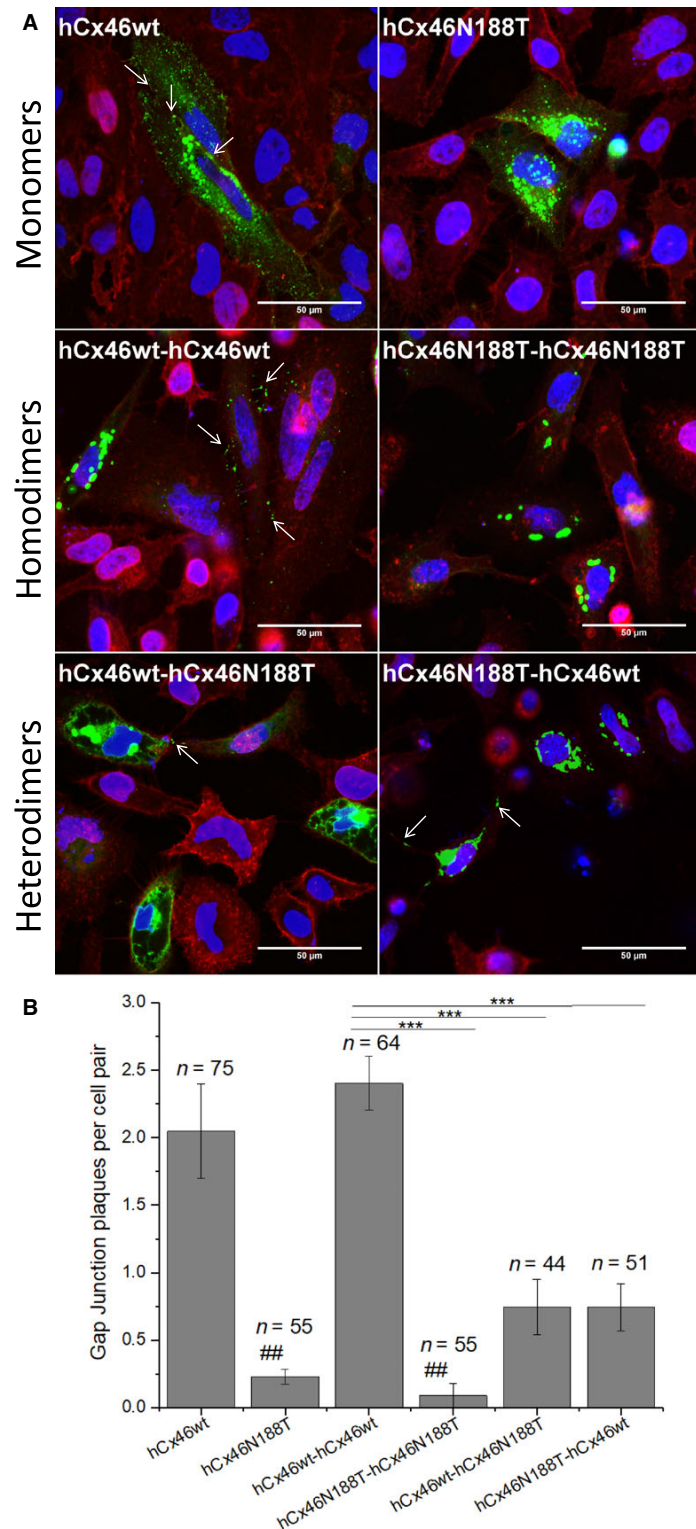
P. Schadzek *et al.*

Impaired docking of hCx46wt-hCx46N188T connexons

Fig. 1. Formation of gap junction plaques by the different variants. (A) Representative micrographs of the HeLa cells expressing eGFP-labeled hCx46wt, hCx46N188T, and the four possible homodimeric and heterodimeric tandems. The cells were stained with Hoechst 33342 (nuclei; blue) and WGA-Alexa-Fluor® 555 (Molecular Probes) (membrane; red). Gap junction plaques are indicated by arrows. The cell indicated by an asterisk (bottom left panel) shows a green GFP label distributed all over the cell membrane. Such single cells were occasionally found for all variants. They probably represent excessive overexpression of the transfected protein. Scale bar = 50 μm. (B) Quantification of the number of gap junction plaques formed by eGFP-labeled hCx46 monomers and the four different homo- and heterodimers between HeLa cell pairs. IMAGEJ (U. S. National Institutes of Health, Bethesda, MD, USA) was used for the analysis. The average number of gap junction plaques per cell pair for the different variants is given as for n considered pairs in at least three transfection experiments for each variant. Error bars represent the SEM. The significance of difference between the variants and hCx46 ($^{##}P \leq 0.01$) or between the variants and hCx46wt-hCx46wt ($^{***}P \leq 0.001$) was evaluated by Student's *t*-test.

Impaired docking of hCx46wt-hCx46N188T connexons   P. Schadzek *et al.*
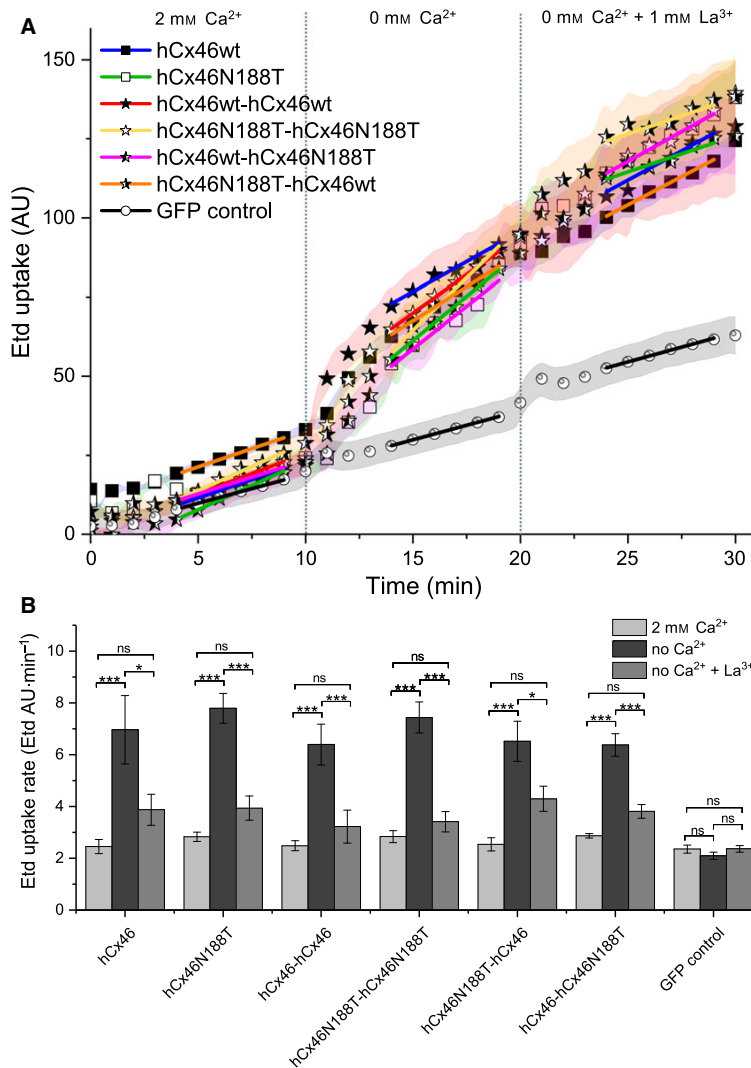

Fig. 2. Analysis of the functionality of the hemichannels by dye uptake experiments. HeLa cells expressing the IRES-GFP Plasmids grown on coverslips to a confluency of about 40–50% were used to perform dye uptake experiments with 5 μM Etd. (A) The cells were perfused with media containing 2 mM Ca^{2+}, no Ca^{2+}, or no Ca^{2+} but 1 mM La^{3+} for 10 min each. The mean fluorescence signal of Etd during the dye uptake experiments showed that all tested hemichannels allowed dye uptake when Ca^{2+} was removed. The data are given as average for at least ten experiments for each construct in at least three different transfections for each construct, resulting in at least 190 analyzed cells. The error bars represent the SEM. (B) The dye uptake rate was quantified for all tested constructs and the backbone control in presence or absence of Ca^{2+} and La^{3+}. For each variant, at least 190 cells from at least three independent transfections were analyzed. The data were evaluated by using a one-way ANOVA followed by a Tukey test (*$P \leq 0.05$, ***$P \leq 0.001$). The error bars represent the SEM.

suggested that the presence of the hCx46N188T would reduce the efficiency to form hCx46 gap junction channels between lens fibers.

Discussion

The N188T mutation is located in the E2 domain of human lens Cx46 and has been linked to an autosomal dominant zonular pulverulent cataract [11]. As dominantly inherited disease, it is possible that the mutant variant affects the co-expressed wt Cx and/or its interaction with other cellular components [9]. Our previous results showed that the hCx46N188T mutant did not affect hexamerization in connexons and the trafficking to and insertion of the connexons in the membrane to form gap junction hemichannels. Electrophysiological experiments showed that hCx46wt and hCx46N188T expressed in *Xenopus* oocytes or HeLa cells formed hemichannels, which responded to depolarizing voltages by similar currents [13]. The present report supports the previous data using dye uptake experiments. As shown, similar dye uptake rates were observed in cells expressing hCx46N188T as compared to cells expressing hCx46wt (Fig. 2). The results indicate that an effect of the hCx46N188T mutation on association of the Cx with other proteins such as those involved in trafficking is unlikely. By observing the formation of gap junction plaques formed by GFP-labeled hCx46wt and hCx46N188T, we found that hCx46N188T hemichannels had a
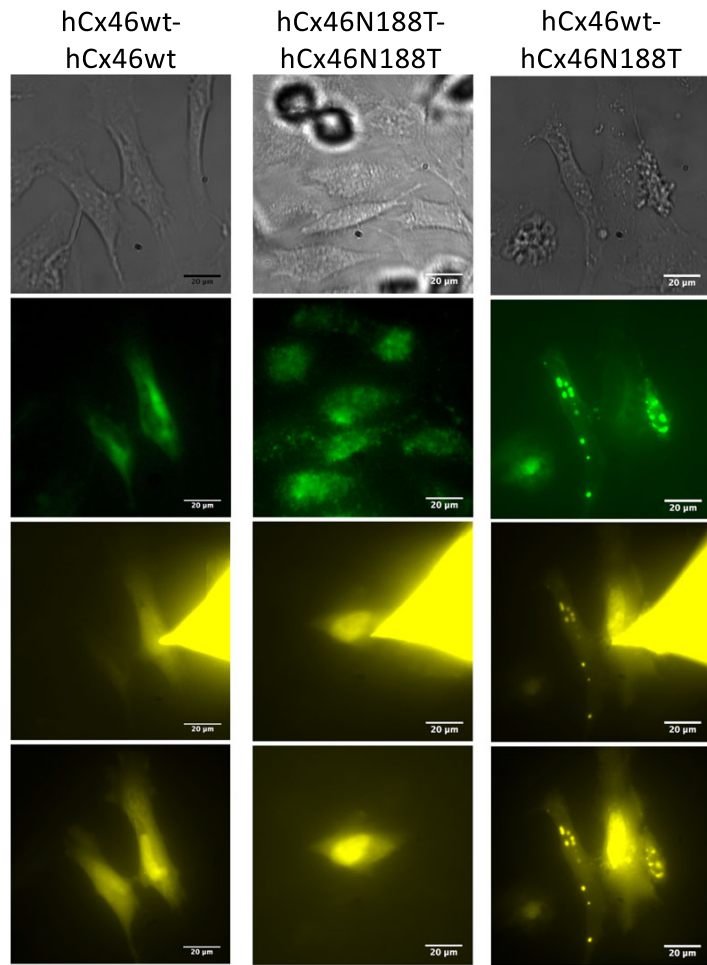
P. Schadzek *et al.*

Fig. 3. Dye transfer experiments to analyze the gap junction functionality. A whole-cell patch-clamp configuration with pipette filling solution containing LY (1 mg·mL^{-1}) was established on one cell of a cell pair expressing the different variants. Mock transfected HeLa cells were used as control. Representative micrographs of cells expressing hCx46wt-hCx46wt, hCx46N188T-hCx46N188T, or hCx46wt-hCx46N188T before (first and second row, phase contrast, and GFP, respectively), during (third row, LY signal 5 min after establishment of the whole-cell configuration) and after (fourth row, 10 min after removal of the dye filled capillary) dye coupling experiments are shown. Scale bar = 20 μm. The cells were considered as coupled if the fluorescence intensity, which was measured in the unpatched cell of a cell pair after 10 min, was at least twice as bright as the background which was measured at the beginning of the experiment. The probability of dye coupling (bar plot) was estimated as a ratio of the sum of LY coupled cell pairs and the total amount of tested cell pairs. The average percentages of the LY dye coupling for the different variants for *n* considered cell pairs in at least three transfection experiments for each variant is given. The error bars represent the SEM. The significance of the difference to control cell pairs which did not express any variant (**$P \leq 0.01$, ***$P \leq 0.001$) and to cells pairs expressing hCx46wt ($^{\#}P \leq 0.05$, $^{\#\#}P \leq 0.01$) was evaluated by Student's *t*-test.

Impaired docking of hCx46wt-hCx46N188T connexons

P. Schadzek *et al.*
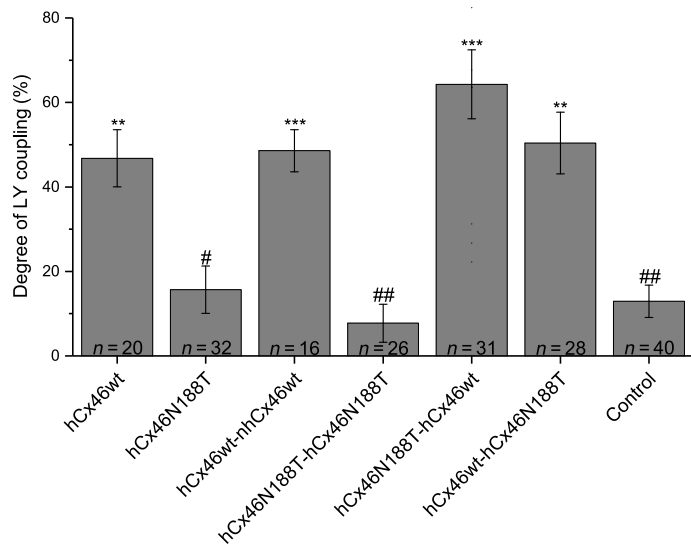
problem with the docking of the channels [13]; therefore, we hypothesized that the co-expression of the wt and the mutant variant would negatively affect the docking of the hemichannels. For the heterodimeric concatenated hCx46wt-hCx46N188T and hCx46N188T-hCx46wt, a reduced number of gap junction plaques compared to the homodimeric concatenated hCx46wt-hCx46wt variant could be observed, even if the heterodimeric concatenated variants showed an increased number of gap junction plaques compared to the homodimeric concatenated hCx46N188T-hCx46N188T (Fig. 1). Concerning the number of gap junction plaques, the concatenation as technique did not alter the number of gap junction plaques, since we observed that the concatenated homodimers hCx46wt-hCx46wt and hCx46N188T-hCx46N188T showed a similar number of gap junction plaques like the hCx46wt and hCx46N188T monomers, respectively (Fig. 1).

The structural models have showed that the docking between connexons required a tight interaction network, mostly governed by HB interactions. The crystallized Cx26 showed that the N176 residue in the E2 domain formed HBs with K168, T177, and D179 of the opposing Cx molecule in the counterpart connexon of the adjacent cells [12,32]. According to the model, 6 HBs were formed between the E2 domains of the interacting

Cx26 protomers between the docked hemichannels. Moreover, further 4 HBs were found in the first extracellular loop (E1) domains, where a protomer interacted with two Cx, resulting in a total of 10 HBs per Cx–Cx interaction or 60 HBs per connexon–connexon interaction [32–37]. For hCx46, N188 is homologous to N176 of Cx26. As shown in Fig. 5, the model predicted that the residue N188 of the E2 loop in a hCx46 molecule in a connexon of one cell forms HBs with residues R180 (two HBs), T189 (one HB), and D191 (one HB) of the opposing Cx molecule in the counterpart connexon of the adjacent cells [13,31]. As for the Cx26, 4 HBs would be formed between the E1 domains of a Cx46 (Fig. 5). As results, a maximum of 72 HBs per connexon–connexon interaction can be assumed for one hCx46wt channel. MD modeling showed that the sum of HBs oscillated between 42 and 68 between the adjacent connexons formed by hCx46wt (Fig. 4, black trace). The formed gap junction channels are stabilized enough to allow a dye coupling (Fig. 3) and an assembly in the gap junction plaques (Fig. 1). In contrast, the MD simulation showed that the sum of HBs between adjacent connexons composed of hCx46N188T oscillated between 24 and only four HBs (Fig. 4, pink trace). These HBs, which might be mostly contributed by interactions in E1 domains, do not support stable gap
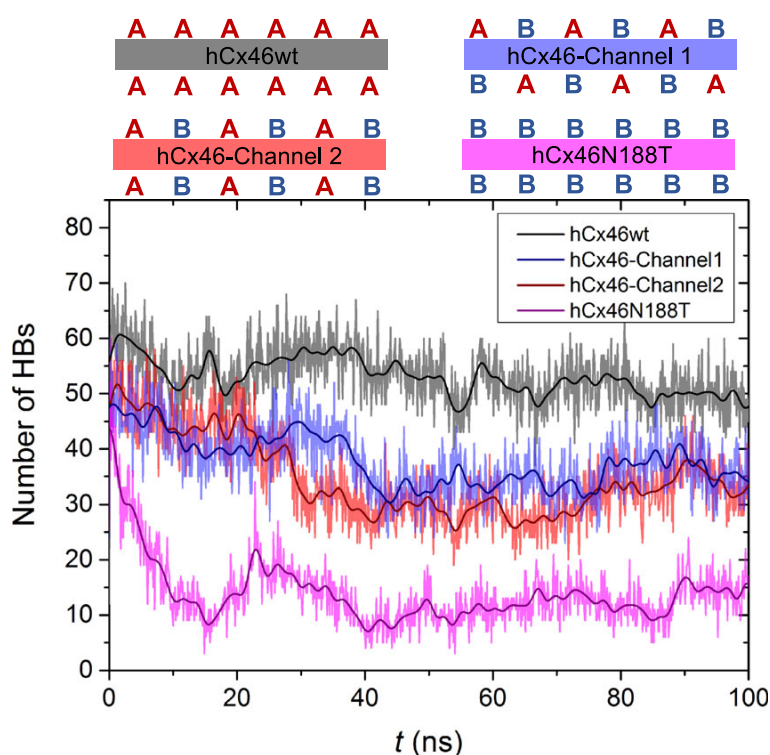

Fig. 4. Number of HBs between interacting connexons over simulation time. Composition of the docking interfaces of the four gap junction channels are shown at the top with a red capital A representing a hCx46wt Cx and the blue capital B depicting hCx46N188T Cx. An average of 53 HBs were found to stabilize the hCx46wt connexon binding interface (black) over a total simulation time of 100-ns MD simulations, while 31 HBs were found for the hCx46wt-hCx46N188T interacting with hCx46wt-hCx46N188T (red) and 35 HBs with hCx46N188T-hCx46wt (blue) connexons, respectively. The number of HBs for hCx46N188T connexons interacting with other hCx46N188T connexons (purple) decreased to an average of 12 HBs within the 100 ns.
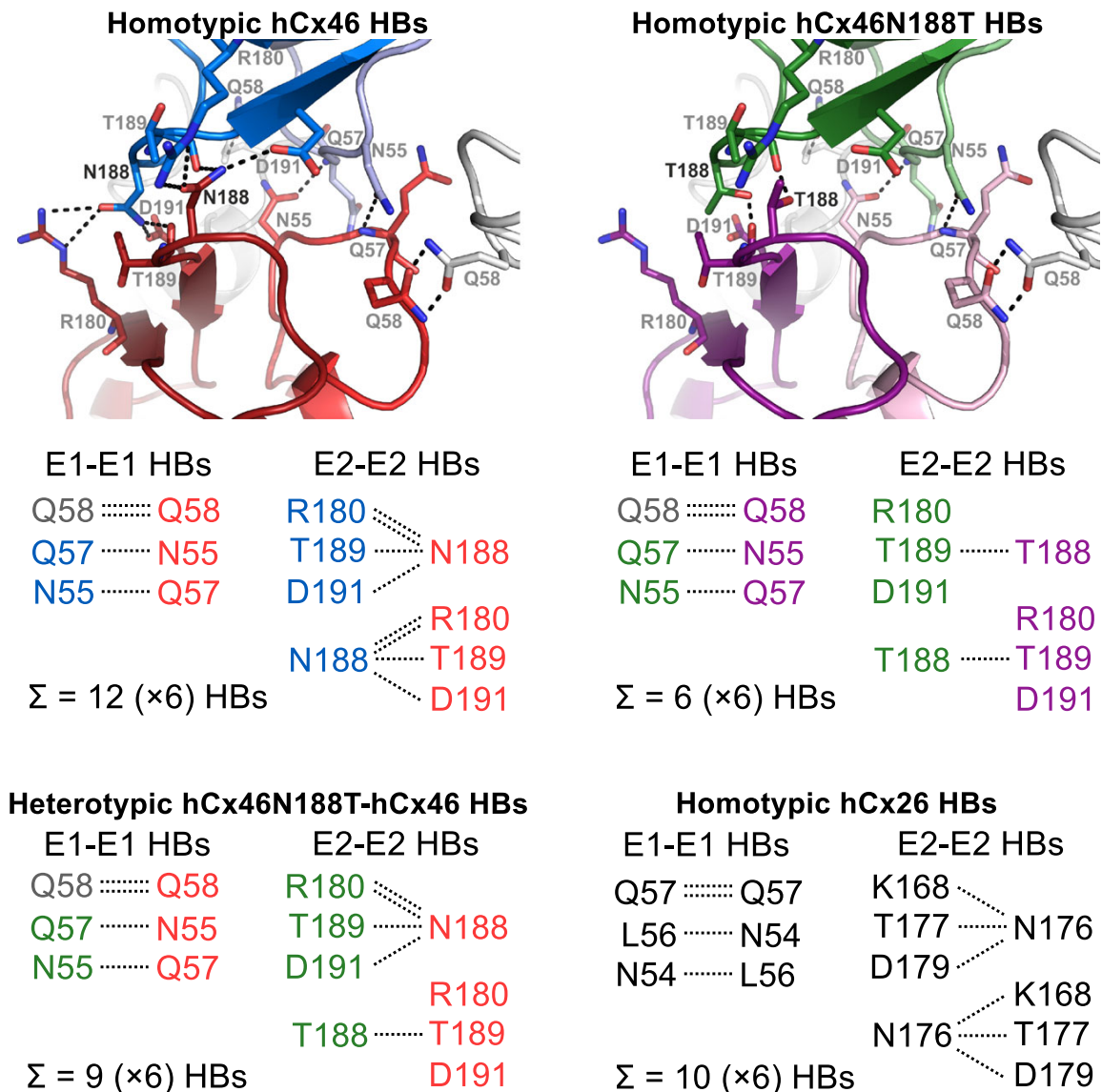
Fig. 5. HB network of the Cx–Cx interaction. The HB network of Cx26 (black, lower right side) is adopted from [12,32]. For a better comparison of the relevant amino acid residues, all homologue residues are displayed. The nondynamic hydrogen bound network of the docking of hCx46 (red and blue) shows 12 relevant HBs per Cx–Cx interaction. Eight HBs were formed in the E2–E2 interaction and four were built for the E1–E1 interaction. Note, that all of the E2-HBs are formed by the residue N188. A channel of hCx46 is theoretically stabilized by 72 HBs. When the hCx46 is mutated at position N188T (green and purple), only 36 HBs could theoretically stabilize the docked channels. The heterotypic hCx46wt-hCx46N188T (green and red) connexon is theoretically stabilized by 54 HBs.

junction channels and corollary gap junction plaques cannot be formed (Fig. 1). In case of hCx46wt and hCx46N188T co-expression, depending on the stoichiometry, different scenarios can be envisaged. For a simplistic model, we considered interactions between hemichannels formed by alternating hCx46wt and hCx46N188T, which also reflects the situation of our experiments with the concatenated heterodimers. Two alternatives are assumed for the formed gap junction channels: wt–mutant interaction (Fig. 4, blue trace) or wt–wt and mutant–mutant (Fig. 4, red trace) interactions. For both alternatives, the MD modeling found that the sum of HBs oscillated between 25 and 45 between the adjacent connexons.

Using a combination of MD modeling and cellular experiments, it was shown that manipulations that reduced the possibility of the formation of HBs between the E2 regions of Cx26 protomers by more than two HBs per Cx–Cx interaction were not functional [35]. How this HB reduction in E2 would affect the total HB binding network between protomers and connexons is so far not clear. However, the results suggest that a minimum number of HBs must be required for stable connexon docking. In this scenario, the mixed hCx46wt/hCx46N188T channels might be affected by this threshold with the consequence of a reduction of the probability to form stable gap junction channels, which correlates with reduction of the number of gap junction plaques as shown in Fig. 1. However, even these reduced gap junction plaques contained gap junction channels that allowed dye transfer experiments (Fig. 3). The dye transfer experiments are evaluated as all-or-nothing process, which shows only that there are gap junction channels between two cells but says almost nothing concerning the density of the gap junction channels. Since we consider cell pairs expressing the variants, the experiments show therefore that concatemers containing N188T together with the wt support LY transfer as well as the wt. Moreover, the observation that the hetero-concatemers hCx46wt-hCx46N188T formed channels that allowed dye coupling agrees very well with the observation that hCx46wt and hCx46N188T formed gap junction hemichannels with similar properties (Fig. 2 and [13]). Therefore, we postulate that cells expressing only hCx46N188T will not form gap junction channels and cells that might co-express hCx46wt and hCx46N188T will form fewer gap junction channels than cells expressing only the wt variant.

Conclusion

The hCx46N188T mutant is dominantly inherited. The usage of concatenated hCx46wt and hCx46N188T in combination with MD simulations shows that the mutation N188T might be negative dominant [11], since the mutant variant might oligomerize with the wt in hemichannels that would inefficiently dock to each other to form gap junction channels between lens fibers. Cx46 gap junction channels participate in lens internal circulation system that is essential for the metabolic homeostasis and, thus, the physiology of the avascular lens [10]. By reducing the formation of hCx46 channels between lens fiber cells, the hCx46N188T mutant would therefore favor the development of a cataract. The degree of participation of the N188T isoform to gap junction channels *in vivo* situation is not known at yet. However, the finding that N188T mutation was linked

to a pulverulent form of cataract [11] might reflect an uneven participation of the mutant isoform in the formation of gap junction channels.

Conflict of interest

The authors declare no conflict of interest.

Author contributions

PS and AN conceptualized the study; PS performed the data curation, and formal analysis; AN performed the funding acquisition and project administration; PS and YS performed the investigation of the article; PS, MP, and AN performed the methodology; MP performed the MD simulations; PS and MP performed the visualization; PS, MP and AN wrote the original draft of the manuscript; PS and AN wrote, reviewed, and edited the article. The paper was proofread by all authors.

References

1 Pogoda K, Kameritsch P, Mannell H and Pohl U (2019) Connexins in the control of vasomotor function. *Acta Physiol (Oxf)* **225**, e13108.

2 Goodenough DA and Gilula NB (1974) The splitting of hepatocyte gap junctions and zonulae occludentes with hypertonic disaccharides. *J Cell Biol* **61**, 575–590.

3 Neijssen J, Herberts C, Drijfhout JW, Reits E, Janssen L and Neefjes J (2005) Cross-presentation by intercellular peptide transfer through gap junctions. *Nature* **434**, 83–88.

4 Bedner P, Niessen H, Odermatt B, Kretz M, Willecke K and Harz H (2006) Selective permeability of different connexin channels to the second messenger cyclic AMP. *J Biol Chem* **281**, 6673–6681.

5 Bennett MVM and Verselis VKV (1992) Biophysics of gap junctions. *Semin Cell Biol* **3**, 29–47.

6 Niessen H, Harz H, Bedner P, Krämer K and Willecke K (2000) Selective permeability of different connexin channels to the second messenger inositol 1,4,5-trisphosphate. *J Cell Sci* **113** (Pt 8), 1365–1372.

7 Söhl G and Willecke K (2004) Gap junctions and the connexin protein family. *Cardiovasc Res* **62**, 228–232.

8 Harris AL (2001) Emerging issues of connexin channels: biophysics fills the gap. *Q Rev Biophys* **34**, 325–472.

9 Berthoud VM and Ngezahayo A (2017) Focus on lens connexins. *BMC Cell Biol* **18**, 6.

P. Schadzek *et al.*   Impaired docking of hCx46wt-hCx46N188T connexons

10 Mathias RT, Kistler J and Donaldson P (2007) The lens circulation. *J Membr Biol* **216**, 1–16.

11 Li Y, Wang J, Dong B and Man H (2004) A novel connexin46 (GJA3) mutation in autosomal dominant congenital nuclear pulverulent cataract. *Mol Vis* **10**, 668–671.

12 Maeda S, Nakagawa S, Suga M, Yamashita E, Oshima A, Fujiyoshi Y and Tsukihara T (2009) Structure of the connexin 26 gap junction channel at 3.5 A resolution. *Nature* **458**, 597–602.

13 Schadzek P, Schlingmann B, Schaarschmidt F, Lindner J, Koval M, Heisterkamp A, Preller M and Ngezahayo A (2015) The cataract related mutation N188T in human connexin46 (hCx46) revealed a critical role for residue N188 in the docking process of gap junction channels. *Biochim Biophys Acta* **1858**, 57–66.

14 Veitia RA (2007) Exploring the molecular etiology of dominant-negative mutations. *Plant Cell* **19**, 3843–3851.

15 Ahring PK, Liao VWY and Balle T (2018) Concatenated nicotinic acetylcholine receptors: a gift or a curse? *J Gen Physiol* **150**, 453–473.

16 Baumann SW, Baur R and Sigel E (2001) Subunit arrangement of gamma-aminobutyric acid type A receptors. *J Biol Chem* **276**, 36275–36280.

17 Im WB, Pregenzer JF, Binder JA, Dillon GH and Alberts GL (1995) Chloride channel expression with the tandem construct of alpha 6-beta 2 GABAA receptor subunit requires a monomeric subunit of alpha 6 or gamma 2. *J Biol Chem* **270**, 26063–26066.

18 Isacoff EY, Jan YN and Jan LY (1990) Evidence for the formation of heteromultimeric potassium channels in Xenopus oocytes. *Nature* **345**, 530–534.

19 Sigel E, Kaur KH, Lüscher BP and Baur R (2009) Use of concatamers to study GABAA receptor architecture and function: application to delta-subunit-containing receptors and possible pitfalls. *Biochem Soc Trans* **37**, 1338–1342.

20 Minier F and Sigel E (2004) Techniques: use of concatenated subunits for the study of ligand-gated ion channels. *Trends Pharmacol Sci* **25**, 499–503.

21 Schadzek P, Hermes D, Stahl Y, Dilger N and Ngezahayo A (2018) Concatenation of human connexin26 (hCx26) and human connexin46 (hCx46) for the analysis of heteromeric gap junction hemichannels and heterotypic gap junction channels. *Int J Mol Sci* **19**, 2742.

22 Gubbels SP, Woessner DW, Mitchell JC, Ricci AJ and Brigande JV (2008) Functional auditory hair cells produced in the mammalian cochlea by *in utero* gene transfer. *Nature* **455**, 537–541.

23 Dieriks B and van Oostveldt P (2012) Spatiotemporal behavior of nuclear cyclophilin B indicates a role in RNA transcription. *Int J Mol Med* **29**, 1031–1038.

24 Schlingmann B, Schadzek P, Busko S, Heisterkamp A and Ngezahayo A (2012) Cataract-associated D3Y mutation of human connexin46 (hCx46) increases the dye coupling of gap junction channels and suppresses

25 Schlingmann B, Schadzek P, Hemmerling F, Schaarschmidt F, Heisterkamp A and Ngezahayo A (2013) The role of the C-terminus in functional expression and internalization of rat connexin46 (rCx46). *J Bioenerg Biomembr* **45**, 59–70.

26 Schindelin J, Arganda-Carreras I, Frise E, Kaynig V, Longair M, Pietzsch T, Preibisch S, Rueden C, Saalfeld S, Schmid B *et al.* (2012) Fiji: an open-source platform for biological-image analysis. *Nat Methods* **9**, 676–682.

27 Jorgensen WL, Chandrasekhar J, Madura JD, Impey RW and Klein ML (1983) Comparison of simple potential functions for simulating liquid water. *J Chem Phys* **79**, 926–935.

28 Phillips JC, Braun R, Wang W, Gumbart J, Tajkhorshid E, Villa E, Chipot C, Skeel RD, Kalé L and Schulten K (2005) Scalable molecular dynamics with NAMD. *J Comput Chem* **26**, 1781–1802.

29 Huang J, Rauscher S, Nawrocki G, Ran T, Feig M, de Groot BL, Grubmüller H and MacKerell AD (2017) CHARMM36 m: an improved force field for folded and intrinsically disordered proteins. *Nat Methods* **14**, 71–73.

30 Darden TA and Pedersen LG (1993) Molecular modeling: an experimental tool. *Environ Health Perspect* **101**, 410–412.

31 Schadzek P, Schlingmann B, Schaarschmidt F, Lindner J, Koval M, Heisterkamp A, Ngezahayo A and Preller M (2016) Data of the molecular dynamics simulations of mutations in the human connexin46 docking interface. *Data Brief* **7**, 93–99.

32 Nakagawa S, Gong X-Q, Maeda S, Dong Y, Misumi Y, Tsukihara T and Bai D (2011) Asparagine 175 of connexin32 is a critical residue for docking and forming functional heterotypic gap junction channels with connexin26. *J Biol Chem* **286**, 19672–19681.

33 Bai D and Wang AH (2014) Extracellular domains play different roles in gap junction formation and docking compatibility. *Biochem J* **458**, 1–10.

34 Bai D, Yue B and Aoyama H (2018) Crucial motifs and residues in the extracellular loops influence the formation and specificity of connexin docking. *Biochim Biophys Acta* **1860**, 9–21.

35 Gong X-Q, Nakagawa S, Tsukihara T and Bai D (2013) A mechanism of gap junction docking revealed by functional rescue of a human-disease-linked connexin mutant. *J Cell Sci* **126**, 3113–3120.

36 Karademir LB, Aoyama H, Yue B, Chen H and Bai D (2016) Engineered Cx26 variants established functional heterotypic Cx26/Cx43 and Cx26/Cx40 gap junction channels. *Biochem J* **473**, 1391–1403.

37 Nakagawa S, Maeda S and Tsukihara T (2010) Structural and functional studies of gap junction channels. *Curr Opin Struct Biol* **20**, 423–430.

Curriculum Vitae

Name	Patrik Klaus Schadzek
Geburtstag	30. August 1986
Geburtsort	Hannover

Bildungsgang

2014 – 2018	Promotionsstudent am Institut für Zellbiologie und Biophysik, Abteilung Biophysik und Zellphysiologie an der Gottfried Wilhelm Leibniz Universität Hannover
2016	FELASA - Kategorie B „Tierschutzgerechter Umgang mit Versuchstieren"
2011 – 2013	Life Science Master-Studium an der Gottfried Wilhelm Leibniz Universität Hannover
	Hauptfächer: Molekularbiologie und Bioprozesstechnik
	Thema der Masterarbeit: Oligomerisierungsverhalten von humanen Connexinen: physiologische und molekularbiologische Analyse
2008 – 2011	Bachelor-Studium des Studiengans Life Science an der Gottfried Wilhelm Leibniz Universität Hannover
	Thema der Bachelorarbeit: Analyse der Rolle des C-Terminus bei der Internalisierung von rCx46
2007 – 2008	Zivildienst im Rettungsdienst beim DRK in Soltau
2007	Humboldtschule Hannover (Gymnasium)
	Abschluss: Allgemeine Hochschulreife

Publikationsliste

Schadzek, P., Stahl, Y., Preller, M., Ngezahayo, A. (2019) Analysis of the dominant mutation N188T of human connexin46 (hCx46) using concatenation and molecular dynamics simulation. FEBS open bio, DOI 10.1002/2211-5463.12624.

Schadzek, P., Hermes, D., Stahl, Y., Dilger, N., Ngezahayo, A. (2018) Concatenation of human connexin26 (hCx26) and human connexin46 (hCx46) for the analysis of heteromeric gap junction hemichannels and heterotypic gap junction channels. Int. J. Mol. Sci. 2018, 19, 2742, DOI 10.3390/ijms19092742.

Harting, T., Stubbendorff, M., Hammer, S. C., **Schadzek, P.**, Ngezahayo, A., Escobar, H. M., Nolte, I. (2017) Dichloroacetate affects proliferation but not apoptosis in canine mammary cell lines. PLoS ONE 12(6):e0178744 (2017) DOI 10.1371/journal.pone.0178744.

Harting, T., Stubbendorff, M., Willenbrock, S., Wagner, S., **Schadzek, P.**, Ngezahayo, A., Escobar, H. M., Nolte, I. (2016) The effect of dichloroacetate in canine prostate adenocarcinomas and transitional cell carcinomas in vitro. Int J Oncol 49 (2016) 2341-2350 DOI 10.3892/ijo.2016.3720.

Kniggendorf, A.-K., Nogueira, R., Kelb, C., **Schadzek, P.**, Meinhardt-Wollweber, M., Ngezahayo, A., Roth, B. (2016) Confocal Raman microscopy and fluorescent in situ hybridization – A complementary approach for biofilm analysis. Chemosphere 161 (2016) 112-118, DOI 10.1016/j.chemosphere.2016.06.096.

Schadzek, P., Schlingmann, B., Schaarschmidt, F., Lindner, J., Heisterkamp, A., Koval, M., Preller, M., Ngezahayo, A. (2016) Data of the molecular dynamics simulations of mutations in the human connexin46 docking interface. Data in Brief 7 (2016) 93-99, DOI 10.1016/j.dib.2016.01.067.

Schadzek, P., Schlingmann, B., Schaarschmidt, F., Lindner, J., Heisterkamp, A., Koval, M., Preller, M., Ngezahayo, A. (2015) The cataract related mutation N188T in human connexin46 (hCx46) revealed a critical role for residue N188 in the docking process of gap junction channels. Biochimica et Biophysica Acta 1858 (2016) 57-66, DOI 10.1016/j.bbamem.2015.10.001.

Schlingmann, B., **Schadzek, P.**, Hemmerling, F., Schaarschmidt, F., Heisterkamp, A., Ngezahayo, A. (2013) The role of the C-terminus in functional expression and internalization of rat connexin46 (rCx46). J Bioenerg Biomembr 45:59-70, DOI 10.1007/s10863-012-9480-x.

Schlingmann, B., **Schadzek, P.**, Busko, S., Heisterkamp, A., Ngezahayo, A. (2012) Cataract-associated D3Y mutation of human connexin46 (hCx46) increases the dye coupling of gap junction channels and suppresses the voltage sensitivity of hemichannels. J Bioenerg Biomembr 44: 607-14, DOI 10.1007/s10863-012-9461-0.

Konferenzbeiträge

Schadzek, P., Hermes, D., Stahl, Y., Ngezahayo, A. Concatemerization of connexins – a tool to analyze the oligomerization behavior of heteromeric connexins. (2017) **Poster**, 2017 ASCB Annual Meeting, Philadelphia, PA, USA.

Stahl, Y., **Schadzek, P.**, Preller, M., Ngezahayo, A. Using concatemerization as a tool to investigate the dominate effect of the mutation N188T of connexin46. (2017) **Poster**, 2017 ASCB Annual Meeting, Philadelphia, PA, USA.

Schadzek, P., Hermes, D., Stahl, Y., Ngezahayo, A. Concatemerisation of connexins – analysis of the oligomerisation behaviour. (2017) **Poster**, International Gap Junction Conference 2017, Glasgow, Schottland, Vereinigtes Königreich.

Schadzek, P., Hermes, D., Ngezahayo, A. Analysis of the oligomerization behavior of concatemeric connexins. (2016) **Poster**, 2016 ASCB Annual Meeting, San Francisco, CA, USA

Schadzek, P., Schlingmann, B., Schaarschmidt, F., Heisterkamp, A., Koval, M., Preller, M., Ngezahayo, A. Functional analysis of the cataract related mutation N188T in human connexin46 (hCx46). (2016) **Poster**, Jahrestagung der Deutschen Physiologischen Gesellschaft, Lübeck, Germany.

Hermes, D., **Schadzek, P.**, Ngezahayo, A. Concatemeric connexins build functional hemichannels and gap junction channels. (2016) **Poster**, Jahrestagung der Deutschen Physiologischen Gesellschaft, Lübeck, Germany.

Schadzek, P., Schlingmann, B., Schaarschmidt, F., Heisterkamp, A., Koval, M., Preller, M., Ngezahayo, A. The cataract related mutation N188T in connexin46 (Cx46) inhibits formation of functional gap junction channels by impairing docking process of Cx46 hemichannels. (2015) **Poster**, 2015 ASCB Annual Meeting, San Diego, CA, USA.

Schadzek, P., Hermes, D., Ngezahayo, A. Generation of concatemeric connexins to investigate the oligomerisation behaviour. (2015) **Poster**, International Gap Junction Conference, Valparaíso, Chile.

Schlingmann, B., **Schadzek, P.**, Preller, M., Schaarschmidt, F., Heisterkamp, A., Ngezahayo, A. Cataract related Mutation N188T in Connexin46 inhibits formation of functional gap junction channels. (2015) **Poster**, International Gap Junction Conference, Valparaíso, Chile.

Schadzek, P., Schlingmann, B., Ngezahayo, A. Investigation the oligomerisation behaviour of connexins by building concatemeric connexins. (2014) **Poster**, Jahrestagung der Deutschen Physiologischen Gesellschaft, Mainz, Germany.

Schadzek, P., Schlingmann, B., Ngezahayo, A. Effects of the Cataract-associated D3Y Mutation of human Connexin46. (2013) **Poster**, Jahrestagung der Deutschen Physiologischen Gesellschaft, Heidelberg, Germany.

Schlingmann, B., **Schadzek, P.**, Ngezahayo, A. The cataract related mutation of human Connexin46 D3Y and N188T affect the voltage sensitivity and the formation of gap junction channels. (2012) **Poster**, annual meeting of the American Society of Cell Biology, San Francisco (CA) USA.

Schadzek, P., Schlingmann, B., Ngezahayo, A. The C-Terminus is Essential for a Functional Expression and Internalization of the Rat Lens Gap Junction Connexin46. (2012) **Vortrag**, Jahrestagung der Deutschen Physiologischen Gesellschaft, Dresden Germany.

Schlingmann, B., **Schadzek, P.**, Busko, S., Hemmerling, F., Ngezahayo, A. The Influence of the C-Terminus in Functional Expression and Internalization of Rat Lens Gap Junction Connexin 46, International Conference on the Lens. (2012) **Vortrag**, Kona (HI) USA.

Danksagung

Herrn Prof. Dr. Anaclet Ngezahayo, meinem Doktorvater, danke ich herzlich für das sehr innovative und zu Beginn auch etwas ungewisse Thema meiner Dissertation. Danke Anaclet, für die großen Freiräume bei der Ausgestaltung des Promotionsprojekts und für die uneingeschränkte Unterstützung. Vielen Dank auch für die sehr interessanten wissenschaftlichen Diskussionen und auch für die vielen Gespräche, die in keinem unmittelbaren wissenschaftlichen Zusammenhang standen. Danke, dass du es mir ermöglich hast, an so vielen Konferenzen teilzunehmen.

Bei meinen Korreferenten Herrn Prof. Dr. Peter Claus und Herrn Prof. Dr. Helge Küster bedanke ich mich herzlichst für die schnelle und freundliche Zusage, dass Sie die Evaluation und Gutachtenerstellung für meine Dissertation übernehmen. Des Weiteren danke ich Herrn Prof. Dr. Helge Küster, dass er den Vorsitz der Promotionskommission übernehmen wird.

Bei allen meinen Koautoren bedanke ich mich für die Unterstützung beim Schreiben der Publikationen. Mein besonderer Dank gilt hier meinem langfristigen Kooperationspartner Herrn Prof. Dr. Matthias Preller für die Durchführung der Molekül-Dynamik-Simulationen, die meine Ergebnisse hervorragend unterstützt und zu einem visuellen Leckerbissen gemacht haben. Herzlich danken möchte ich meinen Kooperationspartnern Herrn PD Dr. Frank Schaarschmidt und Herrn Prof. Dr. Michael Koval für die statistische und experimentelle Hilfe beim ersten Paper.

Bei meiner guten Freundin Babsi (Frau Dr. Barbara Schlingmann-Molina) möchte ich mich ganz herzlich für die geleistete Vorarbeit, die Hilfestellung und vor allem für die Unterstützung seit den Anfängen meines Wissenschafts-Daseins bedanken. Danke für deine großartige Art.

Bei meinen Ex-HiWis und Bachelor- und Masterstudenten Julia Lindner, Doris Hermes und Yannick Stahl bedanke ich mich für ihre experimentelle Unterstützung.

Bei den Feinmechanikern unserer Werkstatt, Frank Köpcke und Michael Senft, bedanke ich mich für die uneingeschränkte Unterstützung beim Bauen von Messkammern und für den Bau und Umbau der Messsysteme.

Herzlich möchte ich mich vor allem bei allen Mitarbeitern und Studierenden des Instituts für Biophysik für das sehr angenehme Arbeitsklima und die vielen netten Gespräche bedanken. Den technischen Assistentinnen Heidi Bliedung, Ingrid Buchwald und Helma Feierabend danke ich für die vielen angesetzten Medien, mit denen man bestimmt eine Badewanne zum Überlaufen hätte bringen können. Andrea Lika-Gerbing und Bettina Winnat danke ich für alle administrativen Angelegenheiten. Bei Annegret Becker, Anne Dierks und Frederike Ruhe möchte ich mich für die Gute Laune, das Pöbeln, das gemeinsame Lachen und die ein oder andere Krisensitzung bedanken.

Besonders möchte ich meiner geliebten Partnerin Nadine Dilger für alles danken. Danke für die Unterstützung, die ich zu jeder Zeit erhalten habe, und vor allem auch das kritische Lesen dieser Arbeit. Danke, dass es dich gibt!

Nicht zuletzt bedanke ich mich bei meiner Familie und meinen Freunden, die mich stets unterstützt haben. Vielen Dank, dass ihr mich immer wieder gedanklich in die „wissenschaftsfreie Welt" geholt habt.

Danke, dass es Euch gibt, ihr habt mich zu dem gemacht, wer ich bin.

Vielen Dank!